Investigating the host cellular changes associated with plant colonisation by the blast fungus *Magnaporthe oryzae*

BERLAINE QUIME

Thesis submitted to the University of East Anglia for the Degree of Doctor of Philosophy

The Sainsbury Laboratory

Norwich, UK

March 2025

UEA Registration No.: 100325950

Abstract

Rice blast disease, caused by the hemibiotrophic fungus *Magnaporthe oryzae*, significantly impacts rice production worldwide. Key advances in understanding infection processes, such as appressorium formation and host cell entry, have been made through molecular genetics and genomics, with recent insights into the Pmk1-dependent phosphorylation landscape and temporal shifts in fungal gene expression. Despite these advances, gaps remain in understanding the spatial and temporal dynamics of fungal invasion. This thesis addresses these gaps by exploring cellular organisation changes in rice during *M. oryzae* infection. Transgenic rice lines expressing GFP-tagged markers for various organelles were developed, enabling the study of plasma membrane organisation, actin dynamics, and the formation of the biotrophic interfacial complex (BIC) during blast infection. Live-cell imaging results provide evidence that fungal infection led to the development of an extra-invasive hyphal membrane (EIHM) to facilitate invasion and actively alters host plasma membrane integrity, leading to a mosaic pattern of cell death and viability. Actin cytoskeleton remodelling is crucial for fungal invasion, as it supports the formation of EIHM and BICs. The study also quantifies the net increase in plasma membrane during infection, highlighting the role of host membrane biogenesis in supporting invasive hyphal growth. This research sheds light on the host cellular changes induced by *M. oryzae* infection and offers a valuable resource of transgenic rice lines for future studies of host-pathogen interactions. Ultimately, this work is a significant advance in the development of a spatiotemporal atlas of cellular changes during fungal colonisation, which could inform strategies to combat rice blast disease.

Table of Contents

List of Figures

List of Tables

Acknowledgements

First, I would like to express my immense gratitude to Les and Claire Halpin, my very generous sponsors for me to carry out my PhD. I am truly grateful and humbled for this life-changing opportunity.

I am deeply grateful to my primary supervisor, Prof. Nick Talbot, for the opportunity to pursue my studies under his guidance. Thank you for your patience and invaluable advice, as well as for creating opportunities that allowed me to grow in confidence and capability as a researcher. I am proud to have been trained by one of the very best in the field.

I am thankful to my secondary supervisors Prof. Wenbo Ma, for her insightful feedback during our review meetings, and to Prof. Matt Moscou, for his practical and realistic approach to research.

To Dr. Xia Yan, thank you for teaching me patiently and selflessly, and for listening to my setbacks and successes, no matter how small.

To Dr. Vincent Were, whom I've known even before coming to the UK, for the encouragement to believe in myself, the extra push when it was needed, and the honesty to challenge me when self-doubt crept in.

To all the past and present Talbot lab members, Adam, Alice, Andrew, Andy, Angus, Barakat, Bright, Camilla, Camille, Diana, Fabio, Gulnara, Iris, Jave, Juan Carlos, Marisela, Matt, Miriam, Neftaly, Neha, Prince, Sue, Vincent, Weibin, Xia, thank you for creating a supportive and collaborative working environment. I would not survive without all of you. I also thank Jack, Markus, Clinton, and Frank, for the insights and the meaningful connections we shared.

To the TSL tissue culture and transformation team, thank you for helping me generate my transgenic lines. Thank you to the TSL SynBio, for your support in construct design and for teaching me Golden Gate cloning, and to the Media Kitchen, whose work is so important to the success of this research. I am grateful to Simon Foster, Chris Hartley, Chris Rickett, and Matt Castle, for ensuring the smooth running of the laboratory. Thank you to the JIC Horticultural Services for their assistance in all plant-related matters.

I thank the entire TSL community. It is indeed a privilege to be here and to be working with such talented people inside and outside of the lab. I look up to you all.

Thank you to our collaborator Dr. Richard Smith of the Computational and Systems Biology department at the John Innes Centre for sharing his expertise and resources that enabled one of the results chapters in this thesis. I also thank Dr. Robert Bellow, for troubleshooting with me and for helping me survive MorphoGraphX in my final year of PhD.

Special thanks to the JIC Bioimaging and Microscopy Platform, especially to Dr. Eva Wegel, for confocal microscopy training, and to Dr. Sergio Lopez for technical support and troubleshooting.

Thank you Ifeoluwa, for being my best housemate in Norwich.

Thank you to Dr. Alice Eseola, for your friendship and support during challenging times.

Special thanks to my lab bff, Jave, for the constant help, shared meals, and endless cups of *tea*.

To my best friends, Billy and Justine, for the unwavering friendship despite the distance and for keeping my sanity intact.

Thank you to my family, my dad, mom, and brother, for the moral support, encouragement, prayers, and reassurance that you got my back no matter what happens.

To my fiancé, Carmichael, it was not easy, but your love and support never faltered. Thank you for patiently waiting for me to figure out my life [and thesis] chapters.

Thank you, Lord Jesus, for your never-ending kindness and mercy.

Above all, thank you, Almighty Father, for giving me more than I've ever asked or ever hoped to have. May You be glorified through this humble work.

Pasasalamat

Nais kong magpaabot ng aking taos-pusong pasasalamat sa lahat ng sumuporta, naniwala at nanalangin para sa aking tagumpay. Lahat ng ito ay hindi lamang akin, kundi atin.

Nais kong magpasalamat sa mga kapatid sa Lokal ng College, ang aking naging tahanan sa loob ng labindalawang taon. Maraming salamat sa inyong malasakit upang marating ko kung nasaan ako ngayon. Maraming salamat sa pamilya ng Ka Eric at Ka Peewee Pasuquin, sa pamilya ng Ka Romy at Ka Fely Tuiza, Ka Adonna Robles, sa aking mga ka-mang-aawit at ka-maytungkulin sa Pagsamba ng Kabataan, at sa balangay ng Christian Brotherhood International-UPLB. Hindi ko malilimutan ang lahat ng ating pinagsamahan.

Buong puso rin akong nagpapasalamat sa mga kapatid sa Lokal ng Norwich. Kayo ang aking naging mga magulang at kapatid sa nakalipas na limang taon. Napakapalad ko sapagkat kayo ang tugon ng Ama sa aking mga panalangin. Hindi naging madali ang pamamalagi ko rito ngunit sa inyong pagtulong at pagpapalakas ng loob ay naiibsan ang aking pangungulila sa aking mga mahal sa buhay at patuloy akong nakatutupad nang buong kasiglahan sa aking mga tungkulin.

Maraming salamat sa pamilya ng Ka Jhoboy at Ka Melissa Socao sa inyong walang-sawang pagmamalasakit. Wala akong maitutumbas sa pagsasaalang-alang ninyo sa aking kapakanan kundi ang ipanalangin kayo sa ating Ama na punuin ang inyong sambahayan ng lahat ng mabubuting bagay.

Salamat sa aking mga kapatid sa kapisanang KADIWA lalung-lalo na kina Lana, Edelweiss, Ate Keisha at Bea sa tawanan, kainan, at damayan. Nawa'y lahat ng mga pangarap ninyo para sa inyong sarili at sa inyong mga mahal sa buhay ay matupad.

Salamat SB19, sa inyong musika, na nagtawid sa akin sa aking paglalakbay. Salamat sa pagbabahagi ng inyong mga karanasan na nagsilbing inspirasyon upang *huwag huminto sa ordinaryo* at *higitan pa ang sagad na*.

Salamat sa aking mga magulang, na nagsakripisyo at nagsumikap para marating ko ang aking kinalalagyan. Salamat sa pagmamahal kahit anumang mangyari at sa pagpapalakas ng loob sa gitna ng kabiguan at kapaguran. Salamat sa aking kapatid sa pagsisilbing inspirasyon upang maging mabuting halimbawa.

Salamat sa aking minamahal, Carmichael, nagawa ko ang lahat ng ito dahil sa iyong suporta at presensya. Hindi ko kailanman naramdamang malayo ka. Salamat hindi ka nagsawa, bagkus humawak ka nang mahigpit sa mga panahong naging mahirap ang lahat. Handa na ako sa susunod nating kabanata.

Salamat sa Pamamahala, sa walang-sawang paalala at pagmamalasakit para sa aming espiritwal na kapakanan. Salamat rin po sa lahat ng mga ministro at manggagawang nagsilbing gabay sa bawat yugto ng aking buhay.

Maraming salamat Panginoong Hesus. Tunay napakabuti mo. Hindi Mo ako kailanman nilimot.

Higit sa lahat, maraming salamat Ama sa lakas, buhay, talino at pananampalataya. Sa bawat bagay na natutuklasan, lalo kong namamalas ang Iyong kadakilaan.

Heto na, heto na, bunga ng mga hiraya…

-DAM, SB19

Abbreviations

BIC	biotrophic interfacial complex
CLSM	confocal laser scanning microscopy
CM	complete medium
DNA	deoxyribonucleic acid
EIHM	extra-invasive hyphal membrane
EIHMx	extra-invasive hyphal matrix
EHM	extrahaustorial matrix
ER	endoplasmic reticulum
GFP	green fluorescent protein
hpi	hours post-inoculation
MGX	MorphoGraphX
PCR	Polymerase Chain Reaction
RFP	red fluorescent protein
rpm	revolutions per minute

General Introduction

Figures and parts of the text from this chapter have been published in *Journal of Microscopy* as part of a review article by Quime et al., 2025. DOI: https://doi.org/10.1111/jmi.13382

1.1 Rice Blast and Its Global Significance

Rice (*Oryza sativa*) is a major crop that constitutes the staple diet for more than half of the world population (Khush, 2005; Sharma et al., 2012). The rapidly growing human population, which is projected to increase to almost 9 billion by the year 2050, requires rice production to increase in order to meet the growing demand for food (Godfray et al., 2010). Most of this demand comes from Asia as evidenced by its 90% share of the total area under rice cultivation worldwide (Bandumula, 2018). Recently, however, Africa is also becoming a major stakeholder of international rice trade, accounting for up to 32% of global rice imports, equivalent to 9 million tonnes annually. This can be explained by the fact that rice is becoming a preferred staple food in sub-Saharan Africa, especially in urban areas (Balasubramanian et al., 2007). Rice production, however, faces a lot of constraints, because it is affected by both abiotic and biotic stresses that limit the rice harvest (Fahad et al., 2019; Iqbal et al., 2023; Rasheed et al., 2020).

One of the most important threats to rice production is rice blast disease caused by the ascomycete fungus *Magnaporthe oryzae* B. Couch (formerly *Magnaporthe grisea* (T.T. Hebert) M.E. Barr; synonym of *Pyricularia oryzae*) (Zhang et al., 2016). Because of its agronomic significance and high amenability to genetic and molecular genetic manipulation (Jeon et al., 2007; Talbot, 2003; Valent & Chumley, 1991), *M. oryzae* emerged as an important model organism for studying plant-fungal interactions (R. Dean et al., 2012; Ebbole, 2007). Rice blast disease has been identified in more than 85 rice-growing countries around the world (Skamnioti & Gurr, 2009). The disease limits production of upland rice in tropical regions of Latin America, Africa and Asia and severely affects lowland rice in Asia in both temperate and subtropical areas (Savary et al., 2019). Recent estimates showed that the global annual yield loss brought about by rice blast is about 6% (Savary et al., 2019), but epidemics arise and can cause up to 30% yield losses (Nalley et al., 2016; Wilson & Talbot, 2009). It is also estimated that such an annual loss of rice is sufficient to feed 60 million people for a year (Pennisi, 2010). Moreover, *M. oryzae* is capable of infecting over 50 grass species (Kato et al., 2000; Langner et al., 2018; Oh et al., 2002; Tosa et al., 2004), leading to the emergence of new plant diseases such as wheat blast.

Wheat blast first appeared in Brazil following a host jump from a grass-infecting strain of *M. oryzae* and has since spread to neighbouring South American countries (Inoue et al., 2017). In 2016, wheat blast was detected in Bangladesh (Islam et al., 2016), posing a significant threat to the Indian subcontinent, a key wheat-producing region (Islam et al., 2019). More recently, it has been reported in Zambia, raising concerns about its potential spread across Africa (Latorre et al., 2023). Factors such as globalisation, climate change, and the widespread cultivation of cereal monocultures increase the likelihood of blast disease outbreaks in crops such as wheat, rice, millets, oats, and barley, making it a growing concern for global agriculture.

Rice blast disease can occur in several parts of the plant including leaf collars, necks, panicles, pedicels, and seeds, but the most common symptoms are characterized by spindle-shaped lesions with reddish brown margins and greyish, and sporulating centres found on leaves. Lesions appear grey-green and water-soaked with a darker green border and then become light tan with necrotic borders in highly susceptible rice cultivars. Lesions on resistant cultivars are often small (1-2 mm) and are brown to dark brown (Ou, 1980).

Several factors favour rice blast disease development. Severe blast infection is often observed during warm temperatures (around 24ºC) and high moisture and profuse sporulation of the lesions is observed under conditions of high humidity (Ou, 1985; Talbot, 2003). In temperate regions, the primary inoculum comes from overwintered fungus spores released from straw, volunteer plants and infected refuse (Ou, 1980; TeBeest et al., 2007). It was observed that higher amounts of initial inoculum often led to more severe blast infections. Over-fertilization, especially with nitrogen fertilizers and cultivation in incorrect water depths are also conducive conditions for blast disease (Long et al., 2000).

Several options are available to manage rice blast disease. These include various cultural (Ou, 1980) and chemical (Iwai et al., 2007) methods. Low-cost measures are also being employed to prevent blast outbreaks, such as burning crop residues, growing under continuous flooding, and planting disease-free seed, but these are ineffective under high disease pressure (Shafaullah et al., 2011; Skamnioti & Gurr, 2009). Growing genetically resistant cultivars is therefore considered the most economical, effective, and

environmentally friendly measure to control blast disease (Skamnioti & Gurr, 2009). To effectively manage blast disease, a deeper understanding of its biology is crucial. Advances in live-cell imaging, combined with molecular genetics and genomic research on *M. oryzae*, have shed new light on the fungal mechanisms behind invasive growth.

1.2 The advent of live-cell imaging of plant infection by *Magnaporthe oryzae*

Historically, studies on how *M. oryzae* infects host plants were conducted using fixed plant tissues (Heath et al., 1992; Heath et al., 1990; Koga & Kobayashi, 1982; Peng & Shishiyama, 1988, 1989). While these investigations revealed the formation of specialised invasive hyphae, they were unable to capture the dynamic nature of plant-pathogen interactions. To address this limitation, the leaf sheath inoculation method was developed and has since become widely used (Koga, 1994; Sakamoto, 1949). This approach allows for the study of fungal growth in living plant tissues in a simple and effective manner (Kankanala et al., 2007). Since leaf sheath tissues lack chlorophyll, there is no need for tissue clearing before imaging, creating optimal conditions for visualising each stage of infection. Additionally, *M. oryzae* is highly amenable to genetic transformation, making it possible to use functional fluorescent fusion proteins (for a video review of their use see (Eseola et al., 2021)) alongside cytological fluorescent dyes to study infection processes in detail (Jones et al., 2016; Shen et al., 2020). The integration of these techniques with confocal laser scanning microscopy, super-resolution imaging, and electron microscopy has provided unprecedented insight into the major cellular changes that occur during blast infection (Giraldo et al., 2013; Kankanala et al., 2007; Khang et al., 2010; Mentlak et al., 2012; Mochizuki et al., 2015; X. Yan et al., 2023). Live-cell imaging has revolutionised our understanding of blast disease and other fungal plant diseases. Except for *M. oryzae,* a selection of live-cell imaging studies of plant infection by fungal plant pathogens, chosen from a ranked list of the most scientifically/economically important fungal species as identified by plant mycologists (Dean et al., 2012) is presented in Table 1.1.

Table 1.1 List of some live-cell imaging studies of plant infection by fungal pathogens.

Pathogen (Disease)	Host Plant	Imaging Technique	Reference
Blumeria graminis f. sp. *hordei* (barley powdery mildew	*Hordeum vulgare*	CLSM	Miklis et al. (2007)
Botrytis cinerea (grey mould)	*Lactuca sativa, Arabidopsis*	CLSM	Emmanuel et al. (2023)
Colletotrichum destructivum (anthracnose)	*Nicotiana benthamiana*	CLSM	Shan and Goodwin (2005)
Colletotrichum graminicola (anthracnose of maize)	*N. benthamiana*	CLSM	Shan and Goodwin (2005)
Fusarium graminearum (*Fusarium* head blight)	*T. aestivum*	CLSM	Qiu et al. (2019)
Fusarium oxysporum (vascular wilt)	*Arabidopsis, Solanum lycopersicum*	CLSM, multi-photon microscopy	Czymmek et al. (2007), Redkar et al. (2023)
Melapsora lini (flax rust)	*Linum usitatissimum*	CLSM	Zhang et al. (2024)
Puccinia graminis f. sp. *tritici* (wheat stem rust)	*Triticum aestivum*	CLSM	Prabhakaran et al. (2021)
Puccinia striiformis (wheat yellow rust)	*T. aestivum*	CLSM	Sørensen et al. (2012)
Ustilago maydis (corn smut)	*Zea mays*	CLSM	Matei and Doehlemann (2016)

CLSM, confocal laser scanning microscopy

1.3 Infection cycle of the blast fungus *Magnaporthe oryzae*

M. oryzae is a hemibiotrophic filamentous ascomycete (Ou, 1980). Early stages of blast infection are characterized by fungal growth within host living plant cells during its biotrophic stage (Kankanala et al., 2007) and the movement of the fungus through pit fields containing plasmodesmata (Sakulkoo et al., 2018). However, during appearance of lesions, the fungus becomes necrotrophic, deriving nutrition from dead plant cells (Ebbole, 2007; Ou, 1980; Talbot, 2003).

1.3.1 Appressorium formation by the blast fungus

The infection process of *M. oryzae* begins when a three-celled conidium lands on the hydrophobic surface of a rice leaf, adhering via spore tip mucilage released from its apex (Hamer et al., 1988). The conidium tightly attaches to the host surface and germinates rapidly within 2 hours, forming a polarised germ tube. The germ tube then hooks and flattens, differentiating into an appressorium, a dome-shaped infection structure (Figure 1A, B) essential for penetrating the plant surface. The appressorium develops a specialised cell wall containing a chitin-rich layer and a thick melanin layer between the cell

membrane and cell wall (Eseola et al., 2021; Fernandez & Orth, 2018; Hamer et al., 1988; Howard & Ferrari, 1989; Howard & Valent, 1996; Talbot, 2003). Appressorium development requires the perception of a hard, hydrophobic surface free of exogenous nutrients, which activates surface receptors such as the Pth11 G-protein coupled receptor, Msb2, and Sho1 proteins. These receptors act upstream of the Pmk1 MAPK pathway and the cyclic AMP-dependent protein kinase A pathway, which are critical for appressorium formation and function (Eseola et al., 2021). Phosphorylation of the Pmk1 MAPK pathway occurs within 1 hour of spore germination, leading to the phosphorylation of various substrates, including the Vts1 regulator, and Hox7, Far1, and Fkh1 transcription factors (Cruz-Mireles et al., 2024). Phosphorylation of these substrates triggers significant gene expression changes, with 49% of *M. oryzae* genes being differentially regulated during appressorium morphogenesis (Osés-Ruiz et al., 2021). The melanised appressorium generates turgor pressure reaching up to 8.0 MPa due to high intracellular concentrations of solutes like glycerol (de Jong et al., 1997). This turgor pressure exerted at the leaf surface enables the emerging rigid penetration peg to breach the rice leaf cuticle and epidermal cell wall (Howard et al., 1991). A series of cell cycle controls regulate appressorium morphogenesis, requiring S-phase checkpoint activation for initiation, mitotic entry for maturation, and mitosis completion for the development of a functional appressorium (Saunders et al., 2010). Additionally, a metabolically regulated cell-cycle checkpoint necessary for appressorium morphogenesis involves inactivation of the target-of-rapamycin (TOR) kinase, controlled by the Asd4 GATA transcription factor. This process represses nitrogen assimilation genes to maintain low glutamine levels, ensuring optimal appressorium development (Marroquin-Guzman & Wilson, 2015). After mitosis, one daughter nucleus moves into the appressorium, while the other daughter nucleus returns to the apical conidial cell (Figure 1C). The conidium undergoes autophagy-dependent cell death (Kershaw & Talbot, 2009; Veneault-Fourrey et al., 2006), requiring cargo-independent autophagy for the collapse of the conidium and the trafficking of its contents into the developing appressorium (Kershaw & Talbot, 2009; Gang Li et al., 2023; Veneault-Fourrey et al., 2006). Proteins encoded by autophagy genes are crucial for pathogenicity (Kershaw & Talbot, 2009; Gang Li et al., 2023; Veneault-Fourrey et al., 2006). It has been suggested that regulated cell death, potentially involving ferroptosis (Q. Liu et al., 2024; Shen et al., 2020), leads to lipid peroxidation and loss of viability of each cell of the conidium (Figure 1D), although this requires further investigation.

Appressoria expand evenly in all directions, initially undergoing radial or isodiametric growth to form dome-shaped infection structures essential for penetrating the host. Subsequently, repolarisation occurs at the base of the appressorium, where a specialised region known as the appressorium pore is established. The appressorium pore is reinforced by a toroidal network of septin GTPases, which provides structural rigidity and reorganises F-actin at the infection site (Dagdas et al., 2012). As the appressorium matures, the septin ring marks the exact location where the penetration peg will emerge (Figure 1E). On a rice leaf surface, the septin ring forms similarly but constricts to a diameter of approximately 0.9–1.1 μm once the penetration peg is established (Figure 1F). Septins play a crucial role in stabilising F-actin at the appressorium base (Figure 1G) (Dulal et al., 2021). Additionally, the septin ring functions as a lateral diffusion barrier for polarity-related proteins such as Bin-Amphiphysin-Rvs (BAR)-domain proteins like Rvs167 (Figure 1H), the exocyst complex, and actin-binding proteins like Tea1 (Figure 1I) (Dagdas et al., 2012; Gupta et al., 2015). This organisation ensures that actin polymerization, targeted exocytosis, and cell wall synthesis are concentrated at the appressorium base, facilitating penetration peg development and force generation.

Recent advances have introduced new techniques to study how appressoria generate turgor pressure. Membrane tension can now be measured using fluorescence lifetime imaging (FLIM) with a mechanosensitive plasma membrane rotor probe, N^+-BDP. This probe detects spatial variations in membrane tension within *M. oryzae* appressoria (Ryder et al., 2023). At 4 hours post-formation, an early stage appressorium exhibits low and uniform membrane tension, which causes mechanical restriction of the rotor probe movement upon photoexcitation, resulting in longer fluorescence lifetimes (Figure 1J). However, by 24 hours, a fully developed, high turgor appressorium displays increased membrane tension and a more disordered membrane structure, allowing free probe rotation and leading to shorter fluorescence lifetimes (Figure 1K). Notably, high-tension appressorial membranes also exhibit heterogeneity, indicating variations in membrane fluidity within the pressurised cell. In contrast, a non-pathogenic melanin-deficient *alb1*− mutant showed uniformly low membrane tension without spatial variation (Figure 1L) (Ryder et al., 2023).

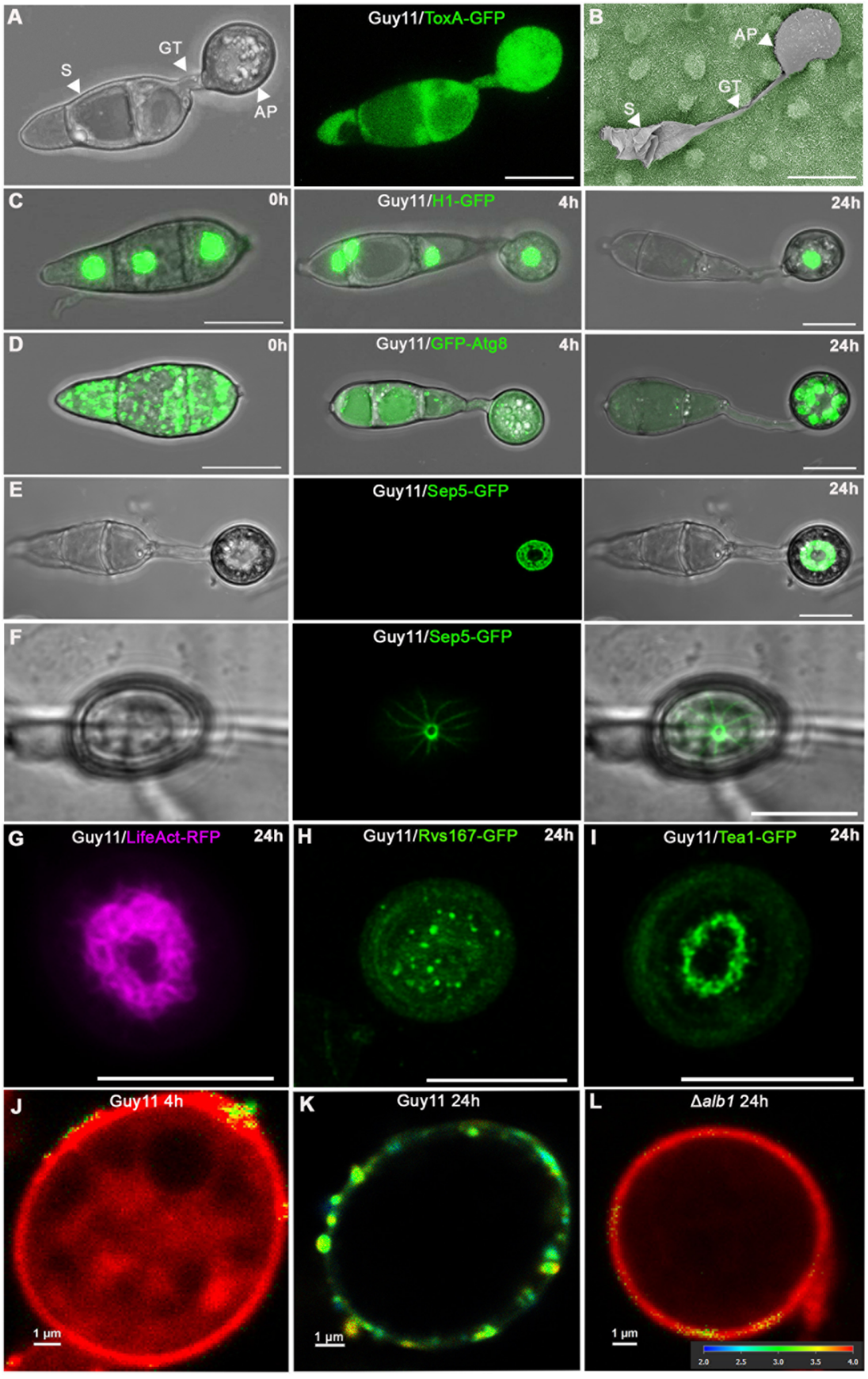
A
S
GT
AP
Guy11/ToxA-GFP
B
AP
GT
S
C
0h
Guy11/H1-GFP
4h
24h
D
0h
Guy11/GFP-Atg8
4h
24h
E
Guy11/Sep5-GFP
24h
F
Guy11/Sep5-GFP
G
Guy11/LifeAct-RFP
24h
H
Guy11/Rvs167-GFP
24h
I
Guy11/Tea1-GFP
24h
J
Guy11 4h
1 µm
K
Guy11 24h
1 µm
L
Δalb1 24h
1 µm
2.0
2.5
3.0
3.5
4.0

Figure 1.1 Infection-related morphogenesis in the rice blast fungus *Magnaporthe oryzae*.

A. Confocal image of appressorium development by *M. oryzae* wild type strain Guy11 expressing cytoplasmic ToxA-GFP. Conidia were germinated on glass coverslips and visualised 6 h post inoculation (hpi). The images represent maximum intensity projections of z-stack series captured on a Leica TCS SP8X confocal laser scanning microscope. Scale bar = 10 μm. **B.** Scanning electron micrograph with false colouring of a dome-shaped appressorium (grey) on a rice leaf surface (green), freeze dried 24 h after inoculation. The contents of the spore undergo autophagy and are recycled to the incipient appressorium, resulting in enormous turgor that is translated into mechanical force to penetrate the waxy rice leaf cuticle. Scale bar = 10 μm. **C.** Conidia were harvested from Guy11 expressing H1-GFP and inoculated onto glass coverslips. Images are maximum projections of z-stack series captured on a Leica TCS SP8X confocal laser scanning microscope at 0, 4 and 24 hpi. Scale bar = 10 μm. **D.** Conidia were harvested from Guy11 expressing GFP-Atg8 and inoculated onto glass coverslips. Images are maximum projections of Z-stack series captured on a Leica TCS SP8X confocal laser scanning microscope at 0, 4 and 24 hpi. Scale bar = 10 μm. **E.** Organisation of Sep5-GFP in the appressorium pore of Guy11 at 24 hpi on glass coverslips. Scale bar = 10 μm. **F.** Organisation of Sep5-GFP in the appressorium pore of Guy11 at 24 hpi on rice leaf sheath cultivar Moukoto. Scale bar = 10 μm. **G.** Organisation of actin with LifeAct-RFP in the appressorium pore of Guy11 at 24 hpi. **H.** Organisation of Bin-Amphiphysin-Rvs (BAR) domain protein Rvs167-GFP in the appressorium pore of Guy11 at 24 hpi. **I.** Organisation actin-binding protein Tea1-GFP in the appressorium pore at 24 hpi. Scale bars = 10 μm. **J.** FLIM image of Guy11 appressorium at 4 hpi stained with N^+-BDP rotor probe. Using FLIM, this rotor probe can detect differences in plasma membrane tension of appressoria during infection-related-development in wild type strain Guy11 and melanin deficient mutant *alb1*$^-$. Red = low tension, green = high tension. **K.** FLIM image of Guy11 appressorium at 24 hpi stained with N^+-BDP rotor probe. **L.** FLIM image of melanin-deficient mutant *alb1*$^-$ appressorium at 24 hpi stained with N^+-BDP rotor probe. The colour corresponds to fluorescence lifetime values expressed in nanoseconds, as shown in the key 2–4 ns. Scale bar = 1 μm. S = spore, GT = germ tube and AP = appressorium. Conidial germination onto glass coverslips **(A, C, D, E, G, H, I)** and leaf sheath infection **(F)** were incubated at 26°C and 24°C, respectively.

1.3.2 Invasive growth by *M. oryzae* in living plant tissue

Invasive growth of *M. oryzae* is characterised by a prolonged biotrophic phase. After breaching the leaf surface, the fungus develops a slender primary hypha, which rapidly differentiates into thicker, bulbous invasive hyphae. These structures initially colonise the first-invaded cell before spreading to neighbouring cells (Heath et al., 1990). Within the first epidermal cell, the bulbous IH is surrounded by the plant-derived extra-invasive hyphal membrane (EIHM) (Kankanala et al., 2007; Mentlak et al., 2012). Despite fungal invasion, these host cells remain healthy and retain their ability to plasmolyse (Koga et al., 2004).

By 24 hours post-inoculation, fungal colonisation can be observed using an *M. oryzae* strain expressing red fluorescent protein under the control of the constitutive *M. oryzae* ribosomal protein 27 (RP27) promoter, as shown in Figure 2A. Within the initially infected cells, invasive hyphae expand, filling the intracellular space while scanning the cell cortex. Hyphal tips probe the cell boundary to identify potential crossing points. To

invade adjacent uninfected cells, the IH transitions from a bulbous to a narrow, filamentous form, enabling it to traverse pit field sites, which contain plasmodesmata (Kankanala et al., 2007). This process of cell-to-cell invasion is regulated by the Pmk1 MAP kinase pathway (Sakulkoo et al., 2018).

When preparing to invade a new cell, the hyphae swell at their tips before undergoing extreme constriction, narrowing to approximately 0.6–0.8 μm, which facilitates movement through pit fields (Cruz-Mireles et al., 2021). These pit fields act as junctions that the fungus exploits to spread. By 36 hours post-inoculation (Figure 2B), *M. oryzae* begins invading neighbouring cells, with further tissue colonisation occurring by 48 hours (Figure 2C).

To successfully traverse pit fields while preserving the integrity of adjacent host cell membranes, the fungus utilises a specialised infection structure known as the transpressorium (Eseola et al., 2021). Additionally, Pmk1 regulates proteins involved in septin organisation, cytoskeletal remodelling, hyphal constriction, and effector gene expression, all of which contribute to fungal proliferation within plant tissue. Notably, during an R-gene-mediated incompatible interaction, invaded host cells lose membrane integrity, exhibit cytoplasmic granulation and autofluorescence, and lose their ability to plasmolyse (Koga et al., 2004).

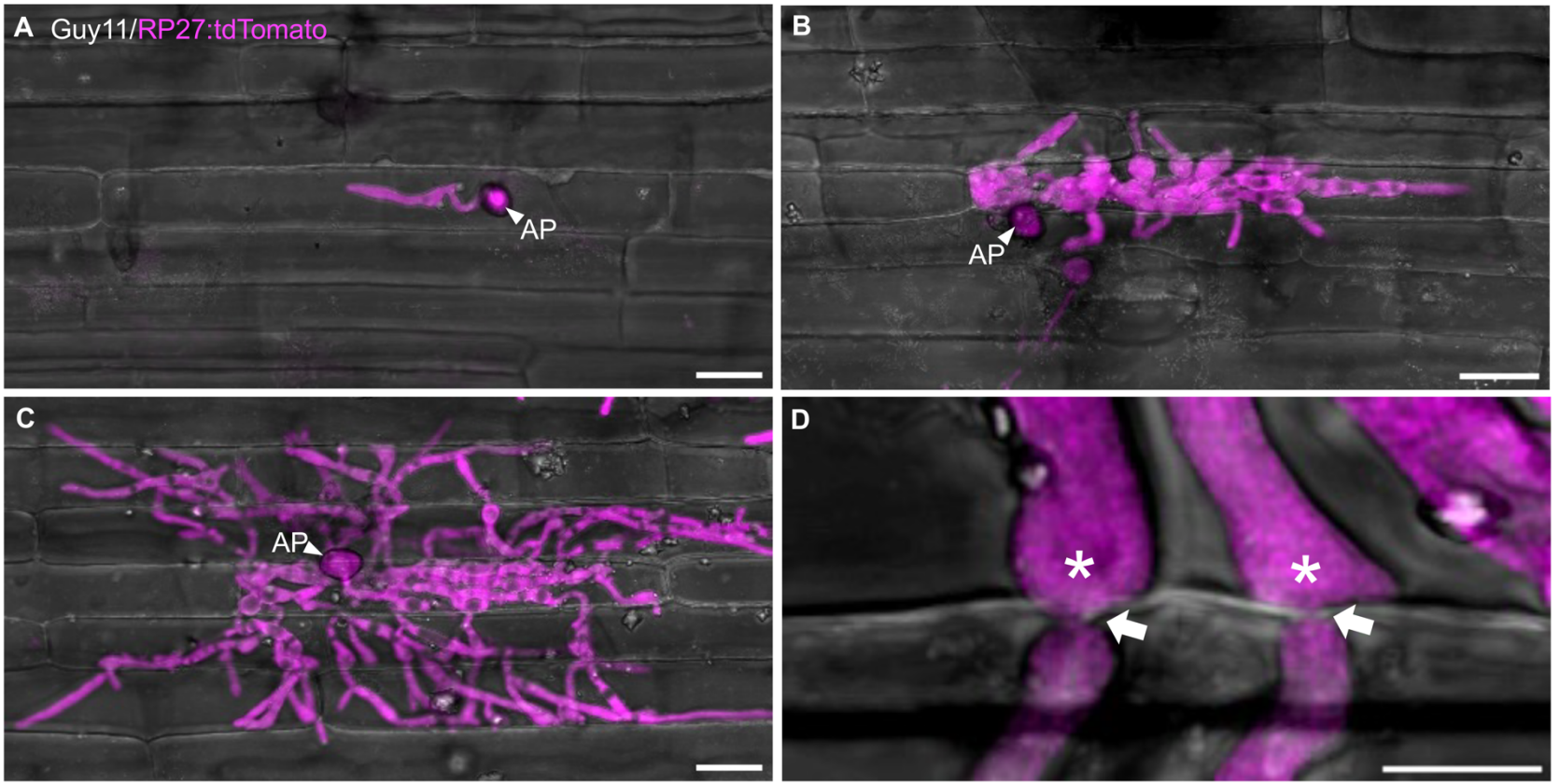

Figure 1.2 Progression of rice tissue invasion by *Magnaporthe oryzae*.

Confocal images of rice cultivar Kitaake leaf sheaths inoculated with *M. oryzae* Guy11 expressing tdTomato driven by *M. oryzae* ribosomal protein 27 (RP27), a constitutive promoter at **(A)** 24 h post-inoculation (hpi), **(B)** 36 hpi and **(C)** 48 hpi. Scale bars = 20 µm. **(D)** Confocal image showing transpessoria (in asterisks), which enables *M. oryzae* to move from cell-to-cell. White arrows indicate crossing points and hyphal constrictions as the fungus moves to the neighbouring host cell. Scale bar = 5 µm. Leaf sheath infections for all time points were incubated at 24°C. All images shown are maximum projections of z-stack series taken using a Leica TCS SP8X confocal laser scanning microscope. AP = appressorium.

1.3.2.1 Secretion and deployment of *M. oryzae* effectors

For pathogens to successfully invade host plants, they must first overcome basal defence mechanisms of plants. These defences are activated by pathogen-associated molecular patterns (PAMPs) or microorganism-associated molecular patterns (MAMPs) (Beck et al., 2012; Dodds & Rathjen, 2010; Jones & Dangl, 2006; Liu et al., 2013). The first line of plant defence called PAMP-triggered immunity (PTI) relies on pattern recognition receptors (PRRs), which are transmembrane receptor kinases and transmembrane receptor-like proteins. Mainly detected in the apoplast, PAMPs, such as chitin for fungi and glucans found in both fungi and oomycetes, initiate defence responses (Block et al., 2008; Jones & Dangl, 2006; Nürnberger et al., 2004). To counteract pathogen effectors, plants have developed intracellular immune receptors that monitor the intracellular environment, detecting either the presence or activity of effectors proteins. Upon recognition, they trigger a robust and effective cell death response to limit pathogen spread within the host (Dodds & Rathjen, 2010; Jones & Dangl, 2006). Building on this defence strategy, plants employ resistance (R) proteins which are specialised intracellular receptors, to detect certain pathogen effectors, known as avirulence (AVR) effectors, through direct binding or indirect interactions. This recognition activates effector-triggered immunity (ETI), representing the second tier of plant defence (Dodds et al., 2020).

To circumvent PTI and successfully colonise living host tissue, *M. oryzae* deploys a diverse array of effector proteins (Figure 1.3) (Boller & He, 2009; de Jonge et al., 2011; Oliveira-Garcia et al., 2023; Yang et al., 2024; S. Zhang & J.-R. Xu, 2014) leading to effector-triggered susceptibility (ETS) (Boller & He, 2009). Recent research has identified 546 putative *Magnaporthe* effector-encoding (*MEP*) genes are expressed during plant infection, displaying distinct temporal co-regulation patterns (Yan et al., 2023). Among these, structurally similar yet sequence-unrelated effectors such as MAX (*Magnaporthe* Avrs and ToxB-like) effectors and putative ADP-ribosylation factor-like effectors are specifically expressed between 24 and 48 hours post-infection, indicating stringent transcriptional control during infection. Supporting this concept, a genetic screen for effector regulators identified *RGS1*, a known regulator of G-protein signalling in appressorium development, as a transcriptional regulator of effector genes. *Rgs1* represses effector expression before fungal penetration, allowing their selective activation upon plant infection (Tang et al., 2023). Similarly, the *Pmk1* MAP kinase, which governs transpressorium development, is

essential for the expression of at least 50 effector genes, including *SLP1, BAS1*, and *BAS3* (Sakulkoo et al., 2018; Yan et al., 2023).

Fluorescent protein tagging has facilitated the classification of effectors based on their localisation within plant tissue. Apoplastic effectors, such as Slp1, which binds fungal cell wall chitin via a LysM domain, are found surrounding invasive hyphae. In contrast, cytoplasmic effectors such as Avr-Pia accumulate in the biotrophic interfacial complex (BIC) before being transported into rice cells. The consistent observation of effector expression in the BIC (Khang et al., 2010; Mosquera et al., 2009; Xia Yan et al., 2023) is consistent with its role as a hub for effector translocation into the host cytoplasm. Further evidence shows that cytoplasmic effectors are secreted through a mechanism insensitive to brefeldin A (BFA), implying a Golgi-independent, unconventional secretion pathway. In contrast, apoplastic effectors such as Slp1 and Bas4 follow a conventional BFA-sensitive secretion route (Giraldo et al., 2013). This suggests that cytoplasmic effectors are released from a specialized BIC-associated hyphal tip through an exocyst-dependent but Golgi-independent mechanism. Once secreted, these effectors accumulate within the BIC, residing outside the fungal cell wall yet enclosed by the extrahaustorial membrane (EIHM). Unconventional secretion in *M. oryzae* further requires tRNA thiolation and alternative codon usage of genes encoding BIC-targeted effectors (G. Li et al., 2023). Using super-resolution imaging, effectors can be detected within the BIC in punctate membranous effector compartments (MECs), initially around 249 nm in diameter but capable of expanding or merging to form larger 500–1000 nm MECs in mature BICs (Oliveira-Garcia et al., 2023). MECs co-localise with plant plasma membrane markers such as LTI6b-GFP and clathrin light chain, suggesting that clathrin-mediated endocytosis facilitates effector uptake into plant cells (Oliveira-Garcia et al., 2023). Inhibiting this process through chemical inhibitors or by silencing *OsCHC1* (Clathrin Heavy Chain 1) or *OsAP2* (AP2/ERF transcription factor family) prevents effector internalisation. However, suppressing clathrin-independent endocytosis via *OsFLOT1* (Flotillin 1) silencing or chemical inhibitors has no impact, reinforcing the role of clathrin-mediated pathways in effector uptake (Oliveira-Garcia et al., 2023). Taken together, these findings indicate that *M. oryzae* employs two distinct secretion pathways depending on effector destination: cytoplasmic effectors utilise an unconventional secretion route and are internalised by plant cells through clathrin-mediated endocytosis, while apoplastic effectors follow a conventional pathway. Remarkably, similar mechanisms have been

observed in the oomycete pathogen *Phytophthora infestans*, despite its evolutionary distance from fungal pathogens. In *P. infestans*, cytoplasmic effectors are also secreted in a BFA-insensitive manner (Wang et al., 2017), and their uptake into host cells from haustoria relies on clathrin-mediated endocytosis, even though a BIC structure is absent. Infections in *Nicotiana benthamiana* have shown that silencing *NbCHC* (clathrin heavy chain) or *NbAra6* (a Rab GTPase associated with late endosomes) reduces *P. infestans* pathogenicity and impairs RXLR effector translocation into host cells (Wang et al., 2023). Collectively, these studies suggest that diverse filamentous pathogens may share a conserved mechanism for effector uptake, despite differences in secretion strategies. However, other pathogens such as *Ustilago maydis* employ distinct secretion mechanisms, potentially involving a translocon for delivering certain effectors (Ludwig et al., 2021), as well as in other fungal pathogens (for a review see (Lo Presti & Kahmann, 2017). Further research is needed to clarify these variations in effector secretion across different fungal pathogens.

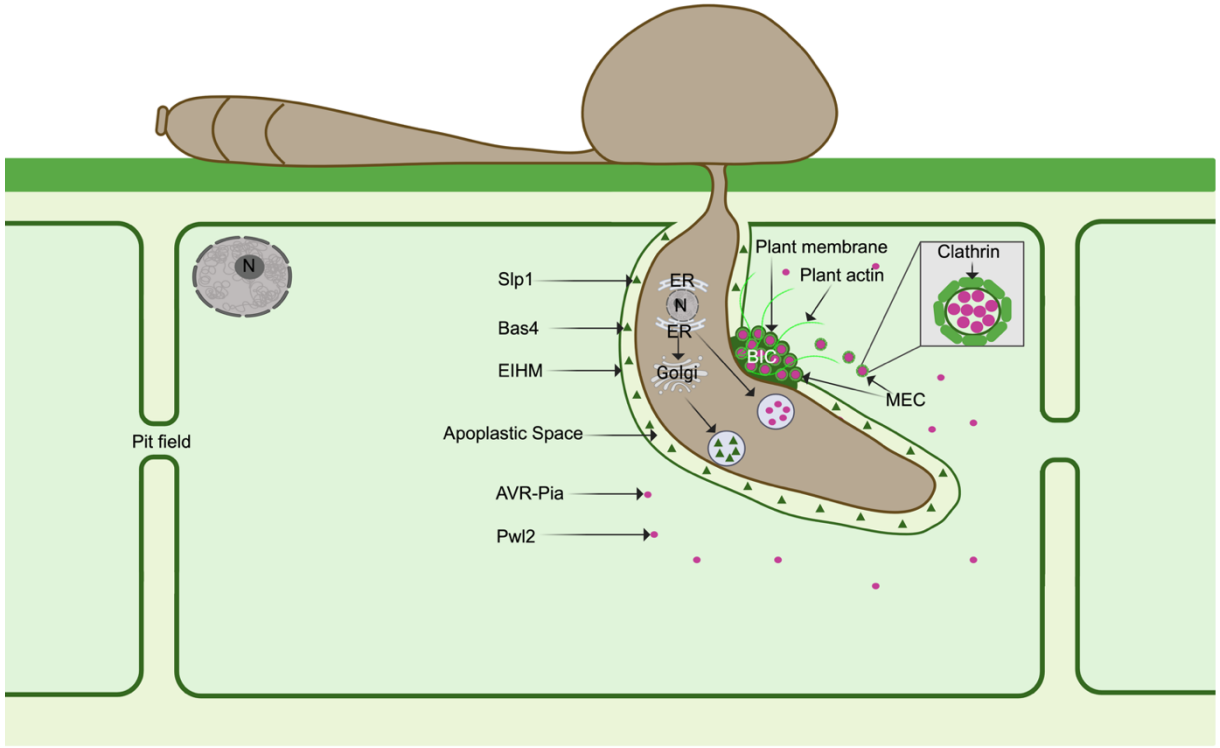

Figure 1.3 Model for the translocation of *M. oryzae* effectors into rice cells.

During biotrophic growth, *M. oryzae* deploys a battery of effector proteins which are either apoplastic or cytoplasmic, to suppress host immune responses and facilitate fungal colonisation. Apoplastic effectors are secreted via the conventional ER-to-Golgi, Brefeldin A (BFA)-sensitive pathway, and reside in the apoplastic or EIHM matrix (EIHMx) enclosed by the extra-invasive hyphal membrane (EIHM). Cytoplasmic effectors are secreted using a nonconventional BFA-insensitive pathway and accumulate in the biotrophic interfacial complex (BIC). Cytoplasmic effectors tagged with fluorescent proteins are observed to be packaged in membranous effector compartments (MECs) which co-localise at the BIC with fluorescently-tagged rice plasma membrane (LTI6b TMD:GFP). Clathrin-mediated endocytosis then results in MECs being taken into the cytoplasm of the host from where effectors are released to fulfil diverse immuno-suppressive functions during fungal infection.

Once secreted, *M. oryzae* effectors adopt distinct functions depending on their target location. For instance, the apoplastic LysM effector Slp1 suppresses chitin-induced immunity by tightly binding chitin oligomers released by the pathogen, that would otherwise trigger a PTI response (Mentlak et al., 2012). This function relies on N-glycosylation for activity in the apoplast (Chen et al., 2014). Similarly, the chitinase Chia1 also binds chitin in the apoplast to suppress immunity; however, in a counter-defence strategy, it is recognised by the rice tetratricopeptide repeat protein OsTPR1 (Yang et al., 2019). Additionally, the ascorbate oxidase AO1 influences apoplastic redox balance, suppressing two rice ascorbate oxidases associated with immunity (Hu et al., 2022). In contrast, cytoplasmic effectors disrupt specific components of pattern-triggered immunity signalling pathways. Some effectors, for example, CDIP4 interacts with the mitochondria-associated OsDjA9-OsDRP1E protein complex to suppress rice immunity (Xu et al., 2020), while AVR-Pita, a metalloprotease, is reported to act on the cytochrome *c* oxidase assembly protein OsCOX11, a key regulator of mitochondrial reactive oxygen species (ROS) metabolism (Han et al., 2021). Other effectors interfere with plant exocytosis; AVR-Pii, for example, targets two rice Exo70 proteins, OsExo70F2 and OsExo70F3 (Fujisaki et al., 2015), and belongs to a zinc-finger effector fold (ZiF) family that specifically binds to a specific Exo70 interface (De la Concepcion et al., 2022). Some effectors, however, interact with multiple host targets. AVR-Pii, in addition to binding OsExo70F2 and OsExo70F3 , also inhibits the activity of NADP-malic enzyme (OsNADP-ME2) (Singh et al., 2016). Even more versatile, AVR-Pizt is known to suppress immunity through interactions with multiple proteins, including the RING-type ubiquitin E3 ligases APIP6 and APIP10 (Park et al., 2012b; Park et al., 2016), the bZIP-type transcription factor APIP5 to inhibit APIP5-triggered cell death (R. Wang et al., 2016), the nucleoporin protein APIP12 (M. Tang et al., 2017), and the potassium channel OsAKT1, where it competes with the kinase OsCIPK23 to regulate K+ channel activity (X. Shi et al., 2018). The evolutionary basis for the broad range of highly distinct interactions of AVR-Pizt, however, remains unclear. Some effectors target entire protein families involved in immune responses, such as those containing heavy metal-associated (HMA) domains, which have diverse immune functions. The MAX effectors AVR1-CO39, AVR-PikD, and Pwl2, for example, all interact with HMA proteins.

In addition to key roles in pathogenesis, a sub-set of *M. oryzae* effectors referred to as avirulence (AVR) effectors, can be detected either directly or indirectly by plant resistance

(R) proteins, triggering race-specific resistance (van der Hoorn & Kamoun, 2008). Among the various types of R proteins, nucleotide-binding leucine-rich repeat receptors (NLRs) form the largest group. They share a multi-domain structure, typically consisting of a central nucleotide-binding (NB-ARC) domain, a C-terminal leucine-rich repeat (LRR) domain, and an N-terminal domain that can be either a coiled-coil (CC) domain, an RPW8-like CC domain, or a Toll/interleukin-1 receptor (TIR) domain. Based on these N-terminal variations, they are classified as CNLs, RNLs, or TNLs, respectively (Takken & Goverse, 2012) (Takken and Goverse, 2012). Additionally, many NLRs possess noncanonical domains known as integrated domains (IDs), such as the heavy metal-associated (HMA) domain, BED domain, RIN4/NOI domain, or WRKY domain, which function as molecular decoys (Cesari et al., 2014; De la Concepcion et al., 2022; Duxbury et al., 2016; Kroj et al., 2016; Shimizu et al., 2022; Wu et al., 2014). When AVRs or AVR-host target complexes bind directly to these IDs, they trigger NLR activation, leading to immune response initiation (Cesari, 2018; Cesari et al., 2014; De la Concepcion et al., 2022; Fujisaki et al., 2015; Fujisaki et al., 2017).The involvement of AVR effectors in both blast susceptibility and resistance paved the way for genetic improvement in rice cultivars and surveillance systems for agronomic decision-making (Gangireddy et al., 2025; Mutiga et al., 2017; Mutiga et al., 2021; Pedrozo et al., 2025; Selisana et al., 2017). A selection of cloned *M. oryzae* AVR effector proteins and their cognate R proteins are listed in Table 1.2.

Table 1.2 Cloned Avr effectors with their corresponding R proteins.

Avr effector	Encoding protein	Secretion site	Corresponding R protein	Encoding Protein	Interaction	Guardee/decoy/cofactors/interacted protein	Reference
Avr1-CO39	MAX	EIHM	RGA4/RGA5	CNL/CNL-HMA	Direct	-	Cesari et al. (2013), Okuyama et al. (2011), Ribot et al. (2013)
Ace1	PSK-NRPS enzyme	n.d.	n.d.	-	Indirect	-	(Böhnert et al., 2004), Collemare et al. (2008),
Avr-Pii	ZiF	BIC	Pii-1/Pii-2	CNL/CNL-RIN4/NOI	-	OsExo70F3, OsNADP-ME2	Fujisaki et al. (2015), Singh et al. (2016), Yoshida et al. (2009)
Avr-Pita	Zinc metalloprotease	BIC	Ptr	CNL	Indirect	OsCOX11	Han et al. (2021), Meng et al. (2020), Xiao et al. (2024), Zhao et al. (2018)
Avr-Pizt	MAX	BIC	Piz-t	CNL	Indirect	APIP4, APIP5, APIP6, APIP7, APIP10, APIP12	Li et al. (2009), Park et al. (2012a), Park et al. (2016), (Shi et al., 2018), C. Zhang et al. (2020), Wang et al. (2016), Tang et al. (2017)
Avr-Pik alleles	MAX	BIC	Pik-1/Pik-2 and alleles	CNL-HMA/CNL	Direct	-	Yoshida et al. (2009), Guo et al. (2024), Oikawa et al. (2024), Yang et al. (2024),
Avr-Pia	MAX	BIC	RGA4/RGA5	CNL/CNL-HMA	Direct	-	Yoshida et al. (2009), Sornkom et al. (2017), Cesari et al. (2013)
Avr-Pib	MAX	BIC	Pib	CNL	Indirect	SH3P2	Zhang et al. (2015), Zhang et al. (2018), Xie et al. (2022)
Avr-Pi9	n.d.	BIC	Pi9	CNL	Indirect	ANIP1, OsWRKY62, OsRGLG5	Shi et al. (2023), Wu et al. (2015), Liu et al. (2023)
Avr-Pi54	n.d.	n.d.	Pi54	CNL	Direct	-	Ray et al. (2016)
Pwl1	n.d.	BIC	-	-	-	-	Khang et al. (2010), Kang et al. (1995)
Pwl2	MAX	BIC	-	-	-	OsHIPP43	Sweigard et al. (1995), Brabham et al. (2024), Were et al. (2025), Zdrzalek et al. (2024)

n.d., not determined; BIC, biotrophic interfacial complex; EIHM, extra-invasive hyphal membrane; CNL, coiled-coil, nucleotide binding, leucine-rich repeat receptors; HMA, heavy metal-associated domain; RIN4/NOI, nitrate-induced/RPMMI-interacting protein 4 domain. Adapted from Liu et al. (2024).

1.4 Host subcellular reorganisation and cytoskeletal remodelling changes accompanying *M. oryzae* infection

Even prior to penetration, host responses to pathogens occur in the form of cytoskeletal remodelling, cytoplasmic aggregation and papilla deposition at attempted penetration sites (Hückelhoven & Panstruga, 2011; Koh et al., 2005). Live cell confocal imaging of fungal invasion showed host membrane polarisation and accumulation of proteins at sites of attempted penetration (Hückelhoven & Panstruga, 2011; Koh et al., 2005; Underwood et al., 2011; Underwood & Somerville, 2008).

Effectors are known to manipulate the host subcellular components for pathogenesis. In human pathogenic bacteria for example, the *Salmonella* effector SptP triggers actin remodelling to direct pathogen internalisation and intracellular bacterial replication (Humphreys et al., 2009) while the effectors SipC, SopE2 and SopB exploit membrane reservoirs for invasion (Zhu et al., 2024). *Vibrio cholerae* effector VopX modulates host actin dynamics to facilitate sustained bacterial colonisation (Ulbrich et al., 2025). Despite the variety of ways in how *M. oryzae* effectors promote susceptibility, it is striking that none of the identified effectors are yet reported to be responsible for altering host cellular organisation to favour pathogen infection (Oliveira-Garcia et al., 2024).

Host subcellular reorganisation during *M. oryzae* pre-penetration stages in a non-adapted host involve an increase of actin filament density (Henty-Ridilla et al., 2013). Inoculation of a mutant strain incapable of penetrating host cells stimulated actin remodelling towards attempted sites of penetration (Xu et al., 1998). During biotrophic growth, the host plasma membrane is invaginated to form the extra-invasive hyphal membrane (Fernandez & Orth, 2018; Kankanala et al., 2007; Khang et al., 2010). Another host plasma membrane-derived focal structure found at the EIHM is the biotrophic interfacial complex (BIC) which appears to be a site of cytoplasmic effector delivery in host cells (Giraldo et al., 2013; Khang et al., 2010; Mentlak et al., 2012).

Despite of our extensive understanding of rice blast infection, our knowledge regarding how host subcellular components change in organisation during *M. oryzae* infection is still very limited.

1.5 Introduction to current study

This study aims to investigate the cell biology of plant infection by the rice blast pathogen, *M. oryzae,* to provide a detailed understanding of the process of plant infection and the major cellular changes associated with plant tissue colonisation by *M. oryzae*.

In Chapter 3, I generated constructs expressing green fluorescent protein (GFP) fusions to visualise the plasma membrane, F-actin, nucleus, mitochondria, early endosomes, late endosomes, cytoplasm, endoplasmic reticulum, Golgi bodies, and peroxisomes of plant cells. One of the reasons why there has been limited knowledge on host cellular responses during *M. oryzae* infection is due to the lack of resources which allows investigation of cell biology questions, in this case, a set of transgenic lines with fluorescently tagged subcellular markers. Although rice transgenic lines with different fluorescent protein-tagged organelle markers have been developed (Chen et al., 2019; Mentlak et al., 2012; Mochizuki et al., 2015; Oliveira-Garcia et al., 2023; Wu et al., 2016). These constructs were individually introduced to rice cv. Kitaake and barley cv. Golden Promise to generate transgenic lines expressing GFP-tagged subcellular markers. I then used a subset of these lines to investigate host cellular changes associated with *M. oryzae* infection. I describe the resource of transgenic lines created for future analysis and their initial genotypic characterisation and maintenance.

In Chapter 4, I set out to characterise the spatial and temporal changes at the host plasma membrane during infection, focusing on the formation and breakdown of the EIHM and the development of the BIC. I also examined the relationship between plasma membrane integrity and cell viability over time using fluorescein diacetate (FDA) as a viability marker. Overall, these findings provide evidence that both the EIHM and BIC emerge during the biotrophic phase, but the EIHM is disrupted as neighbouring cells become colonised by the fungus.

In Chapter 5, I aimed to develop a method for quantifying rice plasma membrane expansion during biotrophic invasion and assessing the amount of additional plant membrane required to sustain the EIHM before its integrity is compromised. I explored the potential of MorphoGraphX (MGX), an open-source tool designed for 3D surface reconstruction in biological imaging (Barbier de Reuille et al., 2015; Strauss et al., 2022),

which has previously been used for analysing and visualising various aspects of plant development. To our knowledge, this represents the first application of MGX to study fungal pathogen infection in plants and the first attempt to quantify the net increase in host plasma membrane during infection using 3D image analysis.

In Chapter 6, I investigated the spatiotemporal dynamics of the rice actin cytoskeleton during the biotrophic growth of *M. oryzae*. I showed that rice actin initially surrounds *M. oryzae* invasive hyphae in both the first-invaded and newly colonised neighbouring cells. Actin also accumulates at cell junctions and BICs. As fungal infection advances, host actin becomes disrupted. Additionally, pharmacological disruption of host F-actin reduced the ability of *M. oryzae* to colonise new cells beyond the initial infection site. Together, these findings suggest that actin remodelling is essential for successful invasion, while its disruption signals the transition from biotrophy to necrotrophy in *M. oryzae* infection.

In Chapter 7, I attempt to synthesise all the findings to date and provide some preliminary results associated with other cellular compartments/organelles for which I have generated transgenic lines.

Overall, this study sheds light on the dynamic behaviour of host subcellular components during *M. oryzae* infection. The preservation and breakdown of host subcellular structures, particularly the plasma membrane and actin cytoskeleton, throughout infection highlight the hemibiotrophic nature of *M. oryzae* infections. The findings provide a basis for future research on additional host subcellular components, and a key resource of transgenic lines, with the goal of constructing a spatiotemporal atlas of cellular changes associated with plant tissue colonisation by the blast fungus *M. oryzae*.

Chapter 2 Materials and Methods

2.1 Fungal growth, maintenance, and storage

Magnaporthe oryzae strains were cultured on complete medium (CM) agar plates and incubated in a controlled growth room at 24 °C with a 12-h light/dark cycle for up to 10 days. CM contains 10 g/L glucose, 2 g/L peptone, 1 g/L yeast extract (BD Biosciences), 1 g/L casamino acids, 0.1% (v/v) trace elements (22 mg/L zinc sulphate heptahydrate, 11 mg/L boric acid, 5 mg/L manganese (II) chloride tetrahydrate, 5 mg/L iron (II) sulphate heptahydrate, 1.7 mg/L cobalt (II) chloride hexahydrate, 1.6 mg/L copper (II) sulphate pentahydrate, 1.5 mg/L sodium molybdate dihydrate, 50 mg/L ethylenediaminetetraacetic acid (EDTA)), 0.1% (v/v) vitamin supplement (0.001 g/L biotin, 0.001 g/L pyridoxine, 0.001 g/L thiamine, 0.001 g/L riboflavin, 0.001 g/L nicotinic acid), 6 g/L $NaNO_3$, 0.5 g/L KCl, 0.5 g/L $MgSO_4$, 1.5 g/L KH_2PO_4, and 15 g/L agar. The pH was adjusted to 6.5 with NaOH. Agar was omitted for liquid cultures. Unless otherwise stated, all chemicals were obtained from Sigma-Aldrich. *M. oryzae* strains were grown on sterile filter paper discs placed on CM agar plates. The paper discs were then dehydrated and stored at -20 °C for long-term preservation. The *M. oryzae* strains used in this study are listed in Table 2.1.

Table 2.1 List of strains used in this study.

Strain	Background	Description/Purpose	Source
RP27p:tdTomato	Guy11	Cytoplasmic marker	This study
Mep1p:tdTomato	Guy11	Cytoplasmic marker	This study
TUB1p:tdTomato	Guy11	Cytoplasmic marker	This study
trpCp:tdTomato	Guy11	Cytoplasmic marker	This study
Mep1:mCherry	Guy11	Apoplastic effector; EIHM integrity reporter	Dr. Xia Yan (TSL)
RP27p:mScarlet3	Guy11	Cytoplasmic marker	This study
Mep1:mCherry/ RP27p:mScarlet	Guy11	Fungal surface area measurement; cytoplasmic marker with EIHM integrity reporter	This study
Pwl2:mRFP	Guy11	Cytoplasmic effector; BIC localisation	Dr. Vincent Were (TSL)

2.2 Plant materials and growth conditions

Rice (*Oryza sativa*) cv. Kitaake seeds were obtained from the United States Department of Agriculture Research Service, National Small Grains Collection (Aberdeen, ID, USA). Rice cv. CO39 seeds were obtained from the International Rice Research Institute (IRRI)

(Laguna, Philippines). Barley (*Hordeum vulgare*) cv. Golden Promise seeds were sourced from the John Innes Centre (JIC). Rice cv. Kitaake and barley cv. Golden Promise were used as host backgrounds for generating transgenic lines with GFP-tagged subcellular markers. Rice cv. CO39 was used to screen the fluorescent protein-tagged *M. oryzae* strains developed in this study through leaf sheath infection, allowing *in-planta* fluorescence observation. Rice plants for leaf sheath infection and seed bulking were grown in John Innes Cereal Mix (65% peat, 25% loam, 10% grit, 3 kg/m³ dolomitic limestone, 1.3 kg/m³ PM mix, 3 kg/m³ Osmocote Exact), while barley plants were cultivated in John Innes Barley Mix (60% peat, 20% grit, 20% perlite, 2.2 kg/m³ dolomitic limestone, 1.3 kg/m³ PG mix, 3 kg/m³ Osmocote Exact). Rice plants were grown in a controlled environment at 25/28°C with a 12/12 h light/dark cycle, a light intensity of 700 µmol/m²/s, and 55–60% humidity. Barley plants were grown in a greenhouse. *Nicotiana benthamiana* plants used for agroinfiltration experiments were cultivated in a controlled environment at 25°C under a 16/8 h light/dark cycle with 45–65% humidity.

2.3 Leaf sheath infection assays

Leaf sheath infection assay procedures for visualising *M. oryzae* colonisation were performed as previously described (Kankanala et al., 2007). *M. oryzae* strains were cultured on CM medium for 7–10 days in a fungal growth chamber. Spores were collected from Petri dish cultures using 5 mL of sterile distilled water and a sterile disposable plastic spreader. The spore suspension was then filtered through sterile Miracloth (Calbiochem) and subjected to centrifugation at 5000 × *g* (Beckman, JA-17) for 5 min at room temperature. The resulting spore pellet was resuspended in 0.2% (w/v) gelatin (BDH), and the spore concentration was determined using a haemocytometer (Improved Neubauer, Hawksley, UK). The spore suspension was adjusted to a final concentration of 5×10^4 spores/mL (or 3×10^4 spores/mL for observations from 36 hpi onwards) before being inoculated into the leaf sheaths. Leaf sheaths were placed horizontally in a square Petri dish lined with a moist paper towel and incubated at 24–26°C. For confocal microscopy visualisation, the leaf sheaths were prepared by thinly sectioning three to four cell layers and mounting them onto glass slides with water, before covering them with cover slips.

2.4 General molecular biology methods

2.4.1 Fungal DNA extraction

Fungal DNA extraction was carried out using a flat plug of fungal mycelium cut from a CM plate culture then placed in a 2 mL microcentrifuge tube with a metal bead. A 500 µL aliquot of DNA extraction buffer (DEB) was added to the fungal plug, and the sample was macerated at 1300 rpm for 1 min in a Geno Grinder tissue homogeniser. The sample was fractionated by centrifugation at 17,000 × *g* for 2 min. To reduce protein content, 450 µL of the top phase was added to an equal amount of phenol-chloroform in a new 1.5 mL microcentrifuge tube then mixed thoroughly. The sample was subjected to centrifugation, 400 µL of the top phase was transferred onto a new 1.5 mL microcentrifuge tube then 1 mL of chilled 100% ethanol was added, and the solution was placed in -20°C for 10 min. The sample was subjected to centrifugation at 17,000 × *g* for 1 min to pellet the DNA. The supernatant was discarded, and the pellet was washed again using 1 mL 70% chilled ethanol. The sample was subjected to centrifugation at 17,000 × *g* for 1 min and the ethanol portion was discarded. To dry the DNA pellet, the tubes were either inverted on a paper towel or placed in a concentrator at 45°C. Once fully dry, the DNA pellet was dissolved in 100 µL sterile distilled water containing RNAse (10 mg/mL.

2.4.2 Polymerase chain reaction

For gene cloning, Q5®High-Fidelity DNA Polymerase (New England Biolabs) was used. The reaction mixture was composed of the following: 10 µL 5X Q5 Reaction buffer, 200 µM dNTPs, 0.5 µM of each primer, 100-200 ng template DNA, 1 unit of Q5®High-Fidelity DNA Polymerase and nuclease-free water to a total volume of 50 µL. The thermocycling conditions were the following: initial denaturation step at 98°C for 30 s followed by 35 cycles of denaturation at 98°C for 10 s, annealing 58°C for 30 s and extension 72°C for 30 s/kb target length, followed by a final extension at 72°C for 10 min and hold at 4°C.

For colony PCR screening, SapphireAmp Fast PCR Master Mix (Clontech, USA) was used. The reaction mix included 12.5 µL of SapphireAmp Fast PCR Mix, 0.2 µM (final concentration) of forward and reverse primers and adjusted with nuclease-free water to a final volume of 20 µL. Bacterial colonies grown overnight were picked with a sterile 200-

µL pipette tip and dipped onto the reaction mix. The PCR conditions were as follows: denaturation at 98°C for 2 min and 35 cycles of PCR cycling parameter: denaturation at 98°C for 10 s, annealing at 55°C for 10 s and extension at 72°C for 10 s/1kb for the desired fragment length, then held at 4°C.

2.4.3 DNA gel electrophoresis

PCR amplification products were fractionated by gel electrophoresis through a 1% (w/v) agarose gel in 1X Tris-borate EDTA (TBE) buffer (0.09 M Tris-borate and 2 mM EDTA). Ethidium bromide was added to molten agarose gel to 0.5 µg/mL final concentration to visualize DNA under UV light. To ensure the right sizes of the PCR products, 1 Kb plus size marker (Invitrogen) was loaded alongside the samples. The DNA fragments in the gel were visualized and recorded using the Syngene G:Box gel documentation system (www.syngene.com).

2.4.4 Gel purification of PCR products

PCR products of interest were excised from the agarose gel on a UV table (Uvitec, www.uvitec.co.uk) using a sterile razor blade and placed in a 2 mL microcentrifuge tube. Wizard® Plus SV Gel and PCR Clean-up System (Southampton, UK) was used to purify fractionated DNA from the agarose gel. Membrane binding solution (4.5 M guanidine isothiocyanate and 0.5 M potassium acetate, pH 5.0) was added to the tube at a ratio of 10 µL per 10mg cut gel. The sample was vortexed and incubated at 50-65°C on a heating block. To bind the DNA, a 750 µL aliquot of the mixture of molten agarose gel and membrane binding solution was transferred onto the Wizard® SV Minicolumn inserted on a supplied 2 mL collection tube and incubated at room temperature for 1 min. The sample was subjected to centrifugation at 17,000 × *g* for 1 min, then the flowthrough was discarded. For the washing step, 700 µL of membrane wash buffer (with 100% ethanol added) was added to the column and subjected to centrifugation at 17,000 × *g* for 1 min. Flowthrough was discarded and the column was reinserted into the collection tube. This step was repeated with 500 membrane wash buffer and processed by centrifugation at 17,000 × *g* for 5 min. The column was transferred on a clean 1.5 mL microcentrifuge tube. The DNA bound in the column was eluted by adding 50 µL of nuclease-free water to the column, incubated at room temperature for 1 min then subjected to centrifugation at 17,000 × *g* for 1 min. Eluted DNA was placed at -20°C for long-term storage.

2.4.5 DNA Cloning

2.4.5.1 In-Fusion cloning procedures

Genes of interest were cloned into pSCBAR backbone (for fungal transformation) or pGWB514 binary vector (for plant transformation) using In-Fusion HD Cloning Kit (Takara-Bio, USA). The cloning reaction mix consisted of the following: 1 µL of 5X In-Fusion HD Enzyme Premix, 50-100 ng of purified PCR fragments and 100 ng linearized vector and sterile distilled water to reach final volume of 10 µL. The reaction mixture was incubated at 50°C for 15 min in a PCR machine then placed on ice for 2 min before proceeding with bacterial transformation.

2.4.5.2 Golden Gate cloning procedures

For level 0 constructs, digestion-ligation reactions were prepared by mixing 100 ng of PCR product or synthesised fragment of interest with the level 0 backbone, 5 U (units) of BpiI (ThermoFisher Scientific), 200 U of T4 DNA ligase (New England Biolabs), 1.5 µL of T4 DNA ligase buffer (New England Biolabs), 1.5 µL of 10X bovine serum albumin (BSA) (New England Biolabs), and sterile distilled water to a final reaction volume of 15 µL.

Level 1 assemblies were carried out by mixing 100 ng of the level 1 acceptor plasmid with level 0 modules in a 2:1 molar ratio of insert to acceptor, 5 U of BsaI-HF (New England Biolabs), 200 U of T4 DNA ligase (New England Biolabs), 1.5 µL of T4 DNA ligase buffer (New England Biolabs), 1.5 µL of 10X bovine serum albumin (BSA) (New England Biolabs), and sterile distilled water to a final reaction volume of 15 µL.

Level 2 assemblies were performed by mixing 100 ng of the level 2 acceptor plasmid with level 1 modules in a 2:1 molar ratio of insert to acceptor, 5 U of BpiI (ThermoFisher Scientific), 200 U of T4 DNA ligase (New England Biolabs), 1.5 µL of T4 DNA ligase buffer (New England Biolabs), 1.5 µL of 10X bovine serum albumin (BSA) (New England Biolabs), and sterile distilled water to a final reaction volume of 15 µL.
All digestion-ligation reactions were incubated at 37°C for 20 s, followed by 26 cycles of 37°C for 3 min, 16°C for 4 min, then 50°C for 5 min, with a final step of 80°C for 5 min.

2.4.6 Bacterial transformation

A 2.5 µL aliquot of the cloning reaction mix was added to 50 µL of thawed *Escherichia coli* Stellar™ (for In-Fusion cloning) or *E. coli* DH5α (for Golden Gate cloning) competent cells, mixed gently and incubated on ice for 30 min. The cells were then incubated at 42°C for 45 s in pre-heated water bath then immediately placed on ice for 2 min. A 500 µL aliquot of pre-warmed SOC media (for Stellar™) (Clontech, USA) or lysogeny broth (LB) medium was added to transformed cells and the mixture was incubated at 37°C with shaking at 225 rpm for 1 h. After incubation, the bacterial culture was plated on LB medium agar containing appropriate antibiotics (50 µg/mL spectinomycin or 50 µg/mL kanamycin or 100 µg/mL carbenicillin). The plates were incubated overnight at 37°C. Successful transformants were identified via colony PCR. Blue-white colony screening was carried out by adding 0.5 mM IPTG (isopropyl b-D-1-thiogalactopyranoside) and 40 µg/mL X-gal to LB agar plates before plating transformed cells if acceptor vector contained a lacZ cassette.

Transformation of *Agrobacterium tumefaciens* AGL1 was performed by electroporation. A 2.5 µL aliquot of construct was mixed with thawed AGL1 electrocompetent cells. The mixture was then transferred to a pre-chilled electroporation cuvette. The cuvette was then placed in an electroporator (BioRad) with the following settings: voltage = 1.8 kV, capacitance = 25 µF, resistance = 200 W. After electroporation, 1 mL of LB medium was added to the cells and pipetted out to a new 1.5 mL microcentrifuge tube. The cells were then incubated at 28°C with shaking at 225 rpm for 1 h. The cells were plated on solid LB medium with the appropriate antibiotics (100 µg/mL rifampicin + 50 µg/mL kanamycin or 100 µg/mL rifampicin + 50 µg/mL spectinomycin) and incubated at 28°C for 48-72 h.

2.4.7 Plasmid DNA preparation

PureYield™ Plasmid Midiprep System (Promega, Madison, Wisconsin, USA) to extract the plasmid DNA for sequencing before fungal or *Agrobacterium* transformation. A positive bacterial colony was inoculated in 10 mL liquid LB media with the appropriate antibiotic. The liquid culture was incubated at 37°C with shaking at 225 rpm overnight. The bacterial pellet was recovered by centrifugation of 1-10 mL of overnight culture in a

2 mL microcentrifuge at 17,000 × *g* for 2 min. The pellet was thoroughly resuspended with 250 µL of cell resuspension solution. An aliquot of 250 µL of cell lysis solution was added and the tube was inverted a few times for mixing. After which, 10 µL of alkaline protease solution was added, the tube was inverted four times to mix and then incubated at room temperature for 5 min. At this point, 350 µL of neutralization solution was added and the tube inverted for mixing. The mixture was processed by centrifugation at 17,000 x *g* at room temperature for 10 min. To bind plasmid DNA, the cleared lysate was decanted into a spin column, which was inserted onto a supplied collection tube, then this was subjected to centrifugation at 17,000 x *g* at room temperature for 1 min. The flowthrough was discarded, and the column reinserted into the collection tube. The column was washed using 750 µL of wash solution (ethanol added) and was subjected to centrifugation at 17,000 x *g* for 1 min. Flowthrough was discarded and the column was reinserted into the collection tube. The washing step was repeated with 250 µL of wash solution, then subjected to centrifugation at 17,000 x *g* for 2 min. The column was then transferred to a sterile 1.5 mL microcentrifuge tube. To elute the plasmid DNA, 50 µL of nuclease-free water was added to the spin column and it was concentrated by centrifugation at 17,000 x *g* for 1 min. The plasmid DNA was stored at -20°C.

2.4.8 Oligonucleotides and sequencing

All oligonucleotides were synthesized by Merck (www.merckmillipore.com) at 100 µM. Sterile distilled water was added to obtain working concentrations of 10 µM. Primer stock and working solutions were kept at -20°C. GENEWIZ® (www.genewiz.com) services were availed for Sanger sequencing.

2.5 Molecular cloning

2.5.1 Molecular cloning for fluorescent protein-tagged *M. oryzae*

Fluorescent protein-tagged fungal strains were generated for better visualization during live cell imaging. To identify a reliable fungal strain, four tdTomato constructs were made, each driven by different promoters namely RP27 (Bourett et al., 2002), Mep1(Yan & Talbot, 2016), α-tubulin and trpC,(Hamer & Timberlake, 1987) and were used to transform *M. oryzae* strain Guy11. The RP27 promoter was amplified from the level 0 module pICSL12033 ordered from TSL SynBio. Mep1 promoter was amplified from a Mep1:GFP construct courtesy of Dr. Xia Yan (The Sainsbury Laboratory) while α-tubulin

and trpC promoters were amplified from constructs provided by Dr. Alice Eseola (The Sainsbury Laboratory). The tdTomato and trpC terminator fragments were amplified from the construct ATG1:tdTomato from Dr. Alice Eseola. The purified PCR products were then introduced to the fungal transformation vector pSCBAR via In-Fusion cloning as previously described. After the constructs were confirmed via sequencing, these were used in DNA-mediated fungal transformation. Primers used in amplifying the PCR inserts and in confirming the correctness of the constructs via sequencing were listed in Table 2.2.

Table 2.2 Oligonucleotide primers used for cloning for tdTomato-tagged constructs for *M. oryzae.*

Primer Name	Primer Sequence (5' to 3')	Purpose
tdtomato_F	ATGGTGAGCAAGGGCGAGGACGTC	to amplify
tdtomato_R	TTACTTGTACAGCTCGTCCATGCC	tdTomato
trpC term_tdtomato OH_F	CATGGACGAGCTGTACAAGTAAAGCGGCCG CCCGGGCTGC	to amplify trpC terminator
trpC term_pSCBAR OH_R	TCGACGGTATCGATAAGCTTAGTGGAGATG TGGAGTGGGC	
RP27 prom_pSC BAR OH_F	TGCAGCCCAATGTGGAATTCGGAGATAAAT GTAGGTATTAC	to amplify RP27 promoter
RP27p_tdtomato OH_R	TCCTCGCCCTTGCTCACCATCATTTTTGAAGA TTGGG	
trpC prom_pSCBAR OH_F	TGCAGCCCAATGTGGAATTCGATATTGAAG GAGCATTTTTG	to amplify trpC promoter
trpC prom_tdtomato OH_R	CCTCGCCCTTGCTCACCATTTGGATGCTTGG GTAG	
tub prom_pSCBAR OH_F	TGCAGCCCAATGTGGAATTCTGTGATATCAA CTTGGGGAC	to amplify TUB1 promoter
tub prom_tdtomato OH_R	TCCTCGCCCTTGCTCACCATCTTGACGGCGT TTTACTTTGG	
Mep1 prom_pSCBAR OH_F	TGCAGCCCAATGTGGAATTCACCCAGCCACA AGTAAAGTC	to amplify Mep1 promoter
Mep1 prom_tdtomato OH_R	TCCTCGCCCTTGCTCACCATTTTGGGGTAGT GAAG	

RP27p:mScarlet3 construct was generated via Golden Gate cloning. Level 0 modules pICSL12033 (RP27 promoter), pICSL80132 (mScarlet3), and pICSL60013 (trpC terminator) were all introduced into the Level 1 acceptor pcb1532H-RFP, a fungal transformation vector carrying hygromycin resistance and RFP screening cassette for colony screening. The resulting construct was introduced to Guy11 and Guy11 Mep1:mCherry backgrounds.

2.5.2 Molecular cloning for transgenic line development

All subcellular component marker constructs were generated by Golden Gate cloning except for the endoplasmic reticulum marker construct pGWB514 ZmUbi:AtWAK2:GFP:HDEL:Nos, which was developed by In-Fusion cloning. The early endosome marker construct 35s:OsAra6:GFP in pGWB502 backbone and the Golgi marker construct 35s:STtmd:GFP:Nos in pVKH18 backbone were readily available in the lab for rice and barley transformation. The 35s:OsAra6:GFP:Nos plasmid was generated by Dr. Magdalena Martin-Urdiroz after a putative Ara6 sequence in rice was identified by a search with the Ara6 protein sequence from *Arabidopsis* (provided by Dr Darren Soanes and Dr. George Littlejohn). Subcellular markers for the plasma membrane (35s:LTI6b TMD:GFP:Nos;pICSL11249), mitochondria (35s:CoxIV:GFP:Nos; pICSL11247), nucleus (35s:NLS:GFP:Nos; pICSL11248) and cytoplasm (ZmUbi:GFP:35s; pICSL11122) were readily available as Level 1 modules from TSL SynBio. LifeAct (actin marker) level 0 module was generated by directly introducing synthesised LifeAct fragment from Merck (www.merckmillipore.com) to level 0 acceptor pICSL01005 (TSL SynBio). Ara7 (late endosome marker) fragment was synthesised by Twist Bioscience (San Francisco, CA, USA) after domestication to remove *BpiI* and *BsaI* sites. The Ara7 fragment was then introduced to level 0 acceptor pICH41308 (TSL SynBio). The GFP:PTS1 fragment was generated by PCR amplification using pICSL50008 (GFP C-terminal tag) as template. A 9 bp overhang was added to the 3' end of GFP which corresponded to the peroxisomal targeting sequence SKL (Serine-Lysine-Leucine) (Nelson et al., 2007; Reumann, 2004).

The organelle-targeting fragments were used to developed Level 0 modules. Level 1 constructs were generated by combining the promoter, organelle-targeting sequence, GFP and terminator modules to form a GFP-tagged organelle marker unit. All subcellular markers were tagged at the C-terminal except for Ara7 which has N-terminal tag. Level 1 modules were generated by combining the promoter, selected signal peptide or organelle targeting sequence, GFP and terminator modules to form a GFP-tagged organelle marker unit. For level 2 constructs, hygromycin B resistance conferred by hygromycin phosphotransferase II gene (HptII; pICSL11509) was placed in position 1 for *in-planta* selection during rice or barley transformation, the organelle marker unit in position 2 and pFAST red (pICSL11199) for seed selection in position 3 to aid in easier advancement and generation of fixed transgenic lines. Descriptions of ordered fragments for synthesis,

requested modules and appropriate acceptors for each level were detailed in Table 2.3. Primer for sequencing assembled modules are listed in Table 2.4.

Table 2.3 Golden Gate cloning modules for organelle marker construct assembly.

Module (subcellular component)	Level	Code	Bacterial Resistance	Size (bp)
Ara7 (late endosome)	0	pICSL80097 (AATG-GCTT)	Spec	2851
LifeAct (actin cytoskeleton)	0	pICSL80101 (AATG-TTCG)	Spec	2301
L0 acceptor for Transcriptional units minus CTAG/terminator	0	pICSL01006 (GGAG-TTCG)/(GGAG-TTCG)	Spec	2845
L0 acceptor for CDS1 no stop (ns) modules	0	pICSL01005 (AATG-TTCG)/(AATG-TTCG)	Spec	2845
L0 acceptor for CDS1 modules	0	pICH41308 (AATG-GCTT)/(AATG-GCTT)	Spec	2845
Ubiquitin (ZmUbi) constitutive promoter	0	pICSL12009 (GGAG-AATG)	Spec	4239
Ubiquitin (ZmUbi) constitutive promoter	0	pICSL13016 (GGAG-CCAT)	Spec	4239
C-terminal GFP tag	0	pICSL50008 (TTCG-GCTT)	Spec	3563
N-terminal GFP tag	0	pICSL30006 (CCAT-AATG)	Spec	2980
Nopaline synthase (Nos) terminator	0	pICH41421 (GCTT-CGCT)	Spec	2514
L1 acceptor (position 2-F)	0	pICH47742 (GGAG-CGCT)/(GCAA-ACTA)	Amp	4968
35s:NLS:GFP:Nos (nucleus)	1	pICSL11248 (GCAA-ACTA)	Carb	6382
35s:CoxIV:GFP:Nos (mitochondria)	1	pICSL11247 (GCAA-ACTA)	Carb	6875
35s:LTI6b TMD:GFP:Nos (plasma membrane)	1	pICSL11249 (GCAA-ACTA)	Carb	6956
ZmUbi:GFP:35s (cytoplasmic GFP)	1	pICSL11122 (ACTA-TTAC)	Carb	7293
Hygromycin resistance	1	pICSL11059 (TGCC-GCAA)	Carb	7225
Barley pFAST red	1	pICSL11199 (ACTA-TTAC)	Carb	9080
Position 2 dummy	1	pICH54022 (GCAA-ACTA)	Carb	4368
End-linker for Level 2	1	pICH41766 (TTAC-GGGA)	Spec	3318
End-linker for Level 2	1	pICH41780 (CAGA-GGGA)	Spec	3318
L2 acceptor	2	pICSL4723 (TGCC-GGGA)	Kan	12948
L2 acceptor	2	pAGM4723_ccdb (TGCC-GGGA)	Kan	6500

Table 2.4 Primers for sequencing assembled Golden Gate modules.

Primer Name	Primer Sequence (5' to 3')	Purpose
F(0015)	CGTTATCCCCTGATTCTGTGGATAAC	to sequence Level 0 assemblies
R(0016)	GTCTCATGAGCGGATACATATTTGAATG	
F(0229)	GAACCCTGTGGTTGGCATGCACATAC	to sequence Level 1 assemblies
R(0230)	CTGGTGGCAGGATATATTGTGGTG	
F(0231)	GTGGTGTAAACAAATTGACGC	to sequence Level 2 assemblies
R(0232)	GGATAAACCTTTTCACGCCC	

2.6 *Nicotiania benthamiana* transient expression assay

Transient expression assay in *N. benthamiana* was carried out to check whether the organelle marker constructs will show the correct subcellular localisation. The organelle marker constructs were introduced into the *Agrobacterium tumefaciens* strain AGL1 except for the Golgi marker which was introduced to EHA105. Transformed strain AGL1 or EHA105 was inoculated in 5 mL LB with appropriate antibiotics and grown overnight at 28°C with shaking at 225 rpm. The bacterial culture was precipitated at 5000 x *g* for 5 min, and the pellet was resuspended in resuspension solution (10 mM $MgCl_2$, 10 mM MES-K (pH 5.6), 100 μM acetosyringone). The final OD_{600} was adjusted to 0.4. *N. benthamiana* leaves were infiltrated using a 1 mL syringe without the needle by pressing the syringe on the underside of the leaf and exerting a counter-pressure with finger on the other side. Observation of GFP fluorescence was carried out 2-3 days after infiltration under the Leica TCS SP8X microscope.

2.7 *Agrobacterium*-mediated transformation in rice and barley

Constructs were streaked onto LB plates with the appropriate antibiotic and were submitted to the TSL tissue culture and transformation team for both rice and barley transformation. Media composition and stock solutions used were detailed in Tables 2.5 and 2.6 for rice and barley transformation, respectively.

Table 2.5 Media and stock solutions for rice transformation.

Medium/Stock Name	Composition and Procedures
Medium R1	4.3 g/L MS salts & vitamins + 30 g/L Sucrose + 0.5 g/L MES + 300 mg/L Casamino acid+ 2.8 g/L L-Proline + 2 mg/L 2，4-D+4g/L Phytagel，pH 5.8with KOH, autoclave.
AAM medium	4.3 g/L MS salts & vitamins + 68.5 g/L Sucrose + 0.5 g/L MES + 36 g/L Glucose + 500 mg/L Casamino acid+ 100 ml 10 x AA amino acids，pH 5.2with KOH and aliquot by 100 ml. Autoclave and store at 4°C. Add 200ul of 20 mg/ml Acetosyringone per 100 ml before use.
10x AA amino acids	Dissolve 8.76 g L-Glutamine, 2.66 g L-Aspartic acid, 1.74 g L-Arginine and 75 mg Glycine in 900 ml distilled water and make up the volume to 1,000 ml. Filter sterilize, aliquot by 100 ml, and store at 4°C.
Medium R2	4.3 g/L MS salts & vitamins + 30 g/L Sucrose + 0.5 g/L MES + 10 g/L Glucose+ 300 mg/L Casamino acid + 2 mg/L 2，4-D + 4 g/L Phytagel, pH 5.2 with KOH. Add 1 ml of 20 mg/ml Acetosyringone to 1 L medium after autoclaving.
Medium R3	4.3 g/L MS salts & vitamins + 30 g/L Sucrose + 0.5 g/L MES + 300 mg/L Casamino acid+ 2.8 g/L L-Proline + 2 mg/L 2，4-D + 4 g/L Phytagel，pH 5.8 with KOH. Add 200mg/L Timentin and 30mg/L Hygromycin (final concentration) after autoclaving.
Medium R4	4.3 g/L MS salts & vitamins + 30 g/L Sucrose + 0.5 g/L MES + 2 g/L Casamino acid + 30 g/L Sorbitol + 2 mg/L Kinetin + 1mg/L NAA + 4g/L Phytagel，pH 5.8 with KOH. Add 200mg/L Timentin and 20mg/L Hygromycin (final concentration) after autoclaving.
Medium R5	2.15g/L MS salts & vitamins + 15g/L Sucrose + 0.5 g/L MES + 2g/L Phytagel，pH 5.8 with KOH. Add 200mg/L Timentin and 20mg/L Hygromycin (final concentration) after autoclaving.
20 mg/ml Acetosyringone stock	Dissolve 200 mg Acetosyringone in 10mlDMSO. Aliquot by 1 ml and store at -20°C.
200 mg/ml Timentin stock	Dissolve 1000 mg Timentin in 5 ml H2O, filter sterilize, aliquot by 1 ml and store at -20°C.
50 mg/ml Hygromycin stock	Dissolve 500 mg Hygromycin in 10 ml H2O, filter sterilize, aliquot by 1 mland store at -20°C.
1.0 mg/ml 2,4-D stock	Dissolve 50 mg 2,4-D in 500 ul Ethanol, add H2O to 50 ml. Store at 4°C.
2.0 mg/ml Kinetin stock	Dissolve 20 mg Kinetin in 200 ul of 1N NaOH, add H2O to 10 ml. Store at 4°C.
1.0 mg/ml NAA stock	Dissolve 50 mg NAA in 200 ul of 1N NaOH, add H2O to 50 ml. Store at 4°C.

Table 2.6 Media and stock solutions for barley transformation.

Medium/Stock Name	Composition and Procedures
Bacterial culture medium MG/L	5.0 g/l tryptone, 5.0 g/l mannitol, 2.5 g/l yeast extract, 1.0 g/l L-glutamic acid, 250 mg/l KH_2PO_4, 100 mg/l NaCl, 100 mg/l $MgSO_4.7H_2O$ and 10 µL Biotin (0.1 mg/l stock). The media is adjusted to pH 7.2 with NaOH. For the preparation of plates 15 g/l agar is added.
Callus induction medium	4.3 g/l Murashige & Skoog plant salt base (Duchefa M0221), 30 g/l maltose, 1.0 g/l casein hydrolysate, 350 mg/l myo-inositol, 690 mg/l proline, 1.0 mg/l thiamine HCl, 2.5 mg/l Dicamba (Sigma-Aldrich D5417), 3.5 g/l Phytagel. The media is adjusted to pH 5.8 with NaOH.
Transition medium	2.7 g/l Murashige & Skoog modified plant salt base (without NH_4NO_3) (Duchefa M0238), 20 g/l maltose, 165 mg/l NH_4NO_3, 750 mg/l glutamine, 100 mg/l myo-inositol, 0.4 mg/l thiamine HCl, 2.5 mg/l 2,4-dichlorophenoxy acetic acid (2,4-D) (Duchefa), 0.1 mg/l 6-benzylaminopurine (BAP) (Duchefa), 3.5 g/l Phytagel. The pH is adjusted to 5.8.
Regeneration medium	2.7 g/l Murashige & Skoog modified plant salt base (without NH_4NO_3) (M0238 Duchefa), 20 g/l maltose, 165 mg/l NH_4NO_3, 750 mg/l glutamine, 100 mg/l myo-inositol, 0.4 mg/l thiamine HCl, 3.5 g/l Phytagel. The pH is adjusted to 5.8.
Callus induction 100x vitamin stock	100 mg/l thiamine HCl, 35 g/l myo-inositol and 690 mg/l proline. This stock should be filter sterilized ready for use and stored at 4°C.
Transition and regeneration 100x vitamin stock	40 mg/l thiamine HCl and 10 g/l myo-inositol. This stock should be filter sterilised ready for use and stored at 4°C.
Dicamba	2.5 mg/l stock made up in water, filter sterilised, divided into 1ml aliquots and stored frozen.
2,4-D	2.5 mg/ml stock made up in 100% ethanol and stored at -20°C
$CuSO_4$ stock	125 mg of $CuSO_4.5H_2O$ dissolved in a total volume of 100 ml water, filter sterilised and store at 4°C.
Hygromycin	Purchased as a sterile 50 mg/ml stock, divided into 1 ml aliquots and stored frozen.
Timentin	160 mg/ml stock made up in water, divided into 1 ml aliquots and stored frozen.
BAP	1 mg/ml stock made up in water with a few drops of 1 *M* NaOH and stored at -20°C.

2.7.1 Rice transformation

Dehulled rice seeds were sterilized with 70% ethanol for 2 min and further sterilized with bleach (2.5% sodium hypochlorite solution) for 15 min, then washed five times in sterile distilled water. Sterilized seeds were inoculated on R1 medium plates and cultured in the light at 32°C for 4 weeks. Fresh secondary calli were transferred onto new R1 medium plates and grown for 3-5 days, then used for transformation. *Agrobacterium* strain AGL1 harboring the binary vector was streaked on LB plate containing appropriate antibiotics and cultured for 2 days at 28°C in the dark. *Agrobacterium* culture was scraped from the plate and suspended with 10 mL AAM medium in a sterile tube to yield an OD_{600} of approximately 0.3-0.5. Calli were immersed in the *Agrobacterium* suspension by gently shaking the tube for 5 min, then blotted dry with sterilized filter paper to remove excess *Agrobacterium*. The infected calli were transferred onto sterilized filter paper on top of R2 medium and cultured in the dark at 25°C for 3 days. Calli were transferred to R3 medium plates and cultured in the light at 32°C for 2 weeks. Living calli were transferred to new R3 plates for two more weeks. Proliferating calli were then transferred to R4 plates and grown in the light at 32°C for 2 weeks or more. Plantlets arising from the calli were transferred to R5 tubes to facilitate root growth. Before transplanting to soil, R5 medium was replaced with water and the tube lid was opened to train the plant. Once rooted plants reach the top of the tubes, the plants were transferred to soil.

2.7.2 Barley transformation

Seeds of barley cv. Golden Promise were sown in a barley growth mix (2:2:1 mix of Levington M3 compost:perlite:grit with slow-release fertilizer Osmocote according to manufacturer's recommended concentration. Seeds were initially sown in 5 diameter pots and then transferred into 13 cm diameter round pots after approximately 30 days in the same growth mix for continued development. Barley spikes were collected when immature embryos were 1.5-2 mm in diameter. The immature seeds were removed from the spike and the awns broken off without damaging the seed coat. The immature seeds were then sterilized by firstly washing in 70% ethanol for 30 s followed by three washes in sterile distilled water. The immature seeds were also sterilized in a solution of sodium hypochlorite (Fluka 71696) diluted 50:50 with water for 4 min followed by four washes in sterile distilled water. The immature seeds were drained but left wet in a screw top

sterile jar. To isolate the immature embryos, sterile seeds approximately 20 at a time, were tipped onto a sterile blue or black tile under a dissecting microscope. The seeds were held firmly with fine forceps and second pair of fine forceps used to expose the immature embryo and remove the embryonic axis. The embryo was then plated scutellum side up on a callus induction medium. Twenty-five embryos were placed on each 9 cm plate for *Agrobacterium* inoculation and stored at 23-24°C in the dark. An overnight *Agrobacterium* culture was prepared by adding a standard inoculum to 10 mL of liquid MG/L medium without any antibiotics. The culture was incubated on a shaker at 180 rpm at 28°C overnight. The full-strength *Agrobacterium* culture was used to inoculate the embryos. Using a 200 µL pipette, a small amount of *Agrobacterium* was dropped onto each embryo. Once all 25 embryos on a plate have been treated, the plate was tilted to allow any excess *Agrobacterium* culture to run off the embryos. A maximum of two plates were treated with *Agrobacterium* before embryos from the first plate were gently removed and transferred to a fresh callus induction plate, scutellum side down. Plates were sealed with Micropore™ surgical tape and incubated at 23-24°C for three days. After three days co-cultivation, the embryos were transferred to fresh callus induction plates containing hygromycin as the selective agent and timentin to remove *Agrobacterium* from the cultures. Embryos were cultured scutellum side down at 23-24°C in the dark. This transfer served as selection 1. After two weeks, embryos were transferred to fresh selection plates as previously described for selection 2. The entire embryo and callus derived from it was transferred as a single unit and not split up. After two more weeks, each embryo was transferred to a third selection plate. After six weeks selection on callus induction medium, the embryo-derived callus was transferred to transition medium, again containing hygromycin and timentin, for two weeks at 24°C under low light. After two weeks on transition medium, the embryo-derived material was transferred to regeneration medium in deep Petri dishes without any growth regulators but still with the same levels of hygromycin and timentin. Once shoots were 2-3 cm in length and roots have formed, the plantlets were removed from the plates and transferred to glass culture tubes containing 12 mL of callus induction medium without any growth regulators but with hygromycin and timentin at the same concentrations. Once rooted plants reach the top of the tubes, the plants were transferred to soil.

2.7.3 Fluorescence checking of transgenic rice and barley lines

From 2-3 weeks after transplanting, ligules from rice transgenic lines and auricles from barley transgenic lines were sampled and mounted onto a glass slide with sterile distilled water and covered with a cover slip. Observations of fluorescence were carried out on a Leica TCS SP8X confocal microscope as previously described (Please see Chapter 2.12).

2.7.4 GFP copy number identification

After checking the fluorescence of transgenic lines, leaf samples of fluorescing plants were submitted to iDNA Genetics/AttoDNA (Norwich Research Park, Norwich, UK) to identify GFP copy number. Transgenic lines with a single copy of GFP at T_0 and two copies of GFP at T_1 were selected for developing stable transgenic lines. The analysis uses qRT-PCR with calibration controls to determine copy number of GFP insertions.

2.7.5 pFast-Red screening in transgenic line seeds

To select T_1 seeds for advancement to the next generation or to confirm non-segregation of T_2 seeds, transgenic lines expressing pFast-Red in seeds were peeled and screened for fluorescence using a Leica M165 fluorescent stereo microscope with a DsRed/red fluorescent protein (RFP) filter. Fluorescent T_1 seeds were picked with forceps and collected in a 1.5 mL microcentrifuge tube. These seeds were then sown and grown into 2-3-week-old seedlings, which were subsequently sampled and submitted to iDNA Genetics/AttoDNA (Norwich Research Park, UK) for GFP copy number determination.

2.8 DNA-mediated fungal transformation of *M. oryzae*

A 2.5 cm^2 section of mycelium from a *M. oryzae* culture grown in CM medium for 7-10 days was cut and transferred to 150 mL liquid CM medium. This was blended to generate small fragments of mycelia. The liquid culture was incubated at 25°C with shaking at 225 rpm for 48 h. The culture was filtered through a sterile Miracloth and the mycelia were washed with sterile distilled water. The mycelium was then transferred to a 50 mL Falcon tube and 40 mL 0.7 M NaCl buffer/500 mg Glucanex (pH 5.5-5.8, filter-sterilized) was added. The mycelia were shaken gently to get rid of hyphal clumps and were incubated at 30°C with shaking at 75 rpm for 3 h. The fungal protoplasts were passed through a sterile Miracloth to sterile Falcon tubes and subjected to centrifugation at 5000 × *g* at 4°C for

10 min in a swinging bucket rotor (Beckman JS-13.1) in a Beckman J2.MC centrifuge. After centrifugation, the supernatant was poured out, the protoplasts were suspended in 50 mL of STC (1.2 M D-sorbitol, 10 mM $CaCl_2$, 10 mM Tris–HCl, pH 7.5) and were subjected to centrifugation at 5000 × *g* for 10 min. The protoplasts were resuspended with 20 mL STC and then counted on a haemocytometer. In a 1.5 mL microcentrifuge tube, the protoplasts ($5x10^6$ cells/mL) were combined with approximately 5-10 μg of DNA. The mixture was incubated on ice for 25 min. Then, 1 mL of PTC (60% PEG 4000, 10 mM Tris-HCl pH 7.5, 10 mM $CaCl_2$) was added, the mixture was mixed gently and incubated at room temperature for 15 min. The transformation mixture was added to 150 ml of BCDM and poured into 5-6 sterile Petri dishes. The plates were incubated in the dark for at least 16 h at 24°C then were overlaid with approximately 15 mL of BCDM top media (minimal medium/1% agar) containing 300 μg/mL sulfonylurea (Sur) or bialophos (Basta). Mycelial growth of transformants were picked using sterile pipette tips and grown in Sur or Basta selection plates and in CM plates. Growing colonies were selected and subjected to more downstream work such as DNA extraction, PCR to confirm successful transformation and checking of fluorescence under a microscope.

2.9 Host plant plasmolysis assay

Infected leaf sheaths were prepared by thinly sectioning three to four cell layers, mounting these onto glass slides with 0.75 M sucrose solution and covering with cover slips (Kankanala et al., 2007).

2.10 Fluorescein diacetate (FDA) cell viability assay

Fluorescein diacetate stain was prepared as previously described (Jones et al., 2016). Briefly, fluorescein diacetate (FDA; F7379-5G, Sigma) was dissolved in acetone to a stock concentration of 1g/ml. A working solution of 2 μg/ml of FDA was prepared by diluting 2 μl of the stock solution in 1ml of water. Inoculated leaf sheaths were trimmed and mounted using the FDA working solution.

2.11 Cytochalasin D treatment of plant tissue

For actin polymerization inhibition, 2-cm rice leaf sheath sections were floated in a 1.5 mL microcentrifuge tube with cytochalasin D solution (in 0.1% v/v DMSO) and vacuum

applied for 1 h. Prior to *M. oryzae* inoculation, the leaf sheath sections were rinsed with sterile distilled water and dried with paper towel.

2.12 Microscopy and Image Processing

Confocal laser scanning microscopy was carried out on a Leica TCS SP8 microscope using a 63x/1.4 oil immersion objective or 40x/1.1 water immersion objective. Images were acquired using the Leica LASX software (Leica Microsystems Inc., Buffalo Grove, IL, USA). The lasers were set as follows: GFP and tdTomato/mCherry/mScarlet3 were excited using 488 and 561 nm laser diodes, respectively. Emitted fluorescence was detected at 500-520 nm for GFP, 570-620 nm for tdTomato, and 580-650 nm for mCherry and mScarlet3 using HyD detectors. Chlorophyll fluorescence was detected at 650-740 nm. Images captured were processed using Fiji software (Schindelin et al., 2012).

Chapter 3 Generation of subcellular component marker transgenic lines in rice (*Oryza sativa*) and barley (*Hordeum vulgare*)

3.1 Introduction

Plant cells, like other eukaryotic cells, carry out a very wide variety of biological processes. To perform highly specialised functions concurrently, eukaryotic cells are therefore organised into compartments, such as membrane-bound organelles (Nelson et al., 2007). Organelles adapt to cellular demands by changing motility, morphology, and distribution (Chan & Marshall, 2012; Heald & Cohen-Fix, 2014; Passmore et al., 2021).

Fluorescent protein tagging has been widely used to visualise the subcellular localisation of organelles in various organisms, including plants. To facilitate organelle visualisation, organelle marker construct sets, and transgenic lines have been developed in plants. A series of constructs tagged with different fluorescent proteins have been established for *Arabidopsis* and other plants (Nelson et al., 2007) as well as for rice (Dangol et al., 2017). More recently, a new set of Golden Gate-based organelle plasmids for plants has been developed (Stellmach et al., 2022). Transgenic plants expressing fluorescent protein-tagged organelle markers were also developed for *Arabidopsis* (Geldner et al., 2009; Kim et al., 2013; Nelson et al., 2007), *Medicago* (Ivanov et al., 2023; Ivanov & Harrison, 2014; Luo & Nakata, 2012) , maize (Krishnakumar et al., 2015; Mohanty et al., 2009; Wu et al., 2013) , and rice (Chen et al., 2019; Wu et al., 2016). Transgenic plants with various organelle markers have also proven useful in studying plant-pathogen interactions including those involving plant pathogenic fungi and oomycetes (Koh et al., 2005; Mochizuki et al., 2015; Takemoto et al., 2003).

For live-cell imaging of major cellular changes during *Magnaporthe oryzae* infection, it is essential to develop fluorescently tagged marker constructs for rice transformation and establish rice transgenic lines with subcellular markers. Although rice transgenic lines with different fluorescent protein-tagged organelle markers have been developed (Chen et al., 2019; Dangol et al., 2017; Wu et al., 2016), I aimed to generate transgenic rice lines in a background suitable for studying both compatible and incompatible interactions. To this end, I selected rice cultivar Kitaake as the background for developing a set of GFP-tagged subcellular marker lines. Kitaake, a *japonica* rice variety (Ichitani et al., 1997), harbours the

resistance (*R*) gene *Pia*, which recognises its corresponding avirulence (*Avr*) gene *Avr-Pia* in *M. oryzae* (Cesari et al., 2013; Yang et al., 2022). When Kitaake is inoculated with an *M. oryzae* strain carrying *Avr-Pia*, an incompatible interaction occurs. Kitaake is also well-suited for research due to its rapid life cycle of approximately nine weeks from seed to seed (Jain et al., 2019; Jung et al., 2008) and its ease of transformation and propagation (Jung et al., 2008; S. L. Kim et al., 2013; Kunihiro et al., 1989). Additionally, the high-quality genome assembly of the model rice plant KitaakeX serves as a valuable reference for rice functional genomics (Jain et al., 2019).

Furthermore, I utilised barley cultivar Golden Promise to generate a set of barley transgenic lines with organelle markers. Golden Promise is a widely used reference variety in barley research for genetic transformation and functional genomics (Harwood, 2014). Golden Promise consistently achieves high shoot recovery from callus (Hensel et al., 2008), exhibits superior transformation efficiency (Ibrahim et al., 2010; Murray et al., 2004), and has a high-quality genome assembly available (Schreiber et al., 2020). Moreover, Golden Promise is a suitable model for studying barley-pathogen interactions due to its susceptibility to barley pathogens such as stem rust (Horvath et al., 2003), powdery mildew (Li et al., 2024), and blast disease (Brabham et al., 2023).

In this chapter, I describe the development of GFP-tagged organelle marker constructs targeting the plasma membrane, actin cytoskeleton, nucleus, mitochondria, early endosome, late endosome, cytoplasm, peroxisome, endoplasmic reticulum, and Golgi bodies. Using these subcellular marker constructs, I generated transgenic rice lines in the Kitaake background and transgenic barley lines in the Golden Promise background. Additionally, I present the subcellular localisation of these GFP-tagged organelle markers in *N. benthamiana* (transient expression), as well as in rice and barley. The transgenic rice and barley lines developed in this study will serve as valuable resources for investigating plant-pathogen interactions and protein colocalisation studies.

3.2 Results

3.2.1 Plasmid construction of GFP-tagged subcellular components markers

To develop transgenic lines expressing GFP-tagged markers that label various plant subcellular components, constructs were generated using either Golden Gate cloning or In-Fusion cloning. Previously identified and characterised signal peptides, targeting

sequences, and full-length protein sequences were used to direct GFP to specific subcellular compartments. For Golden Gate cloning, pICH47742 served as the backbone for level 1 assemblies, while pICSL4723 was used for level 2 assemblies, except for the peroxisome marker, which utilised pAGM4723_ccdb. Level 1 assemblies consisted of a promoter, a marker signal peptide/targeting sequence/full-length protein sequence, a GFP tag (either N-terminal or C-terminal), and a terminator. Level 2 assemblies included the *in planta* hygromycin B resistance selection cassette (pICSL11059), the subcellular marker unit assembled in level 1, the pFast-Red marker for RFP selection in seeds (pICSL11199), and a level 2 end-linker (pICH41766 or pICH41780). For In-Fusion cloning, the backbone used was pGWB514 (linearised with MfeI/SacI), which contains a hygromycin resistance cassette for *in planta* selection. Expression of GFP-tagged sequences targeted to different subcellular compartments including the plasma membrane, actin cytoskeleton, nucleus, mitochondria, early endosome, late endosome, cytoplasm, peroxisome, endoplasmic reticulum, and Golgi body was driven by either the Cauliflower mosaic virus (CaMV) 35S promoter (Amack & Antunes, 2020) or the maize ubiquitin (ZmUbi) promoter (Christensen et al., 1992; Cornejo et al., 1993), both of which are well-established constitutive promoters. All marker constructs were assembled in this study, except for the early endosome and endoplasmic reticulum markers, which were already available in the lab. Details of the subcellular marker constructs used are provided in Table 3.1.

Table 3.1 Overview about constructs used as subcellular component markers.

Subcellular component	Plasmid	Backbone	Marker	Source organism	Reference
Plasma membrane	35S:LTI6b TMD:GFP:Nos	pICSL4723	Low temperature induced protein 6b (LTI6b)	*A. thaliana*	Kurup et al. (2005), Nelson et al. (2007)
Actin	ZmUbi:LifeAct:GFP:Nos	pICSL4723	LifeAct	*S. cerevisiae*	Riedl et al. (2008)
Nucleus	35S:NLS:GFP:Nos	pICSL4723	SV40 NTAG nuclear localisation signal (NLS; MASSPPKKKRKVSWKM)	Simian virus 40	Grützner et al. (2021)
Mitochondria	35S:COXIV:GFP:Nos	pICSL4723	Cytochrome c oxidase IV (aa 1-29)(COXIV)	*S. cerevisiae*	Nelson et al. (2007), Chen et al. (2019)
Early endosome	35S:OsAra6:GFP:Nos	pGWB502	OsAra6	*O. sativa*	Ueda et al. (2001); rice homolog identified by D. Soanes and G. Littlejohn (Talbot lab)
Late endosome	ZmUbi:GFP:Ara7:Nos	pICSL4723	Ara7	*A. thaliana*	Lee et al. (2004), Kotzer et al. (2004)
Cytoplasm	ZmUbi:GFP:35S	pICSL4723	GFP	*Aequorea victoria*	Prasher et al. (1992)
Peroxisome	ZmUbi:GFP:PTS1:Nos	pAGM4723_ccdB	SKL (peroxisome targeting sequence 1, PTS1)	-	Nelson et al. (2007)
Endoplasmic reticulum	ZmUbi:AtWAK2:GFP:HDEL:Nos	pGWB514	Wall-associated kinase2 (aa 1-30)+GFP:HDEL	*A. thaliana*	Nelson et al. (2007), He et al. (1999)
Golgi body	35S:STtmd:mGFP5:Nos	pVKH18	2,6 sialyltransferase (52 aa) (STtmd)	*Rattus norvegicus*	Munro (1995), Boevink et al. (1998), (Saint-Jore et al., 2002)

3.2.2 Generation of transgenic lines expressing GFP–tagged subcellular component markers

To generate transgenic lines expressing GFP-tagged subcellular component markers, I first confirmed whether the assembled marker constructs localise to the correct subcellular component by *N. benthamiana* transient expression assay. The marker constructs were introduced to *Agrobacterium tumefaciens* AGL1 except for the Golgi marker which was introduced to EHA105. Bacterial suspensions were adjusted to a final OD_{600} of 0.4. and infiltrated into *N. benthamiana* leaves using a 1 mL syringe without a needle. GFP fluorescence was observed 2-3 days after infiltration under a Leica TCS SP8X microscope.

Once correct localisation was confirmed, the marker constructs were used to generate transgenic rice (*Oryza sativa* cv. Kitaake) and barley (*Hordeum vulgare* cv. Golden Promise) lines via *Agrobacterium*-mediated transformation. GFP fluorescence was assessed in rice ligules and barley auricles for each clone. Fluorescent T_0 lines exhibiting the correct localisation of the subcellular marker in both rice and barley were subjected to GFP copy number analysis to identify lines containing a single GFP insert. Identified T_0 clones with a single GFP insert were advanced to subsequent generations through self-pollination.

Fluorescence screening and GFP copy number data for all generated T_0 lines are provided in Appendix Table 1 (rice) and Appendix Table 2 (barley). Selected T_0 clones and their self-pollinated progenies were grown under controlled environmental conditions. A total of 452 rice T_0 lines and 165 barley T_0 lines were screened for GFP fluorescence and correct subcellular marker localisation. The number of fluorescent T_0 lines and those with a single GFP insert are summarised in Table 3.2. All constructs had at least one line with a single GFP insert that could be advanced to the T_1 generation, except for rice cv. Kitaake lines expressing the Golgi marker 35S:STtmd:GFP:Nos.

For cv. Kitaake lines expressing the Golgi marker 35S:STtmd:GFP:Nos, fluorescent lines were analysed for the number of hygromycin phosphotransferase II (HptII) inserts instead, as the GFP primers used by iDNA/AttoDNA were incompatible with the GFP variant in the Golgi marker construct.

Table 3.2 Summary of GFP fluorescence screening ang GFP copy number analysis in transgenic rice and barley T_0 lines harbouring subcellular markers.

Background	Construct (subcellular component)	No. of T_0 lines	No. of Fluorescing T_0 lines	No. of T_0 lines with single GFP insert*
Rice cv. Kitaake	35S:LTI6b TMD:GFP:Nos (plasma membrane)	68	20	8
	ZmUbi:LifeAct:GFP:Nos (actin cytoskeleton)	47	30	18
	35S:NLS:GFP:Nos (nucleus)	56	38	18
	35S:COXIV:GFP:Nos (mitochondria)	55	33	28
	35S:OsAra6:GFP:Nos (early endosome)	16	5	1
	ZmUbi:GFP:Ara7:Nos (late endosome)	64	26	11
	ZmUbi:GFP:35S (cytoplasm)	29	24	11
	ZmUbi:GFP:PTS1 (peroxisome)	43	37	1
	ZmUbi:AtWAK2:GFP:HDEL:Nos (endoplasmic reticulum)	9	7	1
	35S:STtmd:GFP:Nos (Golgi)	65	7	0**
	Total no. T0 lines	**452**		
Barley cv. Golden Promise	35S:LTI6b TMD:GFP:Nos (plasma membrane)	25	13	8
	ZmUbi:LifeAct:GFP:Nos (actin cytoskeleton)	20	13	13
	35S:NLS:GFP:Nos (nucleus)	30	9	8
	35S:COXIV:GFP:Nos (mitochondria)	27	14	9
	35S:OsAra6:GFP:Nos (early endosome)	1	1	1
	ZmUbi:GFP:Ara7:Nos (late endosome)	29	11	11
	ZmUbi:GFP:35S (cytoplasm)	33	14	13
	Total no. of T0 lines	**165**		

* Detection of number of GFP inserts was carried out by iDNA Genetics/AttoDNA (Norwich Research Park, United Kingdom).
** Detection of hygromycin phosphotransferase (HptII) gene insert was carried out instead of GFP due to primer incompatibility.

After identifying T_0 lines with a single GFP insert, these lines were self-pollinated to produce T_1 seeds. To establish stable, homozygous transgenic lines, I selected seeds based on pFast-Red fluorescence (Figure 3.1), which eliminated the need to sow seeds, sample tissues, and check for fluorescence in the rice ligule or barley auricle before determining GFP copy number. T_1 lines with two GFP copies were grown for seed bulking.

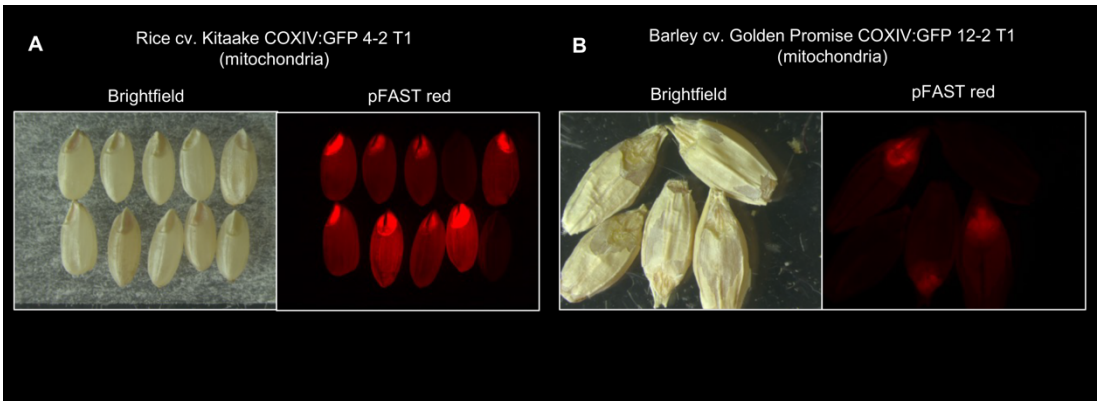

Figure 3.1 pFast-Red aids in seed selection for advancing transgenic rice and barley lines.

Images of segregating T1 seeds in rice cv. Kitaake **(A)** and barley cv. Golden Promise **(B)** under a fluorescent stereomicroscope with RFP filter. pFast-Red fluorescence allows positive seeds to be selected for obtaining stable transgenic lines.

The transgenic rice lines developed in this study are at different generational stages. The status of transgenic lines expressing subcellular markers in rice *cv.* Kitaake and barley cv. Golden Promise is summarised in Table 3.3. Unless otherwise stated, the localisation data for subcellular marker constructs in rice and barley presented in this section are from T_0 clones with a single GFP insert.

Table 3.3 Status of generated transgenic lines expressing GFP-tagged subcellular markers.

Subcellular Component	Construct	Generation (rice cv. Kitaake)	Generation (barley cv. Golden Promise)
Plasma membrane	35S:LTI6b TMD:GFP:Nos	T3	T1
Actin cytoskeleton	ZmUbi:LifeAct:GFP:Nos	T3	T1
Nucleus	35S:NLS:GFP:Nos	T3	T1
Mitochondria	35S:COXIV:GFP:Nos	T3	T1
Early endosome	35S:OsAra6:GFP:Nos	T3	T1
Late endosome	ZmUbi:GFP:Ara7:Nos	T3	T1
Cytoplasm	ZmUbi:GFP:35S	T2	T1
Peroxisome	ZmUbi:GFP:PTS1	T1	-
Endoplasmic reticulum	ZmUbi:AtWAK2:GFP:HDEL:Nos	T1	-
Golgi bodies	35S:STtmd:GFP:Nos	T1	-

3.2.2.1 Plasma membrane marker LTI6b TMD:GFP outlines the cell periphery

To target GFP to the plasma membrane, the transmembrane domain (TMD) of *A. thaliana* Low Temperature-Induced Protein 6b (LTI6b) was introduced into the level 2 binary vector pICSL4723. The LTI6b TMD:GFP fusion correctly labelled the plasma membrane in epidermal leaf cells of *Nicotiana benthamiana* (Figure 3.2A), rice ligules (Figure

3.2B), and barley auricles (Figure 3.2C). LTI6b TMD:GFP appeared as a distinct outline of the cell, consistent with the original reference (Kurup et al., 2005). However, it also showed an intracellular signal which outlines the nucleus (Figure 3.2).

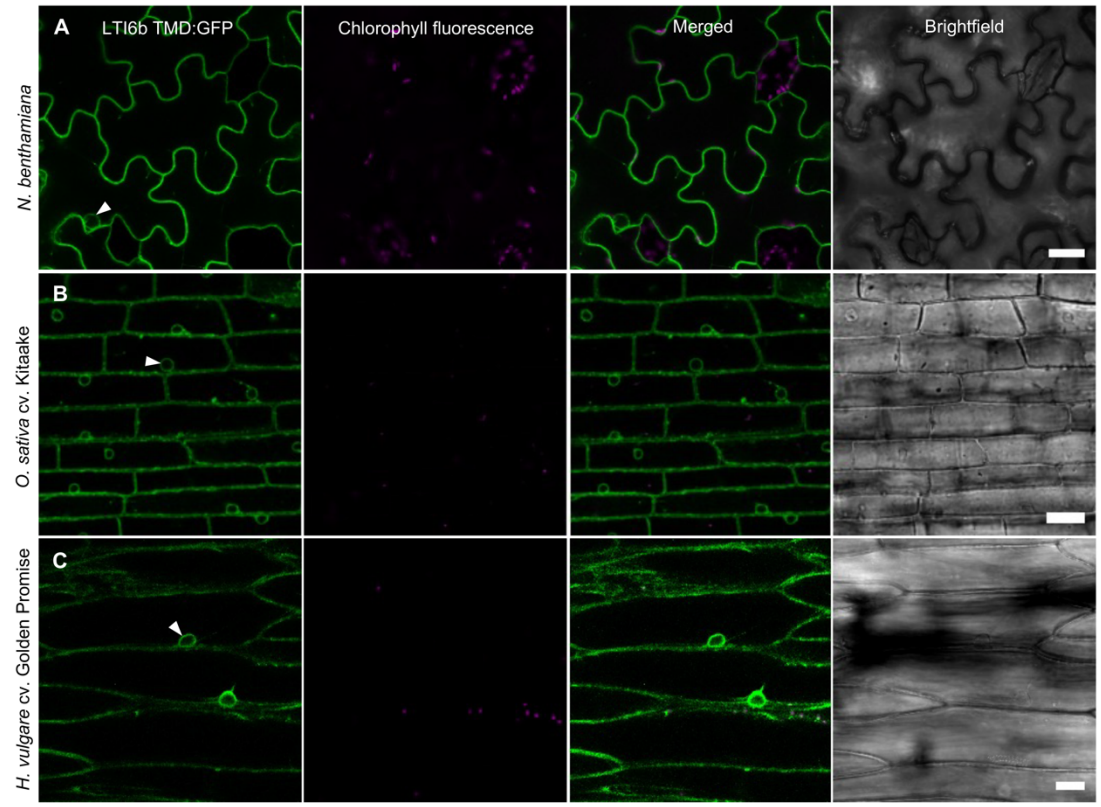

Figure 3.2 Subcellular localisation of the plasma membrane marker LTI6b TMD:GFP.

A. Confocal micrographs showing transiently expressed plasma membrane marker LTI6b TMD:GFP in *Nicotiana benthamiana* 72 h after infiltration. **B.** Confocal micrographs showing plasma membrane marker LTI6b TMD:GFP expression in rice cv. Kitaake ligule. **C.** Confocal micrographs showing plasma membrane marker LTI6b TMD:GFP expression in barley cv. Golden Promise auricle. **A-C.** The marker outlines the cell boundaries but also outlines the nucleus (indicated by white arrowheads). All images shown are maximum projections of z-stack series taken using Leica TCS SP8X confocal laser scanning microscope. Scale bar = 20 μm.

3.2.2.2 Actin cytoskeleton marker LifeAct:GFP labels actin filaments

LifeAct (Riedl et al., 2008) was fused with GFP and introduced into level 2 binary vector pICSL4723 to visualise the actin cytoskeleton. LifeAct, a short peptide consisting of the first 17 amino acids of the yeast protein Abp140p, is a well-established marker for labelling actin filaments (Riedl et al., 2008). LifeAct:GFP successfully labelled actin filaments in epidermal leaf cells of *N. benthamiania* (Figure 3.3A), rice ligules (Figure 3.3B) and barley auricles (Figure 3.3C) consistent with previous reports (Era et al., 2009; Smertenko et al., 2010; Vidali et al., 2009).

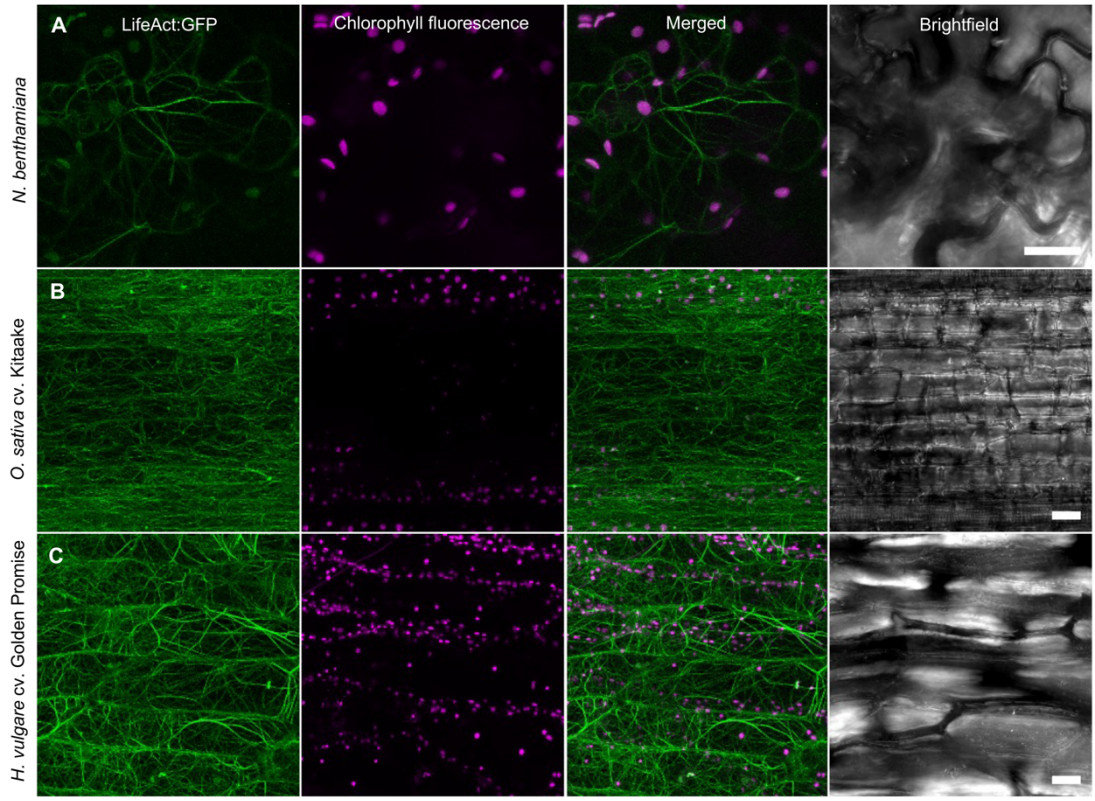

Figure 3.3 Subcellular localisation of the actin cytoskeleton marker LifeAct:GFP.

A. Confocal micrographs showing transiently expressed actin cytoskeleton marker LifeAct:GFP in *Nicotiana benthamiana* 72 h after infiltration. **B.** Confocal micrographs showing actin cytoskeleton marker LifeAct:GFP expression in rice cv. Kitaake ligule. **C.** Confocal micrographs showing actin cytoskeleton marker LifeAct:GFP expression in barley cv. Golden Promise auricle. **A-C.** The marker labels actin filaments. All images shown are maximum projections of z-stack series taken using Leica TCS SP8X confocal laser scanning microscope. Scale bar = 20 μm.

3.2.2.3 Nuclear marker NLS:GFP localises to the nucleus

Organelle marker sets typically do not include a nuclear marker, as the nucleus is easily distinguishable (Geldner et al., 2009; Nelson et al., 2007). To visualise the cell nucleus, GFP was fused with a nuclear localisation signal (NLS) from Simian virus 40 (Grützner et al., 2021) and introduced into the level 2 binary vector pICSL4723. Fluorescence microscopy confirmed that NLS:GFP localised to the nuclei of *N. benthamiana* (Figure 3.4A), rice ligules (Figure 3.4B), and barley auricles (Figure 3.4C).

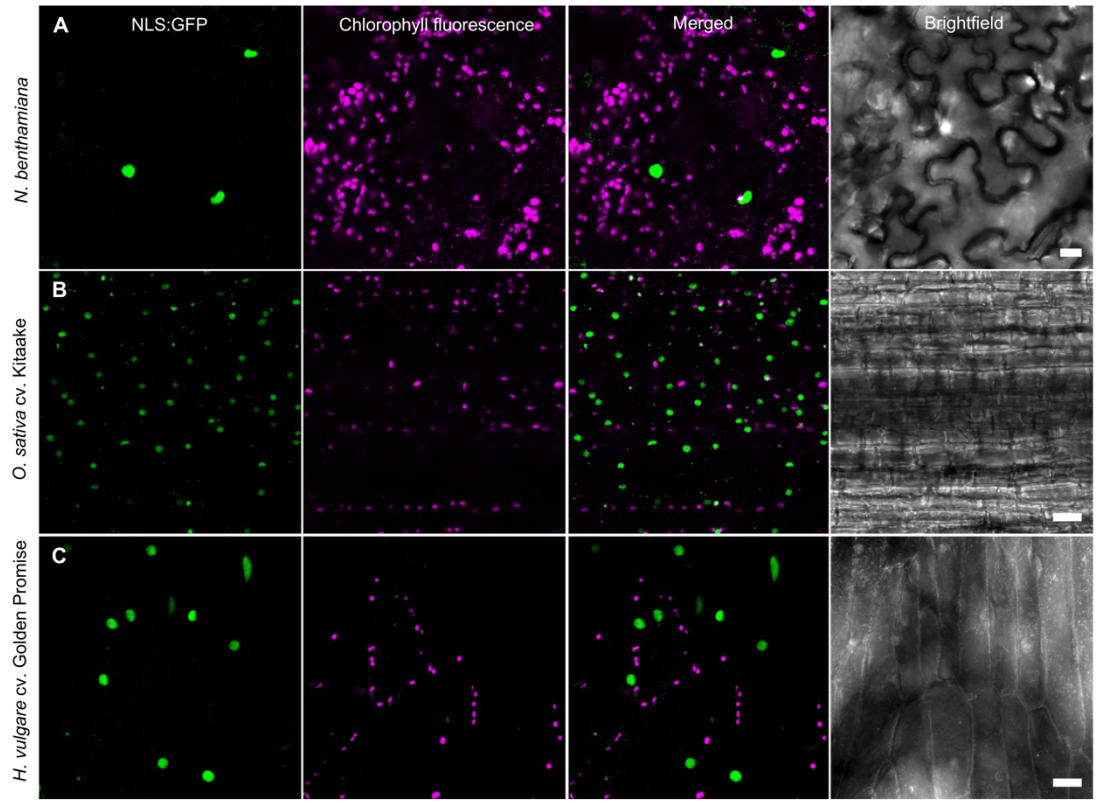

Figure 3.4 Subcellular localisation of the nuclear marker NLS:GFP.

A. Confocal micrographs showing transiently expressed nuclear marker NLS:GFP in *Nicotiana benthamiana* 72 h after infiltration. **B.** Confocal micrographs showing nuclear marker NLS:GFP expression in rice cv. Kitaake ligule. **C.** Confocal micrographs showing nuclear marker NLS:GFP expression in barley cv. Golden Promise auricle. **A-C.** NLS:GFP labels a single nucleus per cell. All images shown are maximum projections of z-stack series taken using Leica TCS SP8X confocal laser scanning microscope. Scale bar = 20 μm.

3.2.2.4 Mitochondrial marker COXIV:GFP appears as small round-oval puncta

To target GFP to the mitochondria, the first 29 amino acids from *Saccharomyces cerevisiae* Cytochrome c oxidase IV (COXIV) were used as a mitochondrial targeting sequence (Chen et al., 2019; Köhler et al., 1997; Nelson et al., 2007), and the fusion was introduced into the level 2 binary vector pICSL4723. The GFP-tagged mitochondrial marker localised to the mitochondria in *N. benthamiana* (Figure 3.5A), rice ligule (Figure 3.5B), and barley auricles (Figure 3.5C), appearing as small round-to-oval spots (Chen et al., 2019; Logan, 2006; Stellmach et al., 2022) or as beads on a string (Logan, 2006).

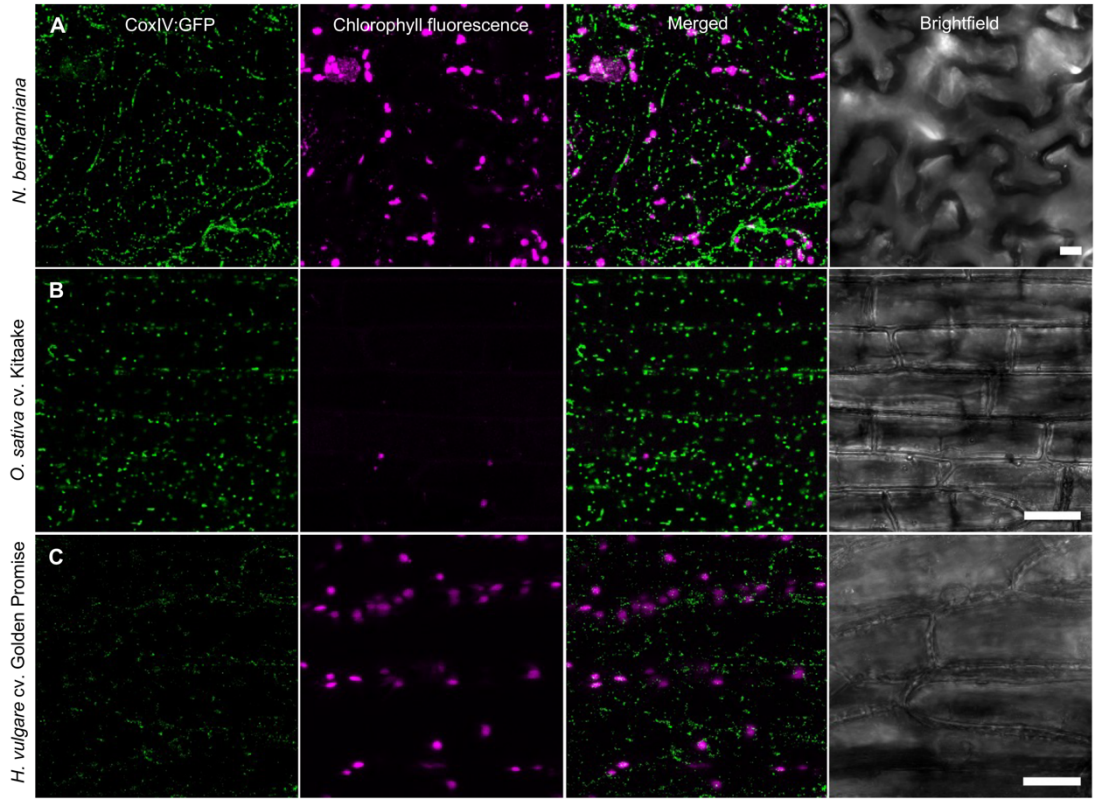

Figure 3.5 Subcellular localisation of the mitochondrial marker COXIV:GFP.

A. Confocal micrographs showing transiently expressed mitochondrial marker COXIV:GFP in *Nicotiana benthamiana* 72 h after infiltration. **B.** Confocal micrographs showing mitochondrial marker COXIV:GFP expression in rice cv. Kitaake ligule. **C.** Confocal micrographs showing mitochondrial marker COXIV:GFP expression in barley cv. Golden Promise auricle. **A-C.** The marker appears as small round-oval structures. All images shown are maximum projections of z-stack series taken using Leica TCS SP8X confocal laser scanning microscope. Scale bar = 20 μm.

3.2.2.5 Early endosome marker OsAra6:GFP labels punctate structures associated with the plasma membrane

To visualise early endosomes, the OsAra6 sequence, identified through a search using the Ara6 sequence from *A. thaliana* (by Dr. Darren Soanes and Dr. George Littlejohn, University of Exeter), was tagged with GFP and was cloned into the pGWB502 vector (construct generated by Dr. Magdalena Martin-Urdiroz, University of Exeter). OsAra6:GFP appeared as punctate structures closely associated with the plasma membrane in *N. benthamiana* epidermal cells (Figure 3.6A), rice ligules (Figure 3.6B), and barley auricles (Figure 3.6C). This is consistent with previous reports regarding the subcellular localisation of Ara6 (Ueda et al., 2001).

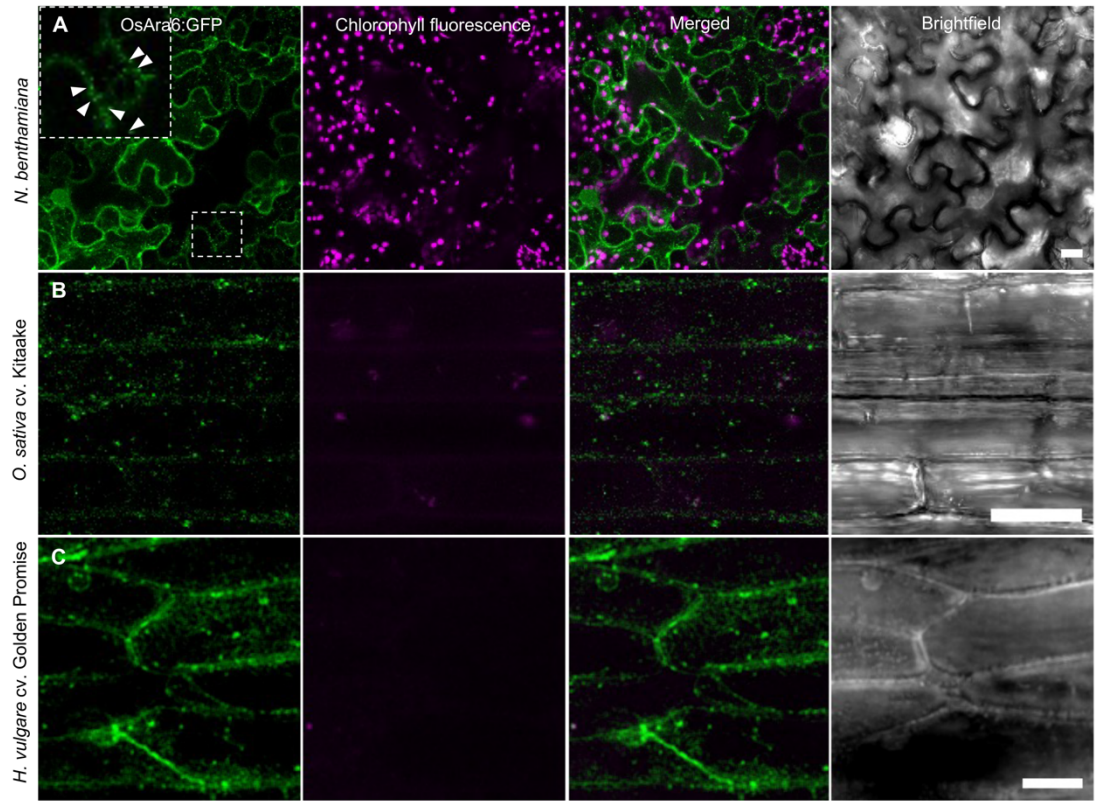

Figure 3.6 Subcellular localisation of the early endosome marker OsAra6:GFP.

A. Confocal micrographs showing transiently expressed early endosome marker OsAra6:GFP in *Nicotiana benthamiana* 72 h after infiltration. Inset shows puncta indicated by white arrowheads. **B.** Confocal micrographs showing early endosome marker OsAra6:GFP expression in rice cv. Kitaake ligule. **C.** Confocal micrographs showing early endosome marker OsAra6:GFP expression in barley cv. Golden Promise auricle. **A-C.** OsAra6:GFP appeared as punctate structures. All images shown are maximum projections of z-stack series taken using Leica TCS SP8X confocal laser scanning microscope. Scale bar = 20 μm.

3.2.2.6 Late endosome marker GFP:Ara7 localises to punctate structures

To visualise late endosomes, Ara7, a well-known late endosome marker, was tagged at the N-terminus with GFP and introduced to the level 2 binary vector pICSL4723. Ara7 is a member of the Rab5 family of small GTPases, which regulate membrane trafficking between different organelles. It localises to multivesicular bodies and is involved in vacuolar trafficking (Jia et al., 2013; Kotzer et al., 2004; Lee et al., 2004; Sohn et al., 2003). GFP:Ara7 appeared as punctate structures distributed within the cytoplasm of *N. benthamiana* (Figure 3.7A), rice ligules (Figure 3.7B), and barley auricles (Figure 3.7C), as previously reported (Jia et al., 2013; Kotzer et al., 2004; Lee et al., 2004; Sohn et al., 2003).

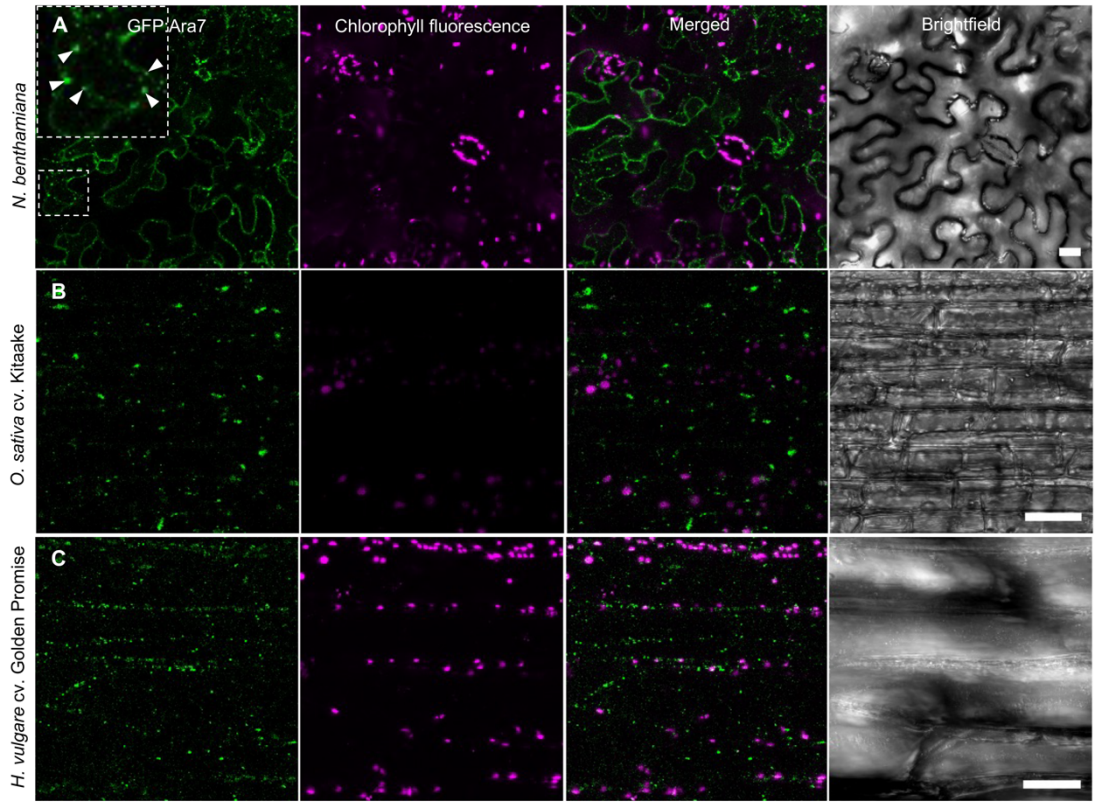

Figure 3.7 Subcellular localisation of the late endosome marker GFP:Ara7.

A. Confocal micrographs showing transiently expressed late endosome marker GFP:Ara7 in *Nicotiana benthamiana* 72 h after infiltration. Inset shows puncta indicated by white arrowheads**. B.** Confocal micrographs showing late endosome marker GFP:Ara7 expression in rice cv. Kitaake ligule. **C.** Confocal micrographs showing late endosome marker GFP:Ara7 expression in barley cv. Golden Promise auricle. **A-C.** GFP:Ara7 appeared as punctate structures. All images shown are maximum projections of z-stack series taken using Leica TCS SP8X confocal laser scanning microscope. Scale bar = 20 μm.

3.2.2.7 Cytoplasmic GFP labels the cytoplasm and the nucleus

To label the cytoplasm, I generated a construct with GFP alone, driven by maize ubiquitin promoter (ZmUbi). Free cytoplasmic GFP fluorescence was observed throughout the entire cell and labelled the nucleus in *N. benthamiana* (Figure 3.8A), rice ligules (Figure 3.8B), and barley auricles (Figure 3.8C).

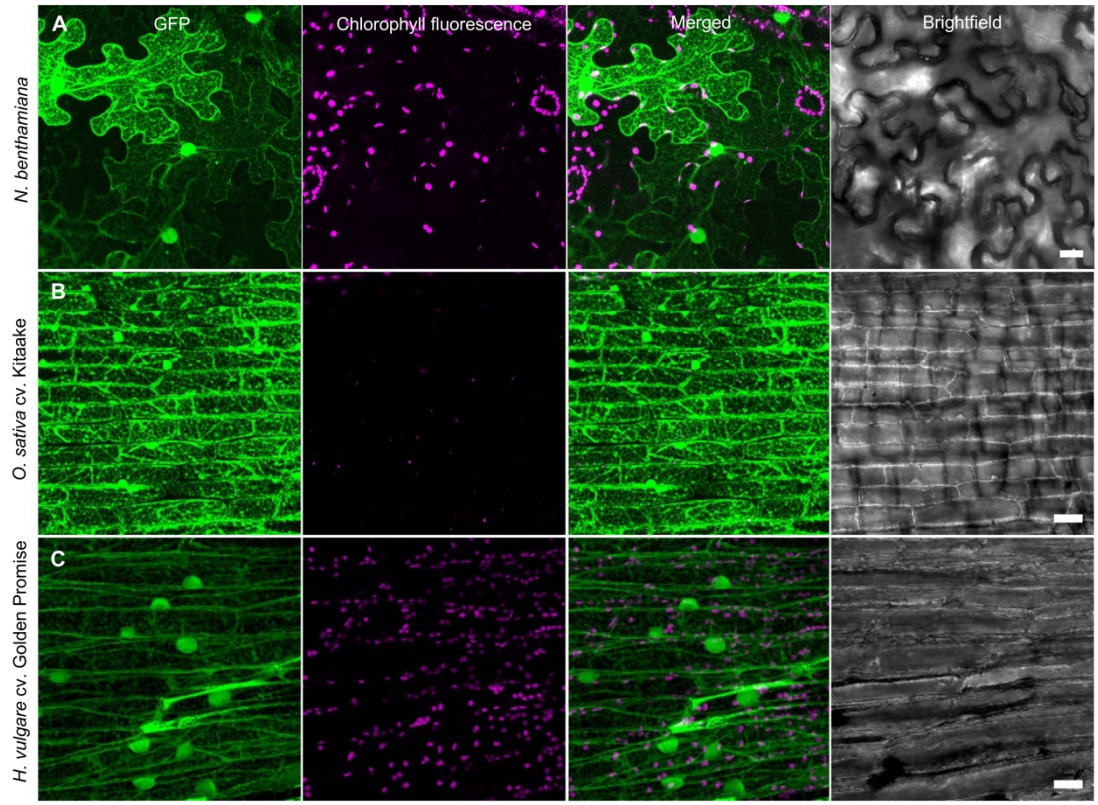

Figure 3.8 Subcellular localisation of free cytoplasmic GFP.

A. Confocal micrographs showing transiently expressed cytoplasmic GFP in *Nicotiana benthamiana* 72 h after infiltration. **B.** Confocal micrographs showing cytoplasmic GFP expression in rice cv. Kitaake ligule. **C.** Confocal micrographs showing cytoplasmic GFP expression in barley cv. Golden Promise auricle. **A-C.** GFP fluorescence appeared in the entirety of the cell and labelled the nucleus. All images shown are maximum projections of z-stack series taken using Leica TCS SP8X confocal laser scanning microscope. Scale bar = 20 μm.

3.2.2.8 Peroxisome marker GFP:PTS1 appears as punctate structures

To label peroxisomes, I tagged peroxisome targeting sequence 1 (PTS1) which consists of the amino acid sequence Serine-Lysine-Leucine (SKL) (Gould et al., 1989; Nelson et al., 2007; Reumann, 2004). GFP:PTS1 appeared as punctate structures in *N. benthamiana* epidermal cells (Figure 3.9A) and rice ligules (Figure 3.9B) consistent with previous reports (Nelson et al., 2007; Stellmach et al., 2022).

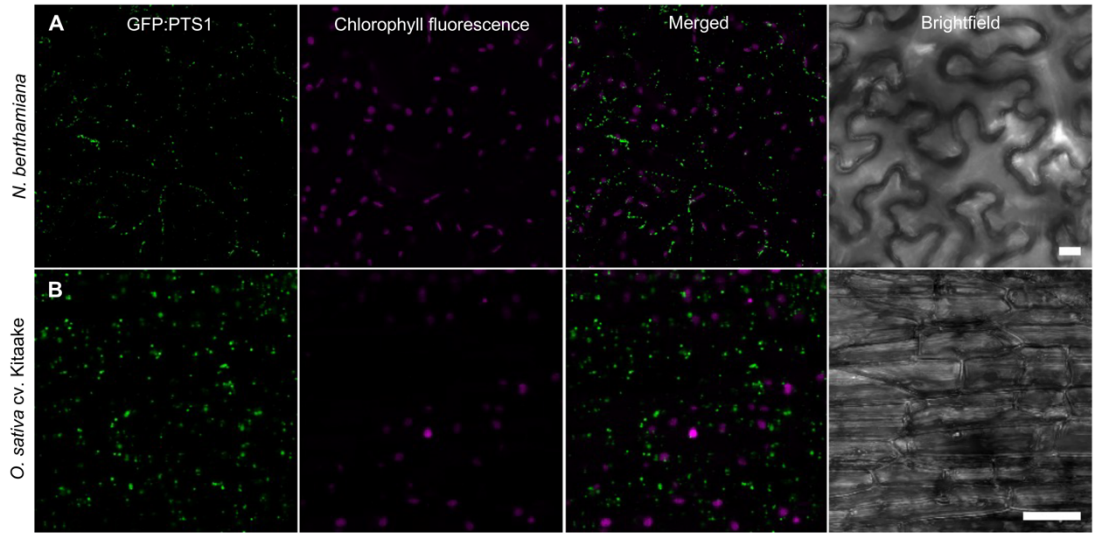

Figure 3.9 Subcellular localisation of peroxisome marker GFP:PTS1.

A. Confocal micrographs showing transiently expressed peroxisome marker GFP:PTS1 in *Nicotiana benthamiana* 72 h after infiltration. **B.** Confocal micrographs showing peroxisome marker GFP:PTS1 expression in rice cv. Kitaake ligule. **A-B.** GFP:PTS1 appeared as dot-like structures distributed within the cell. All images shown are maximum projections of z-stack series taken using Leica TCS SP8X confocal laser scanning microscope. Scale bar = 20 μm.

3.2.2.9 Endoplasmic reticulum marker AtWAK2:GFP:HDEL shows a reticulate pattern

To visualise the endoplasmic reticulum (ER), I positioned the first 30 amino acids of wall-associated kinase 2 (WAK2) from *A. thaliana*, which served as an ER signal peptide, at the N-terminus of GFP, and added the ER retention motif His-Asp-Glu-Leu (HDEL) sequence at the C-terminus. AtWAK2:GFP:HDEL expression displayed reticulated patterns throughout the cytoplasm of *N. benthamiana* (Figure 3.10A) and rice ligule (Figure 3.10B) consistent with previous reports (Chen et al., 2019; Luo & Nakata, 2012; Nelson et al., 2007).

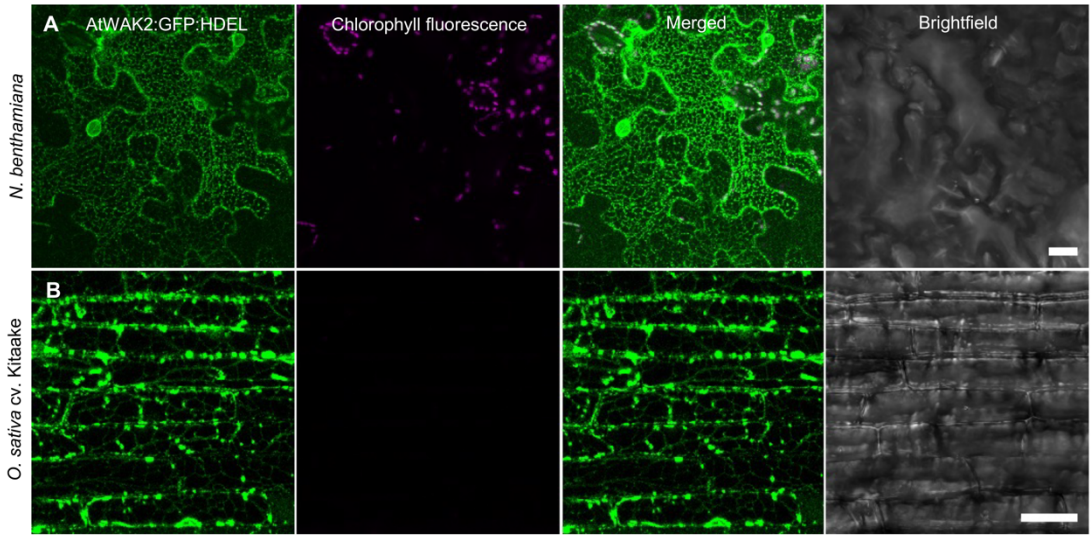

Figure 3.10 Subcellular localisation of endoplasmic reticulum marker AtWAK2:GFP:HDEL.

A. Confocal micrographs showing transiently expressed endoplasmic reticulum marker AtWAK2:GFP:HDEL in *Nicotiana benthamiana* 72 h after infiltration. **B.** Confocal micrographs showing endoplasmic reticulum marker AtWAK2:GFP:HDEL expression in rice cv. Kitaake ligule. **A-B.** AtWAK2:GFP:HDEL labelled reticulate networks in cells. All images shown are maximum projections of z-stack series taken using Leica TCS SP8X confocal laser scanning microscope. Scale bar = 20 μm.

3.2.2.10 Golgi marker STtmd:GFP appears as small round organelles

To label Golgi bodies, I used a readily available construct from Dr. Chris Hawes (Oxford Brookes University) which tagged the signal anchor sequences of a rat sialyltransferase, consisting of a transmembrane domain and short cytoplasmic tail (52 amino acids) of a rat α-2,6-sialyltransferase (STtmd)(Hawes, 2005). When transiently expressed in *N. benthamiana*, STtmd:GFP appeared as small, rounded structures (Figure 3.11A). In rice ligules, in addition to appearing as dot-like structures, the marker also localised around the nucleus (Figure 3.11B). The dot-like appearance of STtmd:GFP is consistent with other studies (Boevink et al., 1998; Saint-Jore et al., 2002). In some cases, Golgi bodies were surrounded by a reticulate network reminiscent of an endoplasmic reticulum (Figure 3.11C). These cases corresponded to fluorescing T_0 lines with two or more construct marker integrations.

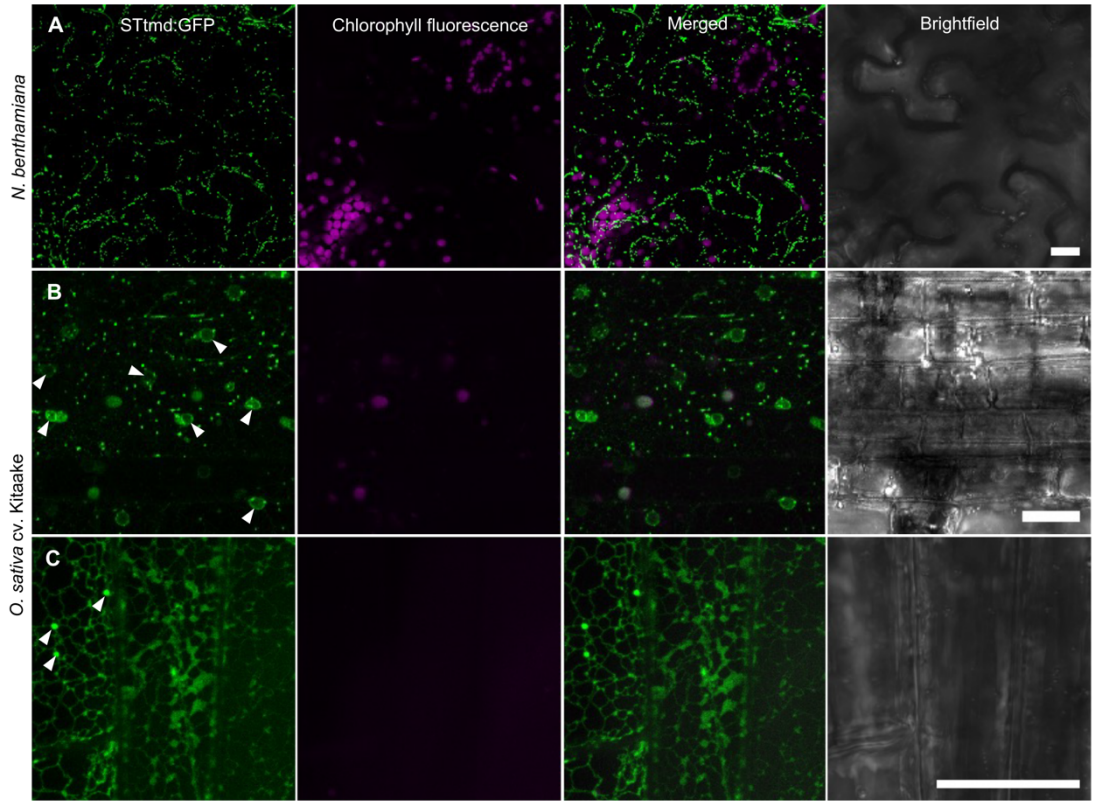

Figure 3.11 Subcellular localisation of Golgi marker STtmd:GFP.

A. Confocal micrographs showing transiently expressed Golgi marker STtmd:GFP in *Nicotiana benthamiana* 72 h after infiltration. STtmd:GFP appeared as dot-like structures. **B.** Confocal micrographs showing Golgi marker STtmd:GFP expression in rice cv. Kitaake ligule. STtmd:GFP appeared as dot-like structures but also localised to the perinuclear-membrane. **C.** Confocal micrographs showing Golgi marker STtmd:GFP expression in rice cv. Kitaake ligule as dot-like structures but surrounded with a reticulate network reminiscent of the endoplasmic reticulum. All images shown are maximum projections of z-stack series taken using Leica TCS SP8X confocal laser scanning microscope. Scale bar = 20 μm.

3.3 Discussion

This chapter reports the development of GFP-based subcellular marker constructs. The markers were designed to label various organelles based on well-established localisation motifs, signal peptides or full-length sequences. These constructs were developed to generate a set of transgenic rice and barley lines to investigate major cellular changes associated with *M. oryzae* infection. Before transforming rice and barley, all subcellular marker constructs were transiently expressed in *N. benthamiana* to ensure correct localisation to the target organelle.

Fluorescence imaging revealed that the organelle marker constructs localised to their expected subcellular compartments when transiently expressed in *N. benthamiana*. These markers were therefore deemed suitable for *Agrobacterium*-mediated transformation in rice

and barley to generate transgenic organelle marker lines. After fluorescence screening of T_0 lines in rice and barley, the localisation and appearance of the subcellular markers in rice and barley were found to be consistent with the localisation observed in *N. benthamiana* and in previous reports.

However, in some cases, the marker correctly labelled the target subcellular compartment but also labelled additional structures. For example, the plasma membrane marker LTI6b TMD:GFP localised to the plasma membrane, outlining cells in *N. benthamiana,* rice and barley. However, in addition to plasma membrane localisation, the marker also outlined the nucleus, which may be caused by overexpression. This peripheral nuclear signal suggests that a pool of LTI6b is associated with the endoplasmic reticulum. A previous rice transgenic line with LTI6b plasma membrane marker does not exhibit the same ER localisation despite using the same CaMV35S promoter (Mentlak et al., 2012). The ER localisation of LTI6b could be attributed to the additional Ω (omega) leader sequence between the CaMV35S promoter and the LTI6b sequence. The Ω leader sequence is a 5' untranslated region (UTR) originally derived from tobacco mosaic virus (TMV) which acts as a translation enhancer (Gallie et al., 1987; Gallie & Walbot, 1992; Goelet et al., 1982; Sleat et al., 1987; Sleat et al., 1988; Takamatsu et al., 1991). The combination of CaMV35S which is a highly constitutive promoter and the Ω leader sequence could overwhelm the ER causing retention. The removal of the Ω leader sequence or the use of a monocot promoter like ZmUbi might help in preventing ER mislocalisation. Nevertheless, the transgenic lines expressing the plasma membrane marker remain useful for our purposes. The Golgi marker STtmd:GFP labelled punctate structures consistent with previous studies (Boevink et al., 1998; Saint-Jore et al., 2002). However, artefacts were observed in fluorescing rice ligules with multiple inserts; aside from dot-like structures, fluorescence signal was also observed surrounding the nucleus and in reticulate networks throughout the cytoplasm. Given the close association between the Golgi and ER, it is possible that the Golgi marker also faintly labelled the ER (Brandizzi et al., 2002). Mislocalisation of Golgi-resident proteins may also result from a very strong promoter (Stellmach et al., 2022). Since the CaMV35S promoter is highly constitutive, exploring alternative promoters may help prevent mislocalisation. Other options include repeating transformation and selecting for single inserts or using other Golgi markers known to work in rice (Chen et al., 2019; Wu et al., 2016).

After T_0 transgenic lines were obtained, fluorescence screening enabled the selection of lines that were fluorescing and exhibited the correct subcellular localisation based on the introduced organelle marker construct. The GFP copy number in these lines was determined by qPCR, facilitating the selection of T_0 lines to advance to T_1. T_0 lines with a single GFP insert were chosen for ease of obtaining stable homozygous T_2 lines. With single integration, segregation is more manageable than with double or multiple inserts. For every subcellular marker, at least one line was suitable for advancement to T_1, except for the Golgi marker transformed in rice. T_0 lines with a single GFP copy were allowed to self-pollinate to obtain T1 seeds. Screening T_1 seeds was made easier by the inclusion of a pFast-Red selection cassette during Golden Gate cloning. All constructs generated via Golden Gate cloning contained the pFast-Red. However, the early endosome, endoplasmic reticulum, and Golgi body marker constructs did not have a pFast-Red selection cassette. Therefore, transgenic lines with these constructs were advanced to T_2 by first planting T_1 seeds, screening rice ligules for fluorescence, and then sampling the positive lines for GFP copy number determination.

It is worth noting that the stable transgenic lines developed did not exhibit any growth phenotypes associated with expression levels and were comparable to the overall phenotype of the background cultivars. During initial screening, several T_0 lines expressing LifeAct:GFP produced sterile seeds. Overexpression of LifeAct-based markers in *Arabidopsis* has previously been reported to cause growth defects (Cvrčková & Oulehlová, 2017), while even moderate expression levels can lead to reduced root growth (Dyachok et al., 2014). LifeAct:GFP T_0 lines that exhibited wild-type morphology and yielded viable seeds were therefore selected and advanced to the next generations.

In summary, I have developed constructs to enable visualisation of different organelles, including the plasma membrane, actin cytoskeleton, mitochondria, nucleus, late endosome, cytoplasm, and peroxisome. Constructs for the early endosome (generated by Dr. Magdalena Martin-Urdiroz) and Golgi bodies (from Dr. Chris Hawes) were readily available in the lab. All these marker constructs were suitable for transient expression in *N. benthamiana*, with their localisations confirmed before introducing them into rice cv. Kitaake and barley cv. Golden Promise. I have generated transgenic rice and barley lines expressing individual subcellular markers. The set of Kitaake transgenic lines are valuable tools for investigating both compatible and incompatible interactions with *M. oryzae*. The

set of Golden Promise transgenic lines will also be useful in host-pathogen and other localisation studies.

Chapter 4 Rice plasma membrane dynamics during *Magnaporthe oryzae* infection

4.1 Introduction

Magnaporthe oryzae has a hemibiotrophic lifestyle. During the biotrophic phase, *M. oryzae* enters the host surface using a specialised infection structure called an appressorium (Hamer et al., 1988; Ryder & Talbot, 2015; Talbot, 2003), which generates mechanical force to breach the host cuticle and cell wall, forming a penetration peg to facilitate fungal entry into host cells (de Jong et al., 1997; Ryder & Talbot, 2015). The penetration peg then expands to form a filamentous primary hypha which then subsequently develops into a bulbous invasive hypha (IH). The bulbous IH fills the first-invaded cell before it uses pit fields containing plasmodesmata (PD) to colonise neighbouring cells (Kankanala et al., 2007; Sakulkoo et al., 2018).A pivotal aspect of the *M. oryzae*-rice interaction is the dynamic behaviour of the rice plasma membrane (PM) during the biotrophic stage of infection, where the PM undergoes significant remodelling to accommodate IH. Central to this interaction are specialized structures which are known to be host PM-derived namely, the extra-invasive hyphal membrane (EIHM) (Fernandez & Orth, 2018; Kankanala et al., 2007; Khang et al., 2010) and the biotrophic interfacial complex (BIC) (Fernandez & Orth, 2018; Giraldo et al., 2013; Khang et al., 2010), which play critical roles in facilitating pathogen invasion and effector delivery (Fernandez & Orth, 2018; Giraldo et al., 2013; Jones et al., 2021; Khang et al., 2010).

As *M. oryzae* invades rice cells, the host PM invaginates to surround IH, forming the EIHM. This plant-derived membrane structure delineates the interface between the host cytoplasm and fungal cell wall (Kankanala et al., 2007; Mentlak et al., 2012). The EIHM creates an apoplastic compartment between the IH and the host cytoplasm called the extra-invasive hyphal matrix (EIHMx) where apoplastic effectors such as Slp1 (Mentlak et al., 2012), Bas4 (Mosquera et al., 2009) and Mep1 (Yan & Talbot, 2016; X. Yan et al., 2023) reside during the biotrophic phase (Fernandez & Orth, 2018; Kankanala et al., 2007).

The BIC is a highly localised, host membrane-derived structure found at the EIHM. The BIC, forms from 22 hours post-inoculation (hpi) during biotrophic growth, and undergoes a two-stage development (Khang et al., 2010). First, a tip BIC is strategically positioned at the tip of a primary hypha. As the primary hypha transitions into a bulbous invasive hypha, the BIC then becomes situated subapically at the BIC-associated cell, and is thus termed a side BIC (Khang et al., 2010). Evidence suggests that the BIC is the site of translocation for cytoplasmic effectors such as Pwl2 (Pathogenicity towards Weeping Lovegrass2) (Giraldo et al., 2013; Khang et al., 2010; Were et al., 2025; S. Zhang & J. R. Xu, 2014), BAS1 (Giraldo et al., 2013; Khang et al., 2010; Oliveira-Garcia & Hamilton, 2024; Oliveira-Garcia et al., 2023) and Avr-Pita1 (Khang et al., 2010) into host cells.
From its initial biotrophic phase, *M. oryzae* later transitions to a necrotrophic stage when it acquires nutrients from dead host cells. When the fungus invades beyond initially-invaded host cell and moves to adjacent cells, the initially colonised cells appear to lose viability, as confirmed by plasmolysis assays (Kankanala et al., 2007). Disruption of the EIHM has also been shown to correlate with the transition from biotrophic to necrotrophic growth phases of *M. oryzae*, highlighting its importance in maintaining the initial biotrophic association (Jones et al., 2021). Additionally, host vacuole integrity is necessary to maintain biotrophy and aid successful invasion (Mochizuki et al., 2015). Previous studies have provided evidence that disease resistance or susceptibility depends on cellular processes preceding cell death depending on the pathogen, and that the vacuole has a central role in such processes (Coll et al., 2011; Dickman & Fluhr, 2013; Hatsugai et al., 2009; Hatsugai et al., 2004; Hirakawa et al., 2015) . Biotrophic pathogens, which rely on living host tissue for survival, often attempt to suppress programmed cell death (PCD) and manipulate host defence signalling to establish infection (Glazebrook, 2005). In contrast, necrotrophic pathogens benefit from host cell death, as they feed on dead and decaying tissue, often actively inducing necrosis through toxin production or by hijacking plant defence mechanisms. For hemibiotrophic pathogens, the timing and regulation of cell death are critical for determining resistance or susceptibility (Glazebrook, 2005).

Cytological studies have been performed in rice leaf sheath infections to look at development of the EIHM and the BIC (Giraldo et al., 2013; Kankanala et al., 2007; Khang et al., 2010; Koga, 1994; Koga et al., 2004; Mentlak et al., 2012), but we have

limited knowledge of whether these host PM-derived structures are always present during the biotrophic phase of infection and how consistently they are observed.

In this chapter, I set out to define the spatial and temporal changes at the host plasma membrane during *M. oryzae* infection while focusing on formation and disruption of the EIHM, and development of the BIC. I expand previous findings regarding the BIC and the EIHM using a rice cv Kitaake transgenic line which I developed that expresses a Low-temperature induced protein 6b fused to green fluorescent protein (LTI6b TMD:GFP) (Kurup et al., 2005) to directly examine the host PM-fungal interface. Here, I show the formation of these structures in initially invaded cells and adjacent rice cells. I also define the relationship between host PM integrity and cell viability in a time course of fungal invasion of the first cell to colonisation of adjacent cells using fluorescein diacetate (FDA), a cell viability marker. Taken together, these findings provide evidence that the EIHM and BIC both form during the biotrophic phase but that the EIHM breaks down rapidly when adjacent cells are colonised by *M. oryzae*.

4.2 Results

4.2.1 Ribosomal protein 27 promoter (RP27p) enables stable expression in *Magnaporthe oryzae* strain Guy11 for time-course experiments

To examine invasive growth of the rice blast fungus during infection time-course experiments, a reliable fungal marker was required to visualise the fungal cytoplasm from early to late biotrophic growth, as well as during cell-to-cell movement. To generate a reliable fluorescent fungal marker, I used tdTomato, a DsRed-derived orange fluorescent protein with low acid sensitivity (Shaner et al., 2004), which has been employed in previous rice blast studies involving time-series experiments (Jones et al., 2016; Jones et al., 2021). Using tdTomato could yield potentially stable fluorescence even at later time points. Four different promoters namely α-tubulin (MGG_06650), Mep1, *M. oryzae* ribosomal protein 27 (RP27), and trpC were used to create constructs that drive the expression of tdTomato. The generated constructs are illustrated in Figure 4.1A. Positive clones harbouring the 1428 bp tdTomato fragment were confirmed by PCR using the primer pair tdTomato-F/tdtomato-R and further validated by sequencing with primers pSCBAR-F and pSCBAR-R to ensure correct assembly (Figure 4.1B). These constructs were used to transform *M. oryzae* strain Guy11, identifying the brightest, most stable fungal transformants for live cell imaging. All promoters successfully drove tdTomato

expression in both conidia (Figure 4.2A) and IH (Figure 4.2B), but the RP27 promoter resulted in the brightest expression of tdTomato in both conidia and IH. To test whether RP27p:tdTomato expression remains stable at latter time points, I performed a leaf sheath infection assay using rice cv CO39 and checked expression at 48 and 72 hours post-inoculation (dpi). At both time points, RP27p:tdTomato expression delineated the limits of fungal cytoplasm during *M. oryzae* invasive growth. Guy11 expressing RP27p:tdTomato was subsequently used for visualising intracellular fungal growth in rice-*M. oryzae* time series experiments.

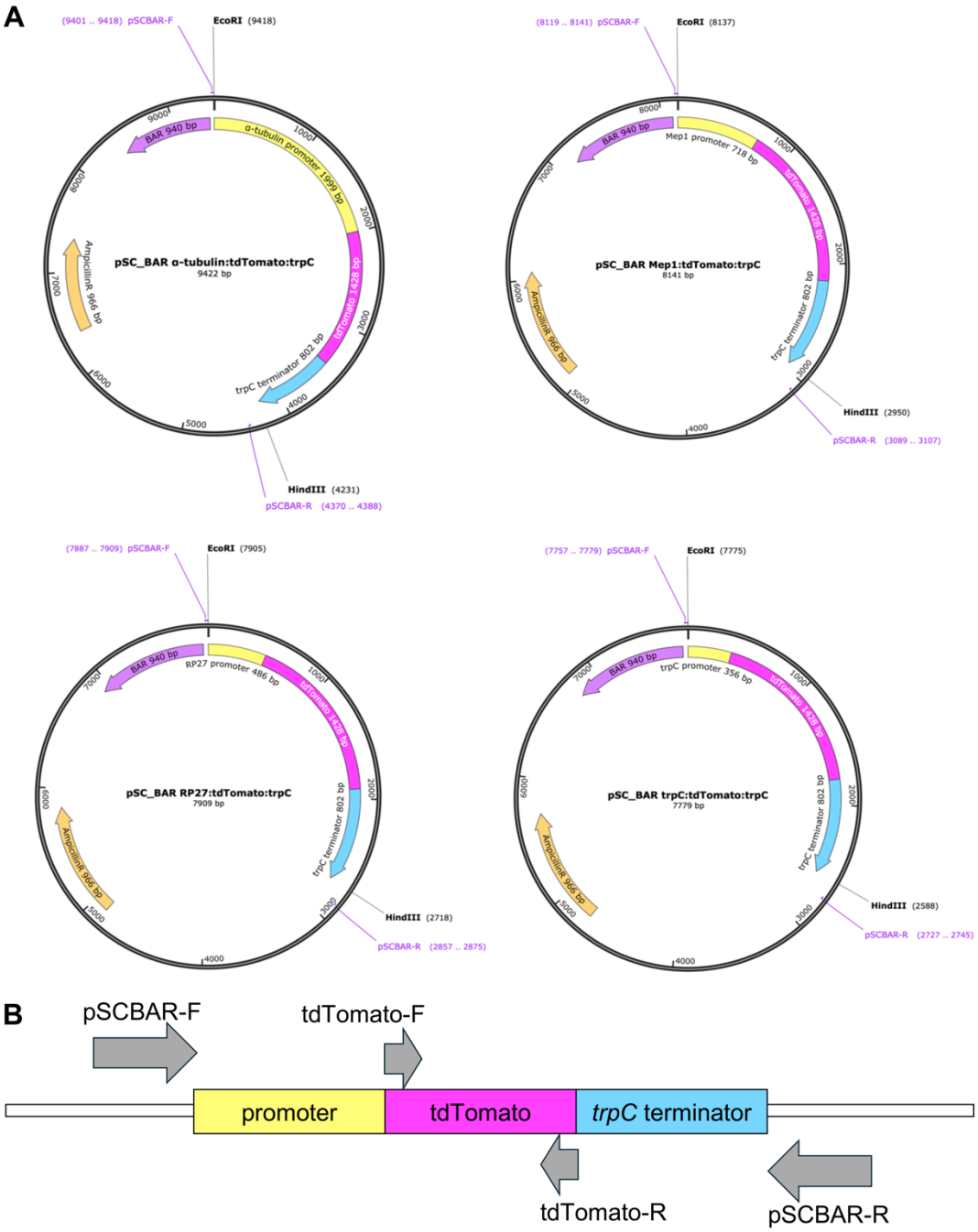

Figure 4.1 Generation of tdTomato vectors with different promoters to select a suitable construct that would enable fluorescent protein expression in *Magnaporthe oryzae* for visualisation of the fungus during plant infection.

A. Constructs of DsRed-derivative tdTomato driven by different promoters were assembled via In-fusion cloning using a linearized pSCBAR vector (Lindsay et al., 2016). Construct maps were exported from the software SnapGene® (from Dotmatics; available at snapgene.com). **B.** Schematic representation of the amplified tdTomato region (1428 bp) for selection of positive clones using primer pair tdTomato-F/tdTomato-R and sequenced region to confirm correct construct assembly using pSCBAR-F and pSCBAR-R.

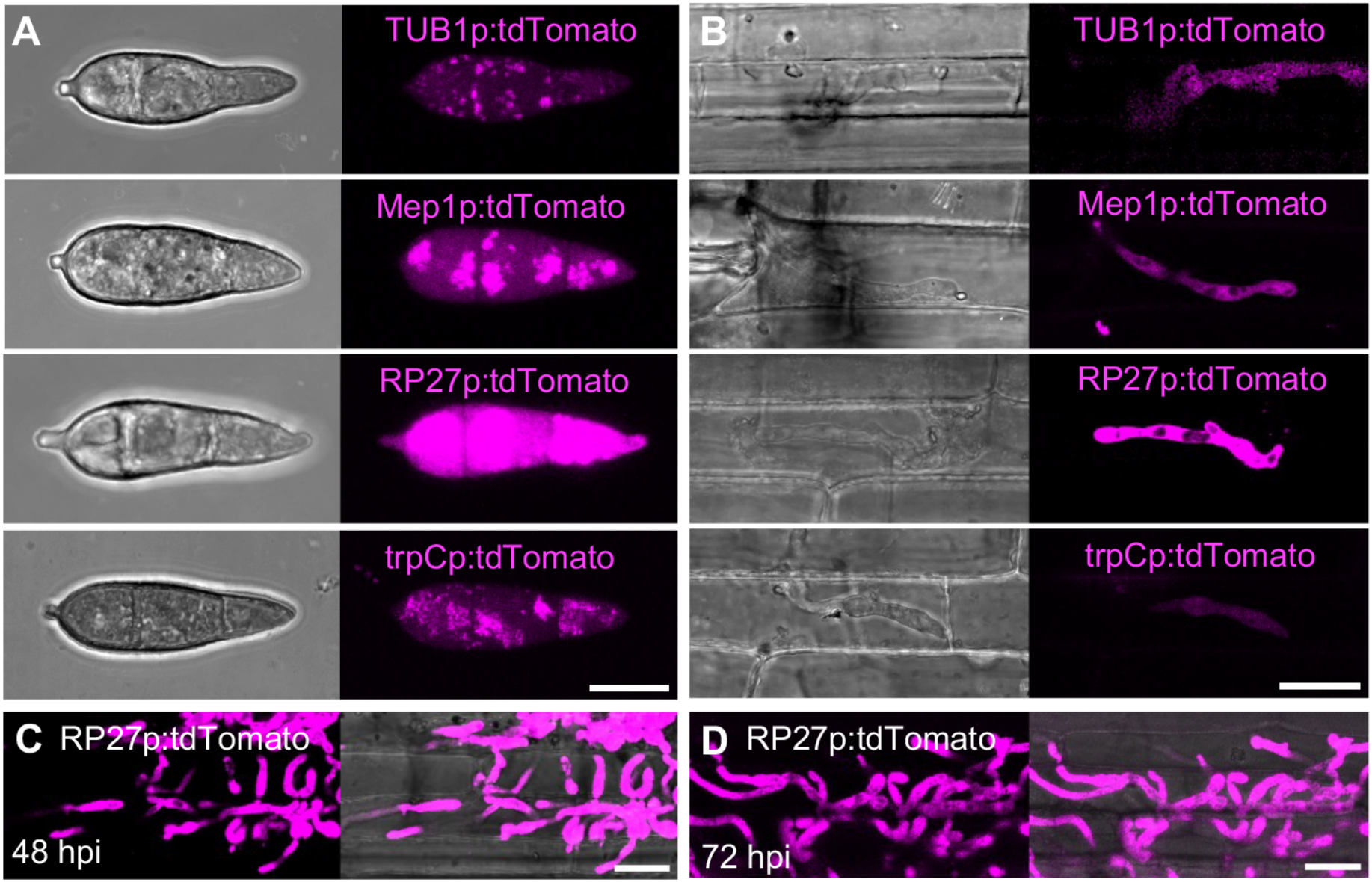
A
TUB1p:tdTomato
Mep1p:tdTomato
RP27p:tdTomato
trpCp:tdTomato
B
TUB1p:tdTomato
Mep1p:tdTomato
RP27p:tdTomato
trpCp:tdTomato
C RP27p:tdTomato
48 hpi
D RP27p:tdTomato
72 hpi

Figure 4.2 The ribosomal protein 27 (RP27p) enables stable tdTomato expression in *Magnaporthe oryzae* Guy11 strain for rice leaf sheath infection time-course experiments.

A. Confocal micrographs of *M. oryzae* Guy11 transformants expressing tdTomato driven by different promoters in conidia. Scale bar = 10 μm. **B.** Confocal micrograph of *M. oryzae* Guy11 expressing tdTomato driven by different promoters in invasive hyphae at 24 hours post-inoculation (hpi) on rice cv CO39. Scale bar = 20 μm. **C.** Confocal images of invasive hyphae at the margins of infection at 48 hpi on rice cv CO39 inoculated with *M. oryzae* Guy11 expressing RP27p:tdTomato. Scale bar = 20 μm. **D.** Confocal images of invasive hyphae at the margins of infection at 72 hpi on rice cv CO39 inoculated with *M. oryzae* Guy11 expressing RP27p:tdTomato. Scale bar = 20 μm. Leaf sheath infections for all time points were incubated at 24 °C. All micrograph shown are maximum projections of z-stack series taken using a Leica TCS SP8X confocal laser scanning microscope

4.2.2 The extra-invasive hyohal membrane (EIHM) is formed and subsequently disrupted during *Magnaporthe oryzae* infection

M. oryzae invasive hyphae have been reported to be sealed in a distinct compartment of the rice plasma membrane called the extra-invasive hyphal membrane (EIHM) (Kankanala et al., 2007). The EIHM prevents FM4-64, an endocytic marker, from reaching the fungal plasma membrane suggesting that the invasive hypha is enveloped in a separate compartment of the host plasma membrane (Kankanala et al., 2007). To confirm this finding, I generated a rice cv Kitaake transgenic line expressing the transmembrane domain of the aquaporin Low-temperature induced protein 6b (LTI6b) fused to green fluorescent protein (LTI6b TMD:GFP) (Kurup et al., 2005) in which GFP is targeted to the plasma membrane, and infected this transgenic line with *M. oryzae* strain Guy11 expressing RP27p:tdTomato. At 24 hpi when the fungus invades the first host cell, I observed that the rice PM invaginates and appears as an intact, tight outline around the IH (Figure 4.3A). However, by 36 hpi when the fungus has already invaded the immediate neighbouring cell, the EIHM in the first-invaded cell appears to be disorganized and disrupted. Quantification of the intact EIHM in first-invaded cells at 24 hpi confirmed that the intact EIHM is always produced during infection but is disrupted after the fungus invades the neighbouring cells at 36 hpi (Figure 4.3B). Quantifying the percentage of intact EIHM in the first-invaded rice cells showed that all infected cells have intact EIHMs at 24 hpi but disrupted EIHMs by 36 hpi (Figure 4.3C). In newly invaded cells, the rice plasma membrane once again invaginates to form an EIHM around new invasive hyphae (Figure 4.3D).

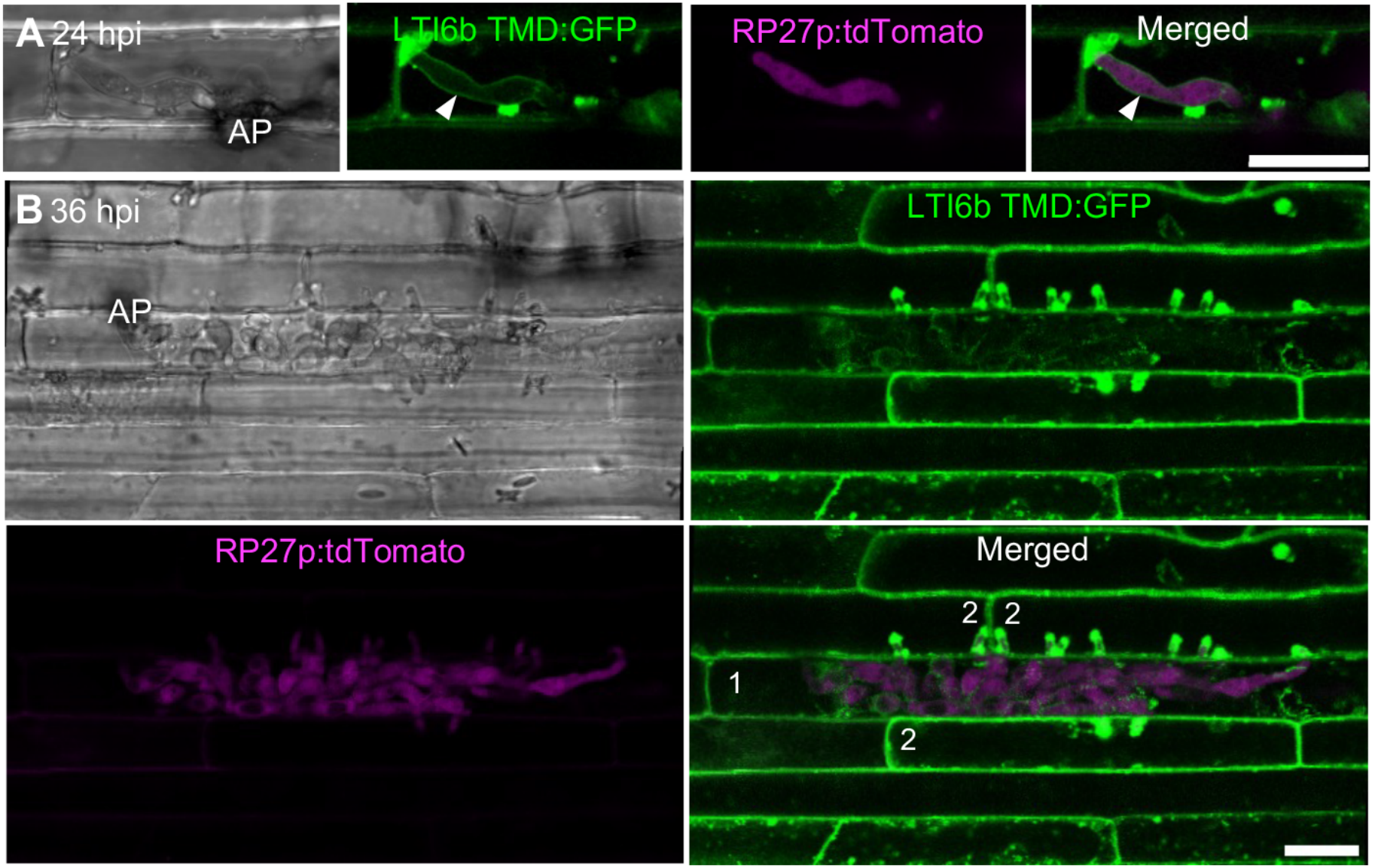
A 24 hpi
AP
LTI6b TMD:GFP
RP27p:tdTomato
Merged
B 36 hpi
AP
LTI6b TMD:GFP
RP27p:tdTomato
Merged
2
2
1
2

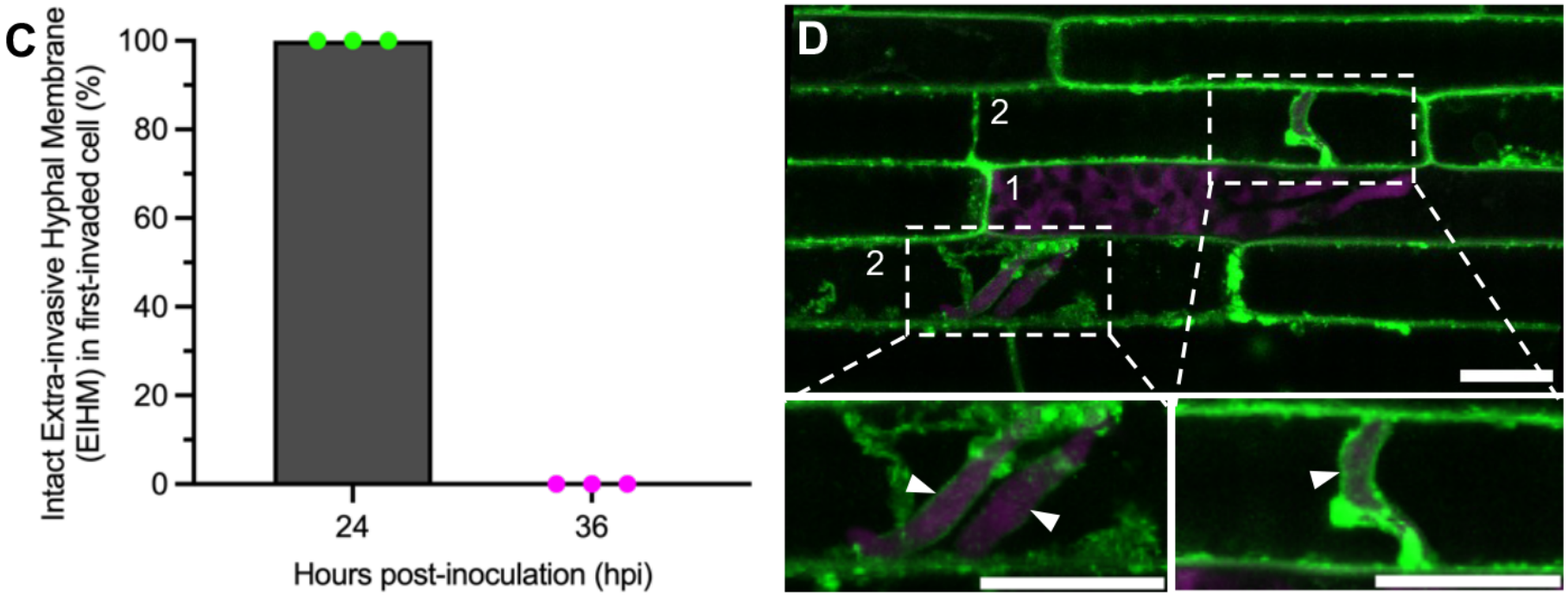

Figure 4.3 The extra-invasive hyphal membrane (EIHM), an invagination of the rice plasma membrane, is formed and subsequently disrupted during *Magnaporthe oryzae* infection.

A. Invasive hyphae (magenta) are enclosed within the intact extra-invasive hyphal membrane (green) at 24 hours post-inoculation (hpi). **B.** The EIHM becomes disrupted in initially invaded cell by 36 hpi. Numbers indicate the order in which the fungus invades the rice cells. **C.** Bar charts quantifying the percentage of intact EIHM within first-invaded cells based on the mean from three biological replicates (n = 50 infection sites per biological replicate; data points show means of individual replicates; error bars indicate the standard deviation). **D.** Invasive hyphae produced in newly invaded cells are once again enclosed within the EIHM. Enlarged views of IH in adjacent cells are shown in the insets. Confocal micrographs were prepared from leaf sheath inoculations using rice cv Kitaake transgenic lines expressing the plasma membrane marker LTI6b TMD:GFP (green) and infected with *M. oryzae* Guy11 RP27p:tdTomato. Leaf sheath infections for all time points were incubated at 24 °C. All images shown are maximum projections of z-stack series recorded using a Leica TCS SP8X confocal laser scanning microscope. Scale bar = 20 μm.

4.2.3 The rice plasma membrane in initially invaded cells maintains integrity during early infection but is disrupted after *Magnaporthe oryzae* invades neighbouring rice cells

To investigate the loss of PM integrity during *M. oryzae* infection more clearly, I carried out plasmolysis assays on infected cells. Intact plasma membrane retains the ability to plasmolyse but disrupted cells lose their ability to plasmolyse (Kankanala et al., 2007; Koga et al., 2004). Using a rice cv Kitaake transgenic line expressing the plasma membrane marker, LTI6b TMD:GFP, healthy, uninfected rice cells mounted in 0.75M sucrose result in plasmolysed cells where the PM recedes from the cell wall due to hyperosmotic conditions outside the cell (Figure 4.4A). During early infection at 24hpi, infected rice cells were fully plasmolysed (100%) consistent with our previous finding that IH are enveloped by an intact PM (Figures 4.4B and D). However, by 36 hpi when the fungus invades neighbouring cells, the initially invaded cells already fail to plasmolyse indicating loss of host PM integrity (see Figures 4.4C and D). It is worth noting that the retracting protoplast shrank around IH (Figure 4.4B) and that this process is repeated each time the fungus invades neighbouring cells (see Figure 4.4C).

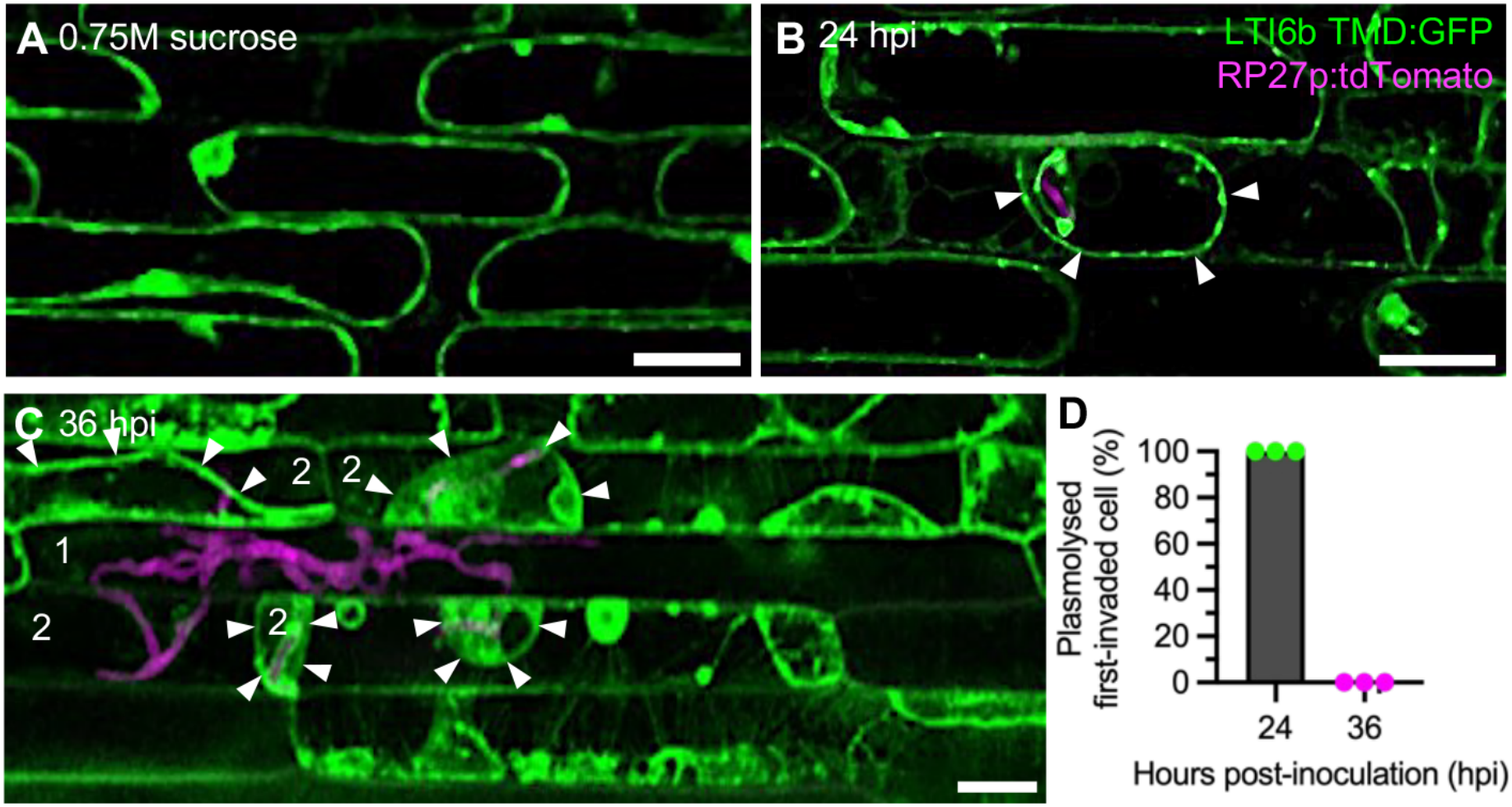
A 0.75M sucrose
B 24 hpi
LTI6b TMD:GFP
RP27p:tdTomato
C 36 hpi
1
2
2
2
2
D
Plasmolysed first-invaded cell (%)
100
80
60
40
20
0
24
36
Hours post-inoculation (hpi)

Figure 4.4 The rice plasma membrane in initially invaded cells maintains integrity during early infection but is disrupted after *Magnaporthe oryzae* invades neighbouring cells.

A. Plasmolysed cells of uninfected rice cv Kitaake transgenic line LTI6b TMD:GFP were mounted in 0.75M sucrose. **B.** Plasmolysed initially infected cell indicates intactness of the rice PM at 24 hpi. **C.** Initially invaded cell loses the ability to plasmolyse after the fungus has invaded neighbouring cells due to loss of PM integrity. Numbers indicate the order in which the fungus invades host cells (1=first-invaded cell, 2=second-invaded cell). White arrowheads indicate the shifting of rice plasma membrane away from the cell wall during plasmolysis. Confocal micrographs were prepared from leaf sheath inoculations using rice cv Kitaake transgenic lines expressing plasma membrane marker LTI6b TMD:GFP (green) and infected with *M. oryzae* Guy11 RP27p:tdTomato. Leaf sheath infections for all time points were incubated at 24 °C. All images shown are maximum projections of z-stack series taken using a Leica TCS SP8X confocal laser scanning microscope. Scale bars = 20 μm. **D.** Bar charts to quantify the percentage of plasmolysed first-invaded cells using 0.75M sucrose based on means from three biological replicates (n = 50 infection sites per biological replicate; data points show means of the individual replicates; error bars indicate the standard deviation.).

4.2.4 Fluorescein staining patterns reveal cytological changes preceding cell death in *Magnaporthe oryzae*-infected rice cells

First-invaded rice cells show intact PM during the early biotrophic stage at 24 hpi but lose PM integrity by 36 hpi when the fungus invades neighbouring cells. However, the time at which infected rice cells lose viability is still unclear, and it is not clear whether the loss of host PM integrity directly equates to loss of cell viability. To assess cell viability and its relation to loss of PM integrity during rice blast infection, I therefore used fluorescein diacetate as a cell viability indicator. Fluorescein diacetate (FDA) is a fluorogenic ester compound that passes through intact plasma membrane and is hydrolysed by intracellular esterases (Figure 4.5A) to produce membrane-impermeable fluorescein which has green fluorescence (Figures 4.5B and C) (adapted from Jones et al., 2016). FDA can therefore serve as an assay for cell viability and show cells that are metabolically active. Dead cells lack fluorescence due to the absence of fluorescein production. In addition, FDA staining can also visualise vacuoles because negatively charged fluorescein selectively accumulates in the cytoplasm but is excluded from the vacuole (Kovarvík & Fojtová, 1999; Saruyama et al., 2013; Steward et al., 1999).

I infected wild type rice cv Kitaake with *M. oryzae* strain Guy11 expressing RP27p:tdTomato, and mounted trimmed infected leaf sheaths in FDA solution (2 μg/mL in 0.2% acetone). At 24 hpi when the fungus has started to invade the first cell, typical cytoplasmic fluorescein was observed in all infected cells upon staining with FDA (Figures 4.6A and 4.7) similar to previous findings that reported that infected cells at this stage are viable (VC) and blast infections are therefore biotrophic in nature (Jones et al., 2016; Kankanala et al., 2007; Koga et al., 2004). By 28 hpi, although more than half of the infected cells are still viable, we started to observe novel fluorescein patterns indicating shrunken (SV) and ruptured (RV) vacuoles (Figures 4.6B and 4.7). Brighter fluorescence was observed in cells with shrunken vacuoles due to enlarged cytoplasm as the fungus occupies more space causing the vacuole to shrink, and for more fluorescein to be accommodated (Mochizuki et al., 2015). Infected cells with ruptured vacuoles were characterized with fluorescein occupying the entirety of the cell (Figure 4.6B). By 32 hpi, the number of viable cells and cells with shrunken vacuoles declined while more cells exhibited ruptured vacuoles (Figures 4.6C and 4.7). As the infection progresses to

neighbouring cells by 36 hpi, most initially invaded cells (84%) exhibited ruptured vacuoles (Figures 4.6D and 4.7). We also started to observe dead cells characterized by a lack of fluorescein fluorescence in the cytoplasm (Figures 4.6E and 4.7). By 48 hpi when the fungus has already infected up to three cells away from the first-invaded cell, the number of cells with ruptured vacuoles declined sharply (~9%) as most initially invaded cells at this stage were not viable (~91%) (Figures 4.6F and 4.7).

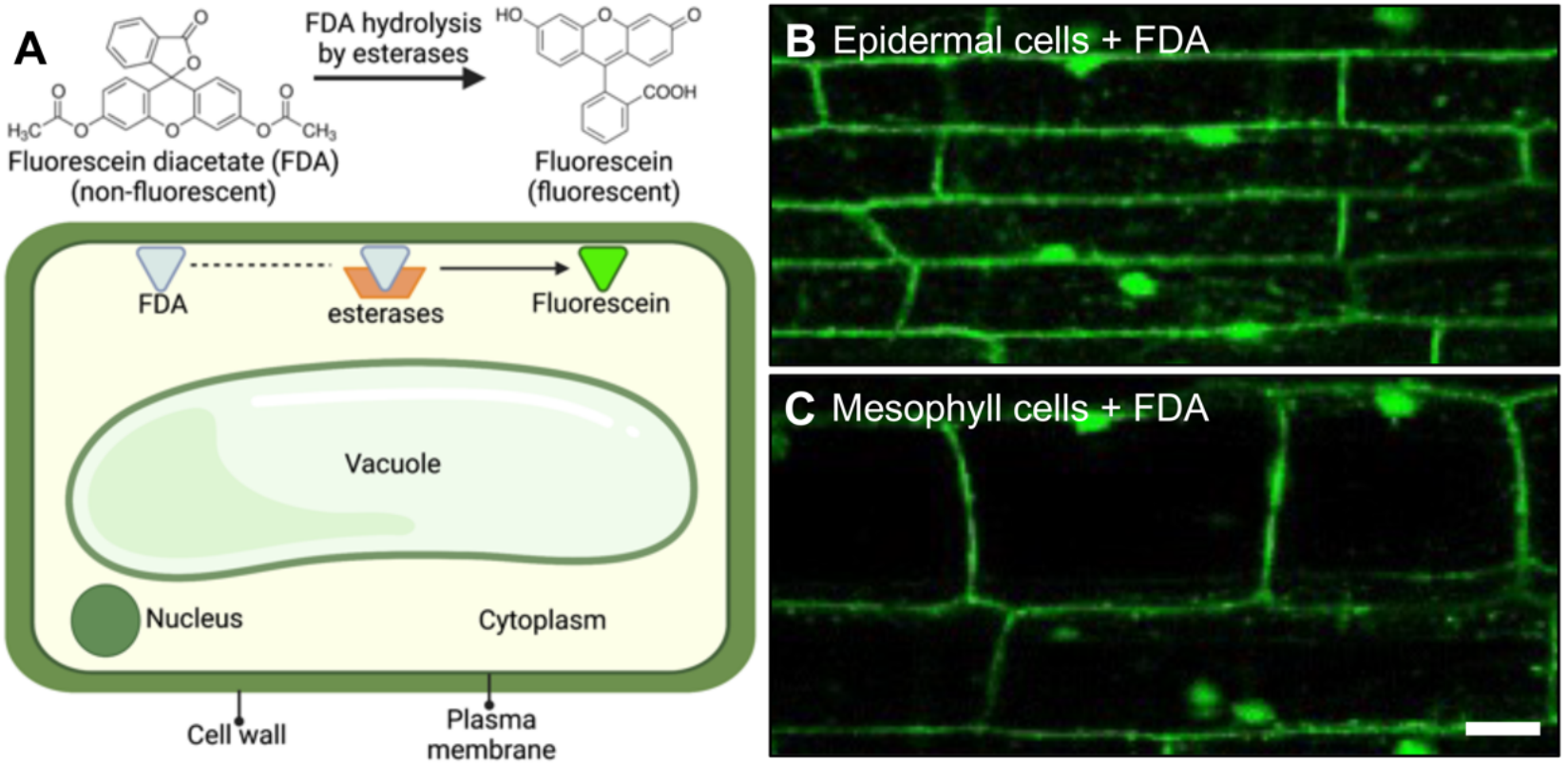

Figure 4.5 Fluorescein diacetate (FDA) is an indicator of cell viability.

A. Diagram showing how fluorescein diacetate is used to assay cell viability. FDA molecules which are non-fluorescent pass through the intact plasma membrane. Upon entering the cell, intracellular esterases hydrolyse FDA molecules, converting them to fluorescein, which is fluorescent. Membrane-impermeable fluorescein accumulates and is retained in the cytoplasm. Diagram adapted from Jones et al. (2016) and created with BioRender.com. **B.** Single plane confocal image of rice sheath epidermal cells. C. Single plane confocal image of immediately underlying rice leaf sheath mesophyll cells. Scale bar = 20 μm. Reproduced from Jones et al. (2016).

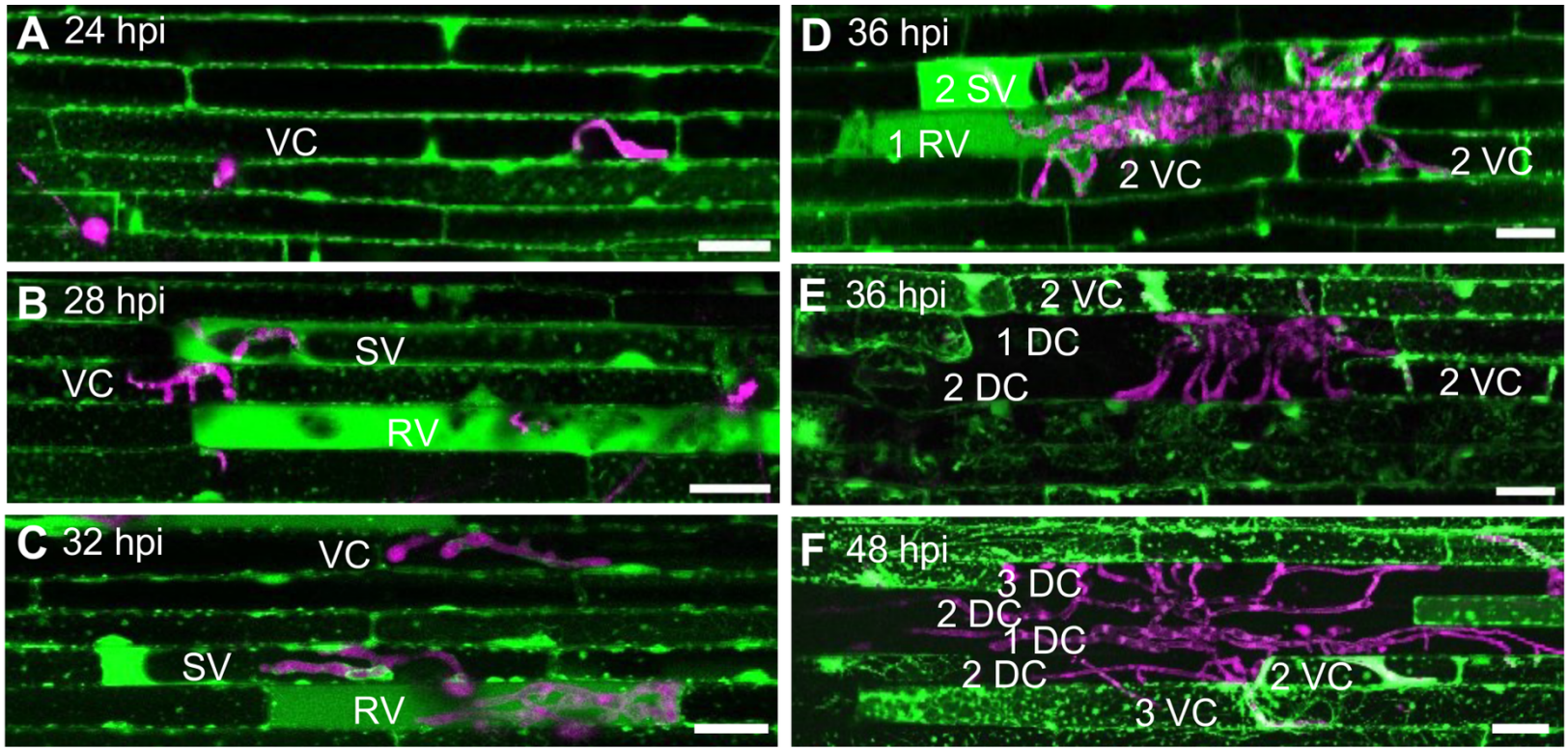

Figure 4.6 Fluorescein staining pattern reveals cytological changes preceding cell death in *Magnaporthe oryzae*-infected rice cells.

A. Fluorescein diacetate (FDA)-derived fluorescein stains the cytoplasm of viable cells (VC) indicating an intact plasma membrane. Typical fluorescein pattern observed in initially invaded cells at 24 hours post-inoculation (hpi). **B.** Cells with shrunken (SV) and ruptured vacuoles (RV) appeared at 28 hpi. Shrunken vacuoles cause more fluorescein accumulation in the cytoplasm while ruptured vacuoles result in fluorescein uptake by the entire cell. **C.** By 32 hpi, viable cells, cells with shrunken and ruptured vacuoles were still observed. **D-E.** By 36 hpi, as the fungus invades neighbouring cells, initially invaded cells appeared to have ruptured vacuoles (D) while others were already dead (DC) (E). **F.** By 48 hpi, initially invaded cells are mostly dead as the infection becomes more advanced. Numbers indicate the order by which the fungus invades the host cells. Confocal images were prepared from leaf sheath inoculations using rice cv. Kitaake stained with FDA (green) and infected with *M. oryzae* Guy11 expressing RP27p:tdTomato (magenta). Leaf sheath infections for all time points were incubated at 24 °C. All images shown are maximum projections of z-stack series taken using a Leica TCS SP8X confocal laser scanning microscope. Scale bars = 20 μm.

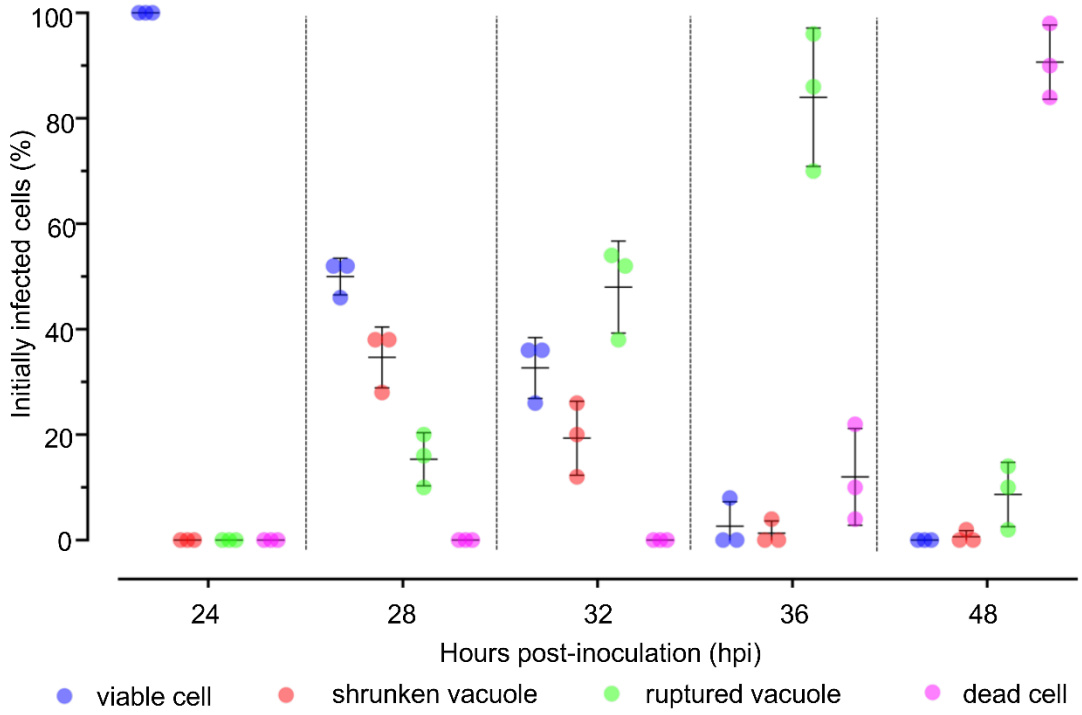

Figure 4.7 Quantification of fluorescein staining pattern cell types in initially invaded cell reflect the sequence of cytological changes preceding cell death during *Magnaporthe oryzae* infection.

Scatter plot showing the mean percentage of initially infected cells showing different cell types based on their fluorescein staining patterns in initially invaded cells. Counts of initially invaded cells which are viable, with shrunken vacuoles, ruptured vacuoles, or non-viable, were recorded to track at which point initially invaded cells begin to undergo cell death and to observe which cells type based on fluorescein staining was prevalent during a course of infection. The scatter plot shows the mean from three biological replicates (n = 50 infection sites per biological replicate; data points show means of individual replicates); error bars indicate the standard deviation.

4.2.5 The rice plasma membrane accumulates at the biotrophic interfacial complex (BIC)

The biotrophic interfacial complex (BIC) is a distinctive, host PM-derived structure (Giraldo et al., 2013) which undergoes two stages of development. Initially, it is found as a 'tip BIC' which is situated at the tip of a primary IH as a membranous cap, which subsequently develops into a 'side BIC' which is positioned subapically as the invasive hypha grows inside the host cell (Khang et al., 2010). The BIC appeared to be a site of cytoplasmic effector delivery in host cells based on several lines of evidence (Mentlak et al., 2012). Using fluorescently labelled cytoplasmic effectors, punctate structures at the outer dome-shaped BIC region were observed and named membranous effector compartments (MECs) (Oliveira-Garcia et al., 2023). I further demonstrated the plant

membrane-rich nature of the BIC using rice cv Kitaake transgenic line expressing the plasma membrane marker LTI6b TMD:GFP and infecting with *M. oryzae* Guy11 expressing fluorescent cytoplasmic effector Pwl2:mRFP, enabling simultaneous imaging of the rice PM and cytoplasmic effector to locate the BIC. First, I confirmed two-stage development of the BIC (Movie 4.1) as reported previously (Khang et al., 2010) as shown in Figure 4.8A. LTI6b TMD:GFP accumulates at the BIC where Pwl2:mRFP puncta could also be observed. Furthermore, fluorescence intensity distribution line scans of both LTI6b TMD:GFP and Pwl2;mRFP signals in individual BIC z-stack slices indicate physical association of the BIC and rice PM (Figure 4.8B) confirming previous findings that the BIC is a host plasma membrane-derived structure (Giraldo et al., 2013; Oliveira-Garcia et al., 2023).

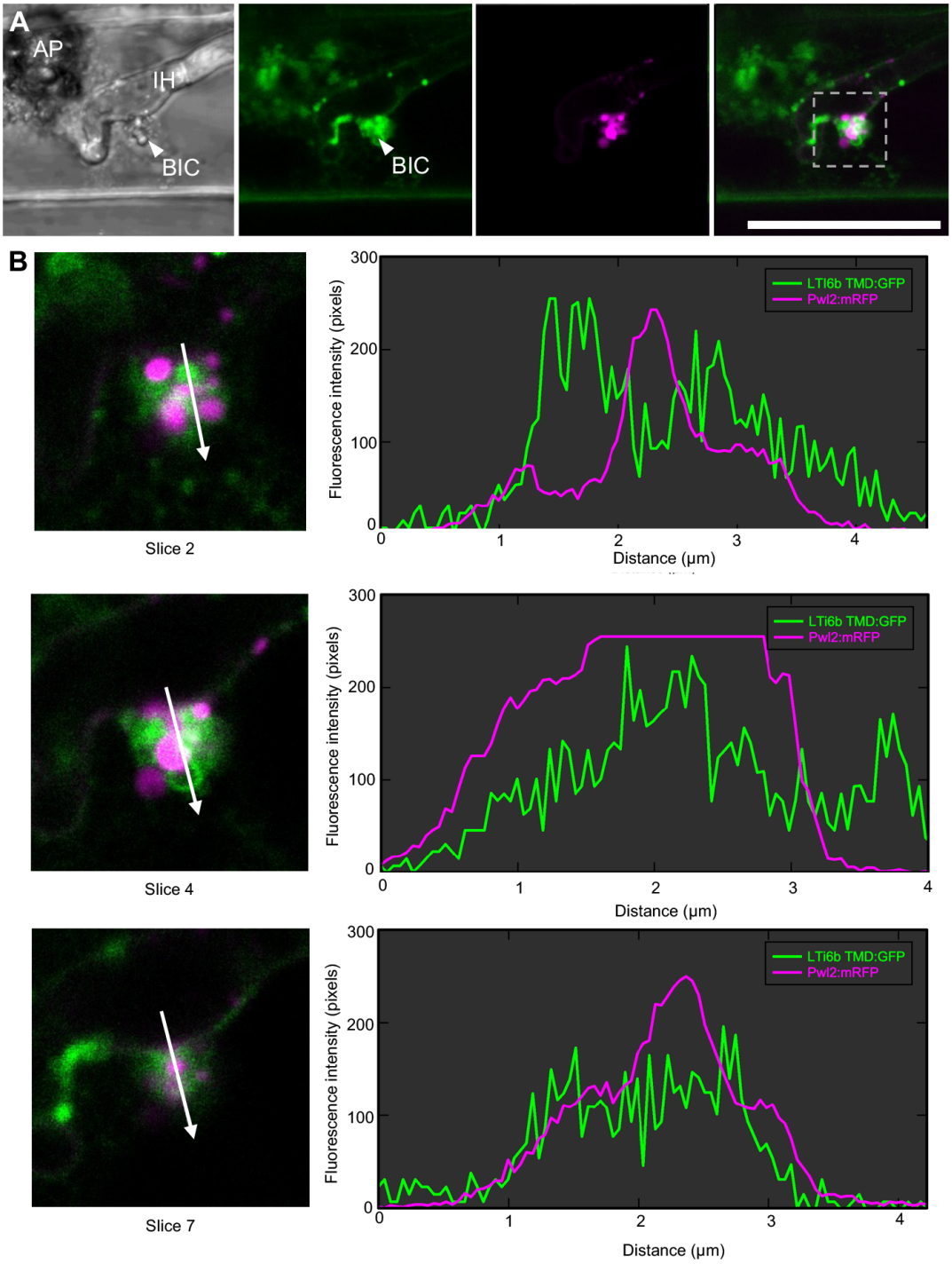

Figure 4.8 Rice plasma membrane accumulates at the biotrophic interfacial complex (BIC).

A. Confocal imaging of rice cv Kitaake transgenic line expressing LTI6b TMD:GFP (green) in cells infected with *M. oryzae* Guy11 expressing Pwl2:mRFP (magenta) showing association of the rice plasma membrane and BIC. Leaf sheath infections were incubated at 24 °C. All images shown are maximum projections of z-stack series taken using Leica TCS SP8X confocal laser scanning microscope. Scale bar = 20 µm. **B.** Single Z-stack slices of the BIC region (enclosed in white dotted lines) shown in (A) showing association of rice plasma membrane and BIC. Association demonstrated by fluorescence intensity distribution through the white arrow is consistent with the host plasma membrane being a component of the BIC.

4.2.6 The biotrophic interfacial complex (BIC) is always formed during *Magnaporthe oryzae* infection

To determine whether the BIC always forms during rice blast infection, I quantified BIC formation in both primary hypha and bulbous IH, and investigated at 'tip BIC' and 'side BIC' formation, respectively, in Guy11 Pwl2:mRFP-infected LTI6b TMD:GFP transgenic rice. At 22 hpi, all primary IH had 'tip BICs' indicated by physical association of the LTI6b TMD:GFP membranous cap and Pwl2:mRFP punctate structures (Figures 4.9A and C). At 24hpi, all bulbous IH had 'side BICs' (Figures 4.9B and C). Notably, only one BIC is produced in the initially invaded cell provided that there is a single infection per host cell (Figures 4.9A and B). However, as the fungus moves to neighbouring cells by 36 hpi, each invasive hypha that branches out from the initial infection site develops a new BIC in the next colonised rice cell (Figure 4.9D).

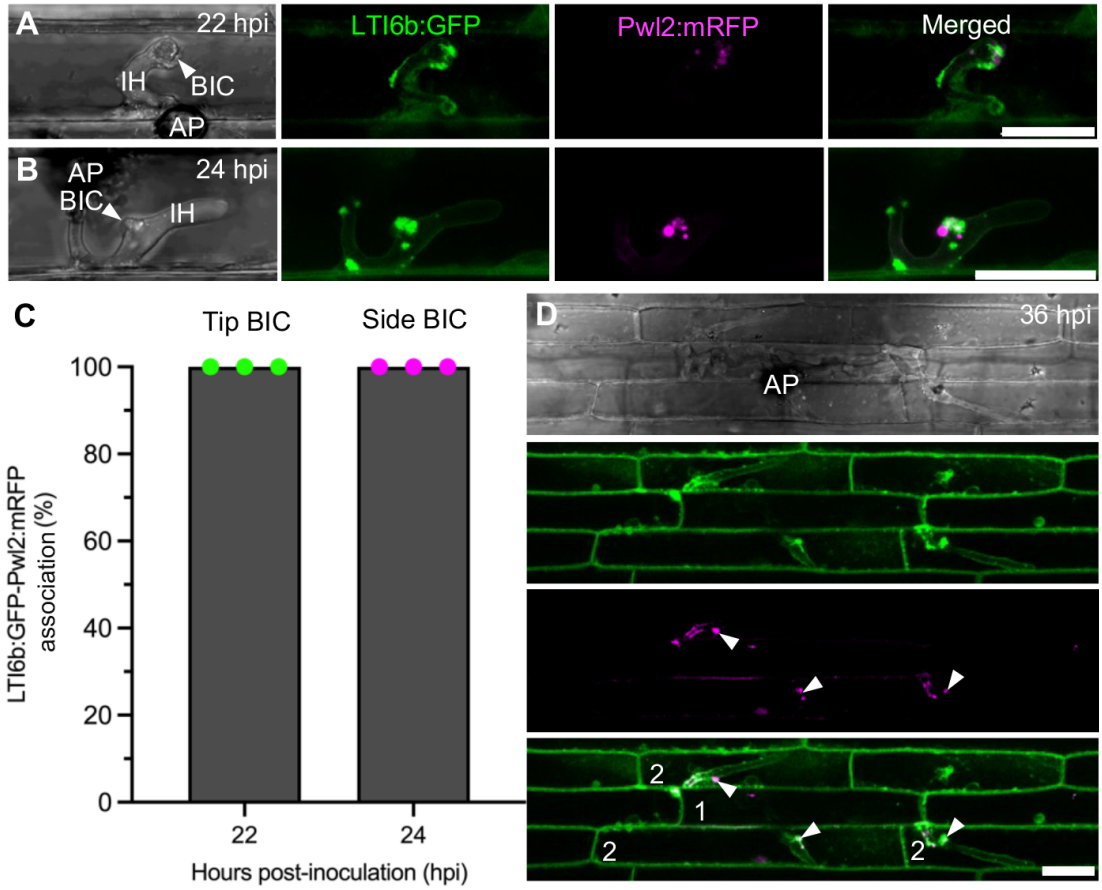

Figure 4.9 The biotrophic interfacial complex (BIC) always forms during *Magnaporthe oryzae* infection in a two-stage development process.

Association of LTI6b TMD:GFP (green) with 'tip' (A) at 22 hours post-inoculation (hpi) and 'side (B) BICs' at 24 hpi using Pwl2:mRFP (magenta), shows that the BIC is always present at all infection sites examined, and follows a two-stage development process. **C.** Bar charts quantifying association of LTI6b TMD:GFP with 'tip' and 'side BICs' based on means from three biological replicates (n = 50 infection sites per biological replicate; data points show means of the individual replicates; error bars indicate standard deviation). **D.** BICs are formed by each invasive hypha as the fungus invades neighbouring cells by 36 hpi. BICs are indicated by white arrowheads. Numbers indicate the order in which the fungus invaded rice cells (1=first-invaded cell, 2=second-invaded cell). Confocal images were prepared from leaf sheath inoculations using rice cv Kitaake transgenic line expressing the plasma membrane marker LTI6b TMD:GFP and Guy11 strain expressing Pwl2:mRFP. Leaf sheath infections for all time points were incubated at 24 °C. All images shown are maximum projections of z-stack series taken using Leica TCS SP8X confocal laser scanning microscope. Scale bars = 20 μm.

4.3 Discussion

This chapter reports the characterization of the *M. oryzae*-rice interface during rice blast infection by specifically investigating changes at the rice plasma membrane during infection. A rice transgenic line reported in Chapter 3 in the Kitaake cultivar background expressing the gene fusion LTI6b TMD:GFP was used to visualise the rice plasma membrane dynamics during live cell imaging experiments of blast infections. Previous studies reported that two distinct structures form during the biotrophic stage of *M. oryzae*

infection—a host PM-derived extra-invasive hyphal membrane (EIHM) and a biotrophic interfacial complex (BIC). In this study, I followed formation of the EIHM and the BIC during early infection in the first-invaded cell (24 hpi) and during infection of the neighbouring cells.

The EIHM is formed by invagination of the host PM as reported previously (Kankanala et al., 2007; Mentlak et al., 2012) using the rice transgenic line expressing LTI6b TMD:GFP. From our findings, the plasma membrane is invaginated and continuously surrounds both young and mature IH until such time that it is disrupted, as also shown in other studies (Kouzai et al., 2014; Mentlak et al., 2012; Mochizuki et al., 2015). The use of other GFP-tagged PM-localised proteins suggests that the EIHM might differ in composition from the bulk host PM. OsCERK1:GFP and EL5:GFP, for example, were found in EIHM of young IH but were absent from EIHM around mature bulbous IH (Kouzai et al., 2014; Mochizuki et al., 2015; Takai et al., 2002). OsCERK1 is a pattern recognition receptor for chitin oligomers (Shimizu et al., 2010) while EL5 is ubiquitin-ligase expressed in response to exposure to chitin oligomers (Takai et al., 2002). It seems that more stable PM-resident proteins such as LTI6b are able to continuously label the EIHM and that defence-related proteins such as pattern recognition receptors may be excluded as a possible mechanism for pathogens to evade host detection (Mochizuki et al., 2015). Similar results have been reported for the EHM of powdery mildews (Koh et al., 2005; Micali et al., 2011) and oomycetes (Caillaud et al., 2012; Lu et al., 2012) in which some PM-resident proteins are excluded such as the aquaporin PIP1;4, calcium ATPase ACA8, arabinogalactan protein (AGP) epitopes, and non-AGP glycoproteins. While the host plasma membrane origin of the EIHM has been confirmed using the LTI6b TMD:GFP transgenic rice line, the partial association of LTI6b with the ER raises the possibility that EIHM may also derive from the ER. This possibility could be experimentally tested by inoculating a transgenic line expressing the ER marker AtWAK2:GFP:HDEL to determine whether the ER becomes invaginated and envelops the IH.

A key feature of biotrophic growth is the formation of plant-derived interfacial membranes that serve as a barrier between the pathogen and host cytoplasm. In biotrophic oomycete plant pathogens such as the late blight pathogen *Pytophthora infestans* and the downy mildew pathogen *Hyaloperonospora arabidopsidis*, haustoria, which are

specialized structures for acquiring nutrients and suppressing defence responses, are enveloped by a plant-derived membrane called the extra-haustorial membrane (EHM) (Jaswal et al., 2020; Jones & Dangl, 2006; Lo Presti et al., 2015; Mims et al., 2004; O'Connell & Panstruga, 2006). The EHM is the interface between the oomycete and its host, and is tethered to neck bands at the site of host cell entry. The sealed compartment between the EHM and the oomycetes is called the extrahaustorial matrix (EHMx) (Bushnell, 1972).

Similarly, during *M. oryzae* infection, the formation of the EIHM marks the biotrophic phase and serves as the interface between *M. oryzae* and rice, and like the EHMx, a sealed compartment is also formed between the EIHM and IH called the extra-invasive hyphal membrane matrix (EIHMx) (Kankanala et al., 2007; Mentlak et al., 2012; Mosquera et al., 2009; Yi & Valent, 2013). However, unlike biotrophic pathogens that maintain EHM integrity and viability of host cells for several days (Perfect & Green, 2001), the *M. oryzae* EIHM loses integrity after the fungus has fully colonised the first cell and invades neighbouring cells (Figure 4.3B). The host cell loses viability as shown by plasmolysis assays (Figure 4.4C) (Kankanala et al., 2007).

A common cytological method used to indicate cell viability is sucrose-induced plasmolysis, in which the plasma membrane of viable cells pulls away from the cell wall due to exposure to a hyper-osmotic solution (Kankanala et al., 2007; Koga et al., 2004). The ability of the cells to plasmolyse also shows integrity of the plasma membrane. Because it is difficult to discern whether the PM of an infected cell surrounding the EIHM has already disrupted just by looking at the GFP signal, I also used a plasmolysis assay to examine the integrity of the host plasma membrane (Figure 4.4). Results reported here agree with previous cytological studies, that *M. oryzae* early infection is biotrophic as indicated by the ability of infected rice cells to plasmolyse (Kankanala et al., 2007; Koga et al., 2004). The inability of initially invaded cells to plasmolyse indeed shows that these cells have disrupted plasma membrane and rapidly lose viability. Disruption of the EIHM and host cell death are phenomena that separate different infection phases in *M. oryzae* (early biotrophic, late biotrophic, and transient necrotrophic phases) (Jones et al., 2021). Formation and disruption of the EIHM in first-invaded cells and its re-establishment in newly invaded cells reiterate the hemibiotrophic nature of *M. oryzae.* Hemibiotrophy is characterized by a mosaic pattern of inviable initially colonized rice cells, surrounded by

cells still undergoing fungal occupation which are always alive. There is therefore a biotrophic margin to all *M. oryzae* infection with a necrotrophic centre to all disease lesions in compatible (susceptible host) interactions. It is also worth noting that it is also possible for invaded cells at the margin of the infection zone to lose the ability to plasmolyse if the level of infection is at the point where the EIHM has once again disrupted (Figure 4.4C).

Sucrose-induced plasmolysis proved to be useful in looking at the integrity of the infected host PM and viability of the cell. However, this method does not show the different cellular changes that precede host cell death. Fluorescein diacetate (FDA) is a suitable tool to show not only cell viability but also intermediate cell types before cell death (Jones et al., 2016). Non-fluorescent FDA, for example, enters intact plasma membrane, and is hydrolysed in viable cells being converted to fluorescent fluorescein. Fluorescein ions are retained in viable cells while they diffuse out in non-viable cells with damaged membranes. I used FDA to investigate the relationship between host plasma membrane integrity and cell viability during blast infection. As previously reported (Jones et al., 2016), I observed different cell types based on their fluorescein pattern. Typical fluorescein patterns were observed for viable cells, distinct fluorescein pattern for dying cells with shrunken vacuoles and closed plasmodesmata, and a novel fluorescein pattern for cells with ruptured vacuole and closed plasmodesmata or dead cells. Because fluorescein intensity declines after 15 min incubation (Jones et al., 2016), it cannot be used for setting up a time-lapse video without replenishing the dye. To compensate for this, I examined 50 blast-infected cells and performed the experiment with three biological replicates at each time point. By 24, 28, and 32 hpi, infections were limited in the first-invaded cell; by 36 hpi, infections progressed to the immediate neighbouring cell/s; and by 48 hpi, infections progressed two to more cells away from the initial site. Quantifying different cell types across time points revealed a trend which reflected the sequence of events leading to host cell death (Figure 4.7). Firstly, a decline in the number of viable cells was observed (from 28 hpi) and a downward trend of cells showing shrunken vacuoles (from 32 hpi) across time points means that infected cells were losing viability. As the number of viable cells and cells with shrunken vacuoles decreased, the number of cells showing ruptured vacuoles increased by 32 hpi and peaked by 36 hpi. Another point to highlight is that cells at the edges of each infection exhibit either viability or early stages of cell death compared to cells invaded before them (see Figure 4.6C, D and E), which further supports the

findings of plasmolysis assays and recapitulates the successive hemibiotrophic mode of *M. oryzae* invasion.

I also followed formation of the BIC, another host plasma membrane-rich structure. It follows a two-stage developmental process as demonstrated previously (Khang et al., 2010). Together with the host plasma membrane, other host subcellular components such as actin and CLATHRIN LIGHT CHAIN 1(OsCLC1), a component of clathrin-mediated endocytosis, have also been reported to be components of the BIC (Oliveira-Garcia et al., 2023) and evidence has been presented that cytoplasmic effector translocation is mediated by clathrin-mediated endocytosis in BICs. Moreover, because of the perinuclear membrane localisation of the plasma membrane marker LTI6b TMD:GFP in this study, it is also likely that the BIC has a plant ER component. This hypothesis can be directly tested using the ER marker AtWAK2:GFP:HDEL. There is a possibility that other host components such as plant endosomes are also closely associated with the BIC and are being coopted for successful fungal invasion. In the late blight pathogen *P. infestans,* for example, host clathrin and Ara6 are active at haustoria and required for effector delivery (Wang et al., 2023). There is a need to look at other host components to examine how effectors are being translocated to host targets and manipulate the host during infection.

I quantified BIC formation during *M. oryzae* infection using a fluorescently tagged cytoplasmic effector Pwl2:mRFP and found that all intially invaded cells have BICs as indicated by co-localisation of LTI6b TMD:GFP with Pwl2:mRFP. This suggests that BIC is indispensable for biotrophic growth during blast infection (Figure 4.9A, B and C). BIC formation in each individual invasive hypha in neighbouring cells also signifies re-establishment of biotrophy in the next invaded cell as the initially invaded cell dies (Figure 4.9D). A previous study quantified primary BIC formation using an EGFP-tagged cytoplasmic effector, AVR-Pita1, and reported that the primary BIC is visible in more than 98% of the infection sites (Khang et al., 2010). Secondary BICs (BICs formed in the adjacent cells) were also counted and because these are smaller than primary BICs, the counts were reliant on AVR-Pita1:EGFP fluorescence. Fluorescent secondary BICs were observed in approximately 85% of hyphae (Khang et al., 2010). They also reported that BICs in the next invaded cells are smaller than those in initially invaded cells. I hypothesise that the formation of multiple invasive hyphae in neighbouring cells will require more

extensive remodeling of host cytoskeleton and plasma membrane, and trafficking of other host components, leading to smaller BICs. It is worth examining these different host subcellular components in relation to BIC formation and effector translocation for us to have a better insight on *M. oryzae* invasion.

In summary, I observed plasma membrane dynamics during blast infection on live cell imaging experiments. I conclude that initially invaded rice cells are intact and viable until the fungus locates pit filed sites to invade neighbouring cells. At this time, cell viability is affected, and the initially colonised cell will die as the fungus invades a new cell, invaginates its plasma membrane, and invades the cell, leading to formation of new BIC and EIHM.

Chapter 5 Surface area quantification of rice plasma membrane accommodating *Magnaporthe oryzae* invasive hypha during biotrophic growth

5.1 Introduction

Results presented in Chapter 4 provide evidence that the rice plasma membrane invaginates and surrounds invasive hypha during *M. oryzae* infection, forming the extra-invasive hyphal membrane (EIHM) during biotrophic invasion. The formation of an interfacial membrane is a hallmark of biotrophic interactions (Jaswal et al., 2020; Jones & Dangl, 2006; Lo Presti et al., 2015; Mims et al., 2004; O'Connell & Panstruga, 2006; Perfect & Green, 2001) as also observed in other oomycetes and fungal pathogens. In the rice–*M. oryzae* interaction, the host plasma membrane undergoes significant expansion to accommodate rapid hyphal growth before the EIHM ultimately ruptures (Kouzai et al., 2014; Mentlak et al., 2012; Mochizuki et al., 2015).

The mechanism by which the plant plasma membrane-derived EIHM maintains its integrity remains elusive. It is highly unlikely that this is achieved through simple stretching, because plasma membranes have been shown to possess no more than approximately 5% elasticity (Wolfe & Steponkus, 1983). The rapid progression of *M. oryzae* infection indicates that an active mechanism likely drives host membrane biogenesis, or that membrane reservoirs and invaginations are exploited to facilitate plasma membrane expansion and remodelling. In bacterial infections of human cells, recent evidence indicates that host membrane reservoirs are manipulated by bacterial effectors to facilitate cell uptake (Zhu et al., 2024). Whether a similar process occurs during *M. oryzae* infection—where fungal effectors might directly activate plasma membrane biogenesis—remains unclear. To date, no conclusive evidence has identified which *M. oryzae* effectors drive rapid host plasma membrane biogenesis and remodelling. A recent hypothesis suggests that the effector Bas83 may facilitate rapid membrane turnover in biotrophic interfacial complexes (BICs); however, this could not be confirmed due to unsuccessful gene knockout attempts (Oliveira-Garcia et al., 2023). Establishing the relationship between fungal growth and the increase in host plasma membrane surface area is crucial before functionally validating candidate effectors that may co-opt the host plasma membrane during *M. oryzae* invasion.

In order to measure host plasma membrane dynamics, an indicator is needed to distinguish between infections with an intact and or disrupted EIHM. Previously, secreted GFP (sec-GFP), which accumulates in the EIHM but appears in the host cytoplasm upon membrane disruption, was used as an EIHM integrity reporter (Jones et al., 2021). In this study, we employed a similar approach, utilising Mep1, an apoplastic effector residing in the EIHM compartment, to differentiate between intact and disrupted EIHM (X. Yan et al., 2023). The RP27p:mScarlet3 construct was introduced into the Mep1:mCherry *M. oryzae* strain to enable imaging of the fungal cytoplasm and facilitate segmentation for analysing membrane dynamics during infection.

Quantifying invasive hyphal growth via live-cell imaging is not straightforward. In a previous study, *M. oryzae* growth was inferred from the number of fungal nuclei, assuming that each fungal cell contains a single nucleus (Jones et al., 2021). The authors demonstrated that EIHM disruption in the initially invaded cell increased proportionally with growth of invasive hyphae, as the fungus occupied more space within the rice cell (Jones et al., 2021). Traditional live cell imaging relying on confocal microscopy often produces only 2D projections, which underestimate actual sample volume and surface area. This limitation necessitates the use of 3D imaging and quantification. Several software packages and plug-ins support 3D image analysis, including MARS-ALT (Fernandez et al 2020), PlantSeg (Wolny et al., 2020), ImageJ Suite 3D (Ollion et al., 2013), Imaris (Bitplane), and SurfCut (Erguvan et al., 2019). However, the irregular shape, branching, and high curvature of invasive hypha makes their analysis challenging even with these tools.

This chapter reports a study to establish a method to quantify rice plasma membrane expansion during biotrophic invasion of *M. oryzae* and to measure the additional rice plasma membrane required to maintain the EIHM before it loses integrity. We explored the potential of using MorphoGraphX (MGX), an open-source tool developed for 3D surface reconstruction in biological imaging (Barbier de Reuille et al., 2015; Strauss et al., 2022). MGX has been used for analysis and visualisation of plant cell division (Jackson et al., 2019; Yoshida et al., 2019), plant cell growth (Kierzkowski et al., 2019; Kirchhelle et al., 2019; Mollier et al., 2023; Silveira et al., 2021; Vijayan et al., 2021; Z. Zhang et al., 2020), cellular elongation (Aryal et al., 2020; Smith et al., 2020) and other aspects of plant

morphology and development (Dong et al., 2020; Kinoshita et al., 2020; Natonik-Białoń et al., 2020; Tasker-Brown et al., 2024).

MGX represents cell layers using curved, triangulated surface meshes, effectively capturing the 3D shape of organs while preserving the simplicity of 2D segmentation and lineage tracking. These 2.5D images encode sample geometry at two levels: the global organ shape is maintained in the mesh structure, while cellular details are extracted by projecting confocal signals onto the mesh and segmenting them to define individual cell shapes on the surface (Figure 5.1A-C). When combined with time-lapse imaging and lineage tracking, MGX enables the quantification of cell growth and its relationship with gene expression (Figure 5.1D and E). Cellular segmentation and basic quantifications supported by MGX can be found in Figure 5.1 (Strauss et al., 2022).

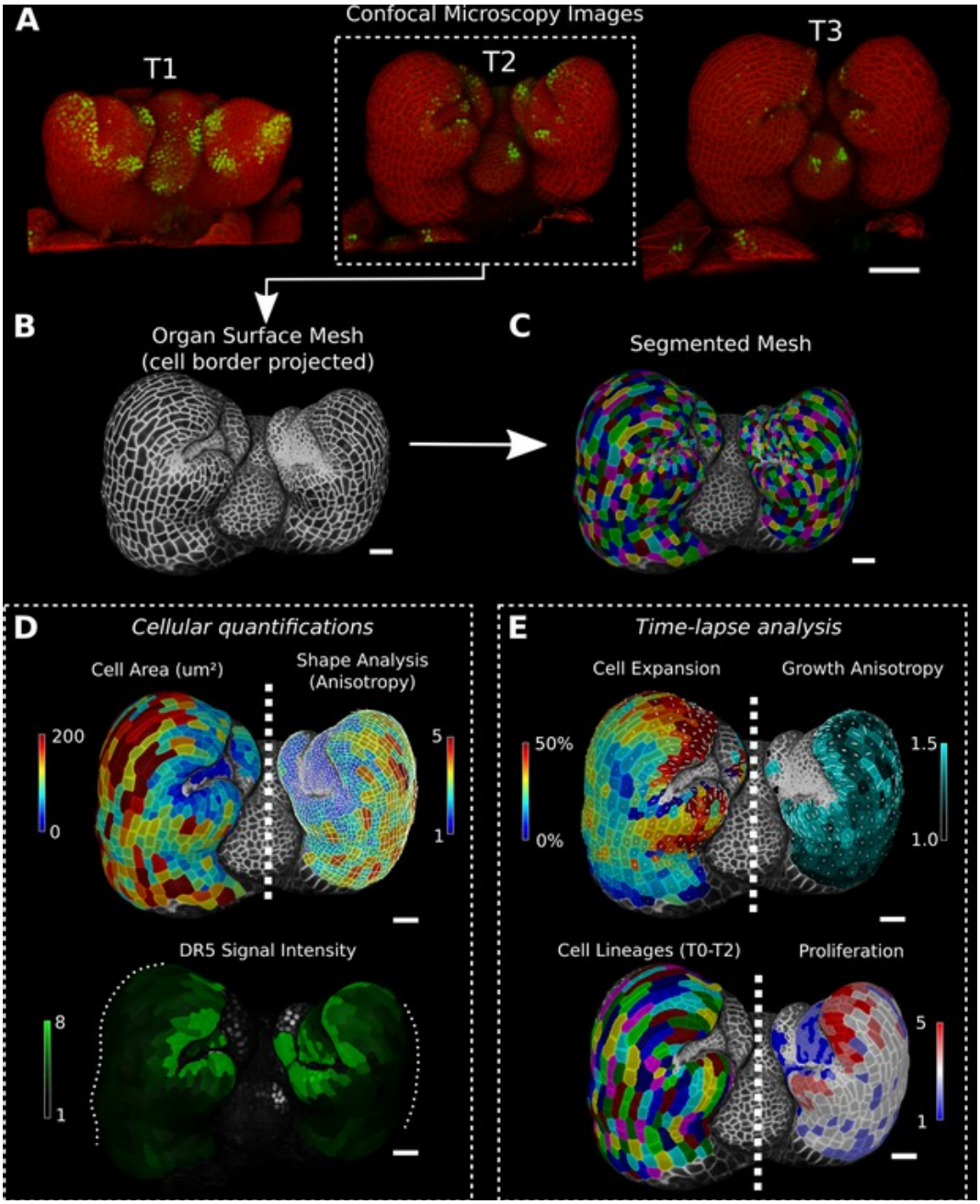

Figure 5.1 Cellular segmentation and basic quantifications supported by MorphoGraphX demonstrated by using a time-lapse series of an *Arabidopsis thaliana* flower meristem.

A. Multichannel confocal microscopy images with a cell wall signal (red) and DR5 marker signal (green). Shown are the last three time points (T1–T3) of a four-image series (T0–T3). **B, C.** Extracted surface mesh of T2. Cell wall signal near the surface was projected onto the curved mesh to enable the creation of the cellular segmentation in C. The segmented meshes provide the base for further analysis within MorphoGraphX as shown in D and E. **D.** Top: MorphoGraphX allows the quantification of cellular properties such as cell area and shape anisotropy (shown as heat maps). The white axes show the max and min axes of the cells. Bottom: heat map of the quantification of the DR5 marker signal (arbitrary units) projected onto the cell surface mesh. **E.** When cell lineages are known, time-lapse data can be analysed. Top: heat maps of cell area expansion and growth anisotropy (computed from T1 to T2). The white crosses inside the cells depict the principal directions of growth. Bottom: visualization of the cell lineages and heat map of cellular proliferation (number of daughter cells), computed from T0 to T2. Scale bars: A = 50 μm; B–E = 20 μm. Figure and figure legend reproduced from Strauss et al. (2022).

Beyond surface-level analysis, MGX also supports the creation and analysis of full 3D meshes with volumetric cell representations. The 3D segmentation process typically starts with a 3D image of a cell boundary marker, followed by preprocessing steps such as noise reduction (via blurring) or background removal filters. MGX utilises the auto-seeded morphological watershed algorithm from the Insight Segmentation and Registration Toolkit (Yoo et al., 2002) for segmentation. Additionally, deep learning approaches using convolutional neural networks (CNNs), such as the 3D U-Net model (Çiçek et al., 2016; Ourselin et al., 2016) have been developed to predict cell boundaries.

The software also includes an intuitive set of 3D voxel (volumetric pixel) editing tools, allowing researchers to manually correct segmentation errors. Furthermore, MGX enables the quantification of cell geometrical properties, including surface area, wall length, and volume, with the option to export data to spreadsheet files for further analysis (Bassel et al., 2014; Strauss et al., 2022).

MGX can render image data from various sources, including confocal laser scanning microscopy (CLSM), magnetic resonance imaging (MRI), and block-face scanning electron microscopy (SEM), all of which provide full 3D volumetric datasets. The software also supports surface processing, with imports from 3D scanners, stereo-SEM reconstructions (Kwiatkowska & Routier-Kierzkowska, 2008), focus-stacking microscopes, and scanning probe techniques such as Cellular Force Microscopy (CFM) (Kwiatkowska & Routier-Kierzkowska, 2008). Additionally, surfaces can be extracted directly within MGX from full 3D datasets (Barbier de Reuille et al., 2015).

In this chapter, we used MGX to quantify the maximum additional plasma membrane generated to accommodate growing invasive hyphae by measuring the surface areas of both rice cell and invasive hyphae. To our knowledge, this is the first application of MGX in the study of fungal pathogen infection in plants and the first attempt to quantify host plasma membrane expansion during infection using 3D image analysis.

5.2 Materials and Methods

5.2.1 Sample Preparation

Samples for imaging were prepared using leaf sheath preparations from 3- to 4-week-old *rice* cv. Kitaake seedlings expressing the plasma membrane marker LTI6b TMD:GFP. These seedlings were inoculated with a *M. oryzae* Guy11 Mep1:mCherry/RP27p:mScarlet3 T1 spore suspension. For standard procedures on plant and fungal growth conditions, as well as leaf sheath inoculation, please refer to Chapter 2. Inoculated leaf sheath preparations were hand-trimmed to remove the sides, exposing the inner epidermis. Lower midvein cells were then discarded to create a thin section consisting of three to four cell layers. The remaining leaf sheath sides were also trimmed. The tissue section was then mounted onto a glass slide with water and covered with a #1.5 cover slip.

5.2.2 Confocal Imaging and Analysis

Confocal imaging was performed using a Leica TCS SP8X equipped with a Leica DMi8 S module (Leica Microsystems Inc., Buffalo Grove, IL, USA) with HyD detectors. Images were collected with a Leica HC PL APO CS2 40x/1.10 NA water immersion objective. Imaging was conducted on samples from *M. oryzae*-infected leaf sheaths at 24, 28, and 30 hours post-inoculation (hpi). The scan speed was set to 600 Hz, with the pinhole adjusted to 1.0 Airy units and the digital zoom set to 1. Excitation was achieved with an argon laser at 488 nm for GFP and 561 nm for mCherry/mScarlet3. Fluorescence signals were collected at 500-530 nm (GFP) and 570-620 nm (mCherry/mScarlet3). For high-quality z-stacks, 16-bit images were captured at a slice interval of 0.2 µm, from above the epidermal cell layer, before the LTI6b TMD:GFP signal appears, to the beginning of the mesophyll cell layer, ensuring complete capture of the infected epidermal cell. Acquired .lif files were opened and separated into distinct channels (GFP for rice cells and mCherry/mScarlet3 for invasive hyphae). Each channel was saved then as a multi-slice TIFF file.

Confocal images were processed using MGX. We collaborated with Dr. Richard Smith from the Computational and Systems Biology Department, John Innes Centre (JIC), with assistance from Dr. Robert Bellow, to establish a pipeline for 3D segmentation and surface area quantification in rice cells and invasive hyphae in infection sites with intact EIHM. The analysis of rice cells and invasive hyphae was conducted separately, with each

following a slightly different pipeline. I performed all 3D segmentation and analyses based on the established pipeline.

For processing rice cells, a multi-slice TIFF stack was loaded onto MGX. The stack was first blurred to reduce noise using "Stack/ITK/Filters/ITK Smoothing Recursive Gaussian". Accurate cell boundary prediction was performed using "Stack/Select CNN/Unet3D Prediction/Bassel Combined UNet". Blurring was then repeated with "Stack/ITK/Filters/ITK Smoothing Recursive Gaussian". Segmentation was carried out with "Stack/ITK/Segmentation/ITK Watershed Auto Seeded". The segmentation process filled the entire sample volume with labels for each segment. Outside labels were removed to isolate the infected rice cell for analysis. After eliminating unnecessary labels using the "Delete Label in Volume" tool, a 3D mesh was generated with "Mesh/Creation/Marching Cubes 3D". If the sample contained multiple segments, these were merged into a single label before mesh creation. Segments were fused into one using the color picker and bucket from the Volume toolbar. Rice cell surface area was quantified with "Heat Map/Analysis/Cell Analysis 3D/Measures 3D/Geometry/Cell Wall Area". The resulting heat map was exported using "Mesh/Heat Map/Heat Map Save", and the numerical data was saved with "Mesh/Attributes/Save to CSV Extended". The pipeline for 3D segmentation and analysis for surface area measurement in rice cells is presented in Figure 5.2.

For processing invasive hyphae, the multi-slice TIFF stack was loaded, followed by blurring using "Stack/ITK/Filters/ITK Gradient Magnitude Recursive Gaussian". Segmentation was performed with "Stack/ITK/Segmentation/ITK Watershed Auto Seeded". Irrelevant labels were removed with "Delete Label in Volume". The cleaned segmented volume often contained multiple labels, but instead of merging them, a mesh was created using "Mesh/Creation/Marching Cubes Surface". A new seed was added, and by running "Mesh/Segmentation/Watershed Segmentation", a single label was assigned to each sample. The "Mesh/Structure/Smooth Mesh" tool was applied to ensure the mesh followed the global shape of the sample. Quantification of invasive hypha surface area, heat map generation, and data saving followed the same procedures as for rice cell analysis. The pipeline for 3D segmentation and analysis for surface area measurement in rice cells is presented in Figure 5.3.

5.2.3 Additional plasma membrane computations and statistical analysis

The percentage of additional plasma membrane produced was calculated using the formula:

$$[(\text{invasive hypha surface area } (\mu m^2)) / (\text{rice cell surface area } (\mu m^2))] \times 100$$

Plasma membrane increase was quantified at three timepoints (24, 28, and 30 hours post-inoculation) by measuring the surface area of invasive hypha relative to host cell surface area. For each timepoint, 15 infection sites were examined across three independent biological replicates, yielding 45 observations per timepoint. Data were log-transformed [log(y+1)] to meet the assumption of homogeneity of variance, which was verified using Levene's test. A linear mixed-effects model was fitted with timepoint as a fixed factor and experiment as a random factor to account for non-independence of observations within experiments. Estimated marginal means were back-transformed to obtain geometric means on the original percentage scale. Post-hoc pairwise comparisons were performed using Tukey's honest significant difference (HSD) test. All analyses were conducted in R (version 4.5.0) using the lme4 and emmeans packages. Statistical significance was set at $\alpha = 0.05$.

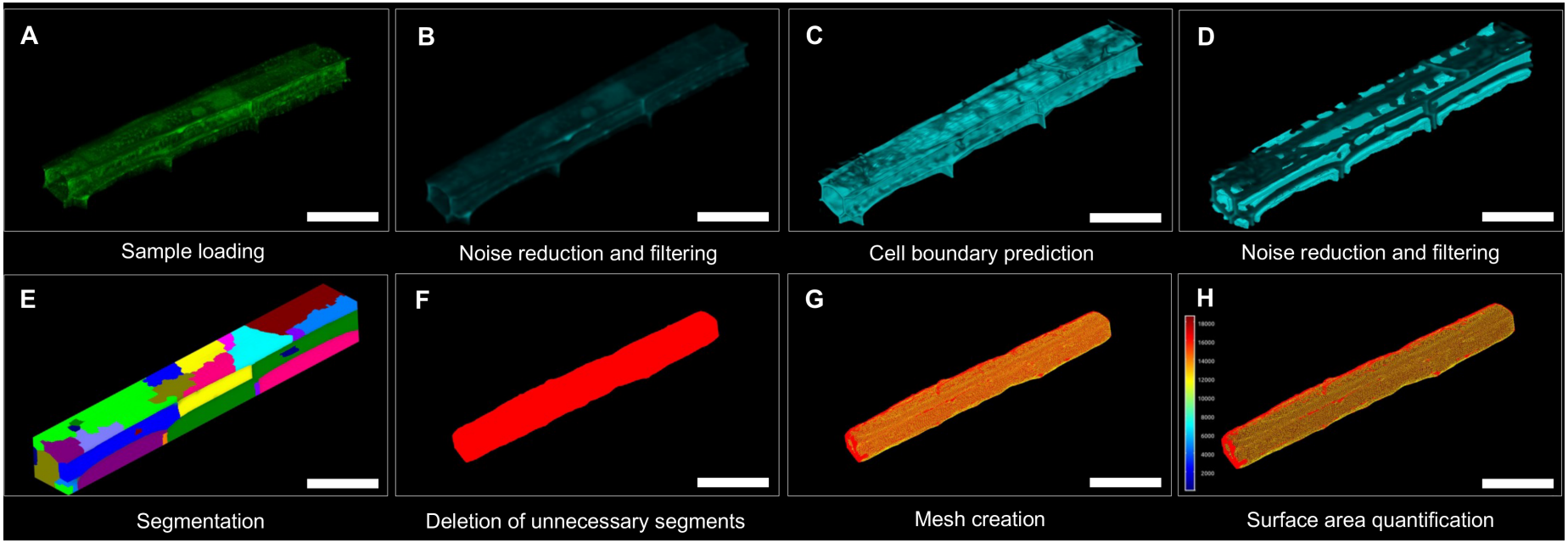

Figure 5.2 3D segmentation and analysis pipeline for surface area quantification in rice cells.

Flowchart showing the pipeline to quantify rice cell surface area in MorphoGraphX (MGX).

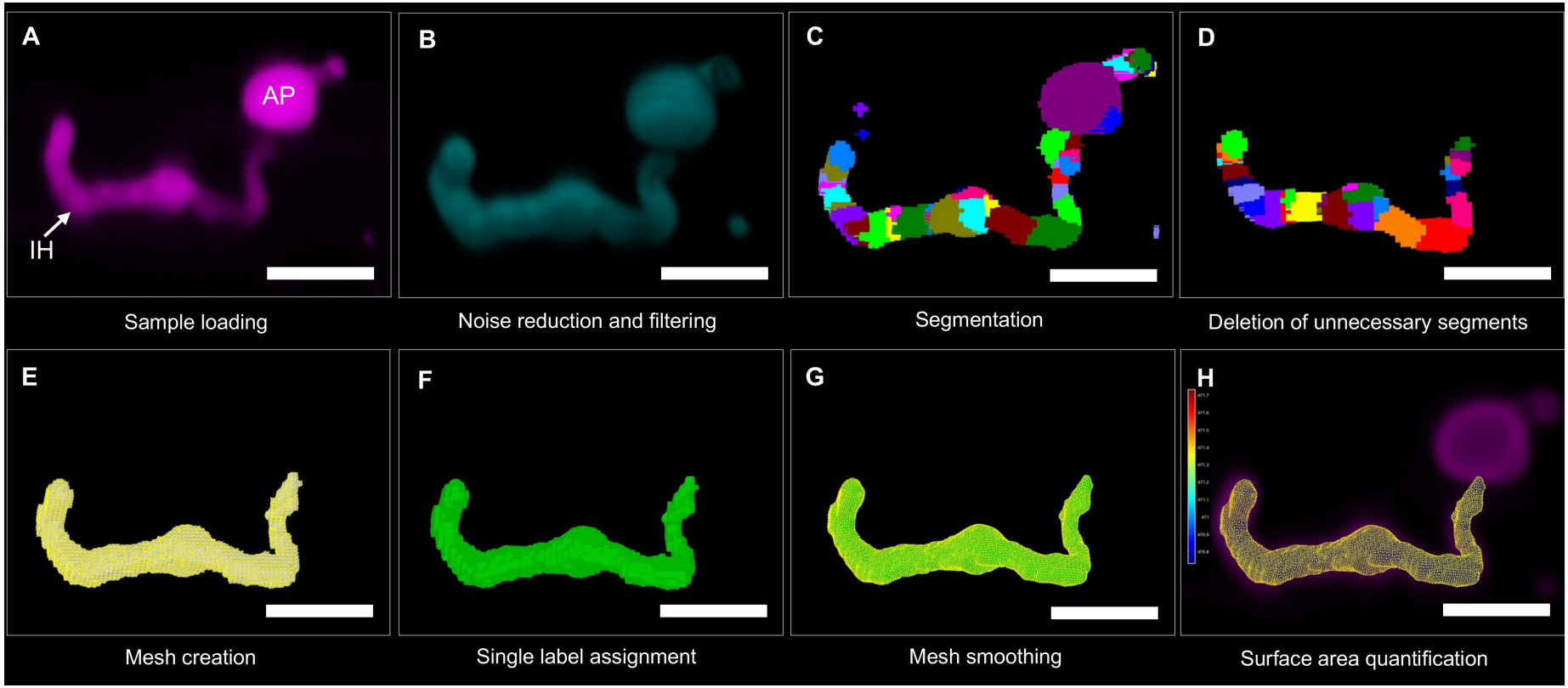

Figure 5.3 3D segmentation and analysis pipeline for surface area quantification in a *M. oryzae* invasive hypha.

Flowchart showing the pipeline to quantify *M. oryzae* invasive hypha surface area in MorphoGraphX (MGX). AP = appressorium, IH = invasive hypha. Scale bar = 10 μm

5.3 Results

5.3.1 The apoplastic effector Mep1 can be used as an indicator of extra-invasive hyphal membrane (EIHM) integrity

Before quantifying host plasma membrane during infection, it is essential to first determine whether the EIHM is intact. I hypothesised that apoplastic effectors present in the extra-invasive hyphal matrix (EIHMx)—the space between the invasive hypha and the EIHM—could serve as indicators of EIHM integrity. If the EIHM is disrupted, these effectors may leak into the host cytoplasm and therefore show the integrity of the invaded rice epidermal cell. To test this, I used a *M. oryzae* Guy11 strain expressing fluorescently tagged Mep1, an apoplastic effector (Yan et al., 2023), provided by Dr. Xia Yan (The Sainsbury Laboratory). At 25 hours post-inoculation (hpi), the Mep1:mCherry signal outlined the invasive hypha, consistent with the typical localization of apoplastic effectors. However, by approximately 28 hpi, Mep1:mCherry began leaking into the host cytoplasm, indicating a loss of EIHM integrity (Figure 5.4). Thus, Mep1:mCherry can serve as a reliable marker for assessing EIHM integrity when imaging *M. oryzae* infection sites.

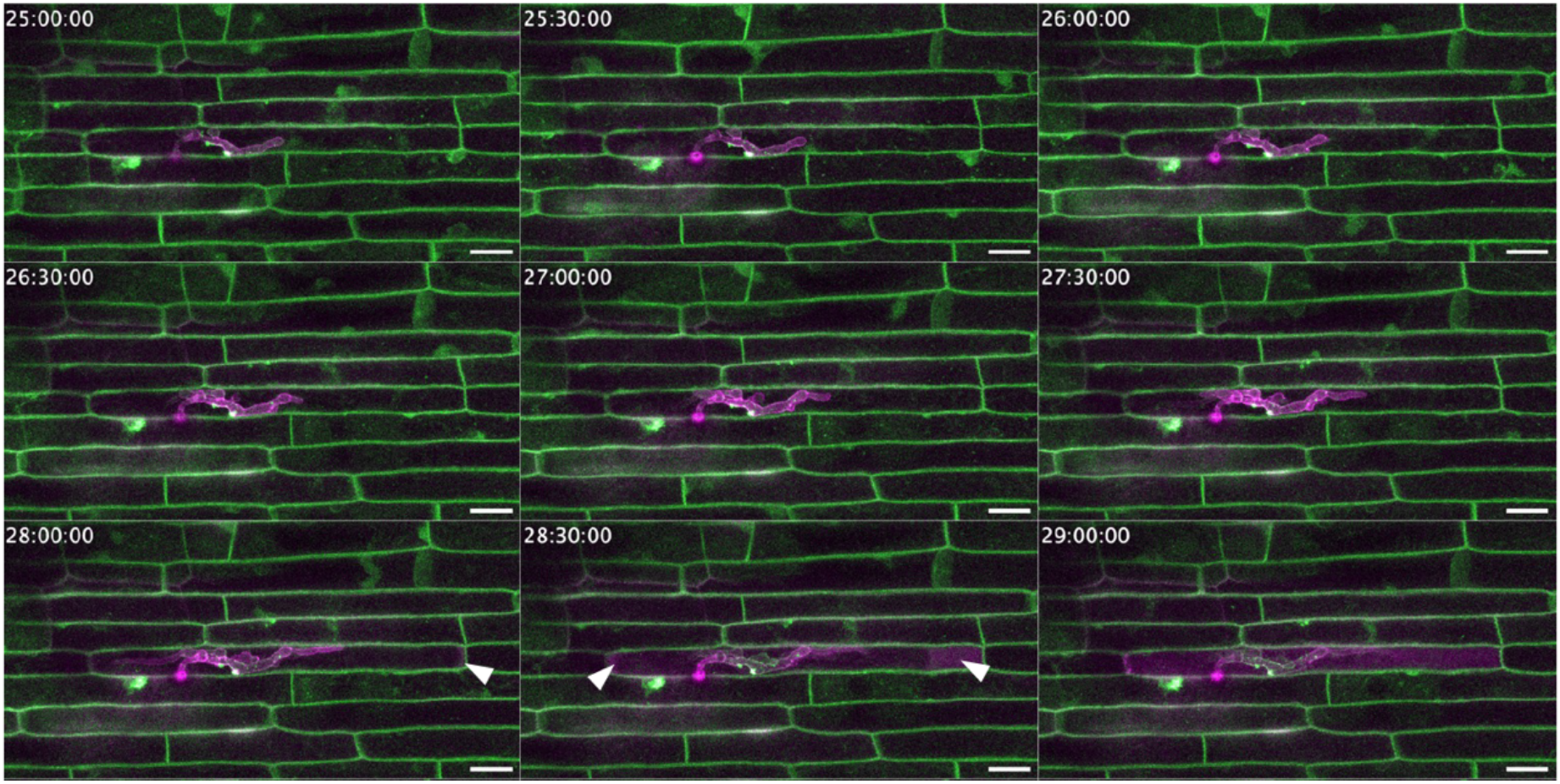
25:00:00
25:30:00
26:00:00
26:30:00
27:00:00
27:30:00
28:00:00
28:30:00
29:00:00

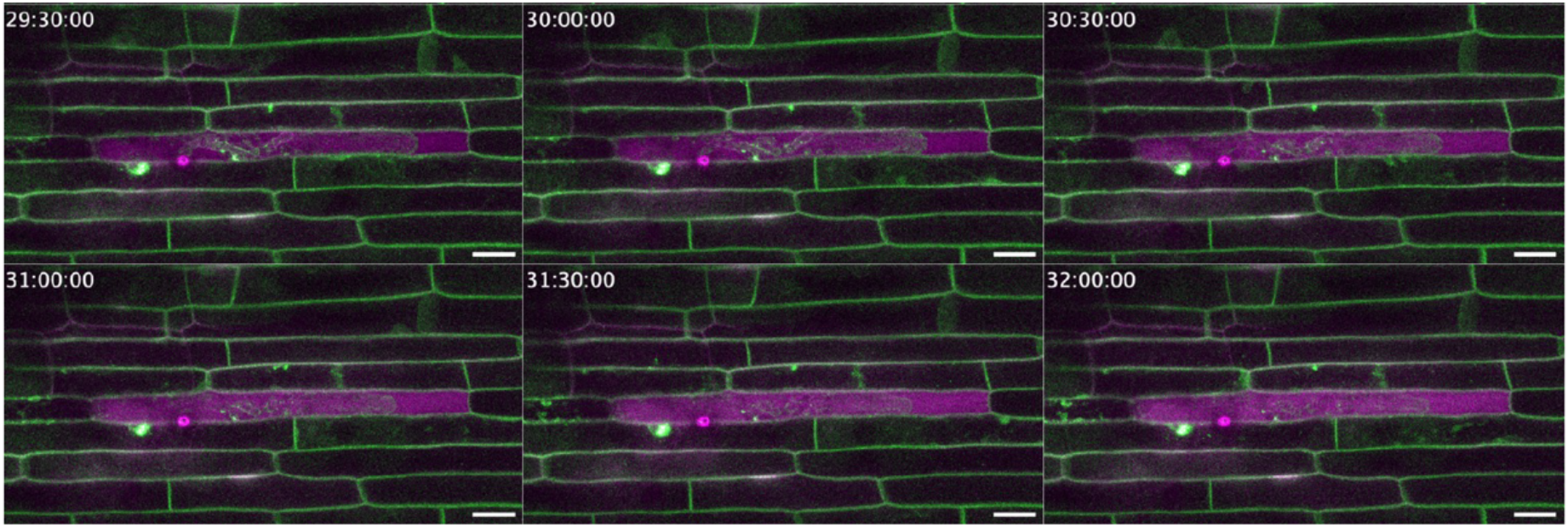

Figure 5.4 The apoplastic effector Mep1 can be used as an indicator of extra-invasive hyphal membrane (EIHM) integrity.
The apoplastic effector Mep1 can be used as an indicator of extra-invasive hyphal membrane (EIHM) integrity. Time-lapse laser confocal scanning microscopy of *M. oryzae* strain Guy11 expressing the apoplastic effector, Mep1:mCherry (in magenta) infecting rice leaf sheath cells of Kitaake transgenic line expressing plasma membrane marker LTi6b TMD:GFP (in green). The infected sample was imaged from 25-32 hours post-inoculation (hpi). Images are still frames taken from a time-lapse (Movie 5.1) captured at 10 min intervals. Selected images shown here are 30 min apart. All images shown are maximum projections of z-stack series recorded using Leica TCS SP8X confocal laser scanning microscope. White arrow heads indicate the start of Mep1:mCherry leakage to the cytoplasm indicating EIHM disruption. Time scale is in hour: min: sec. Scale bar = 20 μm.

5.3.2 Generation of RP27p:mScarlet3 vector for cytoplasmic fluorescent protein expression in *M. oryzae*

As the Mep1:mCherry signal exclusively outlines the invasive hypha (IH), tagging the fungal cytoplasm with a fluorescent protein would facilitate visualisation of the fungus during sample acquisition and segmentation for 3D image analysis. To achieve this, I constructed a fungal cytoplasmic marker using mScarlet3—a red fluorescent protein with low acid sensitivity (Gadella et al., 2023)—driven by the *M. oryzae* ribosomal protein 27 promoter (RP27p) which provides high level constitutive gene expression. The construct was assembled via Golden Gate cloning and is illustrated in Figure 5.5A. Positive clones were validated by sequencing with primers pCB1532-F and pCB1532-R to confirm correct assembly (Figure 5.5B).

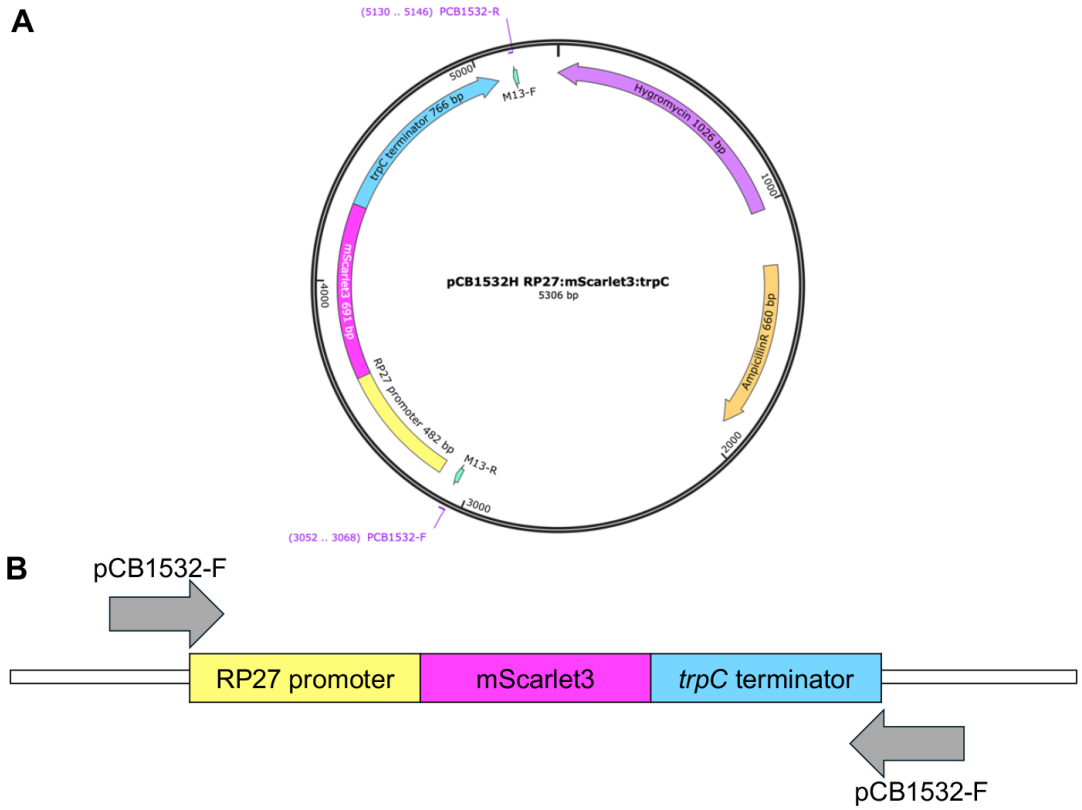

Figure 5.5 Generation of RP27p:mScarlet3 vector for cytoplasmic fluorescent protein expression in *Magnaporthe oryzae*.

A. RP27p:mScarlet3 construct was assembled via Golden Gate cloning using a pCB1532H vector with hygromycin selection. Construct maps were exported from the software SnapGene® (from Dotmatics; available at snapgene.com). **B.** A schematic representation of the sequenced region to confirm correct construct assembly using pCB1532-F and pCB1532-R.

5.3.3 RP27p:mScarlet3 is expressed in conidia and invasive hypha cytoplasm

To confirm that RP27p:mScarlet3 is a suitable fungal cytoplasmic marker, the generated construct was used to transform *M. oryzae* strain Guy11. Fungal transformants were screened for fluorescence using a Leica TCS SP8X laser scanning confocal microscope. For initial screening, conidial suspensions were mounted onto a glass slide and covered with a #1.5 coverslip. The positive transformant, RP27p:mScarlet3 T1, exhibited cytoplasmic fluorescence in conidia (Figure 5.6A). To further assess fluorescence in invasive hyphae, I performed a leaf sheath infection assay using rice cv. CO39 and examined RP27p:mScarlet3 expression at 24 hpi. RP27p:mScarlet3 was strongly expressed in invasive hyphae, clearly delineating the fungal cytoplasm as shown in Figure 5.6B.

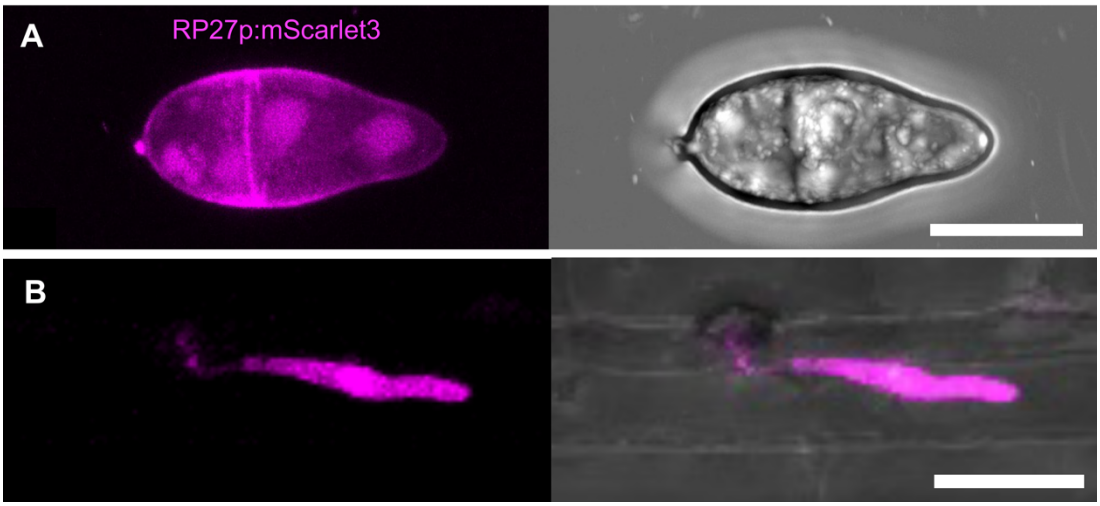

Figure 5.6 RP27p:mScarlet3 is expressed in conidia and invasive hypha cytoplasm.

A. Confocal micrographs of *M. oryzae* Guy11 transformant expressing RP27p:mScarlet3 in conidia. Scale bar = 10 μm. **B.** Confocal micrographs of *M. oryzae* Guy11 expressing RP27p:mScarlet3 in invasive hyphae at 24 hours post-inoculation (hpi) on rice cv CO39. Scale bar = 20 μm. Leaf sheath infection was incubated at 24 °C. All micrographs shown are maximum projections of z-stack series taken using a Leica TCS SP8X confocal laser scanning microscope.

5.3.4 Mep1:mCherry/RP27p:mScarlet3 is expressed in conidia and invasive hypha

After confirming that RP27p:mScarlet3 is a suitable fungal cytoplasmic marker, the construct was used to transform *M. oryzae* strain Guy11 expressing Mep1:mCherry. This new strain enables easier imaging and image analysis while also serving as an indicator of EIHM integrity. The dual-labelled strain (Mep1:mCherry/RP27p:mScarlet3) was

visualised together using the same excitation (561 nm) and emission (580-650 nm) wavelengths. The strain exhibited strong fluorescence in conidia (Figure 5.7A) and invasive hypha (Figure 5.7B) when inoculated onto rice cv. CO39 leaf sheaths and examined at 24 hpi.

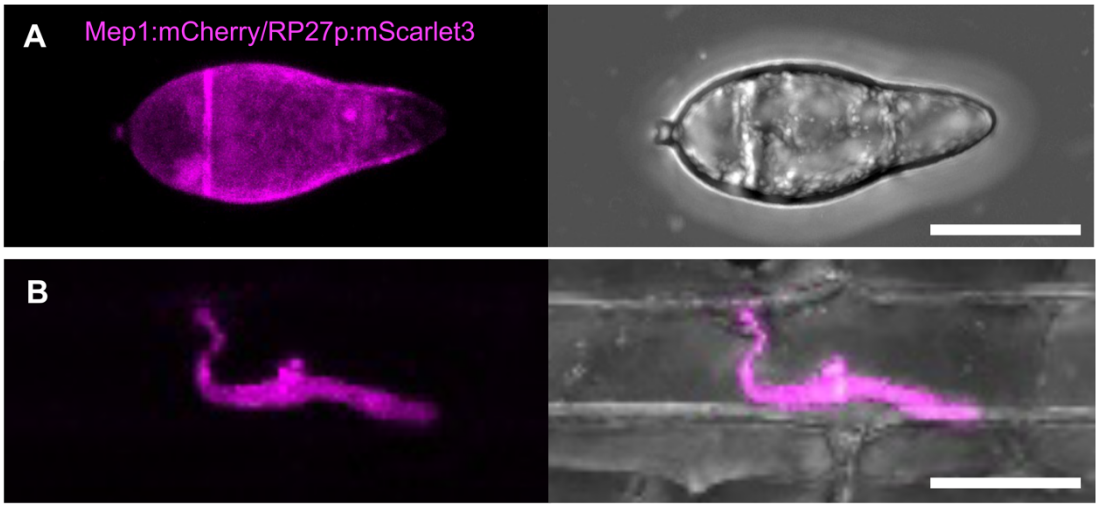

Figure 5.7 Mep1:mCherry/RP27p:mScarlet3 is expressed in conidia and invasive hypha.

A. Confocal micrographs of *M. oryzae* Guy11 transformant expressing Mep1:mCherry/RP27p:mScarlet3 in conidia. Scale bar = 10 μm. **B.** Confocal micrographs of *M. oryzae* Guy11 expressing RP27p:mScarlet3 in invasive hyphae at 24 hours post-inoculation (hpi) on rice cv CO39. Scale bar = 20 μm. Leaf sheath infection was incubated at 24 °C. All micrographs shown are maximum projections of z-stack series taken using a Leica TCS SP8X confocal laser scanning microscope.

5.3.5 Mep1:mCherry/RP27p:mScarlet3 can differentiate between intact and disrupted extra-invasive hyphal membrane (EIHM)

To determine whether *M. oryzae* Guy11 expressing Mep1:mCherry/RP27p:mScarlet3 can differentiate between intact and disrupted EIHM, I inoculated the strain onto leaf sheath preparations of rice cv. Kitaake transgenic lines expressing the plasma membrane marker LTI6b TMD:GFP. Mep1:mCherry leakage into the rice cytoplasm was assessed at 24 h, 28 h, and 30 h post-inoculation (hpi). As expected, at 24 hpi, the EIHM remained intact, with no detectable Mep1:mCherry spillage into the rice cytoplasm (Figure 5.8A). Similarly at both 28 and 30 hpi, infections with intact EIHMs showed fluorescence signals restricted to the fungal cytoplasm and EIHMx. By contrast, infections with disrupted EIHMs exhibited clear Mep1:mCherry leakage into the rice cytoplasm (Figure 5.8B, C). Thus, *M. oryzae* Guy11 expressing Mep1:mCherry/RP27p:mScarlet3 serves as a reliable indicator for distinguishing between infections with intact and disrupted EIHMs. This

strain was subsequently used to inoculate rice cv. Kitaake expressing LTI6b TMD:GFP to acquire images for 3D image analysis in order to quantify the additional plasma membrane formation required to accommodate growing invasive hyphae.

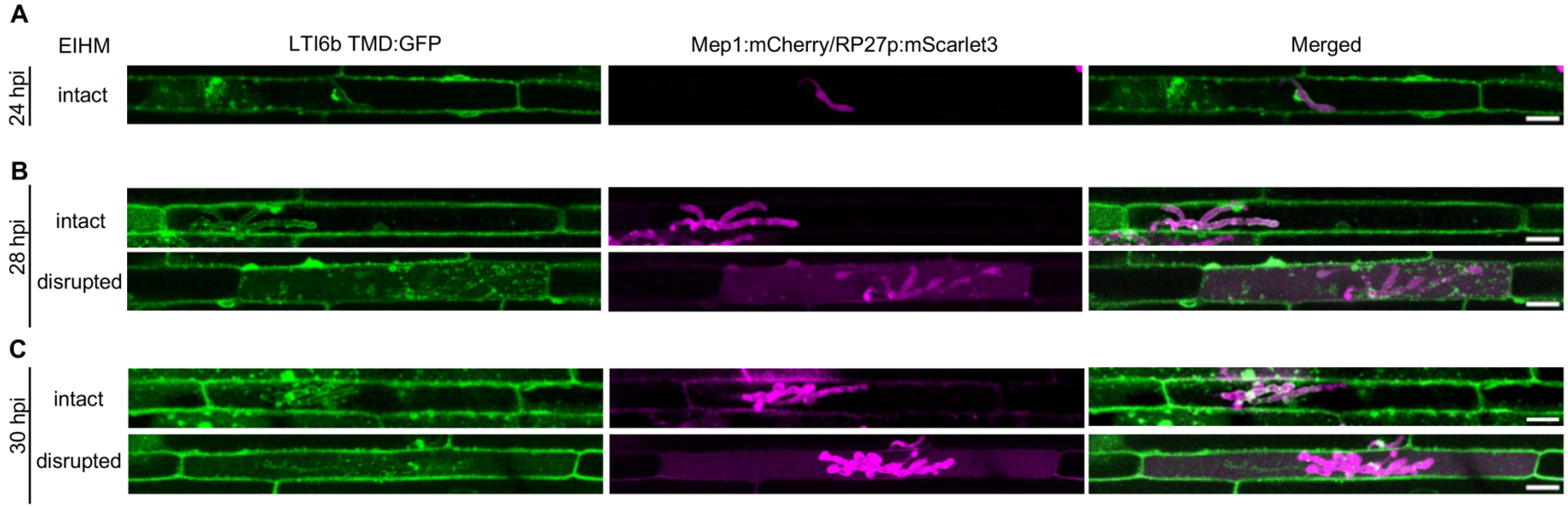

Figure 5.8 Mep1:mCherry/RP27p:mScarlet3 can differentiate between intact and disrupted extra-invasive hyphal membrane (EIHM).

A. Confocal micrographs of infection site showing intact EIHM at 24 hours post-inoculation (hpi). **B.** Confocal micrographs of infection sites showing intact and disrupted EIHM at 28 hpi. **C.** Confocal micrographs of infection sites showing intact and disrupted EIHM at 30 hpi. All confocal micrographs were prepared from leaf sheath inoculations using rice transgenic line expressing the plasma membrane marker LTI6b TMD:GFP (green) and rice blast isolate Guy11 expressing Mep1:mCherry/RP27p:mScarlet3 (magenta). Leaf sheath infections were incubated at 24 °C. All micrographs shown are maximum projections of z-stack series taken using a TCS SP8X confocal laser scanning microscope. Infection sites with intact EIHM from the different time points were used for 3D image analysis and surface area quantification. **A-C**. Scale bars = 20 μm.

5.3.6 MorphoGraphX (MGX) can be used for 3D segmentation and quantification of surface areas in rice cells and *Magnaporthe oryzae* invasive hypha

To quantify the amount of additional plasma membrane generated to accommodate growing invasive hypha during biotrophic invasion, we explored the capabilities of MorphoGraphX (MGX), an open-source application for the visualisation and analysis of biological datasets (Barbier de Reuille et al., 2015; Strauss et al., 2022), in segmenting and measuring the surface areas of rice cells and invasive hyphae. Here, we report a novel method of analysing 3D confocal z-stacks of *M. oryzae*-infected cells and invasive hyphae. We have established pipelines, previously detailed in Figures 5.2 and 5.3, and these have proven to be effective in segmenting and quantifying surface areas from both rice cells and invasive hyphae. Examples of samples processed from different time points are illustrated in Figures 5.9 (0 hpi), 5.10 (24 hpi), 5.11 (28 hpi), and 5.12 (30 hpi). At 0 hpi, prior to infection establishment, the host plasma membrane has not yet undergone any infection-related modifications, serving as a baseline for subsequent comparisons. Plasma membrane increase during M. oryzae infection differed significantly among timepoints ($F_{2,4} = 213.33$, $p < 0.001$). At 24 hpi, plasma membrane increase was 3.16% (geometric mean, 95% CI: 2.72–3.65%), which increased significantly to 11.92% (95% CI: 10.55–13.45%) at 28 hpi ($p < 0.001$). By 30 hpi, membrane increase reached 19.79% (95% CI: 17.59–22.25%), which was significantly higher than both 24 hpi ($p < 0.001$) and 28 hpi ($p < 0.001$). These results demonstrate progressive host plasma membrane production throughout the infection time course, with an approximately 3.8-fold increase from 24 to 28 hpi and 1.7-fold increase from 28 to 30 hpi, indicating substantial membrane increase needed to accommodate invasive hyphal growth. (Figure 5.13).

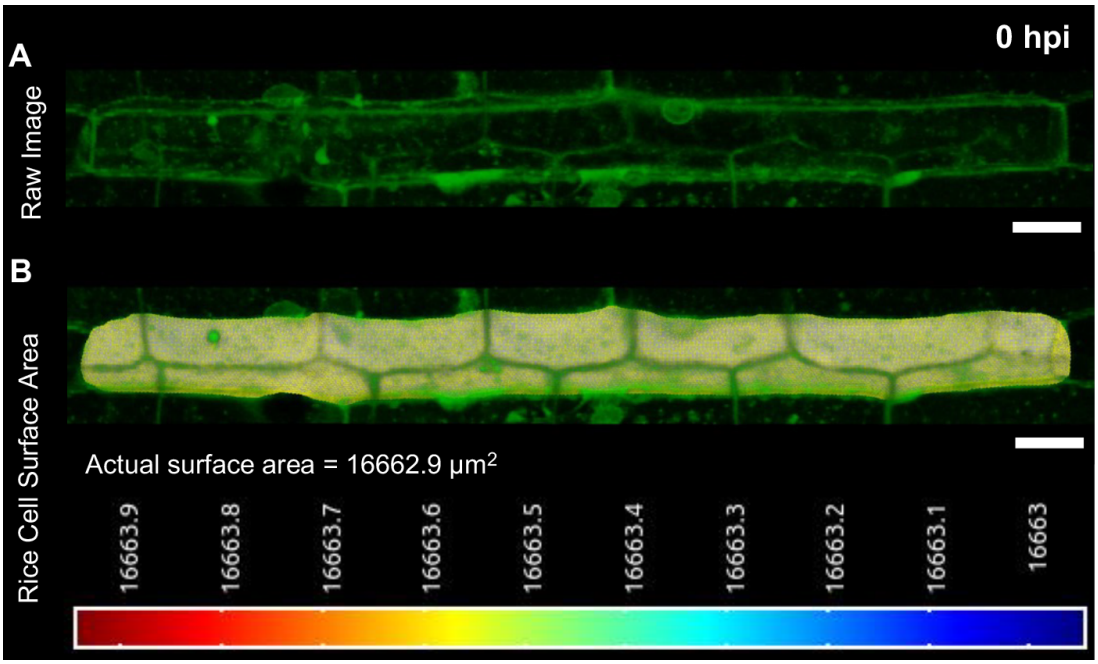

Figure 5.9 Representative 3D segmentation and quantification of surface area in rice cells at 24 hours post-inoculation using MorphoGraphX (MGX).

Snapshots from MorphographX showing **(A)** a raw image of a rice cell labelled with the plasma membrane marker LTI6b TMD:GFP and **(B)** the extracted 3D cell shape or segmented volume, where the surface area was measured. MGX generates a cell geometry heat map for measurements derived from the segmented volume, in this case, the cell surface area. The opacity of the raw image was adjusted to clearly show the cell boundaries. Scale bars = 20 µm.

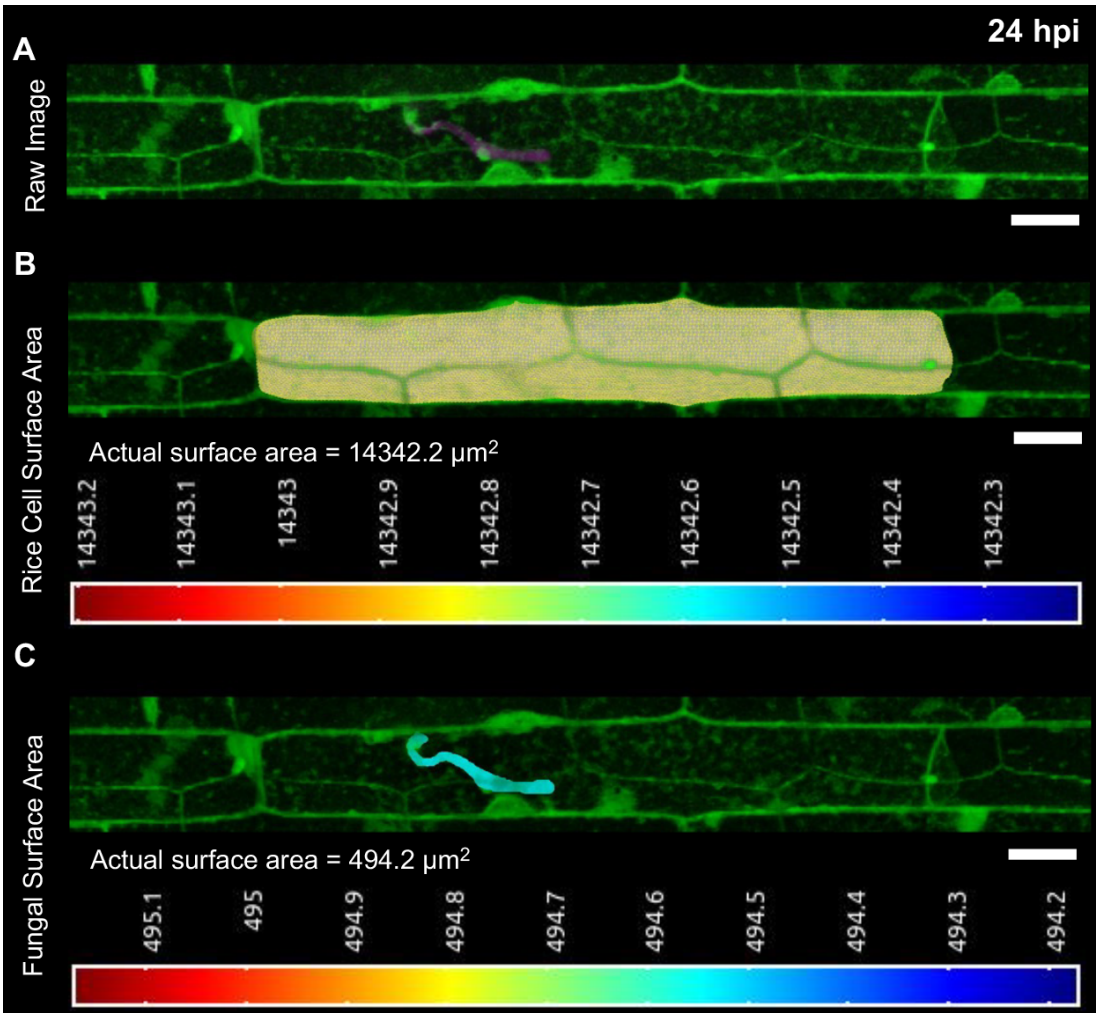

Figure 5.10 Representative 3D segmentation and quantification of surface area in rice cells at 24 hours post-inoculation (hpi) using MorphoGraphX (MGX).

A.Snapshot from MorphographX showing a raw image of a rice cell labelled with the plasma membrane marker LTI6b TMD:GFP (green), infected with *M. oryzae* Guy 11 strain expressing Mep1:mCherry/RP27p:mScarlet3 (magenta) at 24 hours post-inoculation (hpi) **B.** Snapshot showing the extracted 3D rice cell shape or segmented volume where surface area was measured. **C.** Snapshot showing the extracted segmented volume of the invasive hypha where the surface area was measured. MGX generates a cell geometry heat map for measurements derived from the segmented volumes of the rice cell and invasive hypha. The opacity of the raw image was adjusted to clearly show the cell boundaries and the invasive hypha within the cell. Scale bars = 20 µm.

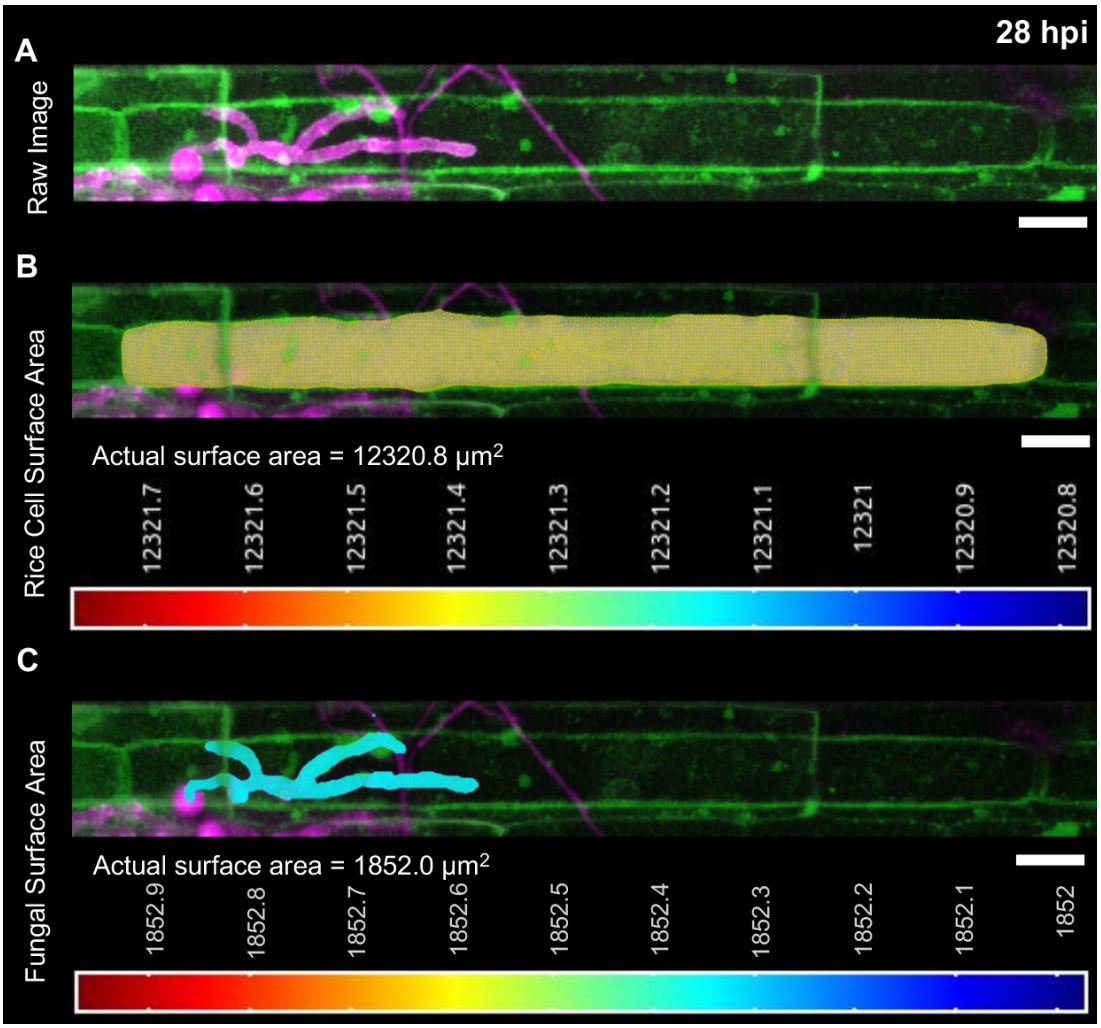

Figure 5.11 Representative 3D segmentation and quantification of surface area in rice cells at 28 hours post-inoculation using MorphoGraphX (MGX).

A.Snapshot from MorphographX showing a raw image of a rice cell labelled with the plasma membrane marker LTI6b TMD:GFP (green), infected with *M. oryzae* Guy 11 strain expressing Mep1:mCherry/RP27p:mScarlet3 (magenta) at 28 hours post-inoculation (hpi) **B.** Snapshot showing the extracted 3D rice cell shape or segmented volume where surface area was measured. **C.** Snapshot showing the extracted segmented volume of the invasive hypha where the surface area was measured. MGX generates a cell geometry heat map for measurements derived from the segmented volumes of the rice cell and invasive hypha. The opacity of the raw image was adjusted to clearly show the cell boundaries and the invasive hypha within the cell. Scale bars = 20 µm.

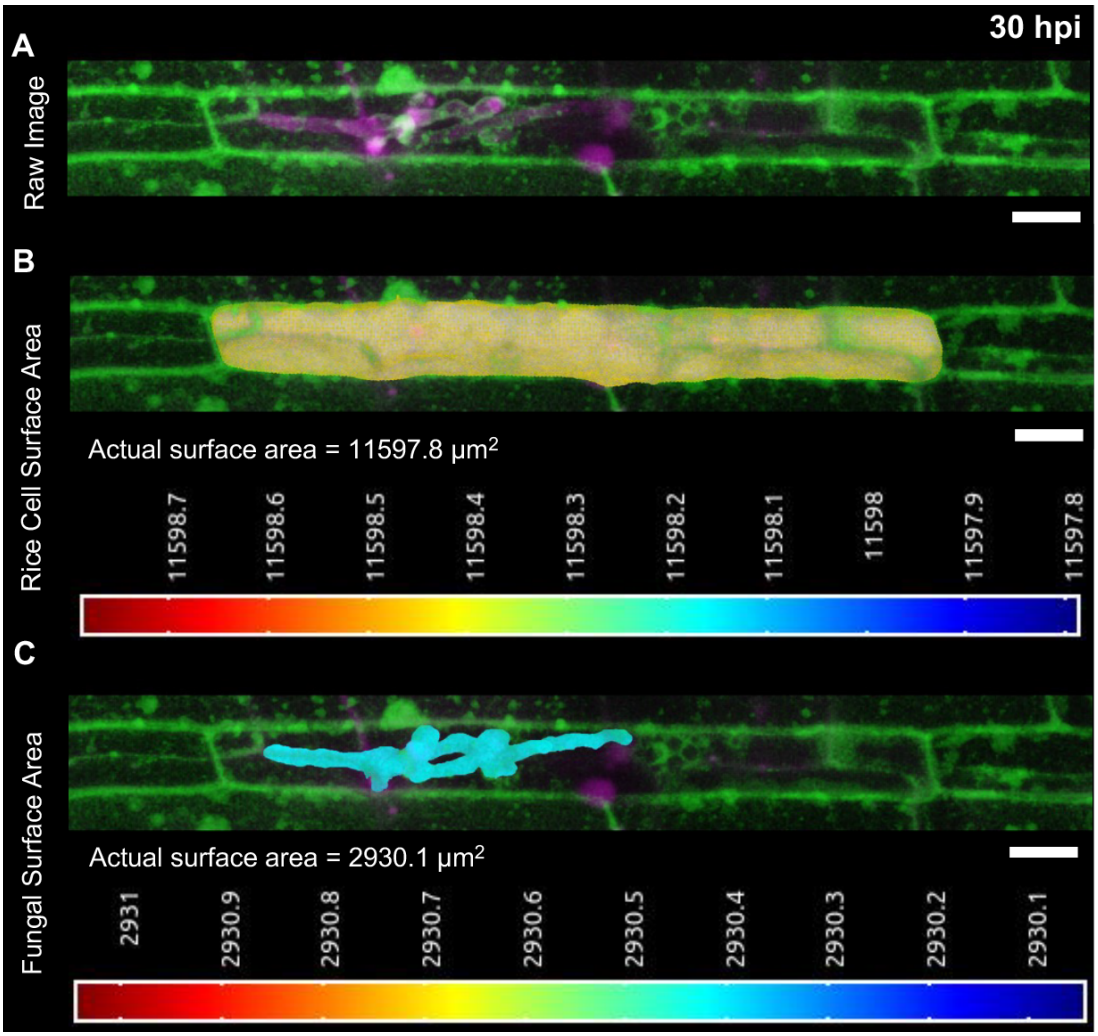

Figure 5.12 Representative 3D segmentation and quantification of surface area in rice cells at 30 hours post-inoculation using MorphoGraphX (MGX).

A.Snapshot from MorphographX showing a raw image of a rice cell labelled with the plasma membrane marker LTI6b TMD:GFP (green), infected with *M. oryzae* Guy 11 strain expressing Mep1:mCherry/RP27p:mScarlet3 (magenta) at 30 hours post-inoculation (hpi) **B.** Snapshot showing the extracted 3D rice cell shape or segmented volume where surface area was measured. **C.** Snapshot showing the extracted segmented volume of the invasive hypha where the surface area was measured. MGX generates a cell geometry heat map for measurements derived from the segmented volumes of the rice cell and invasive hypha. The opacity of the raw image was adjusted to clearly show the cell boundaries and the invasive hypha within the cell. Scale bars = 20 µm.

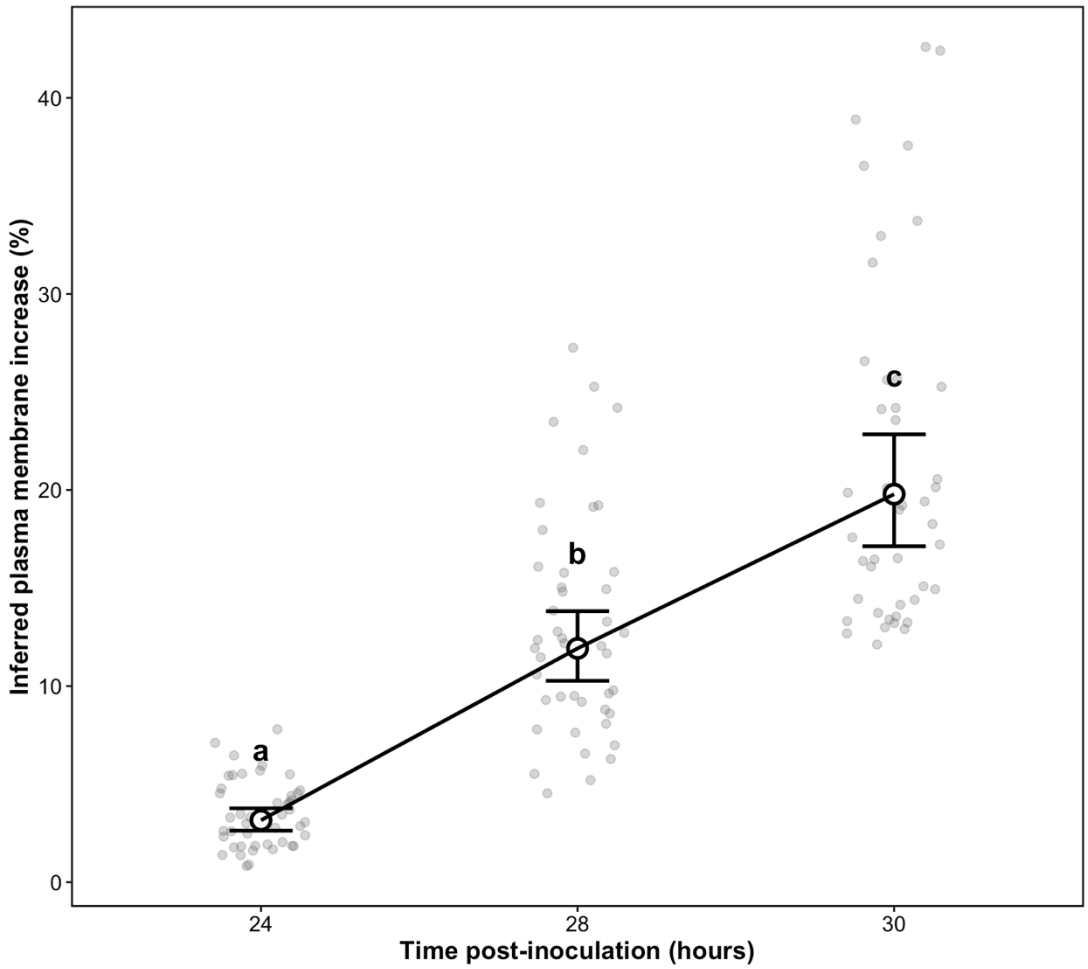

Figure 5.13 Inferred increase in plasma membrane during *M. oryzae* biotrophic growth.

Scatter plot showing the inferred percentage increase of plasma membrane during *M. oryzae* biotrophic growth from measuring the surface area of the fungal invasive hypha. Rice cells were inoculated with *M. oryzae,* and infection sites were examined at 24, 28, and 30 hours post-inoculation (hpi). Values were computed from surface area measurements in rice cells and invasive hyphae at different time points. Gray points represent individual infection sites (n = 15 per experiment, 3 independent experiments per timepoint). Large circles indicate geometric means with error bars showing 95% confidence intervals. The line connects means to illustrate the temporal trend. Letters above error bars denote significant differences based on Tukey's post-hoc test following linear mixed-effects modelling of log-transformed data (different letters indicate $p < 0.05$).

5.4 Discussion

The biotrophic phase of *Magnaporthe oryzae* infection is characterised by development of an interfacial plant plasma membrane-derived structure known as the extra-invasive hyphal membrane (EIHM), which surrounds invasive hyphae of *M. oryzae* (Kankanala et al., 2007). Like other biotrophic fungal pathogens and oomycetes, plant-derived interfacial membranes are essential for establishment and maintenance of biotrophy which requires host cell integrity to be maintained (Bozkurt et al., 2015; Perfect & Green, 2001).

However, the extent of additional membrane required to sustain the EIHM remains unknown.

In this chapter, we have shown that MorphoGraphX (MGX), an open-source tool developed for 3D surface reconstruction in biological imaging (Barbier de Reuille et al., 2015; Strauss et al., 2022), can be utilised to quantify the net additional plasma membrane generated to accommodate rapidly growing invasive hyphae of *M. oryzae*. MGX enables segmentation and quantification of surface areas in both rice cells and invasive hyphae from 3D images of *M. oryzae*-infected sites at different time points. We used the surface area of rice cells as a baseline and the surface area of the invasive hypha as a measure of the net additional plasma membrane generated, allowing us to calculate the percentage of additional plasma membrane required before EIHM integrity is lost. We analysed infection sites at 24 h post-inoculation (hpi), when invasive hyphae had just begun growing inside host cells, and at 28 hpi and 30 hpi, time points by which EIHM disruption is likely to occur. To our knowledge, this is the first application of MorphoGraphX in the context of plant-pathogen interactions and the first study to attempt quantification of EIHM surface area during plant infection.

MGX is an excellent tool for segmenting and analysing 3D image samples. It was able to segment rice cells with ease. Although it is primarily used for processing plant cell images, we successfully applied it to the segmentation of invasive hyphae. In both rice cell and invasive hyphae samples, it was necessary to set an appropriate threshold to ensure accurate segmentation and isolation of the structures for analysis or measurement. Segmenting rice cell images was considerably easier due to their relatively regular shape, whereas invasive hyphae posed greater challenges. The segmentation process for invasive hyphae took longer, as it required meticulous removal of unwanted segments or labels that were not relevant for surface area quantification. Currently, MGX does not support batch processing for segmentation and analysis, making it a time-consuming process, particularly when dealing with extensive fungal infections. Additionally, segmentation requires a trained eye to correctly identify which labels or segments should be included or excluded. For optimal results, it is advisable that the same person who acquires the images also performs the analysis in MGX.

Segmentation and analysis of surface area measurements from rice cells and invasive hyphae revealed a net increase of host plasma membrane during *M. oryzae* infection. The percentage net increase in host plasma membrane increases as the growth of invasive hyphae becomes more extensive. These results are consistent with previous findings that EIHM maintenance and disruption correlate with the stage of hyphal growth (Jones et al., 2021). Jones and colleagues (2021) determined the relationship of EIHM disruption and invasive hyphal growth stage by analysing rice cells infected with *M. oryzae* strain expressing sec-GFP (a secreted GFP from invasive hypha that accumulates at the EIHM compartment but leaks to the cytoplasm when EIHM is compromised) and a translational fusion of tdTomato to Histone1 (H1:tdTomato) as the nuclear marker. The growth stage of the invasive hypha was determined by counting H1:tdTomato-tagged nuclei. By the 13-14 nuclear stage, EIHM disruption frequency reached approximately 50% and by the 21-nucleus stage or beyond, all exhibited EIHM disruption. We expanded on these findings by estimating the amount of plasma membrane required to sustain the EIHM. Furthermore, our results are consistent with membrane biogenesis occurring and being stimulated during fungal infection and this response could be effector-mediated.

The mechanism underlying the origin of the EIHM, or any plant membrane encasing biotrophic hyphal structures, remains unknown. Historically, it has been assumed that plant membranes encasing biotrophic fungal structures are derived by invagination of the host plant plasma membrane (O'Connell & Panstruga, 2006). However, in *Arabidopsis* powdery mildew, the extrahaustorial membrane (EHM) has been clearly differentiated from the plasma membrane by the absence of eight GFP-labelled plasma membrane proteins, namely LTI6a, LTI6b, PIP2a, AtVamp3, SIMIP, PIP1b, Tuba6A, and BRI1 Instead, the plasma membrane is restricted to a collar-like structure encasing the upper part of the haustorial neck region (Koh et al., 2005). From the study by Koh and colleagues (2005), two models for EHM biogenesis have been proposed. In the first model, invagination and stretching of the host plasma membrane by the expanding haustorium is counterbalanced by exocytosis, which supplies new membrane material around the entire cell periphery. In such a scenario, the neckband functions as a selective barrier, permitting certain membrane components to enter the EHM while excluding typical plasma membrane proteins (Koh et al., 2005). The alternative model suggests that the EHM forms *de novo* through targeted secretion of specialised vesicles carrying membrane components unique to this structure, presumably lacking conventional plasma

membrane proteins (Koh et al., 2005). Similar findings have been reported in *Golovinomyces orontii* (powdery mildew infecting *Arabidopsis*), where neither the EHM nor the EHMx was labelled by antibodies recognising arabinogalactan protein (AGP) epitopes and non-AGP glycoproteins, typically present in the plasma membrane (Micali et al., 2011). In *Hyaloperonospora arabidopsidis* (*Hpa*)-*Arabidopsis* and *Phytophthora infestans* (*Pi*)-*Nicotiana benthamiana* interactions, plasma membrane-resident proteins such as the aquaporin PIP1;4 and calcium ATPase ACA8 were also excluded from the EHM (Caillaud et al., 2012; Lu et al., 2012).

To sustain EIHM integrity during *M. oryzae* infection, continuous plasma membrane biogenesis is required. A hypothesis has been proposed which suggests that the EIHM is assembled *de novo* by redeploying host membranes, as supported by FM4-64 dye-loading experiments. The presence of tubular and round vesicles near developing invasive hyphae indicates their potential role in the host cell endocytic network (Kankanala et al., 2007). The substantial plasma membrane surface area generated, particularly before EIHM disruption, also suggests a role for *de novo* lipid biosynthesis (Kankanala et al., 2007). However, an earlier study reported that lipid biosynthesis inhibitors increased plant susceptibility to blast disease, suggesting that *de novo* lipid biosynthesis is not essential for disease development (Koga, 1994). By contrast, phosphoinositides (PIs), a family of anionic phospholipids present in cell membranes, have been found to be enriched, recruited, or localised in biotrophic interfacial membranes (Balla, 2013; Logothetis et al., 2015; Noack & Jaillais, 2017; Posor et al., 2022). Phosphoinositides play key roles in controlling membrane expansion or reduction, interacting with the cytoskeleton and intracellular organelles, mediating protein distribution, and regulating exocytosis and endocytosis (Di Paolo & De Camilli, 2006; Noack & Jaillais, 2017). Specifically, phosphatidylinositol 4,5-bisphosphate [PI(4,5)P2] has been shown to be upregulated and recruited in the EHM-forming powdery mildew fungus *Erysiphe cichoracearum* (Qin et al., 2020) and EIHM-forming *Colletotrichum higginsianum* (Shimada et al., 2019) during *Arabidopsis* infections. In arbuscular mycorrhizal fungi *Rhizophagus irregularis* associated with *Medicago truncatula*, PI(4,5)P2-rich regions were observed at discrete areas of the periarbuscular membrane (PAM) throughout all phases of arbuscule branching. These regions co-localise with membrane marker proteins and are associated with changes in hyphal morphology, specifically the formation of small bulges (Ivanov & Harrison, 2019). Based on these observations, the authors hypothesised that these structures might

resemble the biotrophic interfacial complex (BIC) formed during *M. oryzae* infection. These BIC-like structures appear on hyphae during arbuscule development and might therefore serve as sites for AM fungal effector protein secretion. However, the lack of reliable AM fungal transformation methods makes this hypothesis difficult to test (Ivanov & Harrison, 2019). To further investigate whether specific phosphoinositides (PIs) are enriched and recruited in the *M. oryzae* extrainvasive hyphal membrane (EIHM), specific PI biosensors could be used as done previously (Qin et al., 2020; Shimada et al., 2019).

Other possible mechanisms of plasma membrane expansion during infection include the co-option of membrane reservoirs or invaginations in the host plasma membrane. During *Salmonella* invasion, bacterial effectors SipC, SopE2, and SopB recruit exocyst subunits from membrane reservoirs and other cellular compartments, facilitating exocyst complex assembly and targeted membrane delivery essential for bacterial uptake (Zhu et al., 2024). In *M. oryzae*, the effector Bas83 has been hypothesised to facilitate rapid membrane turnover in biotrophic interfacial complexes (BICs). Bas83 primarily localises to membranous effector compartments (called MECs) clustered around BICs and BIC-associated cells, and also marks the EIHM encasing BIC-associated cells, suggesting potential fusion with the EIHM. However, experimental confirmation of this hypothesis remains unachieved due to unsuccessful targeted gene deletion attempts (Oliveira-Garcia et al., 2023). Once Bas83 knockouts or other candidate effectors become available, the MGX pipeline developed in this study could be employed to functionally validate their role in host plasma membrane expansion during *M. oryzae* infection.

In this chapter, we developed a pipeline using MorphographX for segmentation and surface area quantification in 3D images of rice cells and invasive hyphae during *M. oryzae* infection. Surface area quantifications enabled us to compute the additional plasma membrane required before EIHM integrity is lost. I conclude that during infection, there is a significant net increase in host plasma membrane during infection to sustain the EIHM, thus maintaining the biotrophic stage of *M. oryzae* infection. Our data highlight the extensive plasma membrane expansion is necessary to accommodate rapidly growing hyphae and sustain biotrophic interactions. Although no specific effectors have been identified as responsible for this process, our pipeline provides a valuable tool for functionally validating candidate effectors involved in host plasma membrane expansion. Future improvements could enhance the efficiency of the pipeline by enabling batch

processing, as our current analyses required meticulous manual label removal following segmentation.

Chapter 6 Rice F-actin dynamics during *Magnaporthe oryzae* infection

6.1 Introduction

The plant actin cytoskeleton is a major cellular component that plays essential roles in cell development and various processes, including cellular shape (Blanchoin et al., 2014; Pollard & Cooper, 2009; Szymanski & Staiger, 2018), elongation (Barrero et al., 2002), vesicle trafficking (Baluška et al., 2004; Baluška et al., 2002; Johnson et al., 2012; Lee et al., 2008; Mooren et al., 2012; Robertson et al., 2009; Šamaj et al., 2006; Synek et al., 2014; H. Wang et al., 2016; Wang & Hussey, 2015; Yalovsky et al., 2008; Žárský et al., 2009), cytoplasmic streaming, and organelle distribution (Blanchoin et al., 2014; Geitmann & Nebenführ, 2015; Peremyslov et al., 2015; Pollard & Cooper, 2009; Verchot-Lubicz & Goldstein, 2010; Wada & Kong, 2018).

Actin exists in two main forms: monomeric globular actin (G-actin) and polymerised filamentous actin (F-actin). The physiological functions of actin depend on its structural state, whether as a monomer, oligomer, polymer, or in complex with actin-binding proteins (ABPs). The dynamic organisation of actin structures within the cell is maintained through continuous assembly, disassembly, and reassembly of helical polymer filaments (Dominguez & Holmes, 2011; Fletcher & Mullins, 2010).

Actin filament assembly occurs in two key stages: nucleation and elongation (Pollard, 2016; Pollard & Cooper, 1986). Nucleation involves the initial association of actin monomers, forming dimers and subsequently unstable trimers. Although thermodynamically unstable, these trimers serve as essential 'seeds' for filament formation (Pollard et al., 2000). After nucleation, filament elongation depends on monomer concentration and the filament end where monomers are incorporated. Actin monomers exist in three nucleotide states: ATP-actin, ADP-Pi-actin, and ADP-actin (Pollard, 2016; Pollard & Cooper, 1986; Sedwick, 2011; Zheng et al., 2007). Polymerised actin forms a double-helical filament with head-to-tail orientation, creating a molecular polarity. The barbed (+) end elongates faster than the pointed (−) end. Once an actin monomer is incorporated into a filament, its bound ATP is rapidly hydrolysed to ADP (Blanchoin & Pollard, 2002). After ATP hydrolysis, the inorganic phosphate (Pi) that is cleaved from

actin is released slowly, resulting in the transient ADP-Pi state of actin (Blanchoin & Pollard, 2002; Carlier & Pantaloni, 1986; Pollard & Borisy, 2003). Once Pi dissociates, the filament transitions into the ADP-bound state, which can then depolymerise into G-actin (Pollard, 2016; Pollard & Cooper, 1986). ATP-actin preferentially polymerises at the barbed end, while ADP-actin dissociates from the pointed end. This process is regulated by ATP hydrolysis and phosphate release (Pollard et al., 2000). The continuous turnover of actin monomers establishes a steady-state mechanism known as 'treadmilling,' in which polymerisation at the barbed end is balanced by depolymerisation at the pointed end (Blanchoin et al., 2010; Pollard et al., 2000; Pollard & Cooper, 2009). This process is tightly regulated by essential molecular machines conserved across all eukaryotic organisms (Day et al., 2011; Stradal & Schelhaas, 2018).

Plant cells regulate actin organisation and function through a network of actin-binding proteins (ABPs). ABPs are classified into two functional categories: those that regulate the actin monomer pool by affecting microfilament dynamics and assembly, and those that arrange microfilaments into more complex structures (McCurdy et al., 2001). Key classes of ABPs in plants include actin-depolymerising factors (ADFs)/cofilins, profilins (PRFs), cyclase-associated proteins (CAPs), myosins, fimbrins, villins, LIM domain-containing proteins (LIMs), formins, and capping protein (CP). Actin-depolymerising factors (ADFs)/cofilins bind to both monomeric actin and filamentous actin, and promote severing and loss of actin monomers from the pointed end (Galkin et al., 2011; Suarez et al., 2011; Wioland et al., 2017). Profilins (PRFs) sequester actin monomers to maintain the level of polymerisable actin monomers. PRFs interact with proteins containing proline-rich sequences and phospholipids, which in turn facilitates its binding to actin monomers through multiple mechanisms (Sun et al., 2013). Cyclase-associated proteins (CAPs) are also actin monomer-binding proteins that interact with adenylyl cyclase at the N-terminus and G-actin at the C-terminus via their two distinct domain, allowing them to perform multiple functions (Gerst et al., 1991) such as directly enhancing the rate of nucleotide exchange on G-actin. CAPs help convert ADP-actin back to ATP-actin, ensuring a readily available pool of polymerisation-competent actin monomers (Chaudhry et al., 2007). Myosins are motor proteins which have cargo, actin-binding, and ATPase activities (Peremyslov et al., 2015; Peremyslov et al., 2010). Myosins provide the tensile force to pull an actin filament straight (Sparkes, 2011). Fimbrins contain an actin-binding domain (ABD) consisting of two tandem calponin-homology

(CH) domains. Each fimbrin molecule has two ABDs, allowing it to crosslink actin filaments as a monomer and facilitate the formation of higher-order actin structures (Bretscher & Weber, 1980; Harris et al., 2019). Fimbrins contribute to actin cytoskeleton organization by stabilizing the actin fringe through filament cross-linking (Su et al., 2012), arranging actin filaments into loose networks (Kovar et al., 2000), and forming tightly packed actin bundles (Zhang et al., 2019). Villins regulate actin dynamics by facilitating actin bundling (Huang et al., 2015; Huang et al., 2005; Klahre et al., 2000; Nakayasu et al., 1998; Zhang et al., 2010). These actin-bundling proteins crosslink adjacent actin filaments, forming tightly packed parallel bundles (Thomas et al., 2009). Villins also have Ca^{2+}-dependent actin-severing functions (Zhang et al., 2010). LIM (Lin-11, Isl-1, and Mec-3) domain-containing proteins (LIMs), a group of LIM domain proteins related to animal cysteine-rich proteins, have been identified as key initiators of actin bundle formation, an essential component of the higher-order cytoskeleton (Li et al., 2014; Thomas et al., 2006; Wang et al., 2008). Formins are actin nucleation factors involved in the formation of linear actin bundles (Blanchoin & Staiger, 2010). Characterized by the presence of FH1 and FH2 domains, formin proteins can nucleate actin assembly either from actin monomers or actin-profilin complexes (Blanchoin & Staiger, 2010) and bind to capping protein-bound barbed end to uncap filaments (Shekhar et al., 2015; Shekhar et al., 2016). Formins have been found to have additional capabilities including promotion of supernumerary actin cable formation (Cheung & Wu, 2004), actin filament side-binding (Michelot et al., 2006), filament severing (Gurel et al., 2014; Ren & Xiang, 2007), and microtubule affinity (Deeks et al., 2010). Capping protein (CP) controls actin assembly by tightly binding to the barbed ends of actin filaments, preventing both the addition and removal of actin subunits (Huang et al., 2003).

The plant actin cytoskeleton plays a pivotal role in immune responses against pathogens, including fungi (Kobayashi, Kobayashi, et al., 1997; Kobayashi, Yamada, et al., 1997), bacteria (Henty-Ridilla et al., 2013; Li et al., 2015), oomycetes (Overdijk et al., 2016; Takemoto et al., 2003) and nematodes (Clément et al., 2009; de Almeida Engler et al., 2010; de Almeida Engler et al., 2004). For instance, actin bundles converge at attempted penetration sites, preventing microbial invasion (Kobayashi, Kobayashi, et al., 1997; Opalski et al., 2005; Schmidt & Panstruga, 2007; Takemoto et al., 2003). Actin cytoskeleton remodeling also occurs during both pathogen-triggered immunity (PTI) (Henty-Ridilla et al., 2013) and effector-triggered immunity (ETI) (Li & Staiger, 2018),

and several ABPs have been identified as important players during immune response (Leontovyčová et al., 2020; Li & Staiger, 2018; Qin et al., 2021; Yang et al., 2014; Zou et al., 2021).

Meanwhile, pathogen virulence factors and effectors target the actin cytoskeleton and ABPs to facilitate infection. For example, the nucleocapsid (N) protein from Tomato spotted wilt tospovirus (TSVW) alters endomembrane trafficking by interacting with actin and myosin (Feng et al., 2013). The *Pseudomonas syringae* effector HopW1 disrupts actin organisation and inhibits endocytosis (Kang et al., 2014), while HopG1 induces actin remodeling to promote infection symptoms (Shimono et al., 2016) in *Arabidopsis*.

Despite advances in understanding the role of host actin in plant-pathogen interactions, our knowledge of actin cytoskeleton remodelling during the rice-*M. oryzae* interaction remains very limited. Previous studies have primarily focused on pre-penetration stages, but not during *M. oryzae* biotrophic growth. For instance, in *Arabidopsis*, *M. oryzae* has been shown to induce an increase in actin filament abundance, likely as part of a pathogen-triggered immunity (PTI) response (Henty-Ridilla et al., 2013). Similarly, an earlier study found that *M. oryzae* Δ*mps1* mutants, which are unable to penetrate host cells, still triggered cytoskeletal rearrangement in onion epidermal cells (Xu et al., 1998). Notably, in both cases, there was no compatible interaction between the host and the pathogen.

In this chapter, I report investigations of the spatiotemporal changes in the rice actin cytoskeleton during *M. oryzae* biotrophic growth. I demonstrate that rice actin initially surrounds *M. oryzae* invasive hyphae in both initially invaded and newly invaded adjacent cells. Actin also accumulates at cell crossing points and biotrophic interfacial complexes (BICs). Actin disruption occurs as *M. oryzae* infection progresses. Collectively, these findings suggest that actin remodelling is crucial for successful invasion, while actin disruption marks the transition from biotrophy to necrotrophy in *M. oryzae* infection.

6.2 Results

6.2.1 Rice actin filaments localise around *M. oryzae* invasive hypha

In obligate biotrophs such as *Blumeria graminis* f. sp. *hordei* (barley-adapted powdery mildew) and *Golovinomyces orontii* (*Arabidopsis*-adapted powdery mildew), haustoria at early developmental stages are surrounded by host actin filaments (Inada, 2016; Inada et al.,

2016; Opalski et al., 2005). To investigate whether a similar phenomenon occurs in a hemibiotrophic fungal pathogen like *M. oryzae*, where invasive hyphae are also encased by actin filaments during infection, I inoculated transgenic rice lines expressing LifeAct:GFP with *M. oryzae* Guy11 expressing RP27p:tdTomato. To capture infection site details, I acquired z-stack images from the top to the base of epidermal cells, ensuring full coverage of the cell layer. A comparison of maximum projections from uninfected sites (Figure 6.1A) and infection sites (Figure 6.1C) across the entire epidermal cell layer did not reveal obvious differences. However, a distinct pattern emerged when analysing maximum projections of middle slices. By 24 hours post-inoculation (hpi), actin filaments were observed to surround invasive hyphae in the initially infected cell (Figure 6.1D), whereas in uninfected cells, actin remained more evenly distributed (Figure 6.1B). 3D projections further highlighted these differences. In uninfected cells, actin cables were predominantly located at the cell periphery, contributing to structural integrity (see Movie 6.1). In contrast, in infected cells, actin cables reorganise toward the rice cell interior, accumulating around the site of hyphal growth (see Movie 6.2). To determine whether actin restructuring occurs as the pathogen spreads to neighbouring cells, I analysed actin dynamics at 36 hpi. The results showed that actin cables once again surrounded the newly invading hyphae as they advance into adjacent cells (Figure 6.2). These findings demonstrate that the actin cytoskeleton undergoes remodeling during *M. oryzae* biotrophic growth.

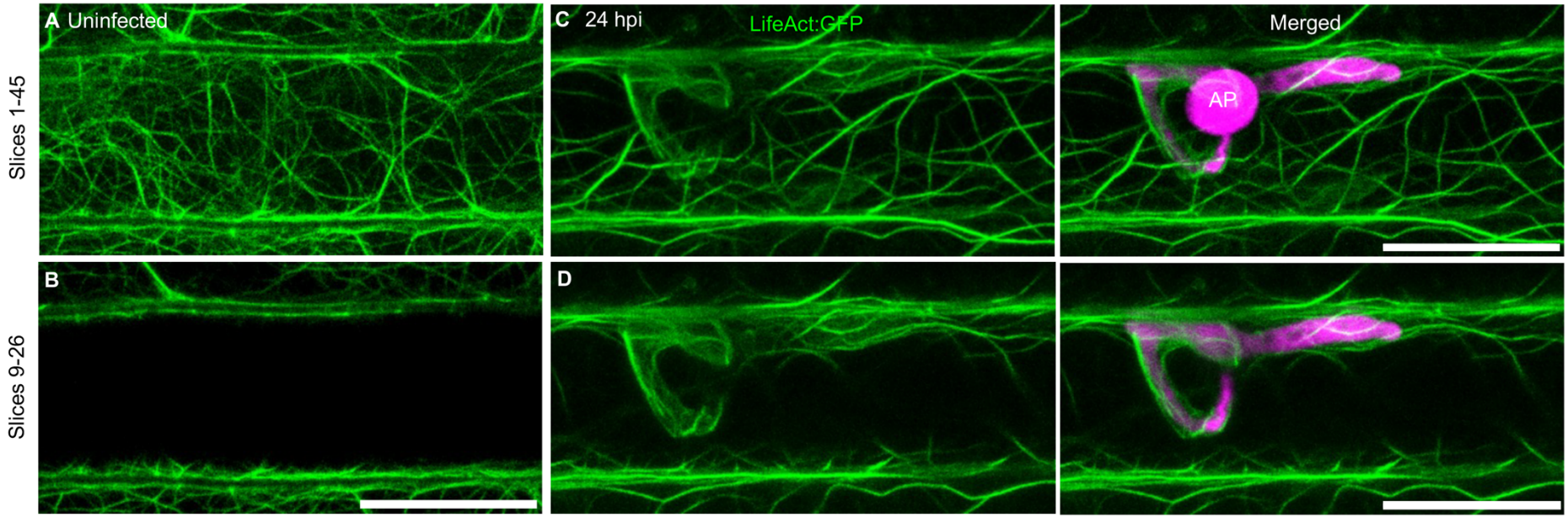

Figure 6.1 Rice F-actin filaments localise around *Magnaporthe oryzae* invasive hyphae during biotrophic growth.

A. Maximum projection of the entire epidermal layer of uninfected rice cell showing GFP-labeled LifeAct. **B.** Maximum projection of middle z-slices of uninfected rice cell to show that the middle portion of the cell has no actin filaments. **C.** Maximum projection of the entire epidermal layer of rice cell expressing GFP-labeled LifeAct inoculated with *M. oryzae* Guy11 expressing RP27p:tdTomato at 24 hours post-inoculation (hpi). **D.** Maximum projection of middle z-slices of infected rice cell expressing GFP-labeled LifeAct inoculated with *M. oryzae* Guy11 expressing RP27p:tdTomato to show that actin filaments surround invasive hypha at 24 hpi. Confocal micrographs were prepared from leaf sheath inoculations using rice cv Kitaake transgenic lines expressing actin marker LifeAct:GFP and infected with *M. oryzae* Guyy1 RP27p:tdTomato. Leaf sheath infections were incubated at 24 °C. All images shown are maximum projections of z-stack series taken using a Leica TCS SP8X confocal laser scanning microscope. AP = appressorium. Scale bars = 20 μm.

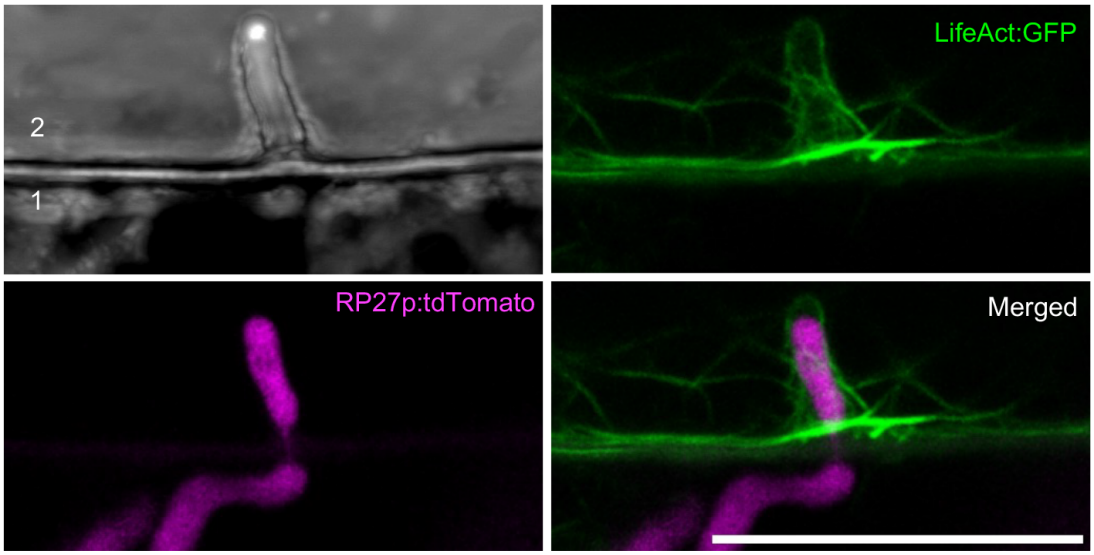

Figure 6.2 Rice F-actin filaments localise around *Magnaporthe oryzae* invasive hyphae in newly invaded cell.

Confocal micrographs of infected rice cell expressing GFP-labeled LifeAct (green) inoculated with *M. oryzae* Guy11 expressing RP27p:tdTomato (magenta) showing actin filaments surrounding invasive hyphae in newly invaded cells at 36 hours post-inoculation (hpi). Confocal micrographs were prepared from leaf sheath inoculations using rice cv Kitaake transgenic lines expressing actin marker LifeAct:GFP infected with *M. oryzae* Guy1 RP27p:tdTomato. Leaf sheath infections were incubated at 24 °C. Numbers indicate the order in which the fungus invades host cells (1=first-invaded cell, 2=second-invaded cell). All images shown are maximum projections of z-stack series taken using a Leica TCS SP8X confocal laser scanning microscope. Scale bars = 20 μm.

6.2.2 Rice F-actin is disrupted as *M. oryzae* infection progresses and invades adjacent host cells

In Chapter 4, I provided multiple lines of evidence showing that during the early stages of infection, the initially invaded rice cells remain viable but lose viability once the fungus spreads to adjacent cells. I hypothesise that the actin cytoskeleton becomes disrupted as fungal infection progresses and the initially invaded cell begins to lose viability. To investigate actin cytoskeleton dynamics during *M. oryzae* infection, I therefore captured time-lapse videos tracking fungal progression from the initially invaded cell to adjacent cells. Observations began at the pre-penetration stage, when the appressorium had already formed, in order to determine whether actin filaments accumulate beneath the attempted penetration site. No actin reorganisation was observed under the appressorium (Figure 6.3, Movie 6.3, Movie 6.4 22h:00min:00sec). However, following fungal penetration, reduction in actin cables was observed starting 28h:00min:00sec (Figure 6.3, Movie 6.4 timepoint 28h:00min:00sec). By 36h:00min:00sec, the initially invaded cell was nearly devoid of actin cables (Figure 6.3, Movie 6.4 timepoint 36h:00min:00sec). These findings indicate that rice actin in the initially invaded cell becomes disrupted as fungal

growth advances and spreads to adjacent cells. It is worth noting that by 31 h, the fungus had begun invading an adjacent cell (2a). However, this cell already lacked actin cables which does not imply that the fungus disrupted actin in an uninfected cell. Rather, the absence of actin is due to a more advanced infection on the opposite side of the cell, which is not visible in Figure 6.3. For clarification, a wider field of view is provided in Figure 6.4.

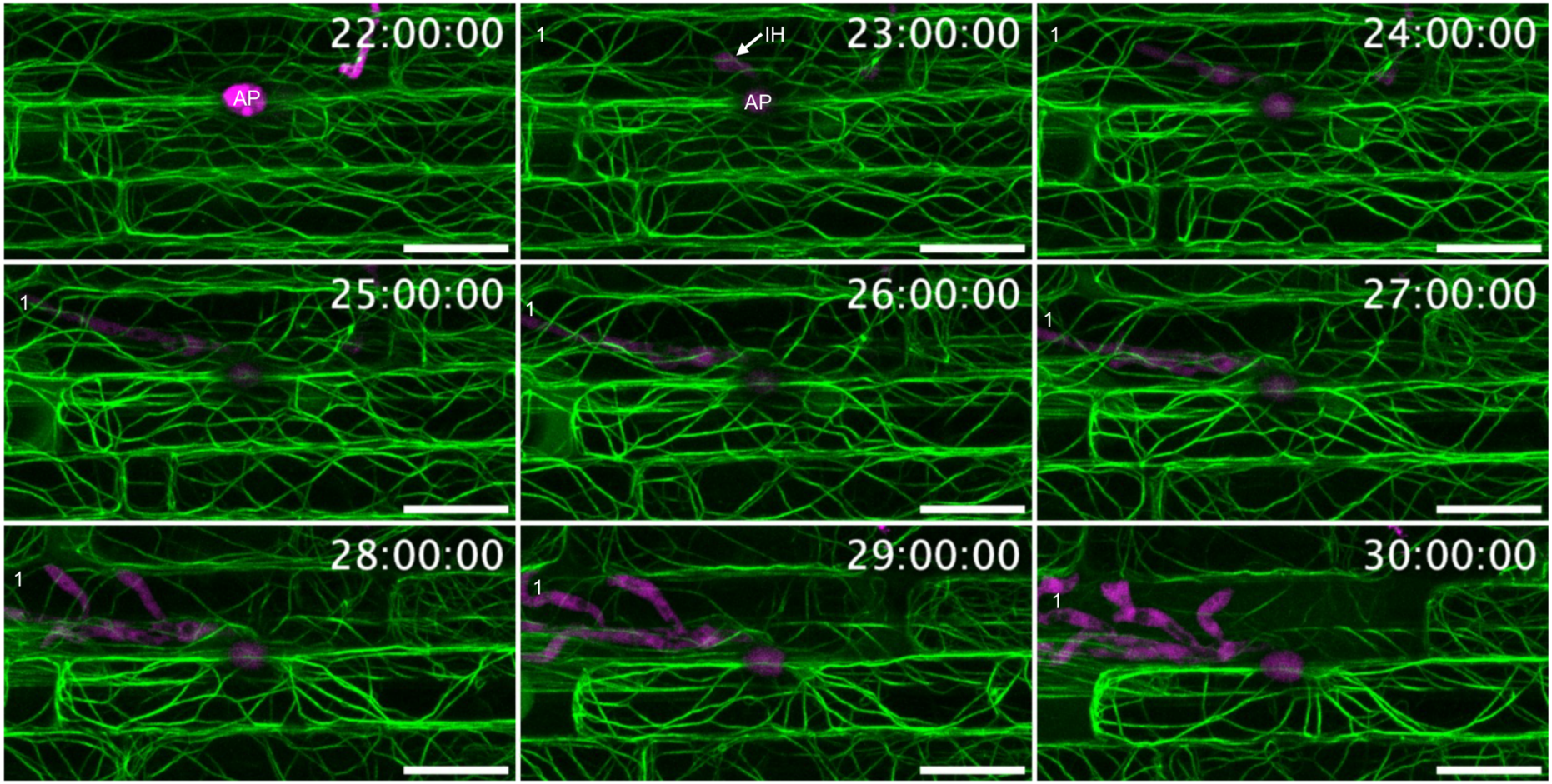
22:00:00
AP
1
IH
23:00:00
AP
1
24:00:00
1
25:00:00
1
26:00:00
1
27:00:00
1
28:00:00
1
29:00:00
1
30:00:00

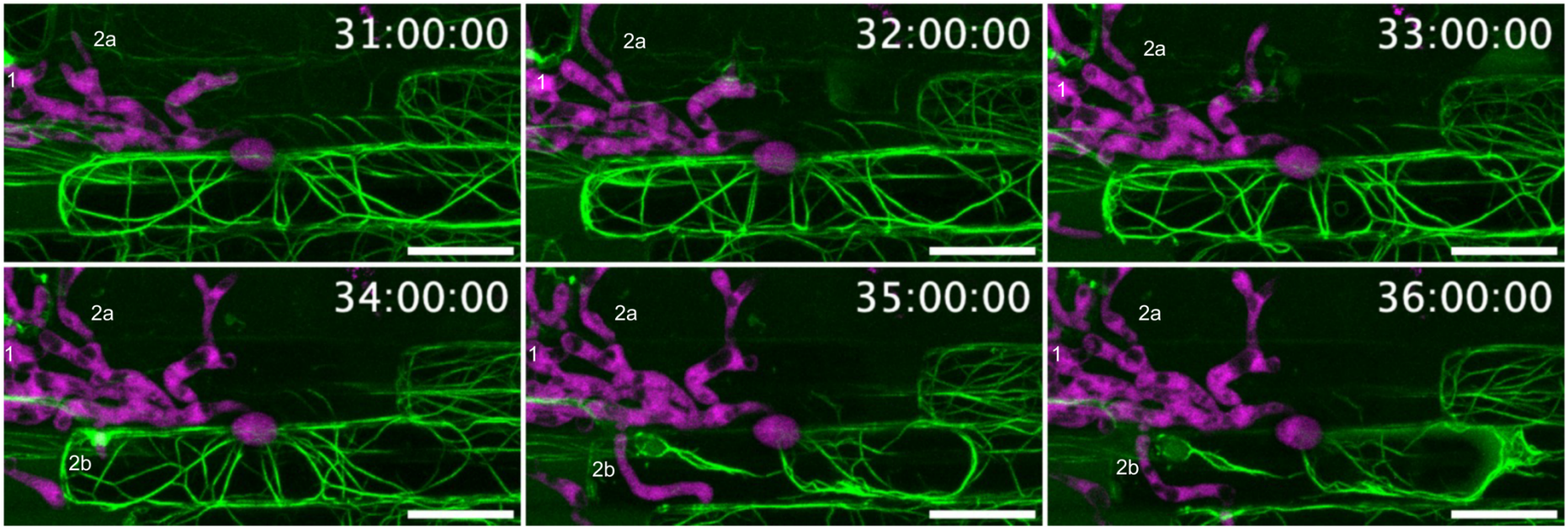

Figure 6.3 Rice F-actin is disrupted as *Magnaporthe oryzae* infection progresses and moves to adjacent cells.

Time-lapse laser confocal scanning microscopy of rice leaf sheath cells of Kitaake transgenic line expressing actin marker LifeAct:GFP (in green) infected with *M. oryzae* Guy11 expressing RP27p:tdTomato (magenta) showing rice actin disruption as *M. oryzae* infection progresses. The infected sample was imaged from 21-36 hours post-inoculation (hpi) using a Leica TCS SP8X confocal laser scanning microscope. Micrographs shown are maximum intensity projections of a z-stack series and correspond to time-lapse series (Movie 6.4) taken at 10 min intervals. Numbers indicate the order in which the fungus invades host cells (1=first-invaded cell, 2=second-invaded cell; 2a=1st adjacent cell colonised; 2b=2nd adjacent cell colonised). Time scale is in h: min: sec. AP=appressorium, IH=invasive hypha. Scale bar = 20 μm.

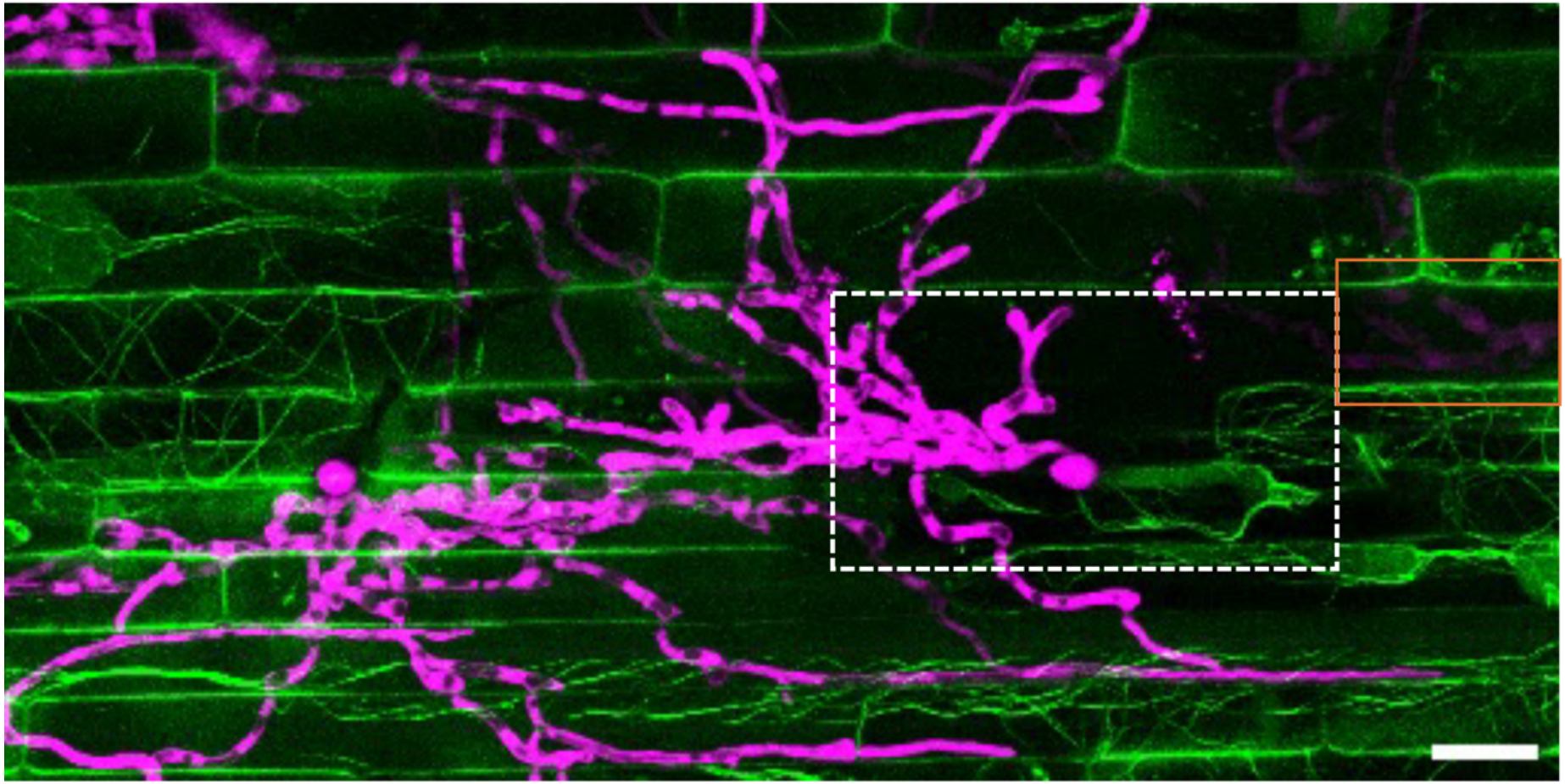

Figure 6.4 Widefield view of infection site captured in the time-lapse video, Movie 6.4 at 36 h post-inoculation.

Confocal micrograph showing a wider field of view of the infection site captured in the time-lapse video, Movie 6.4. The area inside the white dotted lines is the field of view captured in the time-lapse video while the area enclosed in the orange box highlights the more advanced infection that caused actin inhibition in the cell adjacent to the initially invaded cell.

6.2.3 Rice actin accumulates at cell crossing points

From Movie 6.4, I observed that rice actin accumulates at cell crossing points when invasive hyphae from different directions points move from the first-invaded cell into adjacent cells. To monitor rice actin accumulation at cell crossing points, I performed time-lapse imaging capturing the entire first-invaded cell and its neighbouring cells to determine whether actin accumulates at cell crossing points as invasive hyphae invade the adjacent cells. Actin accumulation at cell crossing points was observed starting from 35h:00min:00sec in adjacent cells as invasive hyphae form the initially invaded cell colonised neighbouring cells. However, when two or more invasive hyphae entered the same neighbouring cell, actin accumulation was not always observed at all penetration sites (Figure 6.5; Movie 6.5).

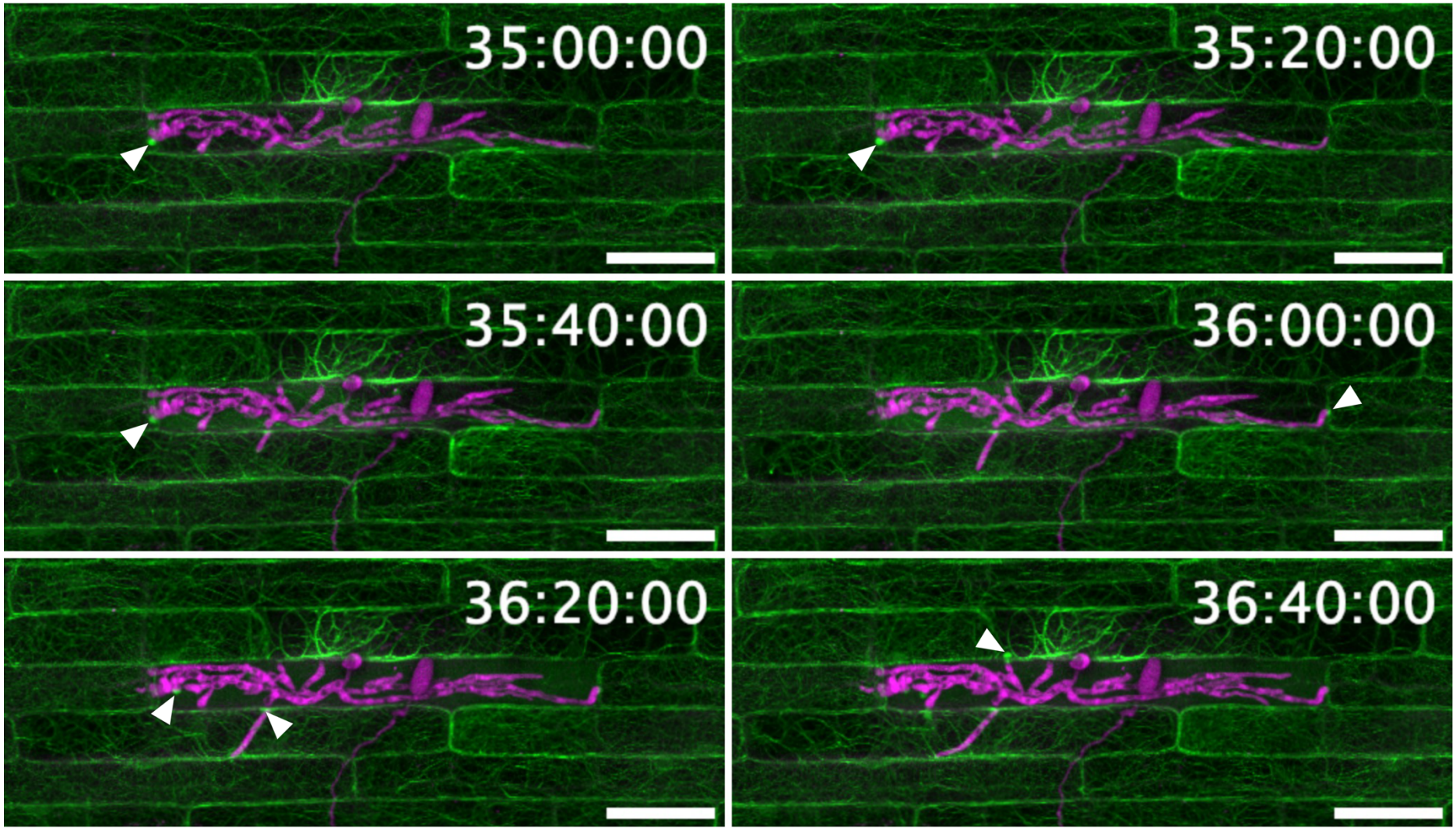
35:00:00
35:20:00
35:40:00
36:00:00
36:20:00
36:40:00

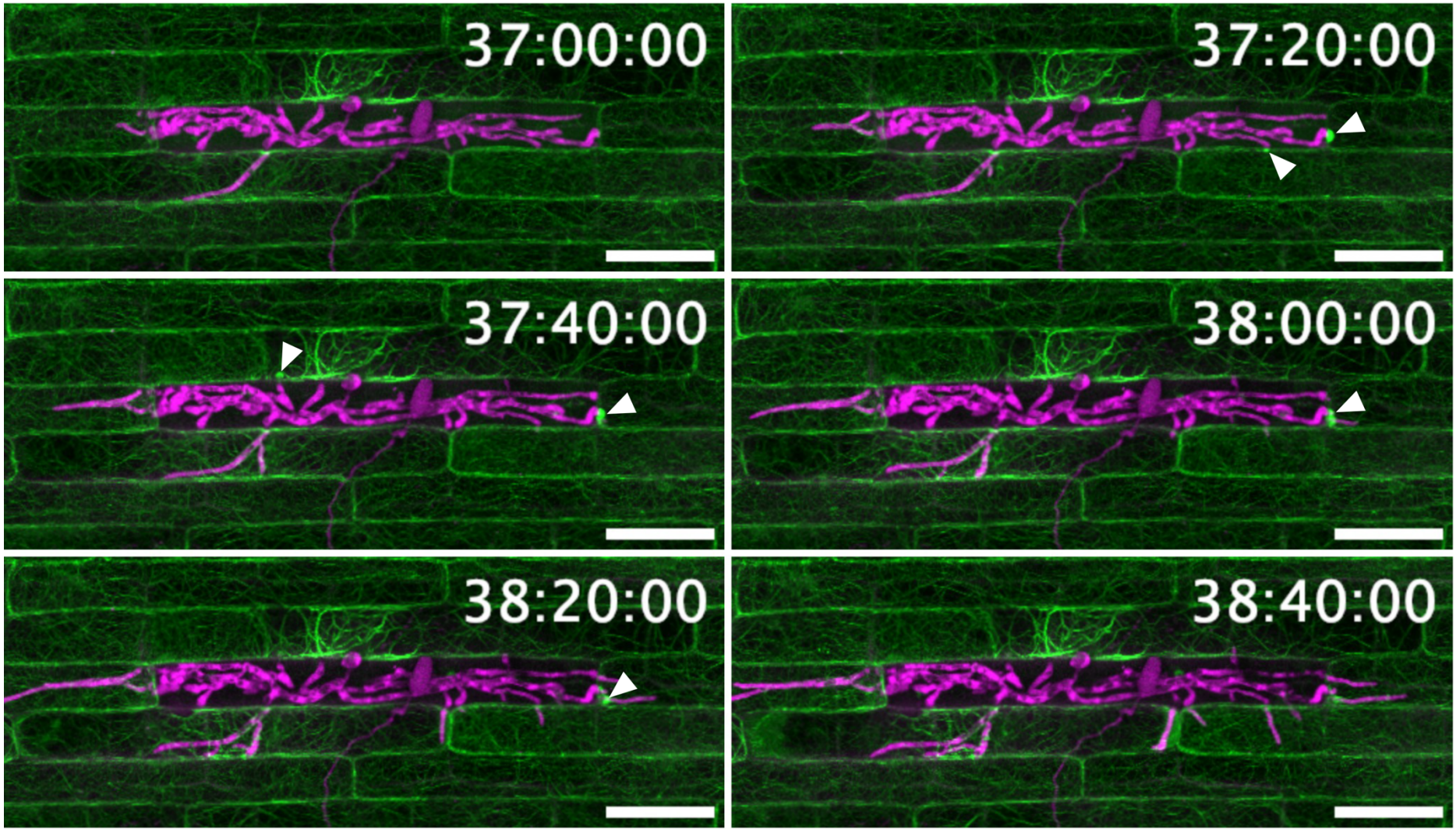
37:00:00
37:20:00
37:40:00
38:00:00
38:20:00
38:40:00

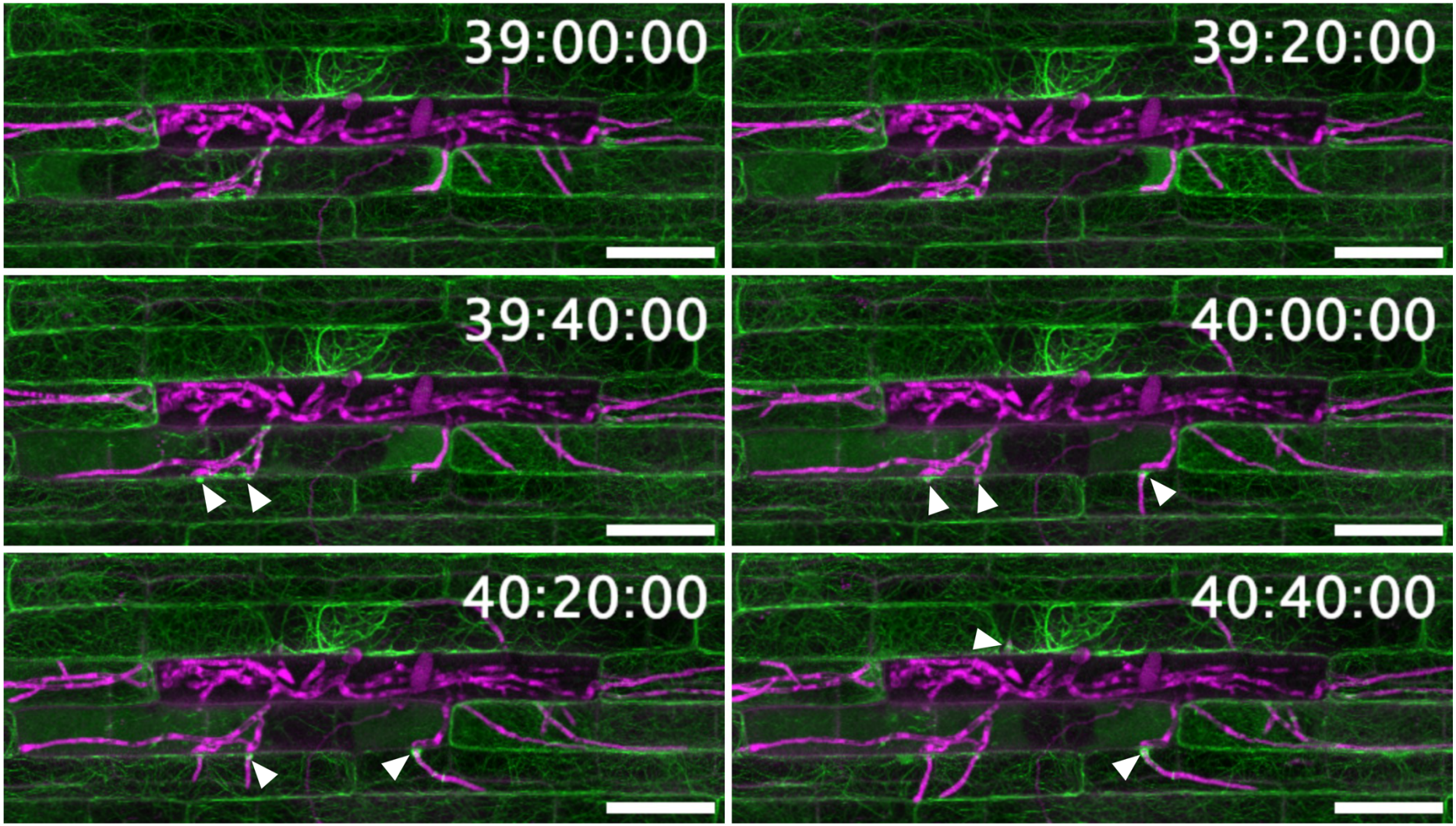
39:00:00
39:20:00
39:40:00
40:00:00
40:20:00
40:40:00

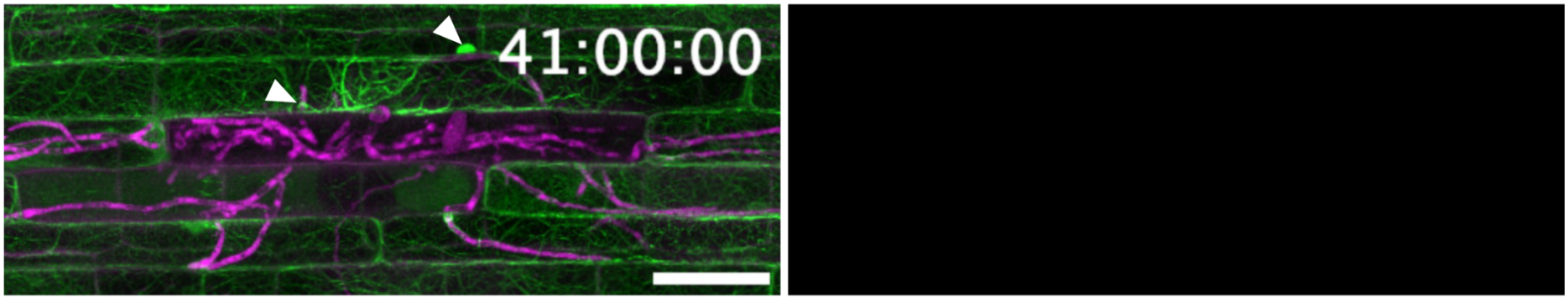

Figure 6.5 Rice F-actin accumulates at cell crossing points.

Time-lapse laser confocal scanning microscopy of rice leaf sheath cells of Kitaake transgenic line expressing actin marker LifeAct:GFP (in green) infected with *M. oryzae* Guy11 expressing RP27p:tdTomato showing rice actin disruption as *M. oryzae* infection progresses. The infected sample was imaged from 24-41 hours post-inoculation (hpi) using a Leica TCS SP8X confocal laser scanning microscope. Micrographs shown are maximum intensity projections of a z-stack series and correspond to a time-lapse series (Movie 6.5) taken at 10 min intervals. White arrows indicate actin accumulation at cell crossing points. Time scale is in h: min: sec. Scale bar = 20 μm.

6.2.4 Rice actin in adjacent cells show thickened filaments during infection in initially invaded cell

From Movie 6.4, the host cell directly beneath the initially infected cell appeared to have thickened actin filaments and reduced dynamic movement while fungal infection progressed. This observation led me to hypothesise that fungal infection in the first-invaded cell might manipulate the adjacent cell, which is most likely to be colonised next. The thickened filaments may for example indicate actin bundling. In *Arabidopsis* infected with *Pseudomonas syringae* DC3000, a significant increase in filament bundling was observed from 18-36 hpi suggesting the involvement of effector-triggered immunity (ETI) (Henty-Ridilla et al., 2013). To investigate whether uninfected cells adjacent to the infection site also exhibit bundling and reduced filament dynamics, I captured time-lapse videos with a wider field of view (Movie 6.6 and Movie 6.7; Movie 6.6 is an uncropped version of Movie 6.5). I focused exclusively on fully imaged, uninfected cells directly adjacent to the infected cell. In both time-lapse videos, uninfected cells which were typically located directly above and below the initially infected sites exhibited thicker actin filaments and reduced actin dynamics. This suggests that infection in the first-invaded cell might have manipulated the neighbouring uninfected cells. However, adjacent cells on either end of initially invaded cells did not display noticeable filament thickening and movement reduction. Uninfected adjacent cells with thickened filaments revert to usual actin filament appearance and movement after some time before the fungus invades the adjacent cell (Figure 6.6). There may be an immune response that is overcome by the invasion of the adjacent cell.

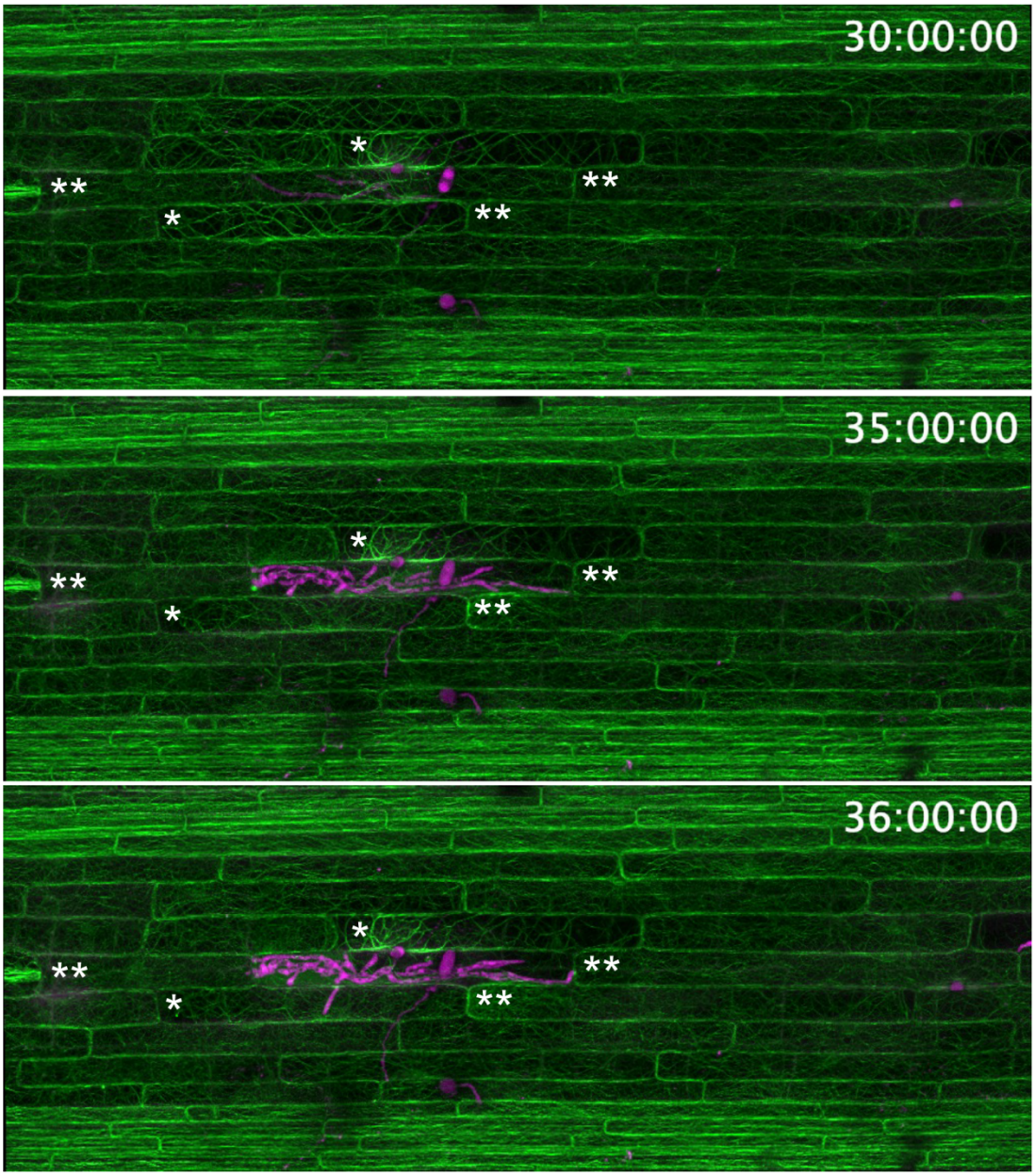

Figure 6.6 Rice F-actin cells directly adjacent to the infected site show thickened filaments.

Confocal micrograph showing thickened filaments in cells directly adjacent to the infected cell (30:00:00). After several hours, these thickened filaments revert to the usual actin appearance such as those observed in uninfected cells away from the infected site (35:00:00) and remain in this appearance as the fungus starts moving to an adjacent cell (36:00:00). Micrographs shown are maximum intensity projections of a z-stack series and correspond to a time-lapse series (Movie 6.6) taken at 10 min intervals. Confocal micrographs were prepared from leaf sheath inoculations using rice cv Kitaake transgenic lines expressing actin marker LifeAct:GFP (in green) and infected with *M. oryzae* Guy1 RP27p:tdTomato (in magenta). Leaf sheath infections were incubated at 24 °C. Single asterisk (*) indicates cells that have thickened actin filaments. Double asterisks (**) indicate cells with normal actin appearance. Time scale is in h: min: sec. Scale bar = 20 μm.

6.2.5 The biotrophic interfacial complex (BIC) contains rice actin

The biotrophic interfacial complex (BIC) is a host membrane-rich structure that serves as an active site for effector translocation (Giraldo et al., 2013; Khang et al., 2010; X. Yan et al., 2023). A recent study reported that *M. oryzae* cytoplasmic effectors, packaged into punctate membranous effector compartments (MECs), are internalised into rice cells via clathrin-mediated endocytosis (CME) at these sites (Oliveira-Garcia et al., 2023). While actin filaments are not essential for internalisation of clathrin-coated vesicles (CCVs) in plants (Johnson, 2024; Narasimhan et al., 2020), they likely play a role in CCV trafficking after endocytosis. To investigate the involvement of actin at the BIC, I localised plant actin using transgenic rice lines expressing the actin marker LifeAct:GFP. Infection by *M. oryzae* strain expressing Pwl2:mRFP, a BIC-localising, cytoplasmic effector, revealed LifeAct:GFP fluorescence at both 'tip' (Figure 6.7A and B) and 'side' (Figure 6.7C and D) BICs. Therefore, BICs do contain filamentous actin during *M. oryzae* biotrophic growth.

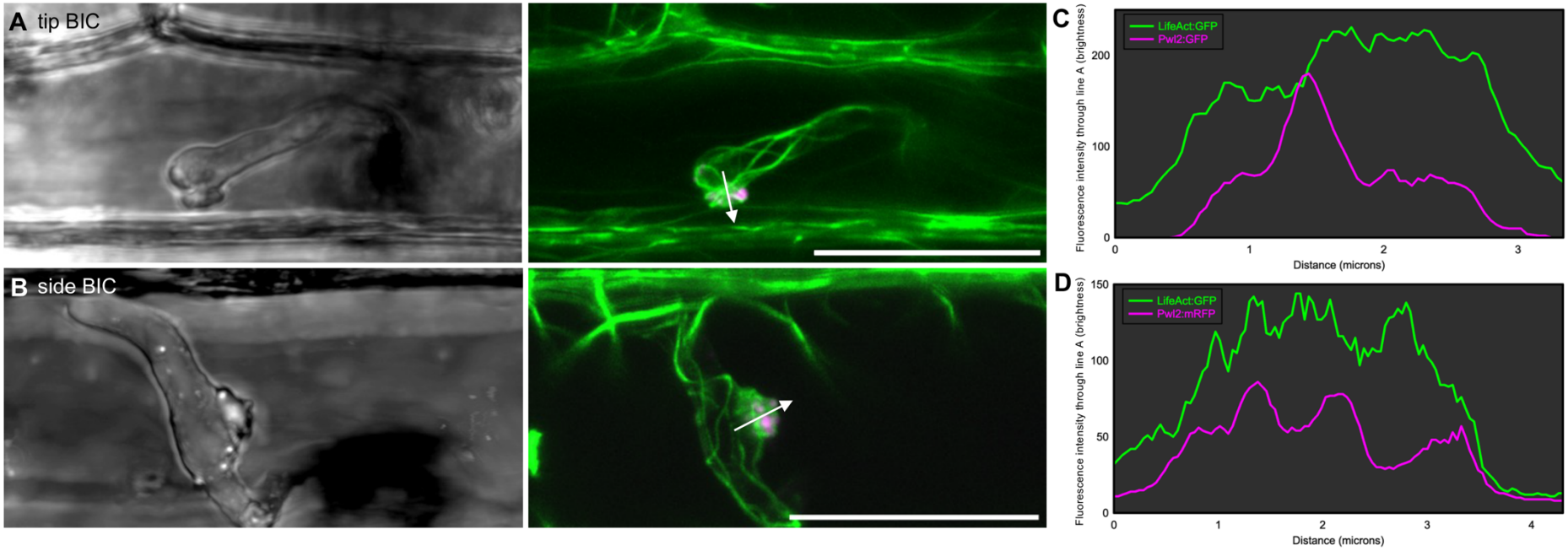

Figure 6.7 The biotrophic interfacial complex (BIC) contains rice actin.

Confocal micrographs of rice cv Kitaake transgenic line expressing LifeAct:GFP (in green) infected with *M. oryzae* Guy11 expressing Pwl2:mRFP (in magenta) showing that both the 'tip' BIC **(A)** and the 'side' BIC **(B)** contains rice actin. Co-localisation demonstrated by fluorescence intensity distribution through line A indicated by the white arrow is consistent with the host actin being a component of 'tip' BIC **(C)** and 'side' BIC **(D)**, respectively. Leaf sheath infections were incubated at 24 °C. All images shown are maximum projections of z-stack series taken using Leica TCS SP8X confocal laser scanning microscope. Scale bars = 20 μm.

6.2.6 Pharmacological interference with actin cytoskeleton reduces *M. oryzae* infection spread

Several studies have shown that when host plants are treated with actin polymerisation inhibitors, hosts become more susceptible to pathogens (Jelenska et al., 2014; Kang et al., 2014), and the penetration rate during nonhost interactions also increases (Kobayashi & Hakuno, 2003; Kobayashi, Kobayashi, et al., 1997; Kobayashi, Yamada, et al., 1997; Miklis et al., 2007; Shimada et al., 2006; Yun et al., 2003). However, in some cases, actin depolymerisation induces transcription of defence-related salicylic acid marker genes, thereby enhancing resistance to pathogens (Kobayashi & Kobayashi, 2007; H. Leontovyčová et al., 2019; Matoušková et al., 2014). To assess the role of the actin cytoskeleton in *M. oryzae* infection, I vacuum-infiltrated leaf sheath sections of transgenic rice lines expressing the actin marker LifeAct:GFP with 10 μM cytochalasin D. Cytochalasins are fungal metabolites that interfere with the polymerisation process by which G-actin builds into F-actin (Brown & Spudich, 1981; Cooper, 1987). After treatment, I washed the leaf sheath surface with sterile distilled water and inoculated leaf sheaths with *M. oryzae* strain Guy11 expressing RP27p:tdTomato. At 36 hpi, I assessed the extent of fungal infection. In the control treatment (0.1% DMSO), *M. oryzae* infection reached either second-invaded cells (69%) or third-invaded cells (31%). However, in cytochalasin D-treated leaf sheaths, most infections were restricted to the first-invaded cells (66%), with fewer spreading to second-invaded (29%) cells and third-invaded cells (5%). These results indicate that inhibiting rice F-actin reduces the spread of *M. oryzae* infection.

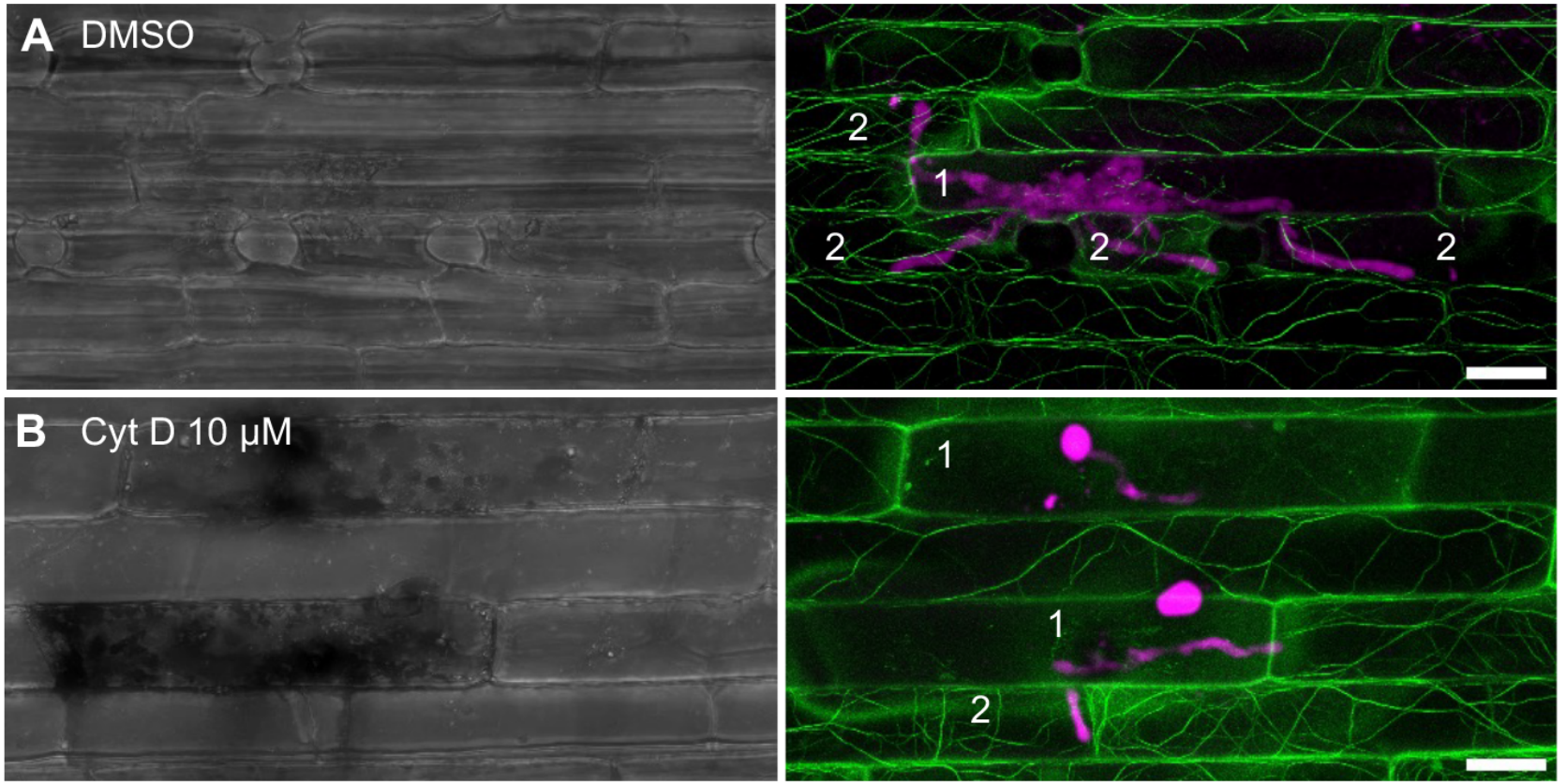

Figure 6.8 Rice F-actin inhibition limits the spread of *Magnaporthe oryzae* infection.

A. Confocal micrographs showing typical *M. oryzae* infection at 36 hours post-inoculation (hpi) in 0.1% DMSO-treated (control) leaf sheaths. **B.** Confocal micrographs showing restricted *M. oryzae* infection spread at 36 hpi in 10 µM cytochalasin D-treated leaf sheaths. Confocal micrographs were prepared from leaf sheath inoculations using rice cv Kitaake transgenic lines expressing the actin marker LifeAct:GFP (in green) and infected with *M. oryzae* Guy11 RP27p:tdTomato (in magenta). Numbers indicate the order in which the fungus invades host cells (1=first-invaded cell, 2=second-invaded cell).Leaf sheath infections for all time points were incubated at 24 °C. All images shown are maximum projections of z-stack series recorded using a Leica TCS SP8X confocal laser scanning microscope. Scale bar = 20 µ

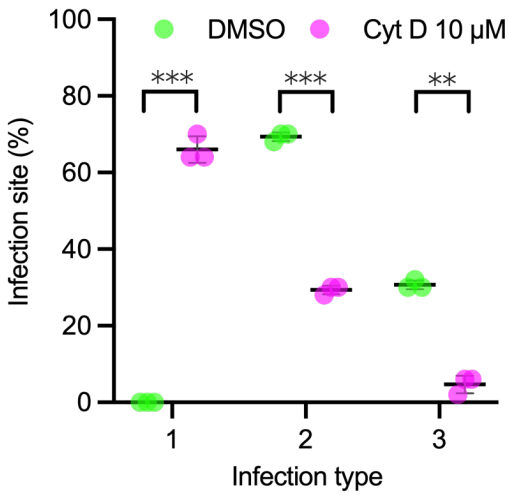

Figure 6.9 Rice F-actin inhibition using cytochalasin D reduces *Magnaporthe oryzae* infection spread.

Scatter plot showing the mean percentage of infection sites reaching different degrees of infection spread. Infection type 1 = only one host cell invaded; 2 = two host cell invaded; and 3 = three host cell invaded. The scatter plot shows the mean from three biological replicates (n = 50 infection sites per biological replicate; data points show means of individual replicates); error bars indicate the standard deviation. ***$P < 0.001$, **$P = 0.002$.

6.3 Discussion

The host actin cytoskeleton undergoes remodeling in response to pathogen attacks. Using rice transgenic lines expressing the actin marker LifeAct:GFP, I monitored the organisational changes in the actin cytoskeleton during *M. oryzae* infection. I report that actin remodels and surrounds *M. oryzae* invasive hyphae during biotrophic growth. This phenomenon is also observed in newly invaded cells once the fungus moves from the initially invaded cell to an adjacent one. This observation aligns with the fact that during biotrophic growth, the extrainvasive hyphal membrane (EIHM) surrounds the invasive hypha as it invaginates the host plasma membrane. The plasma membrane is known to be closely linked to the actin cytoskeleton via actin-binding proteins (ABPs) (Baluška et al., 2003). For the EIHM to accommodate the growing invasive hypha, corresponding actin remodeling must therefore occur. A similar observation has been reported in barley-*Blumeria graminis* f. sp. *hordei* (*Bgh;* barley powdery mildew) where actin filaments closely followed the haustorium when it invaginated the plasma membrane (Opalski et al., 2005).

A link between the EIHM and host actin arises from the possibility that EIHM expansion is dependent on host membrane supply and trafficking, which are actin-mediated processes (Chakrabarti et al., 2021; Lanzetti, 2007; Skruzny, 2022; Stradal & Schelhaas,

2018; Wang & Hussey, 2015). The EIHM forms as invasive hyphae become encased by invaginated host plasma membrane, indicating that host membrane material must be mobilised to the IH-rice interface. Using the lipophilic dye FM4-64, Kankanala et al. (2007) visualised EIHM formation and observed extensive membrane remodelling and connections to peripheral rice membranes as biotrophy progressed (Kankanala et al., 2007). These findings suggest an active, host-directed membrane synthesis pathway at the interface, consistent with the known role of actin in vesicle trafficking and membrane remodelling in plant cells (Wang & Hussey, 2015). Membrane delivery to the EIHM likely proceeds through actin-dependent endomembrane trafficking.

Host actin may also directly regulate EIHM integrity and dynamics. EIHM stability varies with hyphal growth stage and membrane expansion, with disruptions often coinciding with lifestyle switches or interface breakdown, implying that proper actin-membrane coordination is crucial for maintaining EIHM integrity during biotrophy (Jones et al., 2017).

Although imaging data show EIHM formation and host membrane association, direct causal evidence linking plant actin to EIHM biogenesis remains limited. Inhibition of rice actin polymerisation at infection sites could help establish causality by correlating actin disruption with changes in EIHM integrity and hyphal growth. Such experiments would also clarify whether altering actin dynamics affects the localisation of EIHM-associated apoplastic effectors or the progression of EIHM expansion. Additionally, drawing a more definitive conclusion regarding the relationship between host actin and the EIHM would require quantification of the amount of F-actin associated with the EIHM and demonstration of its spatial organisation relative to the EIHM. To achieve this, dual-colour live cell imaging of the host actin and the EIHM could be performed. The resulting image stacks could then be analysed in Imaris (Bitplane) using the *Surfaces* tool to generate 3D reconstructions of each channel. A surface-surface contact area algorithm could subsequently be applied to quantify the extent of contact between the host actin surface and the EIHM surface.

As fungal infection progresses in the initially invaded cell, rice actin filaments become disrupted. Three possible factors could contribute to this actin disruption. First, mechanical stress exerted by the growing invasive hyphae could lead to actin

disorganisation. Time-lapse videos in this study show actin filaments being pulled as the fungus grows inside the host cell. Additionally, actin filament disruption may correlate with the observed EIHM breakdown when the remodeling process can no longer keep pace with extensive fungal growth. Second, *M. oryzae* might produce secondary metabolites that disrupt actin. The *Avirulence Conferring Enzyme1* (*ACE1*) in *M. oryzae* is part of an infection-specific gene cluster encoding a putative polyketide synthase-nonribosomal peptide synthetase (PKS-NRPS) hybrid, which is involved in synthesising non-secreted secondary metabolites (Böhnert et al., 2004; Collemare et al., 2008). While these secondary metabolites have yet to be isolated due to tightly regulated temporal expression, prior studies suggest that the *ACE1* gene cluster encodes the biosynthesis of cytochalasan-like compounds (Nielsen et al., 2016; Song et al., 2015). *ACE1* is recognised by rice cultivars carrying the resistance gene *Pi33*, and its avirulence function is abolished when a critical amino acid in the β-ketoacyl synthase domain is mutated, indicating that its biosynthetic activity is essential for its recognition by *Pi33*. Therefore, its product, or an intermediate that is secreted, may be recognised by the *Pi33* immune receptor. The product may serve a primary role in actin depolymerisation in the host. My data suggests, however, that this is a local response around invasive hyphae and perhaps adjacent cells. Alternatively, unidentified effectors may disrupt actin or regulate ABPs to modulate actin dynamics. Currently, no known *M. oryzae* effectors have been shown to perform such a function, highlighting an area for future research.

Interestingly, during the pre-penetration stage of *M. oryzae*, no significant actin rearrangements were detected, unlike in previous cases where an *M. oryzae* mutant failed to penetrate (Xu et al., 1998) or when the fungus was inoculated onto a non-adapted host (Henty-Ridilla et al., 2013). This suggests that the pathogen either evades or suppresses pathogen-triggered immunity (PTI). However, actin accumulation was observed at penetration sites during cell-to-cell invasion. Actin accumulation may serve as a defence strategy to restrict pathogen spread (Hardham et al., 2007). However, the ability of *M. oryzae* to bypass these physical barriers suggests that actin accumulation at the potentially pit field sites might actually help to facilitate invasion by providing polarized actin structures required for EIHM formation (Takemoto & Hardham, 2004).

Thickened, less dynamic actin filaments were also observed in cells immediately adjacent to the initially invaded cells, particularly above and below them. Compared to host cells

farther from the infection site, these adjacent cells exhibited reduced actin density, likely due to actin bundling. I hypothesise that this response may serve as a defence mechanism, reinforcing the cytoskeleton to hinder pathogen spread. However, no actin polarisation was observed in regions where filament thickening occurred. Alternatively, since actin bundling is associated with reduced filament dynamics, it may impair delivery of organelles and defence-related proteins, ultimately benefiting the pathogen. Actin bundling has previously been implicated in effector-triggered immunity (ETI) (Henty-Ridilla et al., 2013). If this is the case, *M. oryzae* effectors secreted beyond the infection site might induce actin bundling and restrict actin movement in adjacent cells. At present, it remains unclear whether this response primarily benefits the host or the pathogen. Notably, adjacent cells positioned laterally to the initially invaded cell did not exhibit noticeable filament thickening or reduced actin movement. These cells may however have less direct contact with the first-invaded cell, making them less affected by the infection. Quantifying actin bundling and filament density in both infected and adjacent cells, as previously conducted (Henty-Ridilla et al., 2013), would provide clearer insights into the actin response during infection and the timing of these changes.

Additionally, I confirmed previous findings that the biotrophic interfacial complex (BIC) contains host actin. These results align with prior studies demonstrating colocalisation of LifeAct:GFP and rhodamine-phalloidin-stained actin with fluorescently tagged Pwl2 (Oliveira-Garcia et al., 2023). This suggests that actin is involved in intracellular transport of *M. oryzae* membranous effector compartments (MECs) within rice cells, despite not being required for the internalization of clathrin-coated vesicles (CCVs) in plants (Johnson, 2024; Narasimhan et al., 2020). Furthermore, host F-actin in the BIC which is a host plasma membrane-rich region also suggests that the formation of the BIC is driven by processes mediated by F-actin such as vesicle trafficking and *de novo* assembly of membranes (Dörmann et al., 2014).

Lastly, pharmacological disruption of host actin using cytochalasin D reduced the ability of *M. oryzae* to colonise new cells beyond the initial infection site. In this study, I demonstrated that actin surrounds the invasive hyphae during biotrophic growth. The localisation of actin around the IH might suggest that host F-actin is necessary for plasma membrane invagination to form the EIHM. Host F-actin possibly plays a role in membrane and vesicle trafficking to support EIHM expansion. Because EIHM is

indispensable during biotrophic phase, this could be a possible reason why host F-actin is necessary for fungal invasion. Actin disruption might therefore hinder actin-mediated transport, thus, preventing formation of an elaborate EIHM required for biotrophic growth. Infections in control-treated leaf sheaths displayed more extensive fungal growth, nearly filling the entire cell with fungal hyphae. By contrast, infections treated with cytochalasin D exhibited significantly reduced fungal growth. Only 29% of infections were able to colonise adjacent host cells, and 5% spread to host cells two cells away from the initially invaded cell. In comparison, in the control (0.1% DMSO), 69% of infections colonised adjacent cells, while 31% spread two cells away from the initially invaded cell. However, it remains challenging to determine whether this reduction is due to the effect of cytochalasin D on host actin or direct inhibition of the pathogen because its actin cytoskeleton may also be affected by exposure to the drug. Finding a concentration that disrupts host actin without affecting *M. oryzae* is difficult, and washing cytochalasin D from the leaf sheath surface only eliminates potential effects on appressorium formation and early penetration stages but is still potentially problematic in limiting the drug effect to the host.

Aside from host F-actin's possible role in fungal invasion previously mentioned, maintaining host F-actin integrity in the biotrophic stage could also be necessary to prevent activation of immune responses. Although it has been reported that loss of host actin integrity can result in susceptibility in several studies (Henty-Ridilla et al., 2013; Jelenska et al., 2014; Kang et al., 2014; Kobayashi, Kobayashi, et al., 1997; Shimada et al., 2006), actin depolymerisation has also been reported to lead to increased resistance. In cytochalasin-treated tobacco, for example, inoculation with *E. cichoracearum* primed the cells for hypersensitive response-like cell death. Actin perturbation in cytochalasin-treated leaf sections resulted in induced expression of acidic *PR1* and *PR2* genes, suggesting that plant cells actin perturbation may trigger plant defence responses (Kobayashi & Kobayashi, 2007). In *Brassica napus* and *Arabidopsis,* actin depolymerisation also resulted in increased resistance against *Leptosphaeria maculans* and *P. syringae,* respectively by activating salicylic acid signalling pathway via the isochorismate synthase-dependent pathway (Leontovyčová et al., 2019).

In this chapter, I observed actin cytoskeleton dynamics during *M. oryzae* infection in live-cell imaging experiments. My findings indicate that host actin remodelling occurs during

M. oryzae invasion. The presence of actin filaments surrounding invasive hyphae in both initially invaded and newly invaded cells, along with the association of actin filaments with the BIC, suggests that actin remodelling is essential for biotrophic growth. However, as the infection progresses and *M. oryzae* spreads into adjacent cells, actin in the initially invaded cell becomes disrupted, coinciding with host cell death. Thickening of actin filaments in cells adjacent to infected sites suggests that infections in the initially invaded cell influence neighbouring cells. This response could either be a host defence mechanism or a strategy by the pathogen to manipulate the host, as actin bundling restricts filament movement and dynamics. Additionally, actin accumulates at potential pit field sites. This may serve as a host defence response, but it is also possible that actin polarisation at these sites provides the structural support required for EIHM formation. Future quantitative analyses comparing actin density and bundling in adjacent cells at critical time points will be necessary to gain deeper insights into host cellular responses to *M. oryzae* infection.

Chapter 7 General Discussion

Rice blast disease is caused by the hemibiotrophic ascomycete *Magnaporthe oryzae*. Advances in understanding rice blast infection have been made using a combination of molecular genetics, genomics, and live-cell imaging. Fundamental studies of appressorium formation, turgor generation, and repolarisation for host cell entry, for example, have been reported that have provided insight into the establishment of rice blast disease (Dagdas et al., 2012; de Jong et al., 1997; Dulal et al., 2021; Eseola et al., 2021; Gupta et al., 2015; Ryder et al., 2023; Saunders et al., 2010). A significant recent advance is the characterisation of the Pmk1-dependent phosphorylation landscape of appressorium development (Cruz-Mireles et al., 2024), which facilitates the identification of downstream targets within this pathway and their connections to previously identified transcriptional changes during the initial stages of plant infection (Osés-Ruiz et al., 2021). Furthermore, transcriptional analyses of *M. oryzae* during invasive growth in plant tissue has revealed substantial temporal shifts in fungal gene expression, highlighting dynamic changes in primary and secondary metabolism, cell signalling, and transcriptional regulation (Yan et al., 2023).

However, significant gaps remain in our understanding of invasive growth by *M. oryzae*. These gaps largely stem from the historical lack of tools to visualise infections of living plants and thereby study the spatial and temporal dynamics of fungal invasion. In this thesis, I set out to investigate the host cellular changes associated with plant colonisation by the blast fungus *M. oryzae*.

Major advances in live-cell imaging have enabled a more detailed examination of the host-pathogen interface, providing new insight into the key cellular changes that occur during rice blast infection. The tractability of *M. oryzae* (Jeon et al., 2007; Talbot, 2003; Valent & Chumley, 1991), combined with highly efficient protocols for *Agrobacterium*-mediated transformation in rice (Hiei & Komari, 2008), has facilitated the manipulation of both host and pathogen for fluorescent protein tagging, gene complementation, and knockout generation.

Furthermore, the emergence of rice cv. Kitaake as a model for monocotyledonous species presents significant advantages for functional genomics studies (Jain et al., 2019). Kitaake,

a photoperiod-insensitive variety (Ichitani et al., 1997; S. L. Kim et al., 2013; Kunihiro et al., 1989), is characterised by a rapid life cycle and high transformation efficiency (Jain et al., 2019; Jung et al., 2008). The high-quality genome assembly of the model rice plant KitaakeX also serves as a valuable reference for rice functional genomics (Jain et al., 2019).

In the context of plant-pathogen interactions, the Kitaake cultivar provides a useful genetic background for studying both compatible and incompatible interactions. Notably, it carries the resistance (*R*) gene *Pia,* , which recognises the corresponding avirulence (*Avr*) gene *Avr-Pia* in *M. oryzae* (Cesari et al., 2013; Yang et al., 2022). When inoculated with an *M. oryzae* strain expressing *Avr-Pia*, Kitaake triggers an incompatible interaction.

In Chapter 3, I reported the generation of transgenic rice lines in the Kitaake background, each expressing individual GFP-tagged organelle marker constructs. Additionally, I have developed a set of barely lines carrying the same GFP-tagged organelle constructs. Prior to this, I generated GFP-tagged constructs targeted to various subcellular compartments and tested them by transient expression in *N. benthamiana* to confirm their correct predicted subcellular localisation. The development of transgenic rice and barley lines was a large-scale effort, involving screening of 452 and 165 T_0 lines transformed with different organelle marker constructs in Kitaake and Golden Promise, respectively. The incorporation of pFast-Red selection marker greatly facilitated seed selection for most organelle constructs, enabling more rapid screening and efficient generation of stable transgenic lines. GFP copy number analysis was used to determine the genotype of each line before advancing to the next generation. Additionally, pFast-Red served as a secondary validation tool for GFP copy number analysis, because segregation or non-segregation of RFP expression in seeds helped confirm the fixation status of transgenic lines.

In total, I have developed transgenic rice lines expressing GFP-tagged markers for nine subcellular compartments: the plasma membrane, actin cytoskeleton, nucleus, mitochondria, early endosomes, late endosomes, cytoplasm, peroxisome, and endoplasmic reticulum. In barley, six organelle marker constructs have been successfully integrated, covering the plasma membrane, actin cytoskeleton, nucleus, mitochondria, early endosome, and late endosome. These transgenic lines represent valuable resources for future studies on *M. oryzae* infection to investigate host organelles dynamics during

infection and dissect which compartments are recruited or rearranged during invasion and biotrophy. These transgenic lines also allow for comparison of host subcellular component dynamics in incompatible interactions to uncover cellular basis of resistance. The developed transgenic barley lines also allow examination of host cellular dynamics during infection whether similar phenomena exist in different hosts. Beyond host-pathogen studies, they could also serve as versatile tools for protein colocalisation such as effector proteins to identify effector targets and broader cellular research.

The development of transgenic lines in Chapter 3 enabled a series of studies investigating the cellular changes associated with *M. oryzae* invasion. In Chapter 4, I characterised the spatiotemporal changes in host plasma membrane dynamics during infection using the Kitaake transgenic line expressing the plasma membrane marker LTI6b TMD:GFP. My focus was on the formation and breakdown of the extra-invasive hyphal membrane (EIHM) and development of the biotrophic interfacial complex (BIC).

The EIHM is consistently formed during the biotrophic growth of *M. oryzae*, serving as the interface between the pathogen and rice. This is analogous to other biotrophic infections, where the extrahaustorial membrane (EHM) establishes a sealed compartment between the pathogen and host (Jaswal et al., 2020; Jones & Dangl, 2006; Lo Presti et al., 2015; Mims et al., 2004; O'Connell & Panstruga, 2006). The formation of plant-derived interfacial membranes is a key feature of biotrophic invasion (Bozkurt et al., 2015; Perfect & Green, 2001). However, unlike in biotrophic pathogens, where EHM integrity and host cell viability are maintained for several days, the EIHM progressively loses integrity as the fungus colonises neighbouring cells (Perfect & Green, 2001).

There is broad consensus in the rice blast community that the EIHM is derived from the plant plasma membrane-derived (Kankanala et al., 2007; Kouzai et al., 2014; Mentlak et al., 2012; Mochizuki et al., 2015). However, in this study, the plasma membrane marker LTI6b TMD:GFP was also detected at the perinuclear membrane, consistent with localisation to the endoplasmic reticulum. This observation raises the possibility that the EIHM may originate not only from the plant plasma membrane but also, at least in part, from the plant ER. This hypothesis can be tested using the developed ER marker AtWAK2:GFP:HDEL to determine whether plant ER localises around the invasive hyphae.

The integrity of the EIHM and the viability of infected host cells were also assessed using sucrose-induced plasmolysis. Cells with intact plasma membranes retain the ability to plasmolyse, indicating viability, whereas cells with disrupted membranes lose this ability and are therefore non-viable. During early infection (24 hours post-inoculation (hpi)), infected cells plasmolyse when exposed to a hyperosmotic solution, reflecting the biotrophic stage of infection where host viability is maintained (Kankanala et al., 2007; Koga et al., 2004). However, as the fungus moves from the initially invaded cell into neighbouring cells, the initially-invaded cells lose the ability to plasmolyse, suggesting loss of EIHM integrity and cell viability. By contrast, newly invaded cells remain biotrophic and retain the ability to plasmolyse.

I also examined the relationship between plasma membrane integrity and cell viability over time using fluorescein diacetate (FDA) as a cell viability marker. FDA staining revealed different cell types based on fluorescein staining patterns throughout the course of infection, as previously described (Jones et al., 2016). Quantifying these cell types according to their fluorescein staining patterns provided new insight into the cytological changes that occur before cell death.

During the early biotrophic phase, viable cells exhibited a typical fluorescein staining pattern. However, as infection progressed in the initially invaded cell, novel fluorescein patterns began to emerge, characterised by shrunken and subsequently ruptured vacuoles. Dead cells failed to retain fluorescein due to the loss of EIHM integrity. Notably, cells at the edges of each infection site exhibited either viability or early stages of cell death compared to those invaded earlier. This further supports the findings from plasmolysis assays and reinforces the sequential hemibiotrophic invasion strategy of *M. oryzae*.

The formation and subsequent disruption of the extra-invasive hyphal membrane (EIHM) in initially invaded cells, followed by its re-establishment in newly colonised cells, highlights the hemibiotrophic lifestyle of *M. oryzae*. This infection strategy results in a mosaic pattern, where the first-invaded rice cells become non-viable, while neighbouring cells that are still being colonised remain alive. As a consequence, *M. oryzae* infections consistently exhibit a biotrophic margin, with a necrotrophic centre forming at the core of disease lesions in compatible (susceptible host) interactions.

I investigated the formation of the biotrophic interfacial complex (BIC), a highly localised, host membrane-derived structure found at the EIHM. The BIC serves as an active site for effector translocation into the host cytoplasm (Khang et al., 2010; Mosquera et al., 2009; X. Yan et al., 2023). Using Kitaake transgenic lines expressing the plasma membrane marker LTI6b TMD:GFP, I confirmed that BIC development occurs in two stages and that it is derived from the host plasma membrane. In addition, because of the perinuclear membrane localisation of LTI6b TMD:GFP, it is also likely that the BIC has a plant ER component which can be directly tested using the ER marker AtWAK2:GFP:HDEL. A single BIC consistently forms in initially invaded cells, while multiple BICs appear in each invasive hypha as the fungus spreads into neighbouring cells.

I conclude that initially invaded rice cells remain intact and viable until the fungus reaches pit field sites, enabling its spread into adjacent cells. At this stage, cell viability declines, and the originally colonised cell undergoes cell death as the fungus invades the neighbouring cell, invaginates its plasma membrane, and establishes a new BIC and EIHM.

In Chapter 5, I aimed to quantify the net increase in host plasma membrane during infection. The formation of the EIHM during *M. oryzae* infection necessitates the production of large amounts of plasma membrane to accommodate the expanding invasive hyphae. This suggests that an active mechanism may drive host membrane biogenesis or that membrane reservoirs and invaginations are exploited to facilitate plasma membrane remodelling. However, the precise extent of additional plasma membrane required to support the growing invasive hypha was unknown.

I explored the potential of MorphoGraphX (MGX), an open-source tool developed for 3D surface reconstruction in biological imaging (Barbier de Reuille et al., 2015; Strauss et al., 2022), to perform surface area measurements in rice cells and invasive hyphae. Using MGX, I calculated the net increase in plasma membrane in rice cells prior to EIHM disruption. For this analysis, I employed an *M. oryzae* Guy11 strain expressing a fluorescently tagged apoplastic effector, Mep1:mCherry, alongside a cytoplasmic marker, RP27p:mScarlet3. Mep1:mCherry was used to indicate the loss of EIHM integrity,

because leakage of this apoplastic effector into the cytoplasm signals a compromise in membrane integrity. RP27p:mScarlet3 served as a fungal cytoplasmic marker, facilitating the segmentation of invasive hyphae.

For the first time, I have been able to attempt to quantify the net increase in plasma membrane during invasive hyphal development. The EIHM accounted for an additional 3.5% at 24 hpi, 13% at 28 hpi, and 21% at 30 hpi before its eventual disruption. These findings align with previous observations that EIHM maintenance and disruption correlate with hyphal growth stage (Jones et al., 2021). Because of its role as the interface between *M. oryzae* and the host cell, the EIHM plays a crucial role in infection. Loading experiments with the endocytic marker FM4-64 have confirmed that the EIHM acts as a barrier, preventing the dye from reaching the fungal plasma membrane and effectively separating the fungus from the host cytoplasm (Kankanala et al., 2007). The results indicate that the plasma membrane invaginates to form the EIHM, which remains closely associated with both young and mature invasive hyphae (IH) until it eventually ruptures. This observation is consistent with previous studies (Kouzai et al., 2014; Mentlak et al., 2012; Mochizuki et al., 2015). The use of GFP-tagged plasma membrane (PM)-localised proteins suggests that the EIHM has a distinct composition compared to the bulk host PM. For instance, OsCERK1:GFP and EL5:GFP were present in the EIHM surrounding young IH but were absent from the EIHM of mature bulbous IH (Kouzai et al., 2014; Mochizuki et al., 2015; Takai et al., 2002). OsCERK1 functions as a pattern recognition receptor for chitin oligomers (Shimizu et al., 2010), while EL5 is a ubiquitin ligase expressed in response to chitin oligomers (Takai et al., 2002). It appears that more stable PM-integrated proteins, such as LTI6b (used here as the plasma membrane marker), persistently label the EIHM, whereas defence-related proteins, including pattern recognition receptors, are selectively excluded potentially as a strategy for the pathogen to evade host recognition (Mochizuki et al., 2015). Similar findings have been reported for the EHM in powdery mildew (Koh et al., 2005; Micali et al., 2011) and oomycete infections (Caillaud et al., 2012; Lu et al., 2012), where certain PM-resident proteins, such as the aquaporin PIP1;4, calcium ATPase ACA8, arabinogalactan protein (AGP) epitopes, and non-AGP glycoproteins, are also selectively excluded.

The developed MorphoGraphX pipeline to measure additional plasma membrane required to accommodate growing *M. oryzae* invasive hypha is a very valuable tool that

could help to identify effectors responsible for co-opting the host plasma membrane for successful invasion and measure their effects on tissue colonisation. Deleting putative effector-encoding genes involved in co-opting the host plasma membrane to support *M. oryzae* biotrophic growth may, for instance, reduce host plasma membrane biogenesis to accommodate the growing invasive hypha, thereby shortening the biotrophic phase.

In Chapter 6, I investigated the spatiotemporal dynamics of the rice actin cytoskeleton during the biotrophic growth of *M. oryzae* using the rice cv. Kitaake transgenic line expressing the actin marker LifeAct:GFP. The findings revealed that rice F-actin is remodeled during infection and initially surrounds invasive hyphae of *M. oryzae* in both the first-invaded and newly colonised neighbouring cells. This observation aligns with the fact that, during biotrophic growth, the extrainvasive hyphal membrane (EIHM) envelops the invasive hypha as it invaginates the host plasma membrane. The plasma membrane is closely associated with the actin cytoskeleton through actin-binding proteins (ABPs) (Baluška et al., 2003). To accommodate the expanding invasive hyphae, corresponding actin remodelling must therefore occur. A similar phenomenon has been documented in the barley-*Blumeria graminis* f. sp. *hordei* (*Bgh*; barley powdery mildew fungus), where actin filaments closely track the haustorium as it invaginates the plasma membrane (Opalski et al., 2005).

Additionally, actin accumulates at cell junctions and BICs. Accumulation of actin at cell junctions might serve as a defence strategy to hinder further fungal colonisation (Hardham et al., 2007). However, the ability of *M. oryzae* to overcome accumulated actin at cell junctions implies that actin polarisation at these sites may actually aid fungal invasion by providing necessary actin for EIHM formation (Takemoto & Hardham, 2004).

As the infection progresses, host actin becomes disrupted. I confirmed previous findings regarding the accumulation of actin in BICs, suggesting that actin is involved in intracellular transport of membranous effector compartments (MECs) within rice cells (Oliveira-Garcia et al., 2023).

I conclude that during *M. oryzae* invasion, the actin cytoskeleton is remodelled around the invasive hypha, a process linked to plasma membrane invagination and, consequently,

EIHM formation. As fungal infection progresses, the actin cytoskeleton of initially invaded host cells is disrupted as the fungus fills the cell and moves into adjacent cells. This is consistent with the observation that host cells lose viability, correlating with the loss of plasma membrane integrity. In newly invaded cells, actin is remodelled around the invasive hypha, consistent with formation of EIHM in these cells. Actin remodelling is, therefore, crucial for successful fungal invasion, while its disorganisation marks the transition from biotrophy to necrotrophy in *M. oryzae* infection. Quantitative analyses comparing actin density and bundling in adjacent cells could provide more definitive insights into host actin responses during *M. oryzae* infection. Dual labelling actin and plasma membrane would, for example, be necessary to confirm the predicted involvement of actin in EIHM formation.

This study aimed to define the host cellular changes associated with plant colonisation by the blast fungus *M. oryzae*. I have drawn conclusions regarding plasma membrane organisation, BIC development, and actin dynamics using transgenic rice lines developed in this study. The findings highlight how *M. oryzae* co-opts host subcellular compartments for successful invasion and reinforce the hemibiotrophic nature of *M. oryzae* infections, as demonstrated by the maintenance and eventual breakdown of the host plasma membrane and actin cytoskeleton. These findings provide a foundation for future research into additional host subcellular components, as well as a key resource of transgenic rice and barley lines for investigating the dynamics of different organelles. This will contribute to the establishment of a spatiotemporal atlas of cellular changes associated with plant tissue colonisation by *M. oryzae* in both compatible and incompatible interactions. For example, my initial observations suggest that early endosomes are associated with the BIC (Figure 7.1) and may be involved in translocating effectors to the host cytoplasm (Movie 7.1). Comparing this to Figure 4.8, the BIC region also features ring- or bubble-like plasma membrane-containing structures but these do not exhibit Pwl2 signal. Because the BIC is a plasma membrane-rich region, it is likely that the bubble-like structures might be clathrin-coated vesicles arising from the host plasma membrane. The lack of Pwl2 signal in these structures could mean that they carry different cargo. In Figure 7.1, punctate and ring-like OsAra6 structures are associated with the BIC. Some ring-like OsAra6 structures appear to enclose Pwl2 suggesting that Pwl2 could be translocated by early endosomes while those without Pwl2 might be carrying other cargo (Figure 7.1 and Movie 7.1). The observed Pwl2 signal enclosed in OsAra6 detached from

the BIC region (Movie 7.1) could be a step downstream of clathrin-mediated endocytosis in cytoplasmic effector translocation (Oliveira-Garcia et al., 2023). The known next step after clathrin-coated vesicles (CCVs) carrying cargo matures is its uncoating then fusion to early endosomes or the trans-Golgi network for downstream processing (Chen et al., 2011). In the case of OsAra6 ring structures encasing Pwl2 which are in the BIC region, the formation of CCVs, its uncoating and fusion to early endosomes within the BIC region likely occurs because the BIC is associated with early endosomes which are readily available for fusion after uncoating. However, precautions should be taken in interpreting the enclosure of Pwl2:mRFP in ring-like OsAra6 structures because it could also be possible that ring-like structures are pinched-off plasma membrane containing OsAra6 signal (Ebine et al., 2012; Ueda et al., 2001). In this case, it will be more difficult to distinguish whether the observed ring-like structures are pinched off plasma membrane or early endosomes and will necessitate another marker which could clearly differentiate these subcellular structures. Moreover, the model proposed in Figure 7.2 further supports the possibility that both the EIHM and the BIC contain plant ER components, therefore updating the label to "plant-derived membrane" which is more inclusive.

Future studies will be needed to identify the mechanisms by which these subcellular compartments are reorganised during *M. oryzae* invasive growth, as well as the effectors that might be involved in inducing these processes. Answering these fundamental questions will significantly help advance our understanding of the invasive growth of *M. oryzae*.

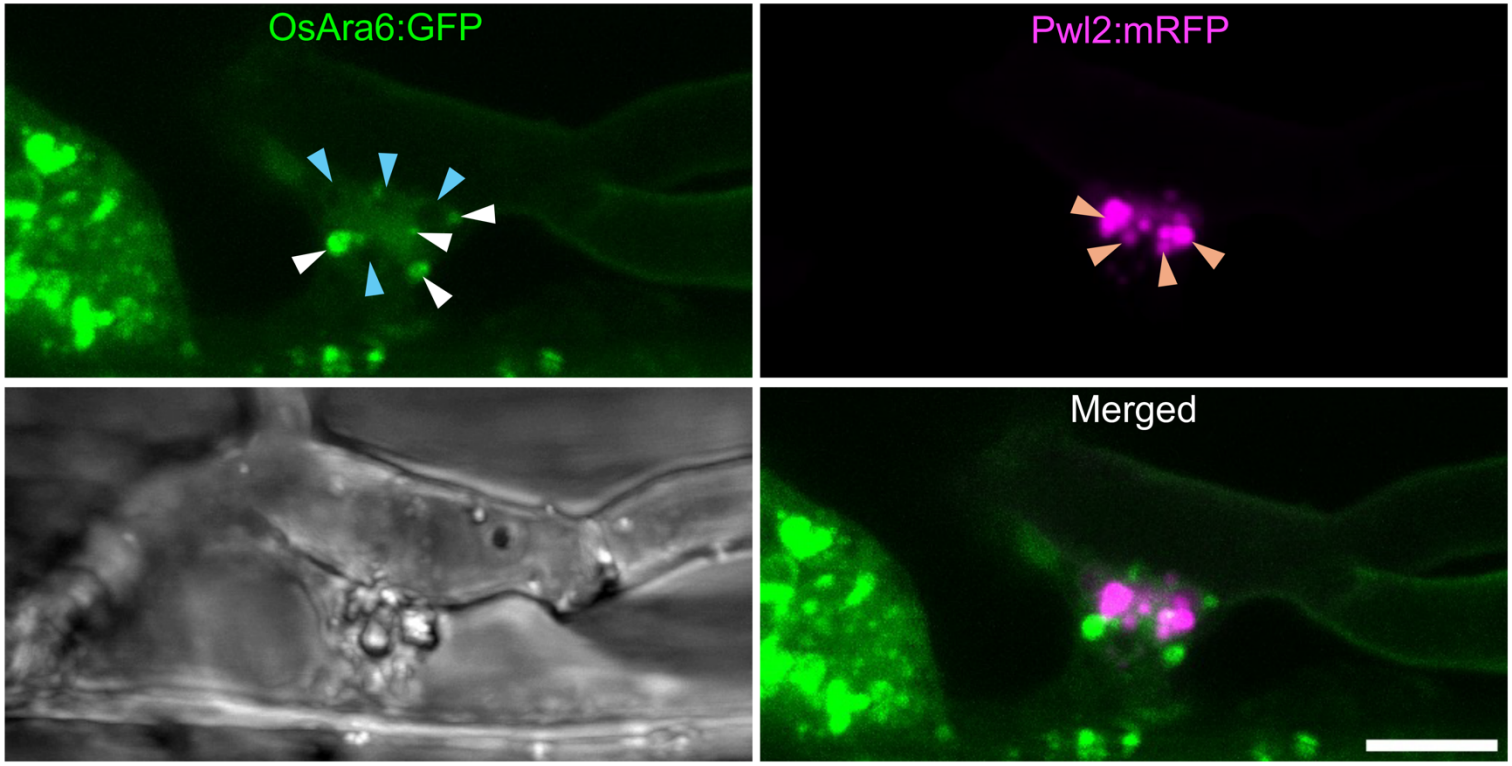

Figure 7.1 Early endosomes are associated with the biotrophic interfacial complex (BIC).
Confocal imaging of rice cv Kitaake transgenic line expressing early endosome marker OsAra6:GFP (green; early endosomes in indicated by white arrowheads) in cells infected with *M. oryzae* Guy11 expressing Pwl2:mRFP (magenta; orange arrowheads indicate membranous effector compartments (MECs)) showing association of rice early endosome and the BIC. A subpopulation of Pwl2:mRFP puncta resides in ring-like early endosomes (blue arrowheads). Micrographs were prepared from leaf sheath infections incubated at 24 °C and observed 26 hours post-inoculation (hpi). Images shown are maximum projections of z-stack series taken using a Leica TCS SP8X confocal laser scanning microscope. Scale bars = 5 μm.

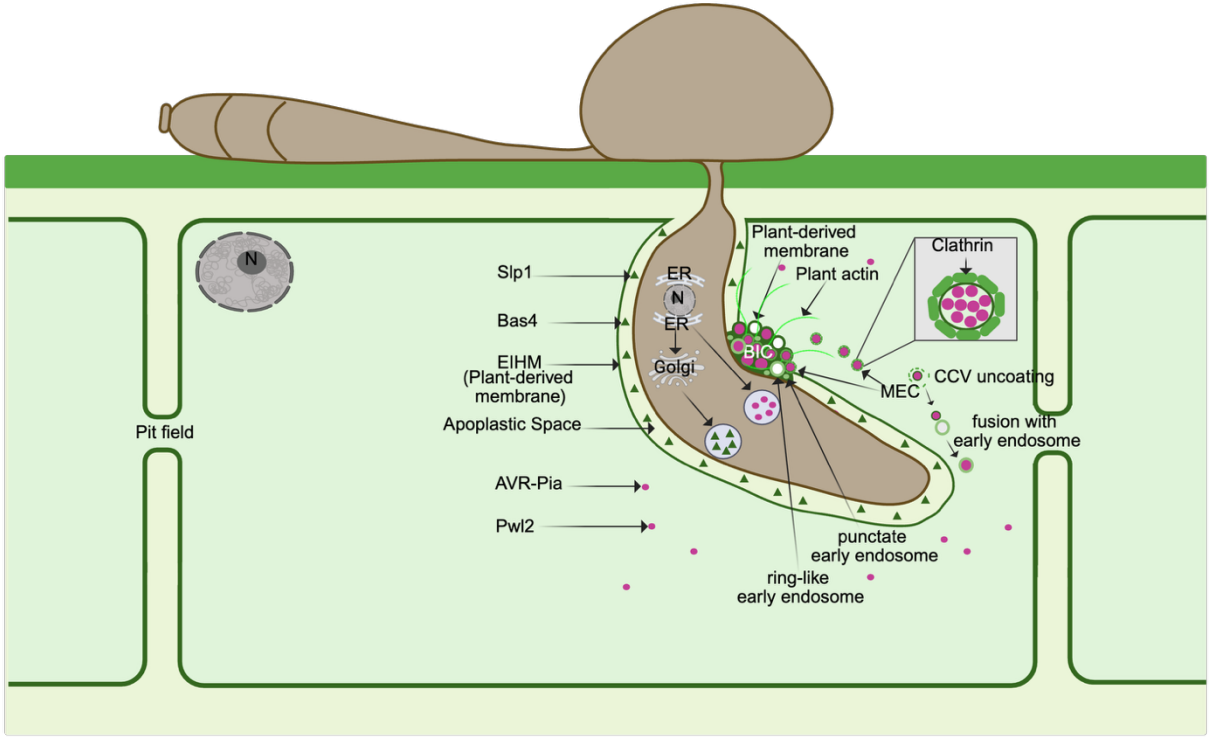

Figure 7.2 Proposed model for the translocation of *M. oryzae* effectors into rice cells.

During biotrophic growth, *M. oryzae* deploys a battery of effector proteins which are either apoplastic or cytoplasmic, to suppress host immune responses and facilitate fungal colonisation. Apoplastic effectors are secreted via the conventional ER-to-Golgi, Brefeldin A (BFA)-sensitive pathway, and reside in the apoplastic or EIHM matrix (EIHMx) enclosed by the extra-invasive hyphal membrane (EIHM). Cytoplasmic effectors are secreted using a nonconventional BFA-insensitive pathway and accumulate in the biotrophic interfacial complex (BIC). Cytoplasmic effectors tagged with fluorescent proteins are observed to be packaged in membranous effector compartments (MECs) which are found at the BIC with fluorescently-tagged rice plasma membrane (LTI6b TMD:GFP). Clathrin-mediated endocytosis subsequently internalises MECs into the host cytoplasm. After clathrin uncoating, MECs likely fuse with early endosomes, which then sort their cargo. At this stage, effector proteins are thought to be released to execute diverse immune-suppressive functions during fungal infection. This process may also occur locally within the BIC region, where early endosomes are frequently associated and thus readily available for fusion with uncoated MECs.

References

Amack, S. C., & Antunes, M. S. (2020). CaMV35S promoter – A plant biology and biotechnology workhorse in the era of synthetic biology. *Current Plant Biology*, *24*, 100179. https://doi.org/https://doi.org/10.1016/j.cpb.2020.100179

Aryal, B., Jonsson, K., Baral, A., Sancho-Andres, G., Routier- Kierzkowska, A.-L., Kierzkowski, D., & Bhalerao, R. P. (2020). Interplay between Cell Wall and Auxin Mediates the Control of Differential Cell Elongation during Apical Hook Development. *Current Biology*, *30*(9), 1733-1739.e1733. https://doi.org/10.1016/j.cub.2020.02.055

Balasubramanian, V., Sie, M., Hijmans, R. J., & Otsuka, K. (2007). Increasing Rice Production in Sub-Saharan Africa: Challenges and Opportunities. In D. L. Sparks (Ed.), *Advances in Agronomy* (Vol. 94, pp. 55-133). Academic Press. https://doi.org/https://doi.org/10.1016/S0065-2113(06)94002-4

Balla, T. (2013). Phosphoinositides: tiny lipids with giant impact on cell regulation. *Physiol Rev*, *93*(3), 1019-1137. https://doi.org/10.1152/physrev.00028.2012

Baluška, F., Šamaj, J., Hlavacka, A., Kendrick-Jones, J., & Volkmann, D. (2004). Actin-dependent fluid-phase endocytosis in inner cortex cells of maize root apices. *Journal of Experimental Botany*, *55*(396), 463-473. https://doi.org/10.1093/jxb/erh042

Baluška, F. e., Hlavacka, A., Sˇamaj, J., Palme, K., Robinson, D. G., Matoh, T., McCurdy, D. W., Menzel, D., & Volkmann, D. (2002). F-actin-dependent endocytosis of cell wall pectins in meristematic root cells. Insights from brefeldin A-induced compartments. *Plant Physiology*, *130*(1), 422-431.

Baluška, F. e., Šamaj, J., Wojtaszek, P., Volkmann, D., & Menzel, D. (2003). Cytoskeleton-Plasma Membrane-Cell Wall Continuum in Plants. Emerging Links Revisited. *Plant Physiology*, *133*(2), 482-491. https://doi.org/10.1104/pp.103.027250

Bandumula, N. (2018). Rice Production in Asia: Key to Global Food Security. *Proceedings of the National Academy of Sciences, India Section B: Biological Sciences*, *88*(4), 1323-1328. https://doi.org/10.1007/s40011-017-0867-7

Barbier de Reuille, P., Routier-Kierzkowska, A.-L., Kierzkowski, D., Bassel, G. W., Schüpbach, T., Tauriello, G., Bajpai, N., Strauss, S., Weber, A., Kiss, A., Burian, A., Hofhuis, H., Sapala, A., Lipowczan, M., Heimlicher, M. B., Robinson, S., Bayer, E. M., Basler, K., Koumoutsakos, P.,…Smith, R. S. (2015). MorphoGraphX: A platform for quantifying morphogenesis in 4D. *eLife*, *4*, e05864. https://doi.org/10.7554/eLife.05864

Barrero, R. A., Umeda, M., Yamamura, S., & Uchimiya, H. (2002). Arabidopsis CAP regulates the actin cytoskeleton necessary for plant cell elongation and division. *The Plant Cell*, *14*(1), 149-163.

Bassel, G. W., Stamm, P., Mosca, G., Barbier de Reuille, P., Gibbs, D. J., Winter, R., Janka, A., Holdsworth, M. J., & Smith, R. S. (2014). Mechanical constraints imposed by 3D cellular geometry and arrangement modulate growth patterns in the Arabidopsis embryo. *Proceedings of the National Academy of Sciences*, *111*(23), 8685-8690.

Beck, M., Heard, W., Mbengue, M., & Robatzek, S. (2012). The INs and OUTs of pattern recognition receptors at the cell surface. *Current Opinion in Plant Biology*, *15*(4), 367-374.

Blanchoin, L., Boujemaa-Paterski, R., Henty, J. L., Khurana, P., & Staiger, C. J. (2010). Actin dynamics in plant cells: a team effort from multiple proteins orchestrates this very fast-paced game. *Current Opinion in Plant Biology*, *13*(6), 714-723.

Blanchoin, L., Boujemaa-Paterski, R., Sykes, C., & Plastino, J. (2014). Actin dynamics, architecture, and mechanics in cell motility. *Physiological reviews*, *94*(1), 235-263.

Blanchoin, L., & Pollard, T. D. (2002). Hydrolysis of ATP by polymerized actin depends on the bound divalent cation but not profilin. *Biochemistry*, *41*(2), 597-602.

Blanchoin, L., & Staiger, C. J. (2010). Plant formins: diverse isoforms and unique molecular mechanism. *Biochimica et Biophysica Acta (BBA)-Molecular Cell Research*, *1803*(2), 201-206.

Block, A., Li, G., Fu, Z. Q., & Alfano, J. R. (2008). Phytopathogen type III effector weaponry and their plant targets. *Current Opinion in Plant Biology*, *11*(4), 396-403.

Boevink, P., Oparka, K., Cruz, S. S., Martin, B., Betteridge, A., & Hawes, C. (1998). Stacks on tracks: the plant Golgi apparatus traffics on an actin/ER network. *The Plant Journal*, *15*(3), 441-447.

Böhnert, H. U., Fudal, I., Dioh, W., Tharreau, D., Notteghem, J. L., & Lebrun, M. H. (2004). A putative polyketide synthase/peptide synthetase from Magnaporthe grisea signals pathogen attack to resistant rice. *Plant Cell*, *16*(9), 2499-2513. https://doi.org/10.1105/tpc.104.022715

Boller, T., & He, S. Y. (2009). Innate immunity in plants: an arms race between pattern recognition receptors in plants and effectors in microbial pathogens. *Science*, *324*(5928), 742-744.

Bourett, T. M., Sweigard, J. A., Czymmek, K. J., Carroll, A., & Howard, R. J. (2002). Reef coral fluorescent proteins for visualizing fungal pathogens. *Fungal Genet Biol*, *37*(3), 211-220. https://doi.org/10.1016/s1087-1845(02)00524-8

Bozkurt, T. O., Belhaj, K., Dagdas, Y. F., Chaparro-Garcia, A., Wu, C.-H., Cano, L. M., & Kamoun, S. (2015). Rerouting of Plant Late Endocytic Trafficking Toward a Pathogen Interface. *Traffic*, *16*(2), 204-226. https://doi.org/https://doi.org/10.1111/tra.12245

Brabham, H. J., Gómez De La Cruz, D., Were, V., Shimizu, M., Saitoh, H., Hernández-Pinzón, I., Green, P., Lorang, J., Fujisaki, K., Sato, K., Molnár, I., Šimková, H., Doležel, J., Russell, J., Taylor, J., Smoker, M., Gupta, Y. K., Wolpert, T., Talbot, N. J.,…Moscou, M. J. (2023). Barley MLA3 recognizes the host-specificity effector Pwl2 from Magnaporthe oryzae. *The Plant Cell*, *36*(2), 447-470. https://doi.org/10.1093/plcell/koad266

Brabham, H. J., Gómez De La Cruz, D., Were, V., Shimizu, M., Saitoh, H., Hernández-Pinzón, I., Green, P., Lorang, J., Fujisaki, K., Sato, K., Molnár, I., Šimková, H., Doležel, J., Russell, J., Taylor, J., Smoker, M., Gupta, Y. K., Wolpert, T., Talbot, N. J.,…Moscou, M. J. (2024). Barley MLA3 recognizes the host-specificity effector Pwl2 from Magnaporthe oryzae. *Plant Cell*, *36*(2), 447-470. https://doi.org/10.1093/plcell/koad266

Brandizzi, F., Snapp, E. L., Roberts, A. G., Lippincott-Schwartz, J., & Hawes, C. (2002). Membrane protein transport between the endoplasmic reticulum and the Golgi in tobacco leaves is energy dependent but cytoskeleton independent: evidence from selective photobleaching. *Plant Cell*, *14*(6), 1293-1309. https://doi.org/10.1105/tpc.001586

Bretscher, A., & Weber, K. (1980). Fimbrin, a new microfilament-associated protein present in microvilli and other cell surface structures. *The Journal of cell biology*, *86*(1), 335-340.

Brown, S. S., & Spudich, J. A. (1981). Mechanism of action of cytochalasin: evidence that it binds to actin filament ends. *Journal of Cell Biology*, *88*(3), 487-491. https://doi.org/10.1083/jcb.88.3.487

Bushnell, W. R. (1972). Physiology of Fungal Haustoria. *Annual Review of Phytopathology*, *10*(Volume 10), 151-176. https://doi.org/https://doi.org/10.1146/annurev.py.10.090172.001055

Caillaud, M. C., Piquerez, S. J., Fabro, G., Steinbrenner, J., Ishaque, N., Beynon, J., & Jones, J. D. (2012). Subcellular localization of the Hpa RxLR effector repertoire identifies a tonoplast-associated protein HaRxL17 that confers enhanced plant susceptibility. *The Plant Journal*, *69*(2), 252-265.

Carlier, M., & Pantaloni, D. (1986). Direct evidence for ADP-inorganic phosphate-F-actin as the major intermediate in ATP-actin polymerization. Rate of dissociation of inorganic phosphate from actin filaments. *Biochemistry*, *25*(24), 7789-7792.

Cesari, S. (2018). Multiple strategies for pathogen perception by plant immune receptors. *New Phytologist*, *219*(1), 17-24.

Cesari, S., Bernoux, M., Moncuquet, P., Kroj, T., & Dodds, P. N. (2014). A novel conserved mechanism for plant NLR protein pairs: the "integrated decoy" hypothesis. *Frontiers in Plant Science*, *5*, 606.

Cesari, S., Thilliez, G., Ribot, C., Chalvon, V., Michel, C., Jauneau, A., Rivas, S., Alaux, L., Kanzaki, H., Okuyama, Y., Morel, J.-B., Fournier, E., Tharreau, D., Terauchi, R., & Kroj, T. (2013). The Rice Resistance Protein Pair RGA4/RGA5 Recognizes the Magnaporthe oryzae Effectors AVR-Pia and AVR1-CO39 by Direct Binding *The Plant Cell*, *25*(4), 1463-1481. https://doi.org/10.1105/tpc.112.107201

Chakrabarti, R., Lee, M., & Higgs, H. N. (2021). Multiple roles for actin in secretory and endocytic pathways. *Current Biology*, *31*(10), R603-R618. https://doi.org/https://doi.org/10.1016/j.cub.2021.03.038

Chan, Y. H., & Marshall, W. F. (2012). How cells know the size of their organelles. *Science*, *337*(6099), 1186-1189. https://doi.org/10.1126/science.1223539

Chaudhry, F., Guérin, C., von Witsch, M., Blanchoin, L., & Staiger, C. J. (2007). Identification of Arabidopsis cyclase-associated protein 1 as the first nucleotide exchange factor for plant actin. *Mol Biol Cell*, *18*(8), 3002-3014. https://doi.org/10.1091/mbc.e06-11-1041

Chen, X., Irani, N. G., & Friml, J. (2011). Clathrin-mediated endocytosis: the gateway into plant cells. *Current Opinion in Plant Biology*, *14*(6), 674-682. https://doi.org/https://doi.org/10.1016/j.pbi.2011.08.006

Chen, X. L., Shi, T., Yang, J., Shi, W., Gao, X., Chen, D., Xu, X., Xu, J. R., Talbot, N. J., & Peng, Y. L. (2014). N-glycosylation of effector proteins by an α-1,3-mannosyltransferase is required for the rice blast fungus to evade host innate immunity. *Plant Cell*, *26*(3), 1360-1376. https://doi.org/10.1105/tpc.114.123588

Chen, Z., Zheng, W., Chen, L., Li, C., Liang, T., Chen, Z., Xu, H., Han, Y., Kong, L., Zhao, X., Wang, F., Wang, Z., & Chen, S. (2019). Green Fluorescent Protein- and Discosoma sp. Red Fluorescent Protein-Tagged Organelle Marker Lines for Protein Subcellular Localization in Rice. *Front Plant Sci*, *10*, 1421. https://doi.org/10.3389/fpls.2019.01421

Cheung, A. Y., & Wu, H.-m. (2004). Overexpression of an Arabidopsis formin stimulates supernumerary actin cable formation from pollen tube cell membrane. *The Plant Cell*, *16*(1), 257-269.

Christensen, A. H., Sharrock, R. A., & Quail, P. H. (1992). Maize polyubiquitin genes: structure, thermal perturbation of expression and transcript splicing, and promoter activity following transfer to protoplasts by electroporation. *Plant Molecular Biology*, *18*, 675-689.

Çiçek, Ö., Abdulkadir, A., Lienkamp, S., Brox, T., & Ronneberger, O. O. (2016). S; Joskowicz, L; Sabuncu, MR; Unal, G; Wells, W. 3D U-Net: learning dense

volumetric segmentation from sparse annotation. International conference on medical image computing and computer-assisted intervention,

Clément, M., Ketelaar, T., Rodiuc, N., Banora, M. Y., Smertenko, A., Engler, G., Abad, P., Hussey, P. J., & de Almeida Engler, J. (2009). Actin-Depolymerizing Factor2-Mediated Actin Dynamics Are Essential for Root-Knot Nematode Infection of Arabidopsis *The Plant Cell*, *21*(9), 2963-2979. https://doi.org/10.1105/tpc.109.069104

Coll, N. S., Epple, P., & Dangl, J. L. (2011). Programmed cell death in the plant immune system. *Cell Death & Differentiation*, *18*(8), 1247-1256. https://doi.org/10.1038/cdd.2011.37

Collemare, J., Pianfetti, M., Houlle, A.-E., Morin, D., Camborde, L., Gagey, M.-J., Barbisan, C., Fudal, I., Lebrun, M.-H., & Böhnert, H. U. (2008). Magnaporthe grisea avirulence gene ACE1 belongs to an infection-specific gene cluster involved in secondary metabolism. *New Phytologist*, *179*(1), 196-208. https://doi.org/https://doi.org/10.1111/j.1469-8137.2008.02459.x

Cooper, J. A. (1987). Effects of cytochalasin and phalloidin on actin. *J Cell Biol*, *105*(4), 1473-1478. https://doi.org/10.1083/jcb.105.4.1473

Cornejo, M.-J., Luth, D., Blankenship, K. M., Anderson, O. D., & Blechl, A. E. (1993). Activity of a maize ubiquitin promoter in transgenic rice. *Plant Molecular Biology*, *23*, 567-581.

Cruz-Mireles, N., Osés-Ruiz, M., Derbyshire, P., Jégousse, C., Ryder, L. S., Bautista, M. J. A., Eseola, A., Sklenar, J., Tang, B., Yan, X., Ma, W., Findlay, K. C., Were, V., MacLean, D., Talbot, N. J., & Menke, F. L. H. (2024). The phosphorylation landscape of infection-related development by the rice blast fungus. *Cell*, *187*(10), 2557-2573.e2518. https://doi.org/10.1016/j.cell.2024.04.007

Cvrčková, F., & Oulehlová, D. (2017). A new kymogram-based method reveals unexpected effects of marker protein expression and spatial anisotropy of cytoskeletal dynamics in plant cell cortex. *Plant Methods*, *13*(1), 19. https://doi.org/10.1186/s13007-017-0171-9

Czymmek, K. J., Fogg, M., Powell, D. H., Sweigard, J., Park, S.-Y., & Kang, S. (2007). In vivo time-lapse documentation using confocal and multi-photon microscopy reveals the mechanisms of invasion into the Arabidopsis root vascular system by Fusarium oxysporum. *Fungal Genetics and Biology*, *44*(10), 1011-1023. https://doi.org/https://doi.org/10.1016/j.fgb.2007.01.012

Dagdas, Y. F., Yoshino, K., Dagdas, G., Ryder, L. S., Bielska, E., Steinberg, G., & Talbot, N. J. (2012). Septin-mediated plant cell invasion by the rice blast fungus, Magnaporthe oryzae. *Science*, *336*(6088), 1590-1595.

Dangol, S., Singh, R., Chen, Y., & Jwa, N. S. (2017). Visualization of Multicolored in vivo Organelle Markers for Co-Localization Studies in Oryza sativa. *Mol Cells*, *40*(11), 828-836. https://doi.org/10.14348/molcells.2017.0045

Day, B., Henty, J. L., Porter, K. J., & Staiger, C. J. (2011). The pathogen-actin connection: a platform for defense signaling in plants. *Annual Review of Phytopathology*, *49*(1), 483-506.

de Almeida Engler, J., Rodiuc, N., Smertenko, A., & Abad, P. (2010). Plant actin cytoskeleton remodeling by plant parasitic nematodes. *Plant Signaling & Behavior*, *5*(3), 213-217. https://doi.org/10.4161/psb.5.3.10741

de Almeida Engler, J., Van Poucke, K., Karimi, M., De Groodt, R., Gheysen, G., Engler, G., & Gheysen, G. (2004). Dynamic cytoskeleton rearrangements in giant cells and syncytia of nematode-infected roots. *Plant J*, *38*(1), 12-26. https://doi.org/10.1111/j.1365-313X.2004.02019.x

de Jong, J. C., McCormack, B. J., Smirnoff, N., & Talbot, N. J. (1997). Glycerol generates turgor in rice blast. *Nature*, *389*(6648), 244-244. https://doi.org/10.1038/38418

de Jonge, R., Bolton, M. D., & Thomma, B. P. (2011). How filamentous pathogens co-opt plants: the ins and outs of fungal effectors. *Curr Opin Plant Biol*, *14*(4), 400-406. https://doi.org/10.1016/j.pbi.2011.03.005

De la Concepcion, J. C., Fujisaki, K., Bentham, A. R., Cruz Mireles, N., Sanchez de Medina Hernandez, V., Shimizu, M., Lawson, D. M., Kamoun, S., Terauchi, R., & Banfield, M. J. (2022). A blast fungus zinc-finger fold effector binds to a hydrophobic pocket in host Exo70 proteins to modulate immune recognition in rice. *Proc Natl Acad Sci U S A*, *119*(43), e2210559119. https://doi.org/10.1073/pnas.2210559119

Dean, R., Van Kan, J. A., Pretorius, Z. A., Hammond-Kosack, K. E., Di Pietro, A., Spanu, P. D., Rudd, J. J., Dickman, M., Kahmann, R., Ellis, J., & Foster, G. D. (2012). The Top 10 fungal pathogens in molecular plant pathology. *Mol Plant Pathol*, *13*(4), 414-430. https://doi.org/10.1111/j.1364-3703.2011.00783.x

Dean, R., Van Kan, J. A., Pretorius, Z. A., Hammond-Kosack, K. E., Di Pietro, A., Spanu, P. D., Rudd, J. J., Dickman, M., Kahmann, R., & Ellis, J. (2012). The Top 10 fungal pathogens in molecular plant pathology. *Molecular plant pathology*, *13*(4), 414-430.

Deeks, M. J., Fendrych, M., Smertenko, A., Bell, K. S., Oparka, K., Cvrckova, F., Zarsky, V., & Hussey, P. J. (2010). The plant formin AtFH4 interacts with both actin and microtubules, and contains a newly identified microtubule-binding domain. *J Cell Sci*, *123*(Pt 8), 1209-1215. https://doi.org/10.1242/jcs.065557

Di Paolo, G., & De Camilli, P. (2006). Phosphoinositides in cell regulation and membrane dynamics. *Nature*, *443*(7112), 651-657.

Dickman, M. B., & Fluhr, R. (2013). Centrality of Host Cell Death in Plant-Microbe Interactions. *Annual Review of Phytopathology*, *51*(Volume 51, 2013), 543-570. https://doi.org/https://doi.org/10.1146/annurev-phyto-081211-173027

Dodds, P. N., Lawrence, G. J., Pryor, A., & Ellis, J. G. (2020). Genetic analysis and evolution of plant disease resistance genes. *Molecular plant pathology*, 88-107.

Dodds, P. N., & Rathjen, J. P. (2010). Plant immunity: towards an integrated view of plant–pathogen interactions. *Nature Reviews Genetics*, *11*(8), 539-548.

Dominguez, R., & Holmes, K. C. (2011). Actin Structure and Function. *Annual Review of Biophysics*, *40*(Volume 40, 2011), 169-186. https://doi.org/https://doi.org/10.1146/annurev-biophys-042910-155359

Dong, Y., Majda, M., Šimura, J., Horvath, R., Srivastava, A. K., Łangowski, Ł., Eldridge, T., Stacey, N., Slotte, T., Sadanandom, A., Ljung, K., Smith, R. S., & Østergaard, L. (2020). HEARTBREAK Controls Post-translational Modification of INDEHISCENT to Regulate Fruit Morphology in Capsella. *Current Biology*, *30*(19), 3880-3888.e3885. https://doi.org/10.1016/j.cub.2020.07.055

Dörmann, P., Kim, H., Ott, T., Schulze-Lefert, P., Trujillo, M., Wewer, V., & Hückelhoven, R. (2014). Cell-autonomous defense, re-organization and trafficking of membranes in plant–microbe interactions. *New Phytologist*, *204*(4), 815-822. https://doi.org/https://doi.org/10.1111/nph.12978

Dulal, N., Rogers, A. M., Proko, R., Bieger, B. D., Liyanage, R., Krishnamurthi, V. R., Wang, Y., & Egan, M. J. (2021). Turgor-dependent and coronin-mediated F-actin dynamics drive septin disc-to-ring remodeling in the blast fungus Magnaporthe oryzae. *Journal of Cell Science*, *134*(5), jcs251298.

Duxbury, Z., Ma, Y., Furzer, O. J., Huh, S. U., Cevik, V., Jones, J. D., & Sarris, P. F. (2016). Pathogen perception by NLRs in plants and animals: Parallel worlds. *BioEssays*, *38*(8), 769-781.

Dyachok, J., Sparks, J. A., Liao, F., Wang, Y. S., & Blancaflor, E. B. (2014). Fluorescent protein-based reporters of the actin cytoskeleton in living plant cells: fluorophore variant, actin binding domain, and promoter considerations. *Cytoskeleton (Hoboken)*, *71*(5), 311-327. https://doi.org/10.1002/cm.21174

Ebbole, D. J. (2007). Magnaporthe as a model for understanding host-pathogen interactions. *Annu Rev Phytopathol*, *45*, 437-456. https://doi.org/10.1146/annurev.phyto.45.062806.094346

Ebine, K., Miyakawa, N., Fujimoto, M., Uemura, T., Nakano, A., & Ueda, T. (2012). Endosomal trafficking pathway regulated by ARA6, a RAB5 GTPase unique to plants. *Small GTPases*, *3*(1), 23-27. https://doi.org/10.4161/sgtp.18299

Emmanuel, C. J., Schoonbeek, H.-J., & Shaw, M. W. (2023). Microscope studies of symptomless growth of Botrytis cinerea in Lactuca sativa and Arabidopsis thaliana. *Plant Pathology*, *72*(3), 564-581. https://doi.org/https://doi.org/10.1111/ppa.13683

Era, A., Tominaga, M., Ebine, K., Awai, C., Saito, C., Ishizaki, K., Yamato, K. T., Kohchi, T., Nakano, A., & Ueda, T. (2009). Application of Lifeact Reveals F-Actin Dynamics in Arabidopsis thaliana and the Liverwort, Marchantia polymorpha. *Plant and Cell Physiology*, *50*(6), 1041-1048. https://doi.org/10.1093/pcp/pcp055

Erguvan, Ö., Louveaux, M., Hamant, O., & Verger, S. (2019). ImageJ SurfCut: a user-friendly pipeline for high-throughput extraction of cell contours from 3D image stacks. *BMC biology*, *17*(1), 38. https://doi.org/10.1186/s12915-019-0657-1

Eseola, A. B., Ryder, L. S., Osés-Ruiz, M., Findlay, K., Yan, X., Cruz-Mireles, N., Molinari, C., Garduño-Rosales, M., & Talbot, N. J. (2021). Investigating the cell and developmental biology of plant infection by the rice blast fungus Magnaporthe oryzae. *Fungal Genetics and Biology*, 103562. https://doi.org/https://doi.org/10.1016/j.fgb.2021.103562

Fahad, S., Adnan, M., Noor, M., Arif, M., Alam, M., Khan, I. A., Ullah, H., Wahid, F., Mian, I. A., Jamal, Y., Basir, A., Hassan, S., Saud, S., Amanullah, Riaz, M., Wu, C., Khan, M. A., & Wang, D. (2019). Chapter 1 - Major Constraints for Global Rice Production. In M. Hasanuzzaman, M. Fujita, K. Nahar, & J. K. Biswas (Eds.), *Advances in Rice Research for Abiotic Stress Tolerance* (pp. 1-22). Woodhead Publishing. https://doi.org/https://doi.org/10.1016/B978-0-12-814332-2.00001-0

Feng, Z., Chen, X., Bao, Y., Dong, J., Zhang, Z., & Tao, X. (2013). Nucleocapsid of Tomato spotted wilt tospovirus forms mobile particles that traffic on an actin/endoplasmic reticulum network driven by myosin XI-K. *New Phytologist*, *200*(4), 1212-1224.

Fernandez, J., & Orth, K. (2018). Rise of a Cereal Killer: The Biology of Magnaporthe oryzae Biotrophic Growth. *Trends in Microbiology*, *26*(7), 582-597. https://doi.org/https://doi.org/10.1016/j.tim.2017.12.007

Fletcher, D. A., & Mullins, R. D. (2010). Cell mechanics and the cytoskeleton. *Nature*, *463*(7280), 485-492.

Fujisaki, K., Abe, Y., Ito, A., Saitoh, H., Yoshida, K., Kanzaki, H., Kanzaki, E., Utsushi, H., Yamashita, T., & Kamoun, S. (2015). Rice Exo70 interacts with a fungal effector, AVR-Pii, and is required for AVR-Pii-triggered immunity. *The Plant Journal*, *83*(5), 875-887.

Fujisaki, K., Abe, Y., Kanzaki, E., Ito, K., Utsushi, H., Saitoh, H., Białas, A., Banfield, M. J., Kamoun, S., & Terauchi, R. (2017). An unconventional NOI/RIN4 domain

of a rice NLR protein binds host EXO70 protein to confer fungal immunity. *bioRxiv*, *239400*.

Gadella, T. W. J., van Weeren, L., Stouthamer, J., Hink, M. A., Wolters, A. H. G., Giepmans, B. N. G., Aumonier, S., Dupuy, J., & Royant, A. (2023). mScarlet3: a brilliant and fast-maturing red fluorescent protein. *Nature Methods*, *20*(4), 541-545. https://doi.org/10.1038/s41592-023-01809-y

Galkin, V. E., Orlova, A., Kudryashov, D. S., Solodukhin, A., Reisler, E., Schröder, G. F., & Egelman, E. H. (2011). Remodeling of actin filaments by ADF/cofilin proteins. *Proceedings of the National Academy of Sciences*, *108*(51), 20568-20572. https://doi.org/doi:10.1073/pnas.1110109108

Gallie, D. R., Sleat, D. E., Watts, J. W., Turner, P. C., & Wilson, T. M. A. (1987). The 5'-leader sequence of tobacco mosaic virus RNA enhances the expression of foreign gene transcripts in vitro and in vivo. *Nucleic Acids Research*, *15*(8), 3257-3273. https://doi.org/10.1093/nar/15.8.3257

Gallie, D. R., & Walbot, V. (1992). Identification of the motifs within the tobacco mosaic virus 5'-leader responsible for enhancing translation. *Nucleic Acids Research*, *20*(17), 4631-4638.

Gangireddy, A. K., Sreevalli, M. D., Chintala, S., Puchakayala, M., Padherla, L. K., Killada, G. K., Vulusala, B. P., Bommisetty, R., Kotte, B., & Vemireddy, L. R. (2025). Integrating phenotypic and molecular profiling for selection of promising advanced breeding lines for blast resistance in rice (Oryza sativa L.). *Molecular Biology Reports*, *52*(1), 184. https://doi.org/10.1007/s11033-025-10279-8

Geitmann, A., & Nebenführ, A. (2015). Navigating the plant cell: intracellular transport logistics in the green kingdom. *Molecular Biology of the Cell*, *26*(19), 3373-3378.

Geldner, N., Dénervaud-Tendon, V., Hyman, D. L., Mayer, U., Stierhof, Y. D., & Chory, J. (2009). Rapid, combinatorial analysis of membrane compartments in intact plants with a multicolor marker set. *Plant J*, *59*(1), 169-178. https://doi.org/10.1111/j.1365-313X.2009.03851.x

Gerst, J. E., Ferguson, K., Vojtek, A., Wigler, M., & Field, J. (1991). CAP is a bifunctional component of the Saccharomyces cerevisiae adenylyl cyclase complex. *Molecular and cellular biology*, *11*(3), 1248-1257. https://doi.org/10.1128/mcb.11.3.1248-1257.1991

Giraldo, M. C., Dagdas, Y. F., Gupta, Y. K., Mentlak, T. A., Yi, M., Martinez-Rocha, A. L., Saitoh, H., Terauchi, R., Talbot, N. J., & Valent, B. (2013). Two distinct secretion systems facilitate tissue invasion by the rice blast fungus Magnaporthe oryzae. *Nat Commun*, *4*, 1996. https://doi.org/10.1038/ncomms2996

Glazebrook, J. (2005). Contrasting mechanisms of defense against biotrophic and necrotrophic pathogens. *Annu Rev Phytopathol*, *43*, 205-227. https://doi.org/10.1146/annurev.phyto.43.040204.135923

Godfray, H. C. J., Beddington, J. R., Crute, I. R., Haddad, L., Lawrence, D., Muir, J. F., Pretty, J., Robinson, S., Thomas, S. M., & Toulmin, C. (2010). Food Security: The Challenge of Feeding 9 Billion People. *Science*, *327*(5967), 812-818. https://doi.org/10.1126/science.1185383

Goelet, P., Lomonossoff, G. P., Butler, P. J., Akam, M. E., Gait, M. J., & Karn, J. (1982). Nucleotide sequence of tobacco mosaic virus RNA. *Proceedings of the National Academy of Sciences*, *79*(19), 5818-5822. https://doi.org/doi:10.1073/pnas.79.19.5818

Gould, S. J., Keller, G.-A., Hosken, N., Wilkinson, J., & Subramani, S. (1989). A conserved tripeptide sorts proteins to peroxisomes. *The Journal of cell biology*, *108*(5), 1657-1664.

Grützner, R., Martin, P., Horn, C., Mortensen, S., Cram, E. J., Lee-Parsons, C. W. T., Stuttmann, J., & Marillonnet, S. (2021). High-efficiency genome editing in plants mediated by a Cas9 gene containing multiple introns. *Plant Communications*, *2*(2), 100135. https://doi.org/https://doi.org/10.1016/j.xplc.2020.100135

Guo, J., Wu, Y., Huang, J., Yu, K., Chen, M., Han, Y., Zhong, Z., Lu, G., Hong, Y., & Wang, Z. (2024). The Magnaporthe oryzae effector Avr-PikD suppresses rice immunity by inhibiting an LSD1-like transcriptional activator. *The Crop Journal*, *12*(2), 482-492.

Gupta, Y. K., Dagdas, Y. F., Martinez-Rocha, A.-L., Kershaw, M. J., Littlejohn, G. R., Ryder, L. S., Sklenar, J., Menke, F., & Talbot, N. J. (2015). Septin-dependent assembly of the exocyst is essential for plant infection by Magnaporthe oryzae. *The Plant Cell*, *27*(11), 3277-3289.

Gurel, P. S., Ge, P., Grintsevich, E. E., Shu, R., Blanchoin, L., Zhou, Z. H., Reisler, E., & Higgs, H. N. (2014). INF2-mediated severing through actin filament encirclement and disruption. *Current Biology*, *24*(2), 156-164.

Hamer, J. E., Howard, R. J., Chumley, F. G., & Valent, B. (1988). A mechanism for surface attachment in spores of a plant pathogenic fungus. *Science*, *239*(4837), 288-290. https://doi.org/10.1126/science.239.4837.288

Hamer, J. E., & Timberlake, W. E. (1987). Functional organization of the Aspergillus nidulans trpC promoter. *Molecular and cellular biology*, *7*(7), 2352-2359. https://doi.org/10.1128/mcb.7.7.2352-2359.1987

Han, J., Wang, X., Wang, F., Zhao, Z., Li, G., Zhu, X., Su, J., & Chen, L. (2021). The Fungal Effector Avr-Pita Suppresses Innate Immunity by Increasing COX Activity in Rice Mitochondria. *Rice*, *14*(1), 12. https://doi.org/10.1186/s12284-021-00453-4

Hardham, A. R., Jones, D. A., & Takemoto, D. (2007). Cytoskeleton and cell wall function in penetration resistance. *Current Opinion in Plant Biology*, *10*(4), 342-348.

Harris, A. R., Belardi, B., Jreij, P., Wei, K., Shams, H., Bausch, A., & Fletcher, D. A. (2019). Steric regulation of tandem calponin homology domain actin-binding affinity. *Molecular Biology of the Cell*, *30*(26), 3112-3122.

Harwood, W. A. (2014). A protocol for high-throughput Agrobacterium-mediated barley transformation. *Cereal genomics: methods and protocols*, 251-260.

Hatsugai, N., Iwasaki, S., Tamura, K., Kondo, M., Fuji, K., Ogasawara, K., Nishimura, M., & Hara-Nishimura, I. (2009). A novel membrane fusion-mediated plant immunity against bacterial pathogens. *Genes & development*, *23*(21), 2496-2506.

Hatsugai, N., Kuroyanagi, M., Yamada, K., Meshi, T., Tsuda, S., Kondo, M., Nishimura, M., & Hara-Nishimura, I. (2004). A plant vacuolar protease, VPE, mediates virus-induced hypersensitive cell death. *Science*, *305*(5685), 855-858.

Hawes, C. (2005). Cell biology of the plant Golgi apparatus. *New Phytologist*, *165*(1), 29-44. https://doi.org/https://doi.org/10.1111/j.1469-8137.2004.01218.x

He, Z.-H., Cheeseman, I., He, D., & Kohorn, B. D. (1999). A cluster of five cell wall-associated receptor kinase genes, Wak1–5, are expressed in specific organs of Arabidopsis. *Plant Molecular Biology*, *39*, 1189-1196.

Heald, R., & Cohen-Fix, O. (2014). Morphology and function of membrane-bound organelles. *Curr Opin Cell Biol*, *26*, 79-86. https://doi.org/10.1016/j.ceb.2013.10.006

Heath, M. C., Howard, R. J., Valent, B., & Chumley, F. G. (1992). Ultrastructural interactions of one strain of Magnaporthe grisea with goosegrass and weeping lovegrass. *Canadian Journal of Botany*, *70*(4), 779-787. https://doi.org/10.1139/b92-099

Heath, M. C., Valent, B., Howard, R. J., & Chumley, F. G. (1990). Interactions of two strains of Magnaporthe grisea with rice, goosegrass, and weeping lovegrass. *Canadian Journal of Botany*, *68*(8), 1627-1637. https://doi.org/10.1139/b90-209

Hensel, G., Valkov, V., Middlefell-Williams, J., & Kumlehn, J. (2008). Efficient generation of transgenic barley: the way forward to modulate plant–microbe interactions. *Journal of plant physiology*, *165*(1), 71-82.

Henty-Ridilla, J. L., Shimono, M., Li, J., Chang, J. H., Day, B., & Staiger, C. J. (2013). The plant actin cytoskeleton responds to signals from microbe-associated molecular patterns. *PLoS Pathog*, *9*(4), e1003290. https://doi.org/10.1371/journal.ppat.1003290

Hiei, Y., & Komari, T. (2008). Agrobacterium-mediated transformation of rice using immature embryos or calli induced from mature seed. *Nature protocols*, *3*(5), 824-834.

Hirakawa, Y., Nomura, T., Hasezawa, S., & Higaki, T. (2015). Simplification of vacuole structure during plant cell death triggered by culture filtrates of Erwinia carotovora. *Journal of Integrative Plant Biology*, *57*(1), 127-135. https://doi.org/https://doi.org/10.1111/jipb.12304

Horvath, H., Rostoks, N., Brueggeman, R., Steffenson, B., Von Wettstein, D., & Kleinhofs, A. (2003). Genetically engineered stem rust resistance in barley using the Rpg1 gene. *Proceedings of the National Academy of Sciences*, *100*(1), 364-369.

Howard, R. J., & Ferrari, M. A. (1989). Role of melanin in appressorium function. *Experimental Mycology*, *13*(4), 403-418.

Howard, R. J., Ferrari, M. A., Roach, D. H., & Money, N. P. (1991). Penetration of hard substrates by a fungus employing enormous turgor pressures. *Proc Natl Acad Sci U S A*, *88*(24), 11281-11284. https://doi.org/10.1073/pnas.88.24.11281

Howard, R. J., & Valent, B. (1996). BREAKING AND ENTERING: Host Penetration by the Fungal Rice Blast Pathogen Magnaporthe grisea. *Annual Review of Microbiology*, *50*(Volume 50, 1996), 491-512. https://doi.org/https://doi.org/10.1146/annurev.micro.50.1.491

Hu, J., Liu, M., Zhang, A., Dai, Y., Chen, W., Chen, F., Wang, W., Shen, D., Telebanco-Yanoria, M. J., Ren, B., Zhang, H., Zhou, H., Zhou, B., Wang, P., & Zhang, Z. (2022). Co-evolved plant and blast fungus ascorbate oxidases orchestrate the redox state of host apoplast to modulate rice immunity. *Molecular Plant*, *15*(8), 1347-1366. https://doi.org/https://doi.org/10.1016/j.molp.2022.07.001

Huang, S., Blanchoin, L., Kovar, D. R., & Staiger, C. J. (2003). Arabidopsis capping protein (AtCP) is a heterodimer that regulates assembly at the barbed ends of actin filaments. *Journal of Biological Chemistry*, *278*(45), 44832-44842.

Huang, S., Qu, X., & Zhang, R. (2015). Plant villins: versatile actin regulatory proteins. *Journal of Integrative Plant Biology*, *57*(1), 40-49.

Huang, S., Robinson, R. C., Gao, L. Y., Matsumoto, T., Brunet, A., Blanchoin, L., & Staiger, C. J. (2005). Arabidopsis VILLIN1 generates actin filament cables that are resistant to depolymerization. *The Plant Cell*, *17*(2), 486-501.

Hückelhoven, R., & Panstruga, R. (2011). Cell biology of the plant–powdery mildew interaction. *Current Opinion in Plant Biology*, *14*(6), 738-746.

Humphreys, D., Hume, P. J., & Koronakis, V. (2009). The Salmonella effector SptP dephosphorylates host AAA+ ATPase VCP to promote development of its intracellular replicative niche. *Cell Host Microbe*, *5*(3), 225-233. https://doi.org/10.1016/j.chom.2009.01.010

Ibrahim, A. S., El-Shihy, O. M., & Fahmy, A. H. (2010). Highly efficient Agrobacterium tumefaciens-mediated transformation of elite Egyptian barley cultivars. *American-Eurasian Journal of Sustainable Agriculture*, *4*(3), 403-413.

Ichitani, K., Okumoto, Y., & Tanisaka, T. (1997). Photoperiod Sensitivity Gene of Se-1 Locus Found in Photoperiod Insensitive Rice Cultivars of the Northern Limit Region of Rice Cultivation. *Ikushugaku zasshi*, *47*, 145-152. https://doi.org/10.1270/jsbbs1951.47.145

Inada, N. (2016). Visualization of Host Actin Microfilament Dynamicity upon Obligate Biotrophic Pathogen Infection. *CYTOLOGIA*, *81*(2), 119-120. https://doi.org/10.1508/cytologia.81.119

Inada, N., Higaki, T., & Hasezawa, S. (2016). Quantitative analyses on dynamic changes in the organization of host Arabidopsis thaliana actin microfilaments surrounding the infection organ of the powdery mildew fungus Golovinomyces orontii. *Journal of Plant Research*, *129*(1), 103-110. https://doi.org/10.1007/s10265-015-0769-9

Inoue, Y., Vy, T. T., Yoshida, K., Asano, H., Mitsuoka, C., Asuke, S., Anh, V. L., Cumagun, C. J., Chuma, I., & Terauchi, R. (2017). Evolution of the wheat blast fungus through functional losses in a host specificity determinant. *Science*, *357*(6346), 80-83.

Iqbal, J., Zia-ul-Qamar, Yousaf, U., Asgher, A., Dilshad, R., Qamar, F. M., Bibi, S., Rehman, S. U., & Haroon, M. (2023). Sustainable Rice Production Under Biotic and Abiotic Stress Challenges. In C. S. Prakash, S. Fiaz, M. A. Nadeem, F. S. Baloch, & A. Qayyum (Eds.), *Sustainable Agriculture in the Era of the OMICs Revolution* (pp. 241-268). Springer International Publishing. https://doi.org/10.1007/978-3-031-15568-0_11

Islam, M. T., Croll, D., Gladieux, P., Soanes, D. M., Persoons, A., Bhattacharjee, P., Hossain, M. S., Gupta, D. R., Rahman, M. M., & Mahboob, M. G. (2016). Emergence of wheat blast in Bangladesh was caused by a South American lineage of Magnaporthe oryzae. *BMC biology*, *14*, 1-11.

Islam, M. T., Kim, K.-H., & Choi, J. (2019). Wheat blast in Bangladesh: the current situation and future impacts. *The plant pathology journal*, *35*(1), 1.

Ivanov, S., Daniels, D. A., & Harrison, M. J. (2023). A Medicago truncatula Cell Biology Resource: Transgenic Lines Expressing Fluorescent Protein-Based Markers of Membranes, Organelles, and Subcellular Compartments. *Mol Plant Microbe Interact*, *36*(4), 256-259. https://doi.org/10.1094/mpmi-01-22-0023-a

Ivanov, S., & Harrison, M. J. (2014). A set of fluorescent protein-based markers expressed from constitutive and arbuscular mycorrhiza-inducible promoters to label organelles, membranes and cytoskeletal elements in Medicago truncatula. *Plant J*, *80*(6), 1151-1163. https://doi.org/10.1111/tpj.12706

Ivanov, S., & Harrison, M. J. (2019). Accumulation of phosphoinositides in distinct regions of the periarbuscular membrane. *New Phytologist*, *221*(4), 2213-2227. https://doi.org/https://doi.org/10.1111/nph.15553

Iwai, T., Seo, S., Mitsuhara, I., & Ohashi, Y. (2007). Probenazole-Induced Accumulation of Salicylic Acid Confers Resistance to Magnaporthe grisea in Adult Rice Plants. *Plant and Cell Physiology*, *48*(7), 915-924. https://doi.org/10.1093/pcp/pcm062

Jackson, M. D. B., Duran-Nebreda, S., Kierzkowski, D., Strauss, S., Xu, H., Landrein, B., Hamant, O., Smith, R. S., Johnston, I. G., & Bassel, G. W. (2019). Global Topological Order Emerges through Local Mechanical Control of Cell Divisions in the Arabidopsis Shoot Apical Meristem. *Cell Systems*, *8*(1), 53-65.e53. https://doi.org/10.1016/j.cels.2018.12.009

Jain, R., Jenkins, J., Shu, S., Chern, M., Martin, J. A., Copetti, D., Duong, P. Q., Pham, N. T., Kudrna, D. A., Talag, J., Schackwitz, W. S., Lipzen, A. M., Dilworth, D., Bauer, D., Grimwood, J., Nelson, C. R., Xing, F., Xie, W., Barry, K. W.,…Ronald, P. C. (2019). Genome sequence of the model rice variety KitaakeX. *BMC Genomics*, *20*(1), 905. https://doi.org/10.1186/s12864-019-6262-4

Jaswal, R., Kiran, K., Rajarammohan, S., Dubey, H., Singh, P. K., Sharma, Y., Deshmukh, R., Sonah, H., Gupta, N., & Sharma, T. (2020). Effector biology of biotrophic plant fungal pathogens: Current advances and future prospects. *Microbiological research*, *241*, 126567.

Jelenska, J., Kang, Y., & Greenberg, J. T. (2014). Plant pathogenic bacteria target the actin microfilament network involved in the trafficking of disease defense components. *Bioarchitecture*, *4*(4-5), 149-153.

Jeon, J., Park, S.-Y., Chi, M.-H., Choi, J., Park, J., Rho, H.-S., Kim, S., Goh, J., Yoo, S., & Choi, J. (2007). Genome-wide functional analysis of pathogenicity genes in the rice blast fungus. *Nature genetics*, *39*(4), 561-565.

Jia, T., Gao, C., Cui, Y., Wang, J., Ding, Y., Cai, Y., Ueda, T., Nakano, A., & Jiang, L. (2013). ARA7(Q69L) expression in transgenic Arabidopsis cells induces the formation of enlarged multivesicular bodies. *Journal of Experimental Botany*, *64*. https://doi.org/10.1093/jxb/ert125

Johnson, A. (2024). Mechanistic divergences of endocytic clathrin-coated vesicle formation in mammals, yeasts and plants. *Journal of Cell Science*, *137*(16). https://doi.org/10.1242/jcs.261847

Johnson, J. L., Monfregola, J., Napolitano, G., Kiosses, W. B., & Catz, S. D. (2012). Vesicular trafficking through cortical actin during exocytosis is regulated by the Rab27a effector JFC1/Slp1 and the RhoA-GTPase–activating protein Gem-interacting protein. *Molecular Biology of the Cell*, *23*(10), 1902-1916.

Jones, J. D., & Dangl, J. L. (2006). The plant immune system. *Nature*, *444*(7117), 323-329.

Jones, K., Kim, D. W., Park, J. S., & Khang, C. H. (2016). Live-cell fluorescence imaging to investigate the dynamics of plant cell death during infection by the rice blast fungus Magnaporthe oryzae. *BMC Plant Biology*, *16*(1), 69. https://doi.org/10.1186/s12870-016-0756-x

Jones, K., Zhu, J., Jenkinson, C. B., Kim, D. W., Pfeifer, M. A., & Khang, C. H. (2021). Disruption of the Interfacial Membrane Leads to Magnaporthe oryzae Effector Re-location and Lifestyle Switch During Rice Blast Disease [Original Research]. *Frontiers in Cell and Developmental Biology*, *9*. https://doi.org/10.3389/fcell.2021.681734

Jung, K.-H., An, G., & Ronald, P. C. (2008). Towards a better bowl of rice: assigning function to tens of thousands of rice genes. *Nature Reviews Genetics*, *9*(2), 91-101.

Kang, S., Sweigard, J. A., & Valent, B. (1995). The PWL host specificity gene family in the blast fungus Magnaporthe grisea. *Mol Plant Microbe Interact*, *8*(6), 939-948. https://doi.org/10.1094/mpmi-8-0939

Kang, Y., Jelenska, J., Cecchini, N. M., Li, Y., Lee, M. W., Kovar, D. R., & Greenberg, J. T. (2014). HopW1 from Pseudomonas syringae disrupts the actin cytoskeleton to promote virulence in Arabidopsis. *PLOS Pathogens*, *10*(6), e1004232.

Kankanala, P., Czymmek, K., & Valent, B. (2007). Roles for Rice Membrane Dynamics and Plasmodesmata during Biotrophic Invasion by the Blast Fungus. *The Plant Cell*, *19*(2), 706-724. https://doi.org/10.1105/tpc.106.046300

Kato, H., Yamamoto, M., Yamaguchi-Ozaki, T., Kadouchi, H., Iwamoto, Y., Nakayashiki, H., Tosa, Y., Mayama, S., & Mori, N. (2000). Pathogenicity, mating ability and DNA restriction fragment length polymorphisms of Pyricularia populations isolated from Gramineae, Bambusideae and Zingiberaceae plants. *Journal of General Plant Pathology*, *66*, 30-47.

Kershaw, M. J., & Talbot, N. J. (2009). Genome-wide functional analysis reveals that infection-associated fungal autophagy is necessary for rice blast disease. *Proceedings of the National Academy of Sciences*, *106*(37), 15967-15972.

Khang, C. H., Berruyer, R., Giraldo, M. C., Kankanala, P., Park, S. Y., Czymmek, K., Kang, S., & Valent, B. (2010). Translocation of Magnaporthe oryzae effectors into rice cells and their subsequent cell-to-cell movement. *Plant Cell*, *22*(4), 1388-1403. https://doi.org/10.1105/tpc.109.069666

Khush, G. S. (2005). What it will take to feed 5.0 billion rice consumers in 2030. *Plant Molecular Biology*, *59*, 1-6.

Kierzkowski, D., Runions, A., Vuolo, F., Strauss, S., Lymbouridou, R., Routier-Kierzkowska, A.-L., Wilson-Sánchez, D., Jenke, H., Galinha, C., Mosca, G., Zhang, Z., Canales, C., Dello Ioio, R., Huijser, P., Smith, R. S., & Tsiantis, M. (2019). A Growth-Based Framework for Leaf Shape Development and Diversity. *Cell*, *177*(6), 1405-1418.e1417. https://doi.org/10.1016/j.cell.2019.05.011

Kim, Xu, Z.-Y., & Hwang, I. (2013). Generation of transgenic Arabidopsis plants expressing mcherry-fused organelle marker proteins. *Journal of Plant Biology*, *56*, 399-406.

Kim, S. L., Choi, M., Jung, K.-H., & An, G. (2013). Analysis of the early-flowering mechanisms and generation of T-DNA tagging lines in Kitaake, a model rice cultivar. *Journal of Experimental Botany*, *64*(14), 4169-4182.

Kinoshita, A., Vayssières, A., Richter, R., Sang, Q., Roggen, A., van Driel, A. D., Smith, R. S., & Coupland, G. (2020). Regulation of shoot meristem shape by photoperiodic signaling and phytohormones during floral induction of Arabidopsis. *eLife*, *9*, e60661. https://doi.org/10.7554/eLife.60661

Kirchhelle, C., Garcia-Gonzalez, D., Irani, N. G., Jérusalem, A., & Moore, I. (2019). Two mechanisms regulate directional cell growth in Arabidopsis lateral roots. *eLife*, *8*, e47988. https://doi.org/10.7554/eLife.47988

Klahre, U., Friederich, E., Kost, B., Louvard, D., & Chua, N.-H. (2000). Villin-like actin-binding proteins are expressed ubiquitously in Arabidopsis. *Plant Physiology*, *122*(1), 35-48.

Kobayashi, I., & Hakuno, H. (2003). Actin-related defense mechanism to reject penetration attempt by a non-pathogen is maintained in tobacco BY-2 cells. *Planta*, *217*(2), 340-345. https://doi.org/10.1007/s00425-003-1042-3

Kobayashi, Y., & Kobayashi, I. (2007). Depolymerization of the actin cytoskeleton induces defense responses in tobacco plants. *Journal of General Plant Pathology*, *73*, 360-364.

Kobayashi, Y., Kobayashi, I., Funaki, Y., Fujimoto, S., Takemoto, T., & Kunoh, H. (1997). Dynamic reorganization of microfilaments and microtubules is necessary for the expression of non-host resistance in barley coleoptile cells. *The Plant Journal*, *11*(3), 525-537.

Kobayashi, Y., Yamada, M., Kobayashi, I., & Kunoh, H. (1997). Actin microfilaments are required for the expression of nonhost resistance in higher plants. *Plant and Cell Physiology*, *38*(6), 725-733.

Koga, H. (1994). Hypersensitive death, autofluorescence, and ultrastructural changes in cells of leaf sheaths of susceptible and resistant near-isogenic lines of rice (Pi-zt) in relation to penetration and growth of Pyricularia oryzae. *Canadian Journal of Botany*, *72*(10), 1463-1477.

Koga, H., Dohi, K., Nakayachi, O., & Mori, M. (2004). A novel inoculation method of Magnaporthe grisea for cytological observation of the infection process using intact leaf sheaths of rice plants. *Physiological and Molecular Plant Pathology*, *64*(2), 67-72. https://doi.org/https://doi.org/10.1016/j.pmpp.2004.07.002

Koga, H., & Kobayashi, T. (1982). Comparison of the early infection process of Pyricularia oryzae Cav. in rice leaves of compatible and incompatible combinations. *Japanese Journal of Phytopathology*, *48*(4), 506-513.

Koh, S., André, A., Edwards, H., Ehrhardt, D., & Somerville, S. (2005). Arabidopsis thaliana subcellular responses to compatible Erysiphe cichoracearum infections. *The Plant Journal*, *44*(3), 516-529. https://doi.org/https://doi.org/10.1111/j.1365-313X.2005.02545.x

Köhler, R. H., Zipfel, W. R., Webb, W. W., & Hanson, M. R. (1997). The green fluorescent protein as a marker to visualize plant mitochondria in vivo. *The Plant Journal*, *11*(3), 613-621. https://doi.org/https://doi.org/10.1046/j.1365-313X.1997.11030613.x

Kotzer, A. M., Brandizzi, F., Neumann, U., Paris, N., Moore, I., & Hawes, C. (2004). AtRabF2b (Ara7) acts on the vacuolar trafficking pathway in tobacco leaf epidermal cells. *J Cell Sci*, *117*(Pt 26), 6377-6389. https://doi.org/10.1242/jcs.01564

Kouzai, Y., Mochizuki, S., Nakajima, K., Desaki, Y., Hayafune, M., Miyazaki, H., Yokotani, N., Ozawa, K., Minami, E., Kaku, H., Shibuya, N., & Nishizawa, Y. (2014). Targeted Gene Disruption of OsCERK1 Reveals Its Indispensable Role in Chitin Perception and Involvement in the Peptidoglycan Response and Immunity in Rice. *Molecular Plant-Microbe Interactions®*, *27*(9), 975-982. https://doi.org/10.1094/mpmi-03-14-0068-r

Kovarvík, A., & Fojtová, M. (1999). Estimation of viable cell count after fluorescein diacetate staining using phosphorimager analysis. *Biotechniques*, *27*(4), 685-688.

Krishnakumar, V., Choi, Y., Beck, E., Wu, Q., Luo, A., Sylvester, A., Jackson, D., & Chan, A. P. (2015). A maize database resource that captures tissue-specific and subcellular-localized gene expression, via fluorescent tags and confocal imaging (Maize Cell Genomics Database). *Plant and Cell Physiology*, *56*(1), e12-e12.

Kroj, T., Chanclud, E., Michel-Romiti, C., Grand, X., & Morel, J. B. (2016). Integration of decoy domains derived from protein targets of pathogen effectors into plant immune receptors is widespread. *New Phytologist*, *210*(2), 618-626.

Kunihiro, Y., Ebe, Y., Wada, S., Shinbashi, N., Honma, A., Sasaki, T., Sasaki, K., Numao, Y., Morimura, K., & Tan-No, H. (1989). The new rice variety" Kita-ake".

Kurup, S., Runions, J., Kohler, U., Laplaze, L., Hodge, S., & Haseloff, J. (2005). Marking cell lineages in living tissues. *Plant J*, *42*(3), 444-453. https://doi.org/10.1111/j.1365-313X.2005.02386.x

Kwiatkowska, D., & Routier-Kierzkowska, A. (2008). New stereoscopic reconstruction protocol for scanning electron microscope images and its application to in vivo replicas of the shoot apical meristem. *Functional Plant Biology*(9-10).

Langner, T., Białas, A., & Kamoun, S. (2018). The blast fungus decoded: Genomes in flux. *MBio*, *9*(2), 10.1128/mbio. 00571-00518.

Lanzetti, L. (2007). Actin in membrane trafficking. *Current opinion in cell biology*, *19*(4), 453-458. https://doi.org/https://doi.org/10.1016/j.ceb.2007.04.017

Latorre, S. M., Were, V. M., Foster, A. J., Langner, T., Malmgren, A., Harant, A., Asuke, S., Reyes-Avila, S., Gupta, D. R., Jensen, C., Ma, W., Mahmud, N. U., Mehebub, M. S., Mulenga, R. M., Muzahid, A. N. M., Paul, S. K., Rabby, S. M. F., Rahat, A. A. M., Ryder, L.,…Kamoun, S. (2023). Genomic surveillance uncovers a pandemic clonal lineage of the wheat blast fungus. *PLOS Biology*, *21*(4), e3002052. https://doi.org/10.1371/journal.pbio.3002052

Lee, G.-J., Sohn, E. J., Lee, M. H., & Hwang, I. (2004). The Arabidopsis Rab5 Homologs Rha1 and Ara7 Localize to the Prevacuolar Compartment. *Plant and Cell Physiology*, *45*(9), 1211-1220. https://doi.org/10.1093/pcp/pch142

Lee, Y. J., Szumlanski, A., Nielsen, E., & Yang, Z. (2008). Rho-GTPase–dependent filamentous actin dynamics coordinate vesicle targeting and exocytosis during tip growth. *The Journal of cell biology*, *181*(7), 1155-1168.

Leontovyčová, Kalachova, T., Trdá, L., Pospíchalová, R., Lamparová, L., Dobrev, P. I., Malínská, K., Burketová, L., Valentová, O., & Janda, M. (2019). Actin depolymerization is able to increase plant resistance against pathogens via activation of salicylic acid signalling pathway. *Scientific Reports*, *9*(1), 10397. https://doi.org/10.1038/s41598-019-46465-5

Leontovyčová, H., Kalachova, T., & Janda, M. (2020). Disrupted actin: a novel player in pathogen attack sensing? *New Phytologist*, *227*(6), 1605-1609. https://doi.org/https://doi.org/10.1111/nph.16584

Leontovyčová, H., Kalachova, T., Trdá, L., Pospíchalová, R., Lamparová, L., Dobrev, P. I., Malínská, K., Burketová, L., Valentová, O., & Janda, M. (2019). Actin depolymerization is able to increase plant resistance against pathogens via activation of salicylic acid signalling pathway. *Scientific Reports*, *9*(1), 10397. https://doi.org/10.1038/s41598-019-46465-5

Li, G., Dulal, N., Gong, Z., & Wilson, R. A. (2023). Unconventional secretion of Magnaporthe oryzae effectors in rice cells is regulated by tRNA modification and codon usage control. *Nat Microbiol*, *8*(9), 1706-1716. https://doi.org/10.1038/s41564-023-01443-6

Li, G., Gong, Z., Dulal, N., Marroquin-Guzman, M., Rocha, R. O., Richter, M., & Wilson, R. A. (2023). A protein kinase coordinates cycles of autophagy and glutaminolysis in invasive hyphae of the fungus Magnaporthe oryzae within rice cells. *Nature Communications*, *14*(1), 4146. https://doi.org/10.1038/s41467-023-39880-w

Li, J., Henty-Ridilla, J. L., Staiger, B. H., Day, B., & Staiger, C. J. (2015). Capping protein integrates multiple MAMP signalling pathways to modulate actin dynamics during plant innate immunity. *Nature Communications*, *6*(1), 7206.

Li, J., & Staiger, C. J. (2018). Understanding Cytoskeletal Dynamics During the Plant Immune Response. *Annual Review of Phytopathology*, *56*(Volume 56, 2018), 513-533. https://doi.org/https://doi.org/10.1146/annurev-phyto-080516-035632

Li, W., Wang, B., Wu, J., Lu, G., Hu, Y., Zhang, X., Zhang, Z., Zhao, Q., Feng, Q., & Zhang, H. (2009). The Magnaporthe oryzae avirulence gene AvrPiz-t encodes a predicted secreted protein that triggers the immunity in rice mediated by the blast resistance gene Piz-t. *Molecular Plant-Microbe Interactions*, *22*(4), 411-420.

Li, Y., Yue, X., Que, Y., Yan, X., Ma, Z., Talbot, N. J., & Wang, Z. (2014). Characterisation of Four LIM Protein-Encoding Genes Involved in Infection-Related Development and Pathogenicity by the Rice Blast Fungus Magnaporthe oryzae. *PLOS ONE*, *9*(2), e88246. https://doi.org/10.1371/journal.pone.0088246

Li, Z., Velásquez-Zapata, V., Elmore, J. M., Li, X., Xie, W., Deb, S., Tian, X., Banerjee, S., Jørgensen, H. J. L., Pedersen, C., Wise, R. P., & Thordal-Christensen, H. (2024). Powdery mildew effectors AVR(A1) and BEC1016 target the ER J-domain protein HvERdj3B required for immunity in barley. *Mol Plant Pathol*, *25*(5), e13463. https://doi.org/10.1111/mpp.13463

Liu, Hu, X., Tu, Z., Sun, Z., Qin, P., Liu, Y., Chen, X., Li, Z., Jiang, N., & Yang, Y. (2024). The roles of Magnaporthe oryzae avirulence effectors involved in blast resistance/susceptibility [Review]. *Frontiers in Plant Science*, *15*. https://doi.org/10.3389/fpls.2024.1478159

Liu, Q., Long, R., Lin, C., Bi, X., Liang, Z., & Deng, Y. Z. (2024). Phosphatidylethanolamines link ferroptosis and autophagy during appressorium formation of rice blast fungus. *Molecular plant pathology*, *25*(7), e13489. https://doi.org/https://doi.org/10.1111/mpp.13489

Liu, W., Liu, J., Ning, Y., Ding, B., Wang, X., Wang, Z., & Wang, G.-L. (2013). Recent progress in understanding PAMP-and effector-triggered immunity against the rice blast fungus Magnaporthe oryzae. *Molecular Plant*, *6*(3), 605-620.

Liu, Z., Qiu, J., Shen, Z., Wang, C., Jiang, N., Shi, H., & Kou, Y. (2023). The E3 ubiquitin ligase OsRGLG5 targeted by the Magnaporthe oryzae effector AvrPi9 confers basal resistance against rice blast. *Plant Commun*, *4*(5), 100626. https://doi.org/10.1016/j.xplc.2023.100626

Lo Presti, L., & Kahmann, R. (2017). How filamentous plant pathogen effectors are translocated to host cells. *Current Opinion in Plant Biology*, *38*, 19-24. https://doi.org/https://doi.org/10.1016/j.pbi.2017.04.005

Lo Presti, L., Lanver, D., Schweizer, G., Tanaka, S., Liang, L., Tollot, M., Zuccaro, A., Reissmann, S., & Kahmann, R. (2015). Fungal effectors and plant susceptibility. *Annu Rev Plant Biol*, *66*, 513-545. https://doi.org/10.1146/annurev-arplant-043014-114623

Logan, D. C. (2006). Plant mitochondrial dynamics. *Biochim Biophys Acta*, *1763*(5-6), 430-441. https://doi.org/10.1016/j.bbamcr.2006.01.003

Logothetis, D. E., Petrou, V. I., Zhang, M., Mahajan, R., Meng, X. Y., Adney, S. K., Cui, M., & Baki, L. (2015). Phosphoinositide control of membrane protein function: a frontier led by studies on ion channels. *Annu Rev Physiol*, *77*, 81-104. https://doi.org/10.1146/annurev-physiol-021113-170358

Long, D. H., Lee, F. N., & TeBeest, D. O. (2000). Effect of Nitrogen Fertilization on Disease Progress of Rice Blast on Susceptible and Resistant Cultivars. *Plant Dis*, *84*(4), 403-409. https://doi.org/10.1094/pdis.2000.84.4.403

Lu, Y.-J., Schornack, S., Spallek, T., Geldner, N., Chory, J., Schellmann, S., Schumacher, K., Kamoun, S., & Robatzek, S. (2012). Patterns of plant subcellular responses to successful oomycete infections reveal differences in host cell reprogramming and endocytic trafficking. *Cellular microbiology*, *14*(5), 682-697. https://doi.org/https://doi.org/10.1111/j.1462-5822.2012.01751.x

Ludwig, N., Reissmann, S., Schipper, K., Gonzalez, C., Assmann, D., Glatter, T., Moretti, M., Ma, L.-S., Rexer, K.-H., Snetselaar, K., & Kahmann, R. (2021). A cell surface-exposed protein complex with an essential virulence function in Ustilago maydis. *Nature Microbiology*, *6*(6), 722-730. https://doi.org/10.1038/s41564-021-00896-x

Luo, B., & Nakata, P. A. (2012). A set of GFP organelle marker lines for intracellular localization studies in Medicago truncatula. *Plant Science*, *188*, 19-24.

Marroquin-Guzman, M., & Wilson, R. A. (2015). GATA-Dependent Glutaminolysis Drives Appressorium Formation in Magnaporthe oryzae by Suppressing TOR Inhibition of cAMP/PKA Signaling. *PLOS Pathogens*, *11*(4), e1004851. https://doi.org/10.1371/journal.ppat.1004851

Matei, A., & Doehlemann, G. (2016). Cell biology of corn smut disease—Ustilago maydis as a model for biotrophic interactions. *Current Opinion in Microbiology*, *34*, 60-66. https://doi.org/https://doi.org/10.1016/j.mib.2016.07.020

Matoušková, J., Janda, M., Fišer, R., Šašek, V., Kocourková, D., Burketová, L., Dušková, J., Martinec, J., & Valentová, O. (2014). Changes in actin dynamics are involved in salicylic acid signaling pathway. *Plant Science*, *223*, 36-44.

McCurdy, D. W., Kovar, D. R., & Staiger, C. J. (2001). Actin and actin-binding proteins in higher plants. *Protoplasma*, *215*(1-4), 89-104. https://doi.org/10.1007/bf01280306

Meng, X., Xiao, G., Telebanco-Yanoria, M., Siazon, P., Padilla, J., Opulencia, R., Bigirimana, J., Habarugira, G., Wu, J., & Li, M. (2020). The broad-spectrum rice blast resistance (R) gene Pita2 encodes a novel R protein unique from Pita. Rice 13, 19. In.

Mentlak, T. A., Kombrink, A., Shinya, T., Ryder, L. S., Otomo, I., Saitoh, H., Terauchi, R., Nishizawa, Y., Shibuya, N., Thomma, B. P. H. J., & Talbot, N. J. (2012). Effector-Mediated Suppression of Chitin-Triggered Immunity by Magnaporthe oryzae Is Necessary for Rice Blast Disease. *The Plant Cell*, *24*(1), 322-335. https://doi.org/10.1105/tpc.111.092957

Micali, C. O., Neumann, U., Grunewald, D., Panstruga, R., & O'Connell, R. (2011). Biogenesis of a specialized plant–fungal interface during host cell internalization of Golovinomyces orontii haustoria. *Cellular microbiology*, *13*(2), 210-226.

Michelot, A., Derivery, E., Paterski-Boujemaa, R., Guérin, C., Huang, S., Parcy, F., Staiger, C. J., & Blanchoin, L. (2006). A novel mechanism for the formation of actin-filament bundles by a nonprocessive formin. *Current Biology*, *16*(19), 1924-1930.

Miklis, M., Consonni, C., Bhat, R. A., Lipka, V., Schulze-Lefert, P., & Panstruga, R. (2007). Barley MLO modulates actin-dependent and actin-independent antifungal defense pathways at the cell periphery. *Plant Physiol*, *144*(2), 1132-1143. https://doi.org/10.1104/pp.107.098897

Mims, C. W., Richardson, E. A., III, B. F. H., & Dangl, J. L. (2004). Ultrastructure of the host□ pathogen interface in Arabidopsis thaliana leaves infected by the downy mildew Hyaloperonospora parasitica. *Canadian Journal of Botany*, *82*(7), 1001-1008. https://doi.org/10.1139/b04-073

Mochizuki, S., Minami, E., & Nishizawa, Y. (2015). Live-cell imaging of rice cytological changes reveals the importance of host vacuole maintenance for biotrophic invasion by blast fungus, Magnaporthe oryzae. *MicrobiologyOpen*, *4*(6), 952-966. https://doi.org/10.1002/mbo3.304

Mohanty, A., Luo, A., DeBlasio, S., Ling, X., Yang, Y., Tuthill, D. E., Williams, K. E., Hill, D., Zadrozny, T., Chan, A., Sylvester, A. W., & Jackson, D. (2009). Advancing cell biology and functional genomics in maize using fluorescent protein-tagged lines. *Plant Physiol*, *149*(2), 601-605. https://doi.org/10.1104/pp.108.130146

Mollier, C., Skrzydeł, J., Borowska-Wykręt, D., Majda, M., Bayle, V., Battu, V., Totozafy, J.-C., Dulski, M., Fruleux, A., Wrzalik, R., Mouille, G., Smith, R. S., Monéger, F., Kwiatkowska, D., & Boudaoud, A. (2023). Spatial consistency of cell growth direction during organ morphogenesis requires CELLULOSE SYNTHASE INTERACTIVE1. *Cell Reports*, *42*(7). https://doi.org/10.1016/j.celrep.2023.112689

Mooren, O. L., Galletta, B. J., & Cooper, J. A. (2012). Roles for actin assembly in endocytosis. *Annual review of biochemistry*, *81*(1), 661-686.

Mosquera, G., Giraldo, M. C., Khang, C. H., Coughlan, S., & Valent, B. (2009). Interaction transcriptome analysis identifies Magnaporthe oryzae BAS1-4 as Biotrophy-associated secreted proteins in rice blast disease. *Plant Cell*, *21*(4), 1273-1290. https://doi.org/10.1105/tpc.107.055228

Munro, S. (1995). An investigation of the role of transmembrane domains in Golgi protein retention. *The EMBO journal*, *14*(19), 4695.

Murray, F., Brettell, R., Matthews, P., Bishop, D., & Jacobsen, J. (2004). Comparison of Agrobacterium-mediated transformation of four barley cultivars using the GFP and GUS reporter genes. *Plant Cell Rep*, *22*(6), 397-402. https://doi.org/10.1007/s00299-003-0704-8

Mutiga, S. K., Rotich, F., Ganeshan, V. D., Mwongera, D. T., Mgonja, E. M., Were, V. M., Harvey, J. W., Zhou, B., Wasilwa, L., Feng, C., Ouédraogo, I., Wang, G. L., Mitchell, T. K., Talbot, N. J., & Correll, J. C. (2017). Assessment of the Virulence Spectrum and Its Association with Genetic Diversity in Magnaporthe oryzae

Populations from Sub-Saharan Africa. *Phytopathology*, *107*(7), 852-863. https://doi.org/10.1094/phyto-08-16-0319-r

Mutiga, S. K., Rotich, F., Were, V. M., Kimani, J. M., Mwongera, D. T., Mgonja, E., Onaga, G., Konaté, K., Razanaboahirana, C., Bigirimana, J., Ndayiragije, A., Gichuhi, E., Yanoria, M. J., Otipa, M., Wasilwa, L., Ouedraogo, I., Mitchell, T., Wang, G.-L., Correll, J. C., & Talbot, N. J. (2021). Integrated Strategies for Durable Rice Blast Resistance in Sub-Saharan Africa. *Plant Disease*, *105*(10), 2749-2770. https://doi.org/10.1094/PDIS-03-21-0593-FE

Nakayasu, T., Yokota, E., & Shimmen, T. (1998). Purification of an Actin-binding Protein Composed of 115-kDa Polypeptide from Pollen Tubes of Lily. *Biochemical and Biophysical Research Communications*, *249*(1), 61-65. https://doi.org/https://doi.org/10.1006/bbrc.1998.9088

Nalley, L., Tsiboe, F., Durand-Morat, A., Shew, A., & Thoma, G. (2016). Economic and Environmental Impact of Rice Blast Pathogen (Magnaporthe oryzae) Alleviation in the United States. *PLOS ONE*, *11*(12), e0167295. https://doi.org/10.1371/journal.pone.0167295

Narasimhan, M., Johnson, A., Prizak, R., Kaufmann, W. A., Tan, S., Casillas-Perez, B., & Friml, J. (2020). Evolutionarily unique mechanistic framework of clathrin-mediated endocytosis in plants. *eLife*, *9*, e52067.

Natonik-Białoń, S., Borowska-Wykręt, D., Mosca, G., Grelowski, M., Wrzalik, R., Smith, R. S., & Kwiatkowska, D. (2020). Deformation of a cell monolayer due to osmotic treatment: a case study of onion scale epidermis. *Botany*, *98*(1), 21-36. https://doi.org/10.1139/cjb-2019-0027

Nelson, B. K., Cai, X., & Nebenführ, A. (2007). A multicolored set of in vivo organelle markers for co-localization studies in Arabidopsis and other plants. *The Plant Journal*, *51*(6), 1126-1136. https://doi.org/https://doi.org/10.1111/j.1365-313X.2007.03212.x

Nielsen, M. L., Isbrandt, T., Petersen, L. M., Mortensen, U. H., Andersen, M. R., Hoof, J. B., & Larsen, T. O. (2016). Linker Flexibility Facilitates Module Exchange in Fungal Hybrid PKS-NRPS Engineering. *PLOS ONE*, *11*(8), e0161199. https://doi.org/10.1371/journal.pone.0161199

Noack, L. C., & Jaillais, Y. (2017). Precision targeting by phosphoinositides: how PIs direct endomembrane trafficking in plants. *Current Opinion in Plant Biology*, *40*, 22-33. https://doi.org/https://doi.org/10.1016/j.pbi.2017.06.017

Nürnberger, T., Brunner, F., Kemmerling, B., & Piater, L. (2004). Innate immunity in plants and animals: striking similarities and obvious differences. *Immunological reviews*, *198*(1), 249-266.

O'Connell, R. J., & Panstruga, R. (2006). Tête à tête inside a plant cell: establishing compatibility between plants and biotrophic fungi and oomycetes. *New Phytol*, *171*(4), 699-718. https://doi.org/10.1111/j.1469-8137.2006.01829.x

O'Connell, R. J., & Panstruga, R. (2006). Tête à tête inside a plant cell: establishing compatibility between plants and biotrophic fungi and oomycetes. *New Phytologist*, *171*(4), 699-718. https://doi.org/https://doi.org/10.1111/j.1469-8137.2006.01829.x

Oh, H., Tosa, Y., Takabayashi, N., Nakagawa, S., Tomita, R., Don, L., Kusaba, M., Nakayashiki, H., & Mayama, S. (2002). Characterization of an Avena isolate of Magnaporthe grisea and identification of a locus conditioning its specificity on oat. *Canadian Journal of Botany*, *80*(10), 1088-1095.

Oikawa, K., Fujisaki, K., Shimizu, M., Takeda, T., Nemoto, K., Saitoh, H., Hirabuchi, A., Hiraka, Y., Miyaji, N., & Białas, A. (2024). The blast pathogen effector AVR-Pik

binds and stabilizes rice heavy metal-associated (HMA) proteins to co-opt their function in immunity. *PLOS Pathogens*, *20*(11), e1012647.

Okuyama, Y., Kanzaki, H., Abe, A., Yoshida, K., Tamiru, M., Saitoh, H., Fujibe, T., Matsumura, H., Shenton, M., & Galam, D. C. (2011). A multifaceted genomics approach allows the isolation of the rice Pia-blast resistance gene consisting of two adjacent NBS-LRR protein genes. *The Plant Journal*, *66*(3), 467-479.

Oliveira-Garcia, E., & Hamilton, A. J. (2024). A pharmacological approach to investigating effector translocation in rice-Magnaporthe oryzae interactions. *Plant Signal Behav*, *19*(1), 2350869. https://doi.org/10.1080/15592324.2024.2350869

Oliveira-Garcia, E., Tamang, T. M., Park, J., Dalby, M., Martin-Urdiroz, M., Rodriguez Herrero, C., Vu, A. H., Park, S., Talbot, N. J., & Valent, B. (2023). Clathrin-mediated endocytosis facilitates the internalization of Magnaporthe oryzae effectors into rice cells. *The Plant Cell*, *35*(7), 2527-2551. https://doi.org/10.1093/plcell/koad094

Oliveira-Garcia, E., Yan, X., Oses-Ruiz, M., de Paula, S., & Talbot, N. J. (2024). Effector-triggered susceptibility by the rice blast fungus Magnaporthe oryzae. *New Phytologist*, *241*(3), 1007-1020. https://doi.org/https://doi.org/10.1111/nph.19446

Ollion, J., Cochennec, J., Loll, F., Escudé, C., & Boudier, T. (2013). TANGO: a generic tool for high-throughput 3D image analysis for studying nuclear organization. *Bioinformatics*, *29*(14), 1840-1841. https://doi.org/10.1093/bioinformatics/btt276

Opalski, Schultheiss, H., Kogel, K.-H., & Hückelhoven, R. (2005). The receptor-like MLO protein and the RAC/ROP family G-protein RACB modulate actin reorganization in barley attacked by the biotrophic powdery mildew fungus Blumeria graminis f.sp. hordei. *The Plant Journal*, *41*(2), 291-303. https://doi.org/https://doi.org/10.1111/j.1365-313X.2004.02292.x

Osés-Ruiz, M., Cruz-Mireles, N., Martin-Urdiroz, M., Soanes, D. M., Eseola, A. B., Tang, B., Derbyshire, P., Nielsen, M., Cheema, J., Were, V., Eisermann, I., Kershaw, M. J., Yan, X., Valdovinos-Ponce, G., Molinari, C., Littlejohn, G. R., Valent, B., Menke, F. L. H., & Talbot, N. J. (2021). Appressorium-mediated plant infection by Magnaporthe oryzae is regulated by a Pmk1-dependent hierarchical transcriptional network. *Nature Microbiology*, *6*(11), 1383-1397. https://doi.org/10.1038/s41564-021-00978-w

Ou, S. H. (1980). Pathogen Variability and Host Resistance in Rice Blast Disease. *Annual Review of Phytopathology*, *18*(1), 167-187. https://doi.org/10.1146/annurev.py.18.090180.001123

Ourselin, S., Joskowicz, L., Sabuncu, M. R., Unal, G., & Wells, W. (2016). *Medical Image Computing and Computer-Assisted Intervention–MICCAI 2016: 19th International Conference, Athens, Greece, October 17-21, 2016, Proceedings, Part II* (Vol. 9901). Springer.

Overdijk, E. J., De Keijzer, J., De Groot, D., Schoina, C., Bouwmeester, K., Ketelaar, T., & Govers, F. (2016). Interaction between the moss Physcomitrella patens and Phytophthora: a novel pathosystem for live-cell imaging of subcellular defence. *Journal of microscopy*, *263*(2), 171-180.

Park, C.-H., Chen, S., Shirsekar, G., Zhou, B., Khang, C. H., Songkumarn, P., Afzal, A. J., Ning, Y., Wang, R., Bellizzi, M., Valent, B., & Wang, G.-L. (2012a). The Magnaporthe oryzae Effector AvrPiz-t Targets the RING E3 Ubiquitin Ligase APIP6 to Suppress Pathogen-Associated Molecular Pattern–Triggered Immunity in Rice. *The Plant Cell*, *24*(11), 4748-4762. https://doi.org/10.1105/tpc.112.105429

Park, C.-H., Chen, S., Shirsekar, G., Zhou, B., Khang, C. H., Songkumarn, P., Afzal, A. J., Ning, Y., Wang, R., Bellizzi, M., Valent, B., & Wang, G.-L. (2012b). The Magnaporthe oryzae Effector AvrPiz-t Targets the RING E3 Ubiquitin Ligase APIP6 to Suppress Pathogen-Associated Molecular Pattern–Triggered Immunity in Rice *The Plant Cell*, *24*(11), 4748-4762. https://doi.org/10.1105/tpc.112.105429

Park, C. H., Shirsekar, G., Bellizzi, M., Chen, S., Songkumarn, P., Xie, X., Shi, X., Ning, Y., Zhou, B., Suttiviriya, P., Wang, M., Umemura, K., & Wang, G.-L. (2016). The E3 Ligase APIP10 Connects the Effector AvrPiz-t to the NLR Receptor Piz-t in Rice. *PLOS Pathogens*, *12*(3), e1005529. https://doi.org/10.1371/journal.ppat.1005529

Passmore, J. B., Nijenhuis, W., & Kapitein, L. C. (2021). From observing to controlling: Inducible control of organelle dynamics and interactions. *Current opinion in cell biology*, *71*, 69-76. https://doi.org/https://doi.org/10.1016/j.ceb.2021.02.002

Pedrozo, R., Osakina, A., Huang, Y., Nicolli, C. P., Wang, L., & Jia, Y. (2025). Status on Genetic Resistance to Rice Blast Disease in the Post-Genomic Era. *Plants*, *14*(5), 807. https://www.mdpi.com/2223-7747/14/5/807

Peng, Y.-L., & Shishiyama, J. (1988). Temporal sequence of cytological events in rice leaves infected with Pyricularia oryzae. *Canadian Journal of Botany*, *66*(4), 730-735.

Peng, Y.-L., & Shishiyama, J. (1989). Timing of a cellular reaction in rice cultivars associated with differing degrees of resistance to Pyricularia oryzae. *Canadian Journal of Botany*, *67*(9), 2704-2710.

Pennisi, E. (2010). Armed and Dangerous. *Science*, *327*(5967), 804-805. https://doi.org/10.1126/science.327.5967.804

Peremyslov, V. V., Cole, R. A., Fowler, J. E., & Dolja, V. V. (2015). Myosin-powered membrane compartment drives cytoplasmic streaming, cell expansion and plant development. *PLOS ONE*, *10*(10), e0139331.

Peremyslov, V. V., Prokhnevsky, A. I., & Dolja, V. V. (2010). Class XI myosins are required for development, cell expansion, and F-Actin organization in Arabidopsis. *The Plant Cell*, *22*(6), 1883-1897.

Perfect, S. E., & Green, J. R. (2001). Infection structures of biotrophic and hemibiotrophic fungal plant pathogens. *Molecular plant pathology*, *2*(2), 101-108. https://doi.org/https://doi.org/10.1046/j.1364-3703.2001.00055.x

Pollard, T. D. (2016). Actin and actin-binding proteins. *Cold Spring Harbor perspectives in biology*, *8*(8), a018226.

Pollard, T. D., Blanchoin, L., & Mullins, R. D. (2000). Molecular mechanisms controlling actin filament dynamics in nonmuscle cells. *Annual review of biophysics and biomolecular structure*, *29*(1), 545-576.

Pollard, T. D., & Borisy, G. G. (2003). Cellular motility driven by assembly and disassembly of actin filaments. *Cell*, *112*(4), 453-465.

Pollard, T. D., & Cooper, J. A. (1986). Actin and actin-binding proteins. A critical evaluation of mechanisms and functions. *Annual review of biochemistry*, *55*(1), 987-1035.

Pollard, T. D., & Cooper, J. A. (2009). Actin, a central player in cell shape and movement. *Science*, *326*(5957), 1208-1212.

Posor, Y., Jang, W., & Haucke, V. (2022). Phosphoinositides as membrane organizers. *Nature Reviews Molecular Cell Biology*, *23*(12), 797-816. https://doi.org/10.1038/s41580-022-00490-x

Prabhakaran, N., Kumar, A., Sheoran, N., Singh, V. K., & Nallathambi, P. (2021). Tracking and assessment of Puccinia graminis f. sp. tritici colonization on rice phyllosphere by integrated fluorescence imaging and qPCR for nonhost resistance

phenotyping. *Journal of Plant Diseases and Protection*, *128*(2), 457-469. https://doi.org/10.1007/s41348-020-00405-y

Prasher, D. C., Eckenrode, V. K., Ward, W. W., Prendergast, F. G., & Cormier, M. J. (1992). Primary structure of the Aequorea victoria green-fluorescent protein. *Gene*, *111*(2), 229-233. https://doi.org/10.1016/0378-1119(92)90691-h

Qin, L., Liu, L., Tu, J., Yang, G., Wang, S., Quilichini, T. D., Gao, P., Wang, H., Peng, G., Blancaflor, E. B., Datla, R., Xiang, D., Wilson, K. E., & Wei, Y. (2021). The ARP2/3 complex, acting cooperatively with Class I formins, modulates penetration resistance in Arabidopsis against powdery mildew invasion. *The Plant Cell*, *33*(9), 3151-3175. https://doi.org/10.1093/plcell/koab170

Qin, L., Zhou, Z., Li, Q., Zhai, C., Liu, L., Quilichini, T. D., Gao, P., Kessler, S. A., Jaillais, Y., Datla, R., Peng, G., Xiang, D., & Wei, Y. (2020). Specific Recruitment of Phosphoinositide Species to the Plant-Pathogen Interfacial Membrane Underlies Arabidopsis Susceptibility to Fungal Infection[OPEN]. *The Plant Cell*, *32*(5), 1665-1688. https://doi.org/10.1105/tpc.19.00970

Qiu, H., Zhao, X., Fang, W., Wu, H., Abubakar, Y. S., Lu, G.-d., Wang, Z., & Zheng, W. (2019). Spatiotemporal nature of Fusarium graminearum-wheat coleoptile interactions. *Phytopathology Research*, *1*(1), 26. https://doi.org/10.1186/s42483-019-0033-7

Rasheed, R., Ashraf, M. A., Iqbal, M., Hussain, I., Akbar, A., Farooq, U., & Shad, M. I. (2020). Major Constraints for Global Rice Production: Changing Climate, Abiotic and Biotic Stresses. In A. Roychoudhury (Ed.), *Rice Research for Quality Improvement: Genomics and Genetic Engineering: Volume 1: Breeding Techniques and Abiotic Stress Tolerance* (pp. 15-45). Springer Singapore. https://doi.org/10.1007/978-981-15-4120-9_2

Ray, S., Singh, P. K., Gupta, D. K., Mahato, A. K., Sarkar, C., Rathour, R., Singh, N. K., & Sharma, T. R. (2016). Analysis of Magnaporthe oryzae Genome Reveals a Fungal Effector, Which Is Able to Induce Resistance Response in Transgenic Rice Line Containing Resistance Gene, Pi54 [Original Research]. *Frontiers in Plant Science*, *7*. https://doi.org/10.3389/fpls.2016.01140

Redkar, A., Di Pietro, A., & Turrà, D. (2023). Live-cell visualization of early stages of root colonization by the vascular wilt pathogen Fusarium oxysporum. In *Plant-Pathogen Interactions* (pp. 73-82). Springer.

Ren, H., & Xiang, Y. (2007). The function of actin-binding proteins in pollen tube growth. *Protoplasma*, *230*, 171-182.

Reumann, S. (2004). Specification of the Peroxisome Targeting Signals Type 1 and Type 2 of Plant Peroxisomes by Bioinformatics Analyses *Plant Physiology*, *135*(2), 783-800. https://doi.org/10.1104/pp.103.035584

Ribot, C., Césari, S., Abidi, I., Chalvon, V., Bournaud, C., Vallet, J., Lebrun, M. H., Morel, J. B., & Kroj, T. (2013). The Magnaporthe oryzae effector AVR1-CO39 is translocated into rice cells independently of a fungal-derived machinery. *Plant J*, *74*(1), 1-12. https://doi.org/10.1111/tpj.12099

Riedl, J., Crevenna, A. H., Kessenbrock, K., Yu, J. H., Neukirchen, D., Bista, M., Bradke, F., Jenne, D., Holak, T. A., Werb, Z., Sixt, M., & Wedlich-Soldner, R. (2008). Lifeact: a versatile marker to visualize F-actin. *Nat Methods*, *5*(7), 605-607. https://doi.org/10.1038/nmeth.1220

Robertson, A. S., Smythe, E., & Ayscough, K. R. (2009). Functions of actin in endocytosis. *Cellular and Molecular Life Sciences*, *66*, 2049-2065.

Ryder, L. S., Lopez, S. G., Michels, L., Eseola, A. B., Sprakel, J., Ma, W., & Talbot, N. J. (2023). A molecular mechanosensor for real-time visualization of appressorium

membrane tension in Magnaporthe oryzae. *Nature Microbiology*, *8*(8), 1508-1519. https://doi.org/10.1038/s41564-023-01430-x

Ryder, L. S., & Talbot, N. J. (2015). Regulation of appressorium development in pathogenic fungi. *Curr Opin Plant Biol*, *26*, 8-13. https://doi.org/10.1016/j.pbi.2015.05.013

Saint-Jore, C. M., Evins, J., Batoko, H., Brandizzi, F., Moore, I., & Hawes, C. (2002). Redistribution of membrane proteins between the Golgi apparatus and endoplasmic reticulum in plants is reversible and not dependent on cytoskeletal networks. *Plant J*, *29*(5), 661-678. https://doi.org/10.1046/j.0960-7412.2002.01252.x

Sakamoto, M. (1949). On the new method of sheath-inoculation of rice plants with blast fungus, Pyricularia oryzae Cav. for the study of the disease-resistant nature of the plant. *Bull. Inst. Agr. Res. Tohoku Univ. Jpn*, *1*, 120-129.

Sakulkoo, W., Osés-Ruiz, M., Oliveira Garcia, E., Soanes, D. M., Littlejohn, G. R., Hacker, C., Correia, A., Valent, B., & Talbot, N. J. (2018). A single fungal MAP kinase controls plant cell-to-cell invasion by the rice blast fungus. *Science*, *359*(6382), 1399-1403. https://doi.org/10.1126/science.aaq0892

Šamaj, J., Müller, J., Beck, M., Böhm, N., & Menzel, D. (2006). Vesicular trafficking, cytoskeleton and signalling in root hairs and pollen tubes. *Trends in Plant Science*, *11*(12), 594-600. https://doi.org/https://doi.org/10.1016/j.tplants.2006.10.002

Saruyama, N., Sakakura, Y., Asano, T., Nishiuchi, T., Sasamoto, H., & Kodama, H. (2013). Quantification of metabolic activity of cultured plant cells by vital staining with fluorescein diacetate. *Anal Biochem*, *441*(1), 58-62. https://doi.org/10.1016/j.ab.2013.06.005

Saunders, D. G., Dagdas, Y. F., & Talbot, N. J. (2010). Spatial uncoupling of mitosis and cytokinesis during appressorium-mediated plant infection by the rice blast fungus Magnaporthe oryzae. *Plant Cell*, *22*(7), 2417-2428. https://doi.org/10.1105/tpc.110.074492

Savary, S., Willocquet, L., Pethybridge, S. J., Esker, P., McRoberts, N., & Nelson, A. (2019). The global burden of pathogens and pests on major food crops. *Nature Ecology & Evolution*, *3*(3), 430-439. https://doi.org/10.1038/s41559-018-0793-y

Schindelin, J., Arganda-Carreras, I., Frise, E., Kaynig, V., Longair, M., Pietzsch, T., Preibisch, S., Rueden, C., Saalfeld, S., Schmid, B., Tinevez, J.-Y., White, D. J., Hartenstein, V., Eliceiri, K., Tomancak, P., & Cardona, A. (2012). Fiji: an open-source platform for biological-image analysis. *Nature Methods*, *9*(7), 676-682. https://doi.org/10.1038/nmeth.2019

Schmidt, S. M., & Panstruga, R. (2007). Cytoskeleton functions in plant–microbe interactions. *Physiological and Molecular Plant Pathology*, *71*(4-6), 135-148.

Schreiber, M., Mascher, M., Wright, J., Padmarasu, S., Himmelbach, A., Heavens, D., Milne, L., Clavijo, B. J., Stein, N., & Waugh, R. (2020). A Genome Assembly of the Barley 'Transformation Reference' Cultivar Golden Promise. *G3 Genes|Genomes|Genetics*, *10*(6), 1823-1827. https://doi.org/10.1534/g3.119.401010

Sedwick, C. (2011). How Actin Filaments Doff Their Pi Cap. *PLOS Biology*, *9*(9), e1001163. https://doi.org/10.1371/journal.pbio.1001163

Selisana, S. M., Yanoria, M. J., Quime, B., Chaipanya, C., Lu, G., Opulencia, R., Wang, G. L., Mitchell, T., Correll, J., Talbot, N. J., Leung, H., & Zhou, B. (2017). Avirulence (AVR) Gene-Based Diagnosis Complements Existing Pathogen Surveillance Tools for Effective Deployment of Resistance (R) Genes Against Rice Blast Disease. *Phytopathology*, *107*(6), 711-720. https://doi.org/10.1094/phyto-12-16-0451-r

Shafaullah, M. A. K., Khan, N. A., & Mahmood, Y. (2011). Effect of epidemiological factors on the incidence of paddy blast (Pyricularia oryzae) disease. *Pakistan Journal of Phytopathology*, *23*(2), 108-111.

Shan, X., & Goodwin, P. (2005). Reorganization of filamentous actin in Nicotiana benthamiana leaf epidermal cells inoculated with Colletotrichum destructivum and Colletotrichum graminicola. *International Journal of Plant Sciences*, *166*(1), 31-39.

Shaner, N. C., Campbell, R. E., Steinbach, P. A., Giepmans, B. N. G., Palmer, A. E., & Tsien, R. Y. (2004). Improved monomeric red, orange and yellow fluorescent proteins derived from Discosoma sp. red fluorescent protein. *Nature Biotechnology*, *22*(12), 1567-1572. https://doi.org/10.1038/nbt1037

Sharma, T. R., Rai, A. K., Gupta, S. K., Vijayan, J., Devanna, B. N., & Ray, S. (2012). Rice Blast Management Through Host-Plant Resistance: Retrospect and Prospects. *Agricultural Research*, *1*(1), 37-52. https://doi.org/10.1007/s40003-011-0003-5

Shekhar, S., Kerleau, M., Kühn, S., Pernier, J., Romet-Lemonne, G., Jégou, A., & Carlier, M.-F. (2015). Formin and capping protein together embrace the actin filament in a ménage à trois. *Nature Communications*, *6*(1), 8730.

Shekhar, S., Pernier, J., & Carlier, M.-F. (2016). Regulators of actin filament barbed ends at a glance. *Journal of Cell Science*, *129*(6), 1085-1091.

Shen, Q., Liang, M., Yang, F., Deng, Y. Z., & Naqvi, N. I. (2020). Ferroptosis contributes to developmental cell death in rice blast. *New Phytologist*, *227*(6), 1831-1846.

Shi, Xuetao, Long, Y., He, F., Zhang, C., Wang, R., Zhang, T., Wu, W., Hao, Z., Wang, Y., & Wang, G.-L. (2018). The fungal pathogen Magnaporthe oryzae suppresses innate immunity by modulating a host potassium channel. *PLOS Pathogens*, *14*(1), e1006878.

Shi, X., Long, Y., He, F., Zhang, C., Wang, R., Zhang, T., Wu, W., Hao, Z., Wang, Y., Wang, G.-L., & Ning, Y. (2018). The fungal pathogen Magnaporthe oryzae suppresses innate immunity by modulating a host potassium channel. *PLOS Pathogens*, *14*(1), e1006878. https://doi.org/10.1371/journal.ppat.1006878

Shi, X., Xiong, Y., Zhang, K., Zhang, Y., Zhang, J., Zhang, L., Xiao, Y., Wang, G. L., & Liu, W. (2023). The ANIP1-OsWRKY62 module regulates both basal defense and Pi9-mediated immunity against Magnaporthe oryzae in rice. *Mol Plant*, *16*(4), 739-755. https://doi.org/10.1016/j.molp.2023.03.001

Shimada, C., Lipka, V., O'Connell, R., Okuno, T., Schulze-Lefert, P., & Takano, Y. (2006). Nonhost Resistance in Arabidopsis-Colletotrichum Interactions Acts at the Cell Periphery and Requires Actin Filament Function. *Molecular Plant-Microbe Interactions®*, *19*(3), 270-279. https://doi.org/10.1094/mpmi-19-0270

Shimada, T. L., Betsuyaku, S., Inada, N., Ebine, K., Fujimoto, M., Uemura, T., Takano, Y., Fukuda, H., Nakano, A., & Ueda, T. (2019). Enrichment of Phosphatidylinositol 4,5-Bisphosphate in the Extra-Invasive Hyphal Membrane Promotes Colletotrichum Infection of Arabidopsis thaliana. *Plant and Cell Physiology*, *60*(7), 1514-1524. https://doi.org/10.1093/pcp/pcz058

Shimizu, M., Hirabuchi, A., Sugihara, Y., Abe, A., Takeda, T., Kobayashi, M., Hiraka, Y., Kanzaki, E., Oikawa, K., & Saitoh, H. (2022). A genetically linked pair of NLR immune receptors shows contrasting patterns of evolution. *Proceedings of the National Academy of Sciences*, *119*(27), e2116896119.

Shimizu, T., Nakano, T., Takamizawa, D., Desaki, Y., Ishii-Minami, N., Nishizawa, Y., Minami, E., Okada, K., Yamane, H., & Kaku, H. (2010). Two LysM receptor molecules, CEBiP and OsCERK1, cooperatively regulate chitin elicitor signaling in rice. *The Plant Journal*, *64*(2), 204-214.

Shimono, M., Lu, Y.-J., Porter, K., Kvitko, B. H., Henty-Ridilla, J., Creason, A., He, S. Y., Chang, J. H., Staiger, C. J., & Day, B. (2016). The Pseudomonas syringae type

III effector HopG1 induces actin remodeling to promote symptom development and susceptibility during infection. *Plant Physiology*, *171*(3), 2239-2255.

Silveira, S. R., Le Gloanec, C., Gómez-Felipe, A., Routier-Kierzkowska, A.-L., & Kierzkowski, D. (2021). Live-imaging provides an atlas of cellular growth dynamics in the stamen. *Plant Physiology*, *188*(2), 769-781. https://doi.org/10.1093/plphys/kiab363

Singh, R., Dangol, S., Chen, Y., Choi, J., Cho, Y.-S., Lee, J.-E., Choi, M.-O., & Jwa, N.-S. (2016). Magnaporthe oryzae Effector AVR-Pii Helps to Establish Compatibility by Inhibition of the Rice NADP-Malic Enzyme Resulting in Disruption of Oxidative Burst and Host Innate Immunity. *Molecules and Cells*, *39*(5), 426-438. https://doi.org/https://doi.org/10.14348/molcells.2016.0094

Skamnioti, P., & Gurr, S. J. (2009). Against the grain: safeguarding rice from rice blast disease. *Trends in Biotechnology*, *27*(3), 141-150. https://doi.org/https://doi.org/10.1016/j.tibtech.2008.12.002

Skruzny, M. (2022). The endocytic protein machinery as an actin-driven membrane-remodeling machine. *European Journal of Cell Biology*, *101*(4), 151267. https://doi.org/https://doi.org/10.1016/j.ejcb.2022.151267

Sleat, D. E., Gallic, D. R., Jefferson, R. A., Bevan, M. W., Turner, P. C., & Wilson, T. M. A. (1987). Characterisation of the 5'-leader sequence of tobacco mosaic virus RNA as a general enhancer of translation in vitro. *Gene*, *60*(2-3), 217-225.

Sleat, D. E., Hull, R., Turner, P. C., & Wilson, T. M. A. (1988). Studies on the mechanism of translational enhancement by the 5'-leader sequence of tobacco mosaic virus RNA. *European journal of biochemistry*, *175*(1), 75-86.

Smertenko, A. P., Deeks, M. J., & Hussey, P. J. (2010). Strategies of actin reorganisation in plant cells. *J Cell Sci*, *123*(Pt 17), 3019-3028. https://doi.org/10.1242/jcs.071126

Smith, S. J., Davidson, L. A., & Rebeiz, M. (2020). Evolutionary expansion of apical extracellular matrix is required for the elongation of cells in a novel structure. *eLife*, *9*, e55965. https://doi.org/10.7554/eLife.55965

Sohn, E. J., Kim, E. S., Zhao, M., Kim, S. J., Kim, H., Kim, Y.-W., Lee, Y. J., Hillmer, S., Sohn, U., & Jiang, L. (2003). Rha1, an Arabidopsis Rab5 homolog, plays a critical role in the vacuolar trafficking of soluble cargo proteins. *The Plant Cell*, *15*(5), 1057-1070.

Song, Z., Bakeer, W., Marshall, J. W., Yakasai, A. A., Khalid, R. M., Collemare, J., Skellam, E., Tharreau, D., Lebrun, M.-H., Lazarus, C. M., Bailey, A. M., Simpson, T. J., & Cox, R. J. (2015). Heterologous expression of the avirulence gene ACE1 from the fungal rice pathogen Magnaporthe oryzae [10.1039/C4SC03707C]. *Chemical Science*, *6*(8), 4837-4845. https://doi.org/10.1039/C4SC03707C

Sørensen, C. K., F., J. A., & and Hovmøller, M. S. (2012). 3-D imaging of temporal and spatial development of Puccinia striiformis haustoria in wheat. *Mycologia*, *104*(6), 1381-1389. https://doi.org/10.3852/11-401

Sornkom, W., Miki, S., Takeuchi, S., Abe, A., Asano, K., & Sone, T. (2017). Fluorescent reporter analysis revealed the timing and localization of AVR-Pia expression, an avirulence effector of Magnaporthe oryzae. *Mol Plant Pathol*, *18*(8), 1138-1149. https://doi.org/10.1111/mpp.12468

Sparkes, I. (2011). Recent Advances in Understanding Plant Myosin Function: Life in the Fast Lane. *Molecular Plant*, *4*(5), 805-812. https://doi.org/10.1093/mp/ssr063

Stellmach, H., Hose, R., Räde, A., Marillonnet, S., & Hause, B. (2022). A New Set of Golden-Gate-Based Organelle Marker Plasmids for Colocalization Studies in Plants. *Plants*, *11*(19), 2620. https://www.mdpi.com/2223-7747/11/19/2620

Steward, N., Martin, R., Engasser, J., & Goergen, J. (1999). A new methodology for plant cell viability assessment using intracellular esterase activity. *Plant Cell Reports*, *19*(2), 171-176.

Stradal, T. E. B., & Schelhaas, M. (2018). Actin dynamics in host–pathogen interaction. *FEBS Letters*, *592*(22), 3658-3669. https://doi.org/https://doi.org/10.1002/1873-3468.13173

Strauss, S., Runions, A., Lane, B., Eschweiler, D., Bajpai, N., Trozzi, N., Routier-Kierzkowska, A.-L., Yoshida, S., Rodrigues da Silveira, S., Vijayan, A., Tofanelli, R., Majda, M., Echevin, E., Le Gloanec, C., Bertrand-Rakusova, H., Adibi, M., Schneitz, K., Bassel, G. W., Kierzkowski, D.,…Smith, R. S. (2022). Using positional information to provide context for biological image analysis with MorphoGraphX 2.0. *eLife*, *11*, e72601. https://doi.org/10.7554/eLife.72601

Suarez, C., Roland, J., Boujemaa-Paterski, R., Kang, H., McCullough, Brannon R., Reymann, A.-C., Guérin, C., Martiel, J.-L., De La Cruz, E. M., & Blanchoin, L. (2011). Cofilin Tunes the Nucleotide State of Actin Filaments and Severs at Bare and Decorated Segment Boundaries. *Current Biology*, *21*(10), 904. https://doi.org/10.1016/j.cub.2011.05.019

Sun, T., Li, S., & Ren, H. (2013). Profilin as a regulator of the membrane-actin cytoskeleton interface in plant cells [Mini Review]. *Frontiers in Plant Science*, *4*. https://doi.org/10.3389/fpls.2013.00512

Sweigard, J. A., Carroll, A. M., Kang, S., Farrall, L., Chumley, F. G., & Valent, B. (1995). Identification, cloning, and characterization of PWL2, a gene for host species specificity in the rice blast fungus. *The Plant Cell*, *7*(8), 1221-1233. https://doi.org/10.1105/tpc.7.8.1221

Synek, L., Sekereš, J., & Žárský, V. (2014). The exocyst at the interface between cytoskeleton and membranes in eukaryotic cells. *Frontiers in Plant Science*, *4*, 543.

Szymanski, D., & Staiger, C. J. (2018). The Actin Cytoskeleton: Functional Arrays for Cytoplasmic Organization and Cell Shape Control. *Plant Physiol*, *176*(1), 106-118. https://doi.org/10.1104/pp.17.01519

Takai, R., Matsuda, N., Nakano, A., Hasegawa, K., Akimoto, C., Shibuya, N., & Minami, E. (2002). EL5, a rice N-acetylchitooligosaccharide elicitor-responsive RING-H2 finger protein, is a ubiquitin ligase which functions in vitro in co-operation with an elicitor-responsive ubiquitin-conjugating enzyme, OsUBC5b. *The Plant Journal*, *30*(4), 447-455.

Takamatsu, N., Watanabe, Y., Iwasaki, T., Shiba, T., Meshi, T., & Okada, Y. (1991). Deletion analysis of the 5'untranslated leader sequence of tobacco mosaic virus RNA. *Journal of virology*, *65*(3), 1619-1622.

Takemoto, D., & Hardham, A. R. (2004). The Cytoskeleton as a Regulator and Target of Biotic Interactions in Plants. *Plant Physiology*, *136*(4), 3864-3876. https://doi.org/10.1104/pp.104.052159

Takemoto, D., Jones, D. A., & Hardham, A. R. (2003). GFP-tagging of cell components reveals the dynamics of subcellular re-organization in response to infection of Arabidopsis by oomycete pathogens. *The Plant Journal*, *33*(4), 775-792.

Takken, F. L., & Goverse, A. (2012). How to build a pathogen detector: structural basis of NB-LRR function. *Current Opinion in Plant Biology*, *15*(4), 375-384.

Talbot, N. J. (2003). On the trail of a cereal killer: Exploring the biology of Magnaporthe grisea. *Annu Rev Microbiol*, *57*, 177-202. https://doi.org/10.1146/annurev.micro.57.030502.090957

Tang, M, Ning, Y., Shu, X., Dong, B., Zhang, H., Wu, D., Wang, H., Wang, G., & Zhou, B. (2017). The Nup98 homolog APIP12 targeted by the effector AvrPiz-t is involved in rice basal resistance against Magnaporthe oryzae. Rice 10: 5. In.

Tang, B., Yan, X., Ryder, L. S., Bautista, M. J. A., Cruz-Mireles, N., Soanes, D. M., Molinari, C., Foster, A. J., & Talbot, N. J. (2023). Rgs1 is a regulator of effector gene expression during plant infection by the rice blast fungus Magnaporthe oryzae. *Proceedings of the National Academy of Sciences*, *120*(12), e2301358120. https://doi.org/doi:10.1073/pnas.2301358120

Tang, M., Ning, Y., Shu, X., Dong, B., Zhang, H., Wu, D., Wang, H., Wang, G.-L., & Zhou, B. (2017). The Nup98 Homolog APIP12 Targeted by the Effector AvrPiz-t is Involved in Rice Basal Resistance Against Magnaporthe oryzae. *Rice*, *10*(1), 5. https://doi.org/10.1186/s12284-017-0144-7

Tasker-Brown, W., Koh, S. W. H., Trozzi, N., Maio, K. A., Jamil, I., Jiang, Y., Majda, M., Smith, R. S., & Moubayidin, L. (2024). An incoherent feed-forward loop involving bHLH transcription factors, Auxin and CYCLIN-Ds regulates style radial symmetry establishment in Arabidopsis. *The Plant Journal*, *119*(6), 2885-2903. https://doi.org/https://doi.org/10.1111/tpj.16959

Thomas, C., Hoffmann, C., Dieterle, M., Van Troys, M., Ampe, C., & Steinmetz, A. (2006). Tobacco WLIM1 is a novel F-actin binding protein involved in actin cytoskeleton remodeling. *The Plant Cell*, *18*(9), 2194-2206.

Thomas, C., Tholl, S., Moes, D., Dieterle, M., Papuga, J., Moreau, F., & Steinmetz, A. (2009). Actin bundling in plants. *Cell motility and the cytoskeleton*, *66*(11), 940-957.

Tosa, Y., Hirata, K., Tamba, H., Nakagawa, S., Chuma, I., Isobe, C., Osue, J., Urashima, A., Don, L., & Kusaba, M. (2004). Genetic constitution and pathogenicity of Lolium isolates of Magnaporthe oryzae in comparison with host species-specific pathotypes of the blast fungus. *Phytopathology*, *94*(5), 454-462.

Ueda, T., Yamaguchi, M., Uchimiya, H., & Nakano, A. (2001). Ara6, a plant-unique novel type Rab GTPase, functions in the endocytic pathway of Arabidopsis thaliana. *Embo j*, *20*(17), 4730-4741. https://doi.org/10.1093/emboj/20.17.4730

Ulbrich, M., Seward, C. H., Ivanov, A. I., Ward, B. M., Butler, J. S., & Dziejman, M. (2025). VopX, a novel Vibrio cholerae T3SS effector, modulates host actin dynamics. *MBio*, *16*(3), e03018-03024. https://doi.org/doi:10.1128/mbio.03018-24

Underwood, W., Koh, S., & Somerville, S. C. (2011). Visualizing cellular dynamics in plant–microbe interactions using fluorescent-tagged proteins. *Plant Immunity: Methods and Protocols*, 283-291.

Underwood, W., & Somerville, S. C. (2008). Focal accumulation of defences at sites of fungal pathogen attack. *Journal of Experimental Botany*, *59*(13), 3501-3508.

Valent, B., & Chumley, F. G. (1991). Molecular genetic analysis of the rice blast fungus, magnaporthe grisea.

van der Hoorn, R. A., & Kamoun, S. (2008). From guard to decoy: a new model for perception of plant pathogen effectors. *The Plant Cell*, *20*(8), 2009-2017.

Veneault-Fourrey, C., Barooah, M., Egan, M., Wakley, G., & Talbot, N. J. (2006). Autophagic Fungal Cell Death Is Necessary for Infection by the Rice Blast Fungus. *Science*, *312*(5773), 580-583. https://doi.org/doi:10.1126/science.1124550

Verchot-Lubicz, J., & Goldstein, R. E. (2010). Cytoplasmic streaming enables the distribution of molecules and vesicles in large plant cells. *Protoplasma*, *240*(1), 99-107. https://doi.org/10.1007/s00709-009-0088-x

Vidali, L., Rounds, C. M., Hepler, P. K., & Bezanilla, M. (2009). Lifeact-mEGFP reveals a dynamic apical F-actin network in tip growing plant cells. *PLOS ONE*, *4*(5), e5744.

Vijayan, A., Tofanelli, R., Strauss, S., Cerrone, L., Wolny, A., Strohmeier, J., Kreshuk, A., Hamprecht, F. A., Smith, R. S., & Schneitz, K. (2021). A digital 3D reference atlas

reveals cellular growth patterns shaping the Arabidopsis ovule. *eLife*, *10*, e63262. https://doi.org/10.7554/eLife.63262

Wada, M., & Kong, S.-G. (2018). Actin-mediated movement of chloroplasts. *Journal of Cell Science*, *131*(2). https://doi.org/10.1242/jcs.210310

Wang, Ruyi, Ning, Y., Shi, X., He, F., Zhang, C., Fan, J., Jiang, N., Zhang, Y., Zhang, T., Hu, Y., Bellizzi, M., & Wang, G.-L. (2016). Immunity to Rice Blast Disease by Suppression of Effector-Triggered Necrosis. *Current Biology*, *26*(18), 2399-2411. https://doi.org/https://doi.org/10.1016/j.cub.2016.06.072

Wang, H., Wang, S., Wang, W., Xu, L., Welsh, L. R. J., Gierlinski, M., Whisson, S. C., Hemsley, P. A., Boevink, P. C., & Birch, P. R. J. (2023). Uptake of oomycete RXLR effectors into host cells by clathrin-mediated endocytosis. *The Plant Cell*, *35*(7), 2504-2526. https://doi.org/10.1093/plcell/koad069

Wang, H., Zhuang, X., Wang, X., Law, A. H. Y., Zhao, T., Du, S., Loy, M. M., & Jiang, L. (2016). A distinct pathway for polar exocytosis in plant cell wall formation. *Plant Physiology*, *172*(2), 1003-1018.

Wang, H.-J., Wan, A.-R., & Jauh, G.-Y. (2008). An actin-binding protein, LlLIM1, mediates calcium and hydrogen regulation of actin dynamics in pollen tubes. *Plant Physiology*, *147*(4), 1619-1636.

Wang, P., & Hussey, P. J. (2015). Interactions between plant endomembrane systems and the actin cytoskeleton. *Frontiers in Plant Science*, *6*, 422.

Wang, R., Ning, Y., Shi, X., He, F., Zhang, C., Fan, J., Jiang, N., Zhang, Y., Zhang, T., Hu, Y., Bellizzi, M., & Wang, G.-L. (2016). Immunity to Rice Blast Disease by Suppression of Effector-Triggered Necrosis. *Current Biology*, *26*(18), 2399-2411. https://doi.org/https://doi.org/10.1016/j.cub.2016.06.072

Wang, S., Boevink, P. C., Welsh, L., Zhang, R., Whisson, S. C., & Birch, P. R. J. (2017). Delivery of cytoplasmic and apoplastic effectors from Phytophthora infestans haustoria by distinct secretion pathways. *New Phytologist*, *216*(1), 205-215. https://doi.org/https://doi.org/10.1111/nph.14696

Were, V., Yan, X., Foster, A. J., Sklenar, J., Langner, T., Gentle, A., Sahu, N., Bentham, A., Zdrzalek, R., Ryder, L., Kaimenyi, D., Gomez De La Cruz, D., Petit-Houdenot, Y., Eseola, A. B., Smoker, M., Bautista, M. J., Ma, W., Kourelis, J., Maclean, D.,…Talbot, N. J. (2025). The blast effector Pwl2 is a virulence factor that modifies the cellular localisation of host protein HIPP43 to suppress immunity. *bioRxiv*, 2024.2001.2020.576406. https://doi.org/10.1101/2024.01.20.576406

Wilson, R. A., & Talbot, N. J. (2009). Under pressure: investigating the biology of plant infection by Magnaporthe oryzae. *Nat Rev Microbiol*, *7*(3), 185-195. https://doi.org/10.1038/nrmicro2032

Wioland, H., Guichard, B., Senju, Y., Myram, S., Lappalainen, P., Jégou, A., & Romet-Lemonne, G. (2017). ADF/Cofilin Accelerates Actin Dynamics by Severing Filaments and Promoting Their Depolymerization at Both Ends. *Current Biology*, *27*(13), 1956-1967.e1957. https://doi.org/https://doi.org/10.1016/j.cub.2017.05.048

Wolfe, J., & Steponkus, P. L. (1983). Mechanical Properties of the Plasma Membrane of Isolated Plant Protoplasts 1: Mechanism of Hyperosmotic and Extracellular Freezing Injury. *Plant Physiology*, *71*(2), 276-285. https://doi.org/10.1104/pp.71.2.276

Wolny, A., Cerrone, L., Vijayan, A., Tofanelli, R., Barro, A. V., Louveaux, M., Wenzl, C., Strauss, S., Wilson-Sánchez, D., & Lymbouridou, R. (2020). Accurate and versatile 3D segmentation of plant tissues at cellular resolution. *eLife*, *9*, e57613.

Wu, J., Kou, Y., Bao, J., Li, Y., Tang, M., Zhu, X., Ponaya, A., Xiao, G., Li, J., Li, C., Song, M. Y., Cumagun, C. J., Deng, Q., Lu, G., Jeon, J. S., Naqvi, N. I., & Zhou, B. (2015). Comparative genomics identifies the Magnaporthe oryzae avirulence effector AvrPi9 that triggers Pi9-mediated blast resistance in rice. *New Phytol*, *206*(4), 1463-1475. https://doi.org/10.1111/nph.13310

Wu, Q., Luo, A., Zadrozny, T., Sylvester, A., & Jackson, D. (2013). Fluorescent protein marker lines in maize: generation and applications. *The International Journal of Developmental Biology*, *57*(6-7-8), 535-543. https://doi.org/10.1387/ijdb.130240qw

Wu, T.-M., Lin, K.-C., Liau, W.-S., Chao, Y.-Y., Yang, L.-H., Chen, S.-Y., Lu, C.-A., & Hong, C.-Y. (2016). A set of GFP-based organelle marker lines combined with DsRed-based gateway vectors for subcellular localization study in rice (Oryza sativa L.). *Plant Molecular Biology*, *90*(1), 107-115. https://doi.org/10.1007/s11103-015-0397-8

Wu, W., Wang, L., Zhang, S., Li, Z., Zhang, Y., Lin, F., & Pan, Q. (2014). Stepwise arms race between AvrPik and Pik alleles in the rice blast pathosystem. *Molecular Plant-Microbe Interactions*, *27*(8), 759-769.

Xiao, G., Laksanavilat, N., Cesari, S., Lambou, K., Baudin, M., Jalilian, A., Telebanco-Yanoria, M. J., Chalvon, V., Meusnier, I., & Fournier, E. (2024). The unconventional resistance protein PTR recognizes the Magnaporthe oryzae effector AVR-Pita in an allele-specific manner. *Nature Plants*, *10*(6), 994-1004.

Xie, Y., Wang, Y., Yu, X., Lin, Y., Zhu, Y., Chen, J., Xie, H., Zhang, Q., Wang, L., Wei, Y., Xiao, Y., Cai, Q., Zheng, Y., Wang, M., Xie, H., & Zhang, J. (2022). SH3P2, an SH3 domain-containing protein that interacts with both Pib and AvrPib, suppresses effector-triggered, Pib-mediated immunity in rice. *Mol Plant*, *15*(12), 1931-1946. https://doi.org/10.1016/j.molp.2022.10.022

Xu, G., Zhong, X., Shi, Y., Liu, Z., Jiang, N., Liu, J., Ding, B., Li, Z., Kang, H., Ning, Y., Liu, W., Guo, Z., Wang, G.-L., & Wang, X. (2020). A fungal effector targets a heat shock–dynamin protein complex to modulate mitochondrial dynamics and reduce plant immunity. *Science Advances*, *6*(48), eabb7719. https://doi.org/doi:10.1126/sciadv.abb7719

Xu, J.-R., Staiger, C. J., & Hamer, J. E. (1998). Inactivation of the mitogen-activated protein kinase Mps1 from the rice blast fungus prevents penetration of host cells but allows activation of plant defense responses. *Proceedings of the National Academy of Sciences*, *95*(21), 12713-12718. https://doi.org/doi:10.1073/pnas.95.21.12713

Yalovsky, S., Bloch, D., Sorek, N., & Kost, B. (2008). Regulation of Membrane Trafficking, Cytoskeleton Dynamics, and Cell Polarity by ROP/RAC GTPases *Plant Physiology*, *147*(4), 1527-1543. https://doi.org/10.1104/pp.108.122150

Yan, X., Tang, B., Ryder, L. S., MacLean, D., Were, V. M., Eseola, A. B., Cruz-Mireles, N., Ma, W., Foster, A. J., Osés-Ruiz, M., & Talbot, N. J. (2023). The transcriptional landscape of plant infection by the rice blast fungus Magnaporthe oryzae reveals distinct families of temporally co-regulated and structurally conserved effectors. *Plant Cell*, *35*(5), 1360-1385. https://doi.org/10.1093/plcell/koad036

Yan, X., & Talbot, N. J. (2016). Investigating the cell biology of plant infection by the rice blast fungus Magnaporthe oryzae. *Current Opinion in Microbiology*, *34*, 147-153. https://doi.org/https://doi.org/10.1016/j.mib.2016.10.001

Yan, X., Tang, B., Ryder, L. S., MacLean, D., Were, V. M., Eseola, A. B., Cruz-Mireles, N., Ma, W., Foster, A. J., Osés-Ruiz, M., & Talbot, N. J. (2023). The transcriptional landscape of plant infection by the rice blast fungus Magnaporthe oryzae reveals distinct families of temporally co-regulated and structurally

conserved effectors. *The Plant Cell*, *35*(5), 1360-1385. https://doi.org/10.1093/plcell/koad036

Yan, X., Tang, B., Ryder, L. S., MacLean, D., Were, V. M., Eseola, A. B., Cruz-Mireles, N., Ma, W., Foster, A. J., Osés-Ruiz, M., & Talbot, N. J. (2023). The transcriptional landscape of plant infection by the rice blast fungus Magnaporthe oryzae reveals distinct families of temporally co-regulated and structurally conserved effectors. *Plant Cell*, *35*(5), 1360-1385. https://doi.org/10.1093/plcell/koad036

Yang, C., Yu, Y., Huang, J., Meng, F., Pang, J., Zhao, Q., Islam, M. A., Xu, N., Tian, Y., & Liu, J. (2019). Binding of the Magnaporthe oryzae Chitinase MoChia1 by a Rice Tetratricopeptide Repeat Protein Allows Free Chitin to Trigger Immune Responses. *The Plant Cell*, *31*(1), 172-188. https://doi.org/10.1105/tpc.18.00382

Yang, L., Qin, L., Liu, G., Peremyslov, V. V., Dolja, V. V., & Wei, Y. (2014). Myosins XI modulate host cellular responses and penetration resistance to fungal pathogens. *Proceedings of the National Academy of Sciences*, *111*(38), 13996-14001. https://doi.org/doi:10.1073/pnas.1405292111

Yang, L., Zhao, M., Sha, G., Sun, Q., Gong, Q., Yang, Q., Xie, K., Yuan, M., Mortimer, J. C., Xie, W., Wei, T., Kang, Z., & Li, G. (2022). The genome of the rice variety LTH provides insight into its universal susceptibility mechanism to worldwide rice blast fungal strains. *Comput Struct Biotechnol J*, *20*, 1012-1026. https://doi.org/10.1016/j.csbj.2022.01.030

Yang, T., Song, L., Hu, J., Qiao, L., Yu, Q., Wang, Z., Chen, X., & Lu, G.-d. (2024). Magnaporthe oryzae effector AvrPik-D targets a transcription factor WG7 to suppress rice immunity. *Rice*, *17*(1), 14. https://doi.org/10.1186/s12284-024-00693-0

Yi, M., & Valent, B. (2013). Communication Between Filamentous Pathogens and Plants at the Biotrophic Interface. *Annual Review of Phytopathology*, *51*(Volume 51, 2013), 587-611. https://doi.org/https://doi.org/10.1146/annurev-phyto-081211-172916

Yoo, T. S., Ackerman, M. J., Lorensen, W. E., Schroeder, W., Chalana, V., Aylward, S., Metaxas, D., & Whitaker, R. (2002). Engineering and algorithm design for an image processing API: a technical report on ITK-the insight toolkit. In *Medicine Meets Virtual Reality 02/10* (pp. 586-592). IOS press.

Yoshida, K., Saitoh, H., Fujisawa, S., Kanzaki, H., Matsumura, H., Yoshida, K., Tosa, Y., Chuma, I., Takano, Y., Win, J., Kamoun, S., & Terauchi, R. (2009). Association genetics reveals three novel avirulence genes from the rice blast fungal pathogen Magnaporthe oryzae. *Plant Cell*, *21*(5), 1573-1591. https://doi.org/10.1105/tpc.109.066324

Yoshida, S., van der Schuren, A., van Dop, M., van Galen, L., Saiga, S., Adibi, M., Möller, B., ten Hove, C. A., Marhavy, P., Smith, R., Friml, J., & Weijers, D. (2019). A SOSEKI-based coordinate system interprets global polarity cues in Arabidopsis. *Nature Plants*, *5*(2), 160-166. https://doi.org/10.1038/s41477-019-0363-6

Yun, B.-W., Atkinson, H. A., Gaborit, C., Greenland, A., Read, N. D., Pallas, J. A., & Loake, G. J. (2003). Loss of actin cytoskeletal function and EDS1 activity, in combination, severely compromises non-host resistance in Arabidopsis against wheat powdery mildew. *The Plant Journal*, *34*(6), 768-777. https://doi.org/https://doi.org/10.1046/j.1365-313X.2003.01773.x

Žárský, V., Cvrčková, F., Potocký, M., & Hála, M. (2009). Exocytosis and cell polarity in plants–exocyst and recycling domains. *New Phytologist*, *183*(2), 255-272.

Zdrzałek, R., Xi, Y., Langner, T., Bentham, A. R., Petit-Houdenot, Y., De la Concepcion, J. C., Harant, A., Shimizu, M., Were, V., Talbot, N. J., Terauchi, R., Kamoun, S.,

& Banfield, M. J. (2024). Bioengineering a plant NLR immune receptor with a robust binding interface toward a conserved fungal pathogen effector. *Proc Natl Acad Sci U S A*, *121*(28), e2402872121. https://doi.org/10.1073/pnas.2402872121

Zhang, C., Fang, H., Shi, X., He, F., Wang, R., Fan, J., Bai, P., Wang, J., Park, C. H., & Bellizzi, M. (2020). A fungal effector and a rice NLR protein have antagonistic effects on a Bowman–Birk trypsin inhibitor. *Plant Biotechnology Journal*, *18*(11), 2354-2363.

Zhang, H., Qu, X., Bao, C., Khurana, P., Wang, Q., Xie, Y., Zheng, Y., Chen, N., Blanchoin, L., & Staiger, C. J. (2010). Arabidopsis VILLIN5, an actin filament bundling and severing protein, is necessary for normal pollen tube growth. *The Plant Cell*, *22*(8), 2749-2767.

Zhang, N., Luo, J., Rossman, A. Y., Aoki, T., Chuma, I., Crous, P. W., Dean, R., de Vries, R. P., Donofrio, N., Hyde, K. D., Lebrun, M.-H., Talbot, N. J., Tharreau, D., Tosa, Y., Valent, B., Wang, Z., & Xu, J.-R. (2016). Generic names in Magnaporthales. *IMA Fungus*, *7*(1), 155-159. https://doi.org/10.5598/imafungus.2016.07.01.09

Zhang, S., Wang, L., Wu, W., He, L., Yang, X., & Pan, Q. (2015). Function and evolution of Magnaporthe oryzae avirulence gene AvrPib responding to the rice blast resistance gene Pib. *Sci Rep*, *5*, 11642. https://doi.org/10.1038/srep11642

Zhang, S., & Xu, J.-R. (2014). Effectors and Effector Delivery in Magnaporthe oryzae. *PLOS Pathogens*, *10*(1), e1003826. https://doi.org/10.1371/journal.ppat.1003826

Zhang, S., & Xu, J. R. (2014). Effectors and effector delivery in Magnaporthe oryzae. *PLoS Pathog*, *10*(1), e1003826. https://doi.org/10.1371/journal.ppat.1003826

Zhang, X., Catanzariti, A.-M., Lawrence, G. J., Gan, P. H. P., Jones, D. A., Dodds, P. N., & Rathjen, J. P. (2024). Translocation of effector proteins into plant cells by the flax rust pathogen Melampsora lini. *bioRxiv*, 2024.2012.2001.625101. https://doi.org/10.1101/2024.12.01.625101

Zhang, X., He, D., Zhao, Y., Cheng, X., Zhao, W., Taylor, I. A., Yang, J., Liu, J., & Peng, Y.-L. (2018). A positive-charged patch and stabilized hydrophobic core are essential for avirulence function of AvrPib in the rice blast fungus. *The Plant Journal*, *96*(1), 133-146. https://doi.org/https://doi.org/10.1111/tpj.14023

Zhang, Z., Runions, A., Mentink, R. A., Kierzkowski, D., Karady, M., Hashemi, B., Huijser, P., Strauss, S., Gan, X., Ljung, K., & Tsiantis, M. (2020). A WOX/Auxin Biosynthesis Module Controls Growth to Shape Leaf Form. *Current Biology*, *30*(24), 4857-4868.e4856. https://doi.org/10.1016/j.cub.2020.09.037

Zhao, H., Wang, X., Jia, Y., Minkenberg, B., Wheatley, M., Fan, J., Jia, M. H., Famoso, A., Edwards, J. D., & Wamishe, Y. (2018). The rice blast resistance gene Ptr encodes an atypical protein required for broad-spectrum disease resistance. *Nature Communications*, *9*(1), 2039.

Zheng, X., Diraviyam, K., & Sept, D. (2007). Nucleotide effects on the structure and dynamics of actin. *Biophys J*, *93*(4), 1277-1283. https://doi.org/10.1529/biophysj.107.109215

Zhu, H., Sydor, A. M., Boddy, K. C., Coyaud, E., Laurent, E. M. N., Au, A., Tan, J. M. J., Yan, B.-R., Moffat, J., Muise, A. M., Yip, C. M., Grinstein, S., Raught, B., & Brumell, J. H. (2024). Salmonella exploits membrane reservoirs for invasion of host cells. *Nature Communications*, *15*(1), 3120. https://doi.org/10.1038/s41467-024-47183-x

Zou, M., Guo, M., Zhou, Z., Wang, B., Pan, Q., Li, J., Zhou, J.-M., & Li, J. (2021). MPK3- and MPK6-mediated VLN3 phosphorylation regulates actin dynamics during stomatal immunity in Arabidopsis. *Nature Communications*, *12*(1), 6474.

Appendix

Quime, B. G., Ryder, L. S., & Talbot, N. J. (2025). Live cell imaging of plant infection provides new insight into the biology of pathogenesis by the rice blast fungus *Magnaporthe oryzae*. *Journal of Microscopy,* 297, 274-288. https://doi.org/10.1111/jmi.13382.

Received: 11 September 2024 | Revised: 16 December 2024 | Accepted: 23 December 2024

DOI: 10.1111/jmi.13382

Journal of Microscopy RMS

REVIEW ARTICLE

Live cell imaging of plant infection provides new insight into the biology of pathogenesis by the rice blast fungus *Magnaporthe oryzae*

Berlaine G. Quime | **Lauren S. Ryder** | **Nicholas J. Talbot**

The Sainsbury Laboratory, University of East Anglia, Norwich, UK

Correspondence
Nicholas J. Talbot, The Sainsbury Laboratory, University of East Anglia, Norwich Research Park, Norwich NR4 7UH, UK.
Email: nick.talbot@tsl.ac.uk

Funding information
Gatsby Charitable Foundation; Biotechnology and Biological Sciences Research Council, Grant/Award Numbers: BBS/E/J/000PR9797, BB/V016342/1

Abstract

Magnaporthe oryzae is the causal agent of rice blast, one of the most serious diseases affecting rice cultivation around the world. During plant infection, *M. oryzae* forms a specialised infection structure called an appressorium. The appressorium forms in response to the hydrophobic leaf surface and relies on multiple signalling pathways, including a MAP kinase phosphorelay and cAMP-dependent signalling, integrated with cell cycle control and autophagic cell death of the conidium. Together, these pathways regulate appressorium morphogenesis.The appressorium generates enormous turgor, applied as mechanical force to breach the rice cuticle. Re-polarisation of the appressorium requires a turgor-dependent sensor kinase which senses when a critical threshold of turgor has been reached to initiate septin-dependent re-polarisation of the appressorium and plant infection. Invasive growth then requires differential expression and secretion of a large repertoire of effector proteins secreted by distinct secretory pathways depending on their destination, which is also governed by codon usage and tRNA thiolation. Cytoplasmic effectors require an unconventional Golgi-independent secretory pathway and evidence suggests that clathrin-mediated endocytosis is necessary for their delivery into plant cells. The blast fungus then develops a transpressorium, a specific invasion structure used to move from cell-to-cell using pit field sites containing plasmodesmata, to facilitate its spread in plant tissue. This is controlled by the same MAP kinase signalling pathway as appressorium development and requires septin-dependent hyphal constriction. Recent progress in understanding the mechanisms of rice infection by this devastating pathogen using live cell imaging procedures are presented.

KEYWORDS
appressorium, biotrophy, effectors, pathogen, plant immunity, septin

1 | INTRODUCTION

Rice blast disease is one of the most important constraints on global rice production. The disease is caused by the filamentous hemibiotrophic fungus *Magnaporthe oryzae* (syn. *Pyricularia oryzae*), which has emerged as an important model organism for studying plant–fungal interactions.[1] Losses to rice blast each year are estimated to be 6% of the global harvest[2] but epidemics often cause up to 30% yield losses.[3,4] As more than half of the world's population rely on rice for their main calorific intake,[5] blast disease represents a continual threat to global food security. In addition, *M. oryzae* can infect more than fifty grass species,[6–8] leading to emergence of new diseases such as wheat blast, which emerged in Brazil after a host jump from a grass-infecting isolate of *M. oryzae*.[9] Having spread into neighbouring countries in South America, wheat blast appeared in Bangladesh in 2016[10] where it now threatens the Indian subcontinent, a vital wheat-growing region of the world,[11] and more recently appeared in Zambia with the potential now to spread across Africa (Latorre et al., 2023).[12] Globalisation, climate change and intense cultivation of cereal monocultures therefore make blast disease outbreaks more likely on wheat, rice, millets, oats and barley so the disease has the potential to become increasingly important to world agriculture.

In order to control blast disease, it is imperative that the biology of blast is better understood. Breakthroughs in live-cell imaging, coupled with molecular genetic and genomic analysis of *M. oryzae*, have provided new insight into the cell biology of invasive growth by the fungus.[13–15] In this review, we describe the major morphological transitions that the fungus undergoes during plant infection. We then critically evaluate studies of appressorium development, host cell penetration and intracellular colonisation by the blast fungus and review biological consequences of fungal infection induced during disease progression.

2 | THE ADVENT OF LIVE-CELL IMAGING OF PLANT INFECTION by *M. oryzae*

Historically, investigations of host plant infection by *M. oryzae* were made on fixed plant tissues[16–20] and while these revealed the development of specialised invasive hyphae by the fungus,[16] they did not allow the dynamics of the plant-pathogen interaction to be captured. To observe the infection process of *M. oryzae* in living tissues, the leaf sheath inoculation method was developed[21,22] and is now widely used. This provides a simple and effective means of studying fungal growth in living plant tissue.[23] Infecting leaf sheath tissues, which are devoid of chlorophyll, eliminates the need to clear tissues prior to imaging providing optically clear conditions to visualise each stage of fungal infection. Because *M. oryzae* is also easy to genetically transform, the visualisation of functional fluorescent fusion proteins is also widely used (for a video review of their use see Ref. [13], as well as cytological fluorescent dyes.[24,25] Development of these methods, coupled with use of confocal laser scanning microscopy, super-resolution imaging, and electron microscopy, has enabled completely new insights into the major cellular changes that occur during blast infection.[23,26–31] Live cell imaging has, indeed, proven revolutionary in our understanding of blast disease.

3 | APPRESSORIUM FORMATION BY THE BLAST FUNGUS

Plant infection by the blast fungus proceeds when a three-celled conidium lands and attaches to the hydrophobic leaf surface via spore tip mucilage released from its apex.[32] The spore adheres tightly from its tip and germinates rapidly on the leaf surface to form a polarised germ tube within 2 h. The germ tube then hooks and flattens at its tip before differentiating into an appressorium, a dome-shaped infection structure (see Figure 1A and B) with a specialised cell wall containing a layer rich in chitin and a thick layer of melanin between the cell membrane and the cell wall.[32–36] Appressorium development requires perception of an appropriate surface, which must be hard and hydrophobic, as well as free of exogenous nutrients. These conditions are perceived by surface receptors, such as the Pth11 G-protein coupled receptor, the Msb2 and Sho1 proteins which act upstream of the Pmk1 mitogen-activated protein kinase (MAPK) pathway, and the cyclic AMP-dependent protein kinase A pathway, which are necessary for appressorium formation and function.[13] Phosphorylation of the Pmk1 MAPK occurs within 1 h of spore germination and leads to phosphorylation of a large-set of substrates including a novel regulator Vts1, and the Hox7, Far1 and Fkh1 transcription factors.[15] Phosphorylation of these substrates ultimately results in major changes in gene expression in which 49% of the genes of *M. oryzae* are differentially regulated during appressorium morphogenesis.[37] The appressorium undergoes intense melanin biosynthesis and turgor generation which requires high concentrations of intracellular compatible solutes such as glycerol.[38] *M. oryzae* appressoria generate up to 8.0 MPa of pressure, which is applied at the leaf surface to enable a rigid penetration peg to breach the rice leaf cuticle and epidermal cell wall.[39] Appressorium morphogenesis is also regulated by a series of cell cycle controls in which initiation of appressorium formation requires an S-phase checkpoint, appressorium maturation requires

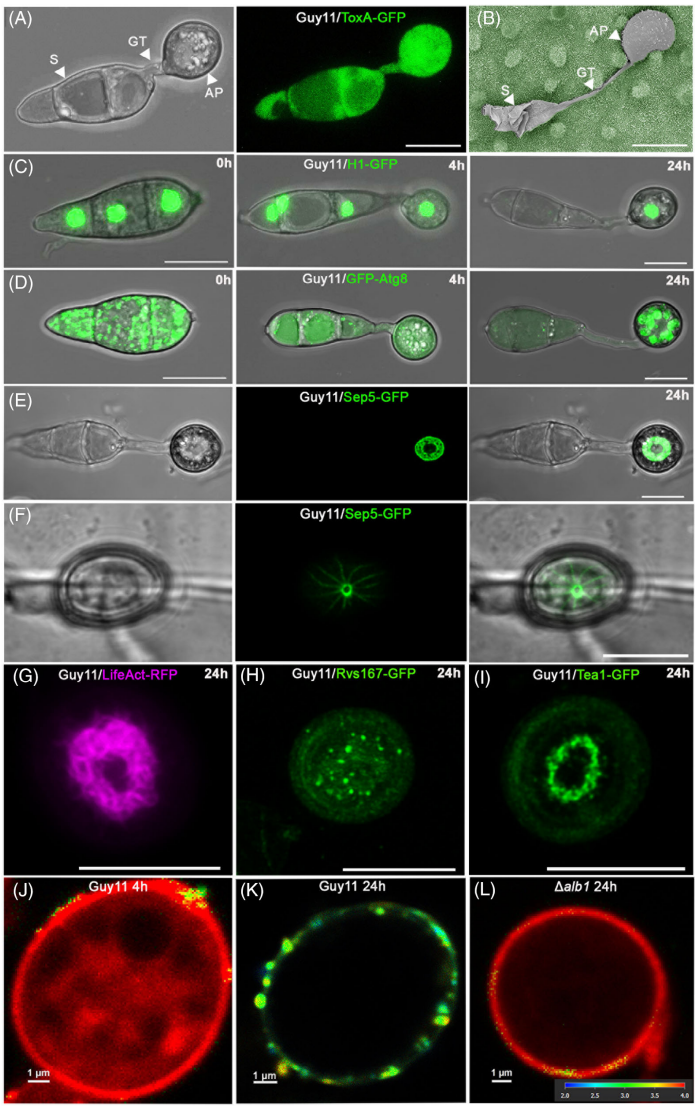

FIGURE 1 Infection-related morphogenesis in the rice blast fungus *Magnaporthe oryzae*. (A) Confocal image of appressorium development by *M. oryzae* wild type strain Guy11 expressing cytoplasmic ToxA-GFP. Conidia were germinated on glass coverslips and visualised 6 h post inoculation (hpi). The images represent maximum intensity projections of Z-stack series captured on a Leica SP8 confocal laser scanning microscope. Scale bar = 10 µm. (B) Scanning electron micrograph with false colouring of a dome-shaped appressorium (grey) on a rice leaf surface (green), freeze dried 24 h after inoculation. The contents of the spore undergo autophagy and are recycled to the incipient appressorium, resulting in enormous turgor that is translated into mechanical force to penetrate the waxy rice leaf cuticle.

mitotic entry, and completion of mitosis is necessary for development of a functionally competent appressorium.[40] A metabolically regulated cell-cycle checkpoint has also been reported to be necessary for appressorium morphogenesis involving inactivation of the target-of-rapamycin (TOR) kinase, which is maintained by the Asd4 GATA transcription factor, thereby repressing expression of genes involved in nitrogen assimilation to maintain low glutamine levels.[41] Following mitosis, one daughter nucleus moves from the germ tube to the appressorium and the second daughter returns to the apical conidial cell (Figure 1C). The conidium then undergoes an autophagy-dependent process leading to cell death.[42,43] This requires cargo-independent autophagy and it has been demonstrated that proteins encoded by genes associated with nonselective autophagy are all required for pathogenicity.[42–44] Autophagy is necessary for collapse of the three-celled conidium and trafficking of its contents into the developing appressorium. Regulated cell death of the spore has, however, also been proposed to require ferroptosis[25,45] which results in lipid peroxidation and loss of viability of each cell of the conidium (see Figure 1D). This suggests that regulated cell death of the conidium requires autophagy but may not be caused by it directly, instead requiring another form of regulated cell death, although further study is essential to confirm these observations.

Appressoria initially undergo radial or isodiametric growth, expanding uniformly in all directions to form dome-shaped infection structures for host penetration. Repolarisation of the appressorium then occurs at its base, where a specific region, the appressorium pore, is defined by a toroidal network of septin GTPases which generates cortical rigidity and re-organises F-actin at the point of plant infection.[46] The septin ring forms during appressorium maturation marking the precise point of penetration peg emergence, as shown in Figure 1E. On a rice leaf surface, the septin ring forms in the same manner, but then undergoes further constriction to a diameter of approximately 0.9–1.1μm once the penetration peg is formed (Figure 1F). Septins are required for scaffolding F-actin at the base of the appressorium[47] as shown in Figure 1G. The septin ring also acts as a lateral diffusion barrier for polarity factors such as Bin-Amphiphysin-Rvs (BAR)-domain proteins like Rvs167 (Figure 1H), the exocyst complex, and actin-binding proteins such as Tea1 (Figure 1I).[46,48] In this way, rapid actin polymerisation, polarised exocytosis and cell wall biogenesis are focused to facilitate peg development and protrusive force generation at the base of the appressorium.

Recently, new tools have been developed to investigate appressorium turgor generation. Changes in membrane tension can be quantified via fluorescence lifetime imaging (FLIM) using a mechanosensor plasma membrane rotor probe, N^+-BDP, which can detect spatial variations in membrane tension in *M. oryzae* appressoria.[14] An incipient appressorium at 4 h shows low and uniform membrane tension causing mechanical restriction of the rotor probe upon photoexcitation and longer average fluorescence lifetimes (Figure 1J), whereas by 24 h, an appressorium with high turgor exhibits high membrane tension, with a disordered membrane, allowing free rotation of the probe, resulting in shorter average fluorescent lifetimes, as shown in Figure 1K. Strikingly, the appressorium membrane under high tension also shows considerable heterogeneity, suggesting that there are regions varying considerably in membrane fluidity in the pressurised cell. By contrast, a nonpathogenic melanin-deficient mutant *alb1*$^-$ was found to exhibit low spatially homogeneous tension (Figure 1L).[14]

4 | INVASIVE GROWTH BY *M. oryzae* IN LIVING PLANT TISSUE

Once the fungus has punctured the leaf surface, it extends a narrow primary hypha that rapidly differentiates into thicker, bulbous invasive hyphae (IH) which

Scale bar = 10 μm. (C) Conidia were harvested from Guy11 expressing H1-GFP and inoculated onto glass coverslips. Images are maximum projections of Z-stack series captured on a Leica SP8 confocal laser scanning microscope at 0, 4 and 24 hpi. Scale bar = 10 μm. (D) Conidia were harvested from Guy11 expressing GFP-Atg8 and inoculated onto glass coverslips. Images are maximum projections of Z-stack series captured on a Leica SP8 confocal laser scanning microscope at 0, 4 and 24 hpi. Scale bar = 10 μm. (E) Organisation of Sep5-GFP in the appressorium pore of Guy11 at 24 hpi on glass coverslips. Scale bar = 10 μm. (F) Organisation of Sep5-GFP in the appressorium pore of Guy11 at 24 hpi on rice leaf sheath cultivar Moukoto. Scale bar = 10 μm. (G) Organisation of actin with LifeAct-RFP in the appressorium pore of Guy11 at 24 hpi. (H) Organisation of Bin-Amphiphysin-Rvs (BAR) domain protein Rvs167-GFP in the appressorium pore of Guy11 at 24 hpi. (I) Organisation actin-binding protein Tea1-GFP in the appressorium pore at 24 hpi. Scale bars = 10 μm. (J) FLIM image of Guy11 appressorium at 4 hpi stained with N^+-BDP rotor probe. Using FLIM, this rotor probe is able to detect differences in plasma membrane tension of appressoria during infection-related-development in wild type strain Guy11 and melanin deficient mutant *alb1*$^-$. Red = low tension, green = high tension. (K) FLIM image of Guy11 appressorium at 24 hpi stained with N^+-BDP rotor probe. (L) FLIM image of melanin-deficient mutant *alb1*$^-$ appressorium at 24 hpi stained with N^+-BDP rotor probe. The colour corresponds to fluorescence lifetime values expressed in nanoseconds, as shown in the key 2–4 ns. Scale bar = 1 μm. S = spore, GT = germ tube and AP = appressorium. Conidial germination onto glass coverslips (A, C, D, E, G, H, I) and leaf sheath infection (F) were incubated at 26°C and 24°C, respectively.

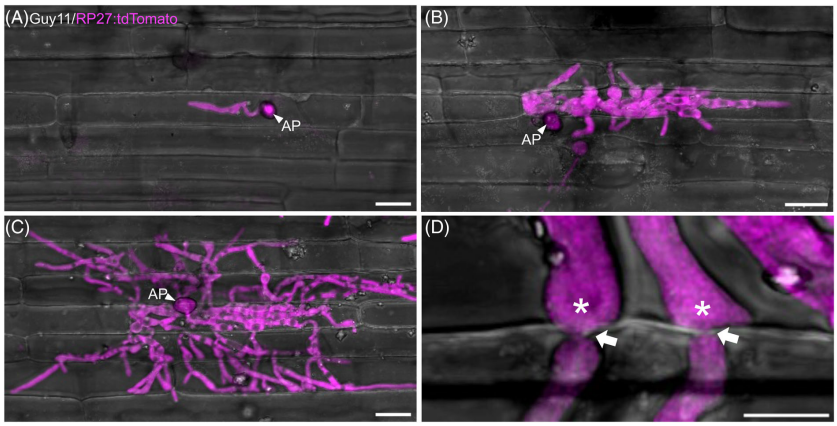

FIGURE 2 Progression of rice tissue invasion by *Magnaporthe oryzae*. Confocal images of of rice cultivar Kitaake leaf sheaths inoculated with *M. oryzae* Guy11 expressing tdTomato driven by *M. oryzae* ribosomal protein 27 (RP27), a constitutive promoter at (A) 24 h post-inoculation (hpi), (B) 36 hpi and (C) 48 hpi. Scale bars = 20 μm. (D) Confocal image showing transpessoria (in asterisks), which enables *M. oryzae* to move from cell-to-cell. White arrows indicate crossing points and hyphal constrictions as the fungus moves to the neighbouring host cell. Scale bar = 5 μm. Leaf sheath infections for all time points were incubated at 24°C. All images shown are maximum projections of Z-stack series taken using Leica SP8 confocal laser scanning microscope. AP = appressorium.

colonise primary-invaded cells before infecting neighbouring cells.[16] Rapid plant tissue colonisation can be visualised from 24 h after inoculation using a *M. oryzae* strain expressing cytoplasmic red fluorescent protein (expressed using the high level constitutive promoter *M. oryzae* ribosomal protein 27 (RP27)[27] driving tdTomato) as shown in Figure 2A. Invasive hyphae initially grow within the first invaded host cells, filling them as they grow and undergoing cortical scanning in which hyphal tips make contact with the edge of the plant cell to locate potential crossing points. To move to uninfected adjacent cells, invasive hyphae swell at the tip and then undergo severe hyphal constriction to a diameter of approximately 0.6-0.8 μm (Cruz-Mireles et al., 2021).[50] Cell-to-cell crossing points located by invasive hyphae correspond to pit field sites, containing plasmodesmata[23] and the fungus utilises these cell junctions to facilitate its spread. The fungus starts to move to neighbouring cells by 36 h after inoculation (Figure 2B) and colonises more cells by 48 h (Figure 2C). The process of cell-to-cell invasion is controlled by the Pmk1 MAPK, mirroring the process of appressorium development.[49] When a conditional *pmk1* analogue-sensitive mutant was generated, it was shown that inhibition of MAPK activity with the ATP analogue kinase inhibitor 1NA-PP1 led to the fungus becoming trapped in the initial infected cell, unable to invade adjacent tissue. Furthermore, Pmk1 appears to regulate a large set of fungal proteins associated with septin and cytoskeletal re-modelling and hyphal constriction, as well as effector-encoding genes required for proliferation of the fungus in plant tissue.[50] Cell-to-cell movement thus requires a specialised infection structure similar to the appressorium, that has been termed a transpressorium (Figure 2C). In this way, the fungus can cross pit field sites, allowing integrity of the plant cell membrane to be maintained in adjacent plant cells as they are invaded.[13,50,51]

5 | RICE PLASMA MEMBRANE DYNAMICS DURING *M. oryzae* INVASION

Expression of fluorescent gene fusions in both rice and *M. oryzae* has recently allowed for much better definition of the fungal-plant interface. Spatiotemporal changes in the rice plasma membrane (PM), for example, can now be directly visualised during *M. oryzae* infection. As the fungus enters the first invaded cell, it is enveloped by the rice plasma membrane, which forms a specialised compartment called the extra-invasive hyphal membrane (EIHM) (Figure 3A). The EIHM surrounds invasive hyphae as they grow in the plant cell but as the fungus moves to previously unoccupied neighbouring cells, integrity of the EIHM in the first invaded cell is lost (Figure 3B). It has been demonstrated that the EIHM forms a sealed compartment that

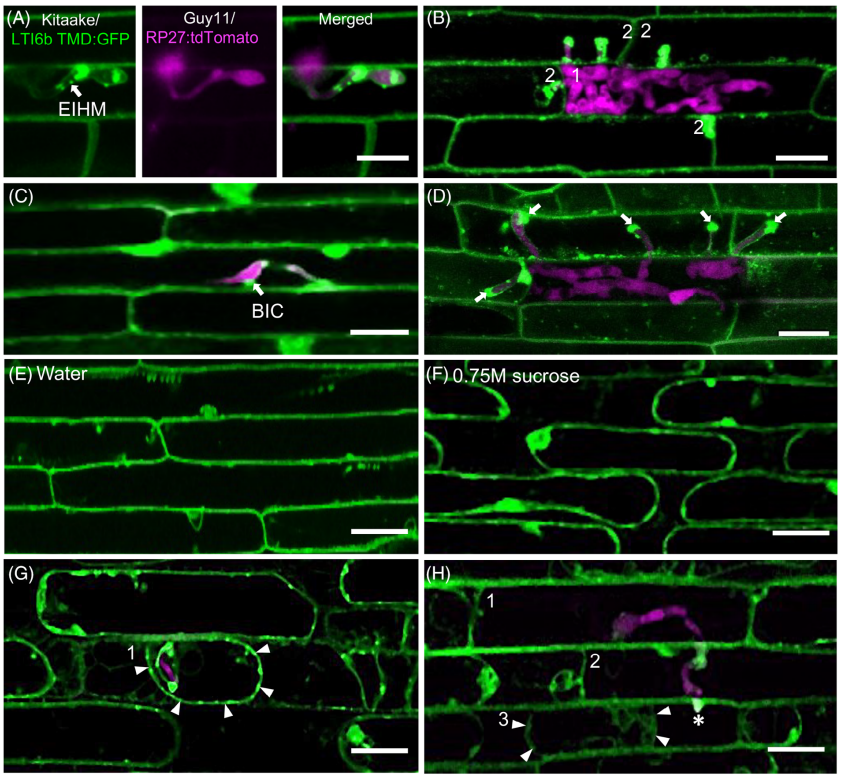

FIGURE 3 Host plasma membrane changes during *Magnaporthe oryzae* infection. (A-B) Extra-invasive hyphal membrane (EIHM) dynamics during *M. oryzae* infection. (A) Invasive hypha (IH) is enclosed with intact EIHM at 24 h post-inoculation (hpi). (B) EIHM becomes disrupted in the initially invaded cell at 36 hpi. Numbers indicate the order by which the fungus invades rice cells. Confocal images were prepared from leaf sheath inoculations using rice transgenic line expressing the plasma membrane marker LTI6b TMD:GFP (green) and rice blast isolate Guy11 RP27:tdTomato (magenta). Scale bars = 20 μm. (C, D) Biotrophic interfacial complex (BIC) formation during *M. oryzae* infection. (C) BIC (indicated by white arrow) is formed as the fungus enters the first cell at 24 hpi. (D) BICs are formed in each invasive hypha as the fungus invades the neighbouring cells at 36 hpi. Confocal images were prepared from leaf sheath inoculations using rice transgenic line expressing the plasma membrane marker LTI6b TMD:GFP (green) and blast isolate Guy11 RP27:tdTomato (magenta). Scale bars = 20 μm. (E–H) Rice plasma membrane dynamics during *M. oryzae* infection. (E) Uninfected rice transgenic line expressing the plasma membrane marker LTI6b TMD:GFP mounted in water. (F) Plasmolysed, uninfected cells of the rice transgenic line LTI6b TMD:GFP mounted in 0.75M sucrose. (G) Plasmolysed initially infected cell indicates intactness of the rice plasma membrane at 24 hpi. (H) Previously invaded cells lose the ability to plasmolyse after the fungus has moved to the neighbouring cells due to loss of plasma membrane integrity. Numbers indicate the order by which the fungus invades the host cells. Confocal images were prepared from leaf sheath inoculations using rice transgenic line expressing the plasma membrane marker LTI6b TMD:GFP (green) and rice blast isolate Guy11 RP27:tdTomato (magenta). White arrowheads indicate the shifting of rice membranes away from the cell wall during plasmolysis. White asterisk indicates new penetration site. Scale bars = 20 μm. (A–H) Leaf sheath infections for all time points were incubated at 24°C. All images shown are maximum projections of Z-stack series taken using Leica SP8 confocal laser scanning microscope.

creates a barrier between the fungus and the host cytoplasm. Labelling with the lipophilic styryl dye FM4-64 allows visualisation of the EIHM, and the inability of the dye to penetrate and label the invasive hyphae has provided evidence that the EIHM forms a sealed compartment.[23] A membrane-rich structure is also found at the EIHM called the biotrophic interfacial complex (BIC). This is a host-derived structure that forms a distinct punctum where fungal effectors are concentrated. In *M. oryzae* strains expressing fluorescently-tagged effector proteins, BIC structures can be visualised clearly. The BIC undergoes a two-stage development as the fungus invades host cells during biotrophic growth. In newly invaded cells, the BIC appears as an EIHM membranous cap, termed a 'tip BIC' that can be observed at the primary hyphal tip.[23] As the filamentous primary penetration hypha differentiates into a bulbous invasive hypha, the BIC develops into a distinctive structure beside the first invasive hyphal cell, where it has been termed a 'side-BIC'.[27] The BIC forms when the fungus penetrates the initial host cell and is consistently visible 24 h after inoculation. The BIC can be readily visualised in rice transgenic lines expressing the plasma membrane marker LTI6b TMD:GFP, as a bright punctate structure as shown in Figure 3C and BICs can be observed as each invasive hypha moves into the next rice cell (Figure 3D). Strikingly, only a single BIC is produced in the initially invaded cell. However, as the fungus spreads to neighbouring cells by 36 h post-inoculation, each invasive hypha that branches from the initial infection site forms a BIC in each newly colonised host cell. The host plasma membrane remains intact during fungal invasion of the initial cell but becomes disrupted as the fungus moves into the neighbouring cell. This can be observed using a plasmolysis assay, where the plasma membrane separates from the cell wall, making it more clearly visible.[23,52] To illustrate the loss of plasma membrane integrity, a plasmolysis assay was carried out on infected rice cells expressing the plasma membrane marker LTI6b-GFP[28] and used to evaluate plasma membrane integrity (Figure 3E). Using a rice transgenic line expressing the LTI6b TMD:GFP, healthy, uninfected rice cells mounted in 0.75M sucrose result in plasmolysed cells where the plasma membrane recedes from the cell wall due to hyperosmotic conditions (Figure 3F). In infected cells, initially invaded cells at 24 hpi also retain their ability to plasmolyse, consistent with host cell membrane integrity being maintained in fungal colonised cells. The EIHM was found also found to shrink around the invasive hypha (Figure 3G). However, as the fungus moves to neighbouring cells, the initial and subsequently invaded cells lose their ability to plasmolyse, indicating that the host plasma membrane is disrupted at this time. Only newly invaded rice cells can plasmolyse (Figure 3H), confirming that *M. oryzae* always colonises living plant cells as it spreads in rice tissue. Biotrophic growth therefore involves a mosaic pattern in which newly invaded plant tissue is alive with intact plasma membranes and a discrete EIHM bounding invasive hyphae, whereas cells from which the fungus spreads lose their viability as soon as adjacent cells are invaded, leading to host cell death. Hemibiotrophy in the blast fungus therefore does not involve distinct switches in growth habit at a precise point following infection, but rather is a consequence of the way in which invasive hyphae move, via transpressoria and pit fields, between host cells always with a growing zone of biotrophic development. As the infection progresses, *Magnaporthe* therefore predominantly appears to switch from a biotrophic phase in which host cells are alive, to a later necrotrophic phase where most cells that the fungus occupies are killed and their nutrients consumed. This leads to the characteristic lesions, sporulation and tissue death associated with rice blast disease.

6 | SECRETION AND DEPLOYMENT OF *M. oryzae* EFFECTORS

To successfully invade living host tissue, *M. oryzae* delivers a complex repertoire of effector proteins to manipulate plant immunity and protect the pathogen from defence responses.[30,53–55] A recent study revealed that 546 putative Magnaporthe effector-encoding (*MEP*) genes are expressed during plant infection and show specific patterns of temporal co-regulation.[31] Structurally related but sequence-unrelated effectors, such as the MAX (Magnaporthe Avrs and ToxB-like) effectors and putative ADP-ribosylation factor-like effectors are expressed specifically between 24 and 48 h after infection. This suggests that effectors are under tight transcriptional control during infection. Consistent with this, a forward genetic screen to search for effector regulators identified *RGS1*, a previously described regulator of G-protein signalling during appressorium development, as a transcriptional regulator of effector gene expression. Rgs1 represses effector expression during the prepenetration phase of development, enabling their specific de-repression upon plant infection.[56] Similarly, the Pmk1 MAP kinase that regulates transpressorium development is also necessary for expression of at least 50 effector-encoding genes, including *SLP1*, *BAS1* and *BAS3*.[31,49] Fluorescent protein tagging has enabled categorisation of effectors based on their localisation patterns *in planta*. Apoplastic effectors delivered to the apoplast, such as *SLP1*,a LysM domain protein binding fungal cell wall chitin, appears around the periphery of invasive hyphae (Figure 4A), whereas cytoplasmic effectors, such as *AVR-Pia*, are concentrated in the BIC before being translocated to the rice cytoplasm (Figure 4B). The

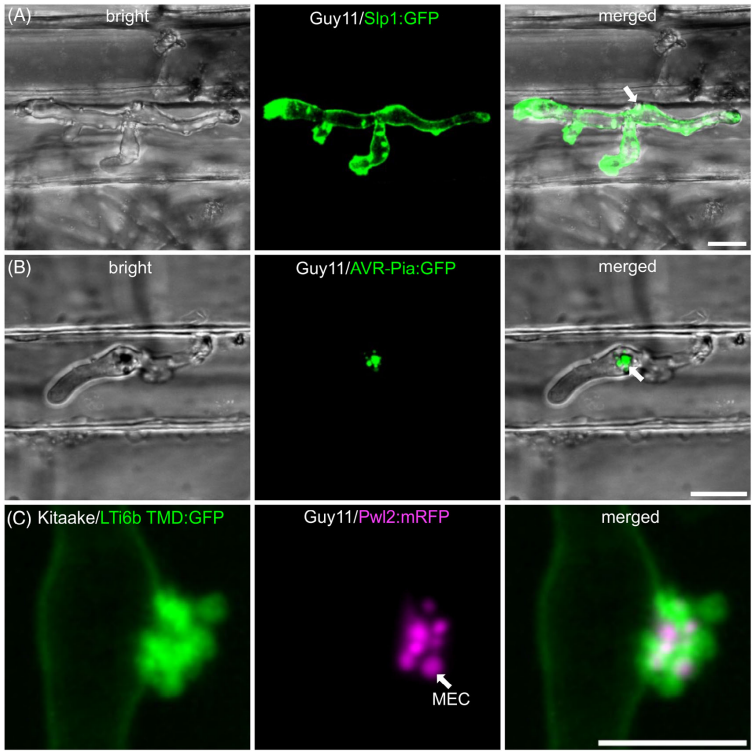

FIGURE 4 Localization of *M. oryzae* effectors during infection. (A) Confocal image shows Guy11 expressing Slp1:GFP, an apoplastic effector, which localizes at the apoplastic space. Note that there is no fluorescence signal in the BIC (white arrow) Scale bars = 10 μm. (B) Confocal image shows Guy11 expressing a known cytoplasmic effector AVR-Pia:GFP. AVR-Pia:GFP preferentially accumulated in the BIC (indicated by white arrow). (C) Confocal image shows a close-up of the biotrophic interfacial complex (BIC). The BIC is plant plasma membrane-derived and colocalizes with Guy11 expressing Pwl2:mRFP. Pwl2 is a known *M. oryzae* cytoplasmic effector localizing at the BIC. Scale bar = 5 μm. Leaf sheath infections were incubated at 24°C. All images were taken 26 h post-inoculation (hpi) and are presented as maximum intensity projections of Z-stack series captured using Leica SP8 confocal laser scanning microscope.

reproducible visualisation of effector expression in the BIC,[27,31,57] is consistent with a role for the BIC as an active site of effector translocation to the host cytoplasm. Evidence to support this hypothesis has been reported in a study which showed that cytoplasmic effectors are secreted in a manner that is insensitive to brefeldin A (BFA), suggesting an unconventional Golgi-independent secretion process. By contrast, apoplastic effectors such as Slp1 and Bas4 are secreted in a BFA-sensitive way, suggesting conventional secretion.[26] Cytoplasmic effectors therefore appear to be secreted from the BIC-associated cell, which is a modified hyphal tip in an exocyst-dependent but Golgi-independent manner. Thereafter they accumulate within the BIC outside of the fungal cell wall but still within the EIHM (Figure 4C). Unconventional secretion of *M*. oryzae furthermore requires tRNA thiolation and alternate codon usage of genes encoding effectors destined for delivery to the BIC.[58] Following secretion, effectors can be visualised within the BIC. between the fungal cell wall and the EIHM, using super resolution imaging within punctate structures called membranous effector compartments (MECs), which have an initial diameter of up to 249 nm, but can enlarge/fuse to form larger 500–1000 nm MECs in mature BICs.[30] MECs co-localise with plant plasma membrane

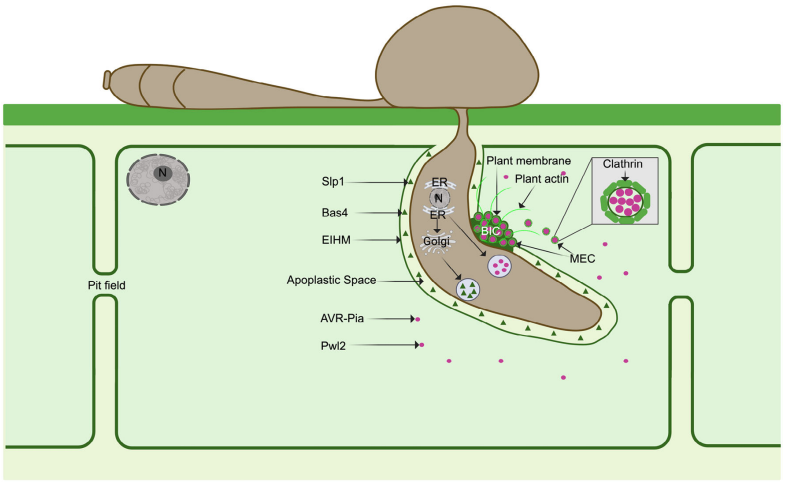

FIGURE 5 Model for the translocation of *M. oryzae* effectors into rice cells. During biotrophic growth, *M. oryzae* deploys a battery of effector proteins which are either apoplastic or cytoplasmic, to suppress host immune responses and facilitate fungal colonisation. Apoplastic effectors are secreted via the conventional ER-to-Golgi, Brefeldin A (BFA)-sensitive pathway, and reside in the apoplastic or EIHM matrix (EIHMx) enclosed by the extra-invasive hyphal membrane (EIHM). Cytoplasmic effectors are secreted using a nonconventional BFA-insensitive pathway and accumulate in the biotrophic interfacial complex (BIC). Cytoplasmic effectors tagged with fluorescent proteins are observed to be packaged in membranous effector compartments (MECs) which co-localise at the BIC with fluorescently-tagged rice plasma membrane (LTI6b:GFP). Clathrin-mediated endocytosis then results in MECs being taken into the cytoplasm of the host from where effectors are released to fulfil diverse immuno-suppressive functions during fungal infection.

markers, such as LTI6b-GFP and also with Clathrin light chain, suggesting a role for clathrin-mediated endocytosis in effector uptake into plant cells from the BIC (Figure 5). Inhibiting clathrin-mediated endocytosis using chemical inhibitors or by virus-mediated gene silencing of OsCHC1 (Clathrin Heavy Chain 1) or OsAP2 (AP2/ERF transcription factor family) prevented effector uptake, whereas inhibition of clathrin independent endocytosis by silencing OsFLOT1 (Flotillin 1), or with chemical inhibitors, had no effect on effector uptake.[30] Taken together, these studies suggest that effector secretion occurs via two routes in *M. oryzae*, depending on the destination of the effector. Cytoplasmic effectors are secreted unconventionally, accumulating in the BIC from where they are taken into plant cells through a mechanism involving clathrin-mediated endocytosis. Interestingly, very similar results have been found in the oomycete pathogen *Phytophthora infestans*, which is only very distantly related to fungal pathogens such as *M. oryzae*. Cytoplasmic effectors of *P. infestans* are secreted in a BFA-insensitive manner[59] and clathrin-mediated endocytosis is also implicated in their uptake during plant infection from haustoria even though a BIC structure is not observed. In *P. infestans* infections of the model host *Nicotiana benthamiana*, transient silencing of *NbCHC*, encoding clathrin heavy chain, or *NbAra6* encoding a Rab GTPase late endosome/multivesicular body marker, attenuates *P. infestans* infection and reduces the translocation of RXLR effector fusions from the pathogen to host cells.[60] When considered together, these studies suggest that there may be a conserved mechanism involved in effector uptake by very diverse filamentous pathogens. There are, however, clearly distinct mechanisms of secretion in pathogens such as *Ustilago maydis*, in which a translocon has been implicated in secretion of at least a subset of its effectors,[61] as well as in other fungal pathogens (for a review see Ref. [62]).

Once secreted, *M. oryzae* effectors take on distinct functions depending on their destination. The apoplastic LysM effector Slp1, for example, suppresses chitin-triggered immunity by acting as a high affinity binder of chitin oligomers released by the pathogen which would normally elicit a pattern-triggered immune response,[28] requiring N-glycosylation for its activity in the apoplast.[63] Similarly, the chitinase Chia1 binds chitin in the apoplast to suppress immunity, but can also be recognised by the rice tetratricopeptide repeat protein OsTPR1 in a

counter-suppression strategy against the effector.[64] An ascorbate oxidase, AO1, also affects apoplastic redox status and suppresses two immunity-associated rice ascorbate oxidases.[65] Cytoplasmic effectors meanwhile target distinct components of pattern-triggered immunity signalling pathways. For example, mitochondria are targeted by at least two *M. oryzae* effectors. CDIP4 targets the mitochondria-associated OsDjA9-OsDRP1E protein complex to reduce rice immunity,[66] while Avr-Pita is a metalloprotease that has been reported to target the cytochrome *c* oxidase assembly protein OsCOX11, which regulates mitochondrial reactive oxygen species (ROS) metabolism.[67] Effectors may also target processes such as plant exocytosis. The Avr-Pii effector, for example, targets two rice Exo70s OsExo70F2 and OsExo70F3[68] and defines a family of zinc-finger effector fold (ZiF) effectors that bind to a specific Exo70 interface.[69] Effectors can, however, also have multiple host targets. Avr-Pii has, for instance, also been reported to interact with NADP-malic enzyme (OsNADP-ME2) to inhibit its activity,[70] while the effector Avr-Pizt is even more promiscuous and has been reported to suppress immunity by binding to the RING-type ubiquitin E3 ligases APIP6 and APIP10,[71, 72] the bZIP-type transcription factor APIP5 to suppress APIP5-triggered cell death,[73] the nucleoporin protein APIP12[74] and the potassium channel OsAKT1 by competing with protein kinase OsCIPK23 to modulate K^+ channel activity.[75] How Avr-Pizt evolved to have such a large number of highly distinct interactors, however, is not clear. Effectors can also target large sets of immune-related proteins such as heavy metal-associated (HMA) domain, which fulfil diverse functions in immunity. The MAX effectors Avr1-CO39, Avr-PikD, and Pwl2, for example, all target HMA proteins and host plants have in turn evolved to recognise them during effector-triggered immunity by integrating HMA domains into NLR immune receptors.[76–80]

7 | FRONTIERS OF OUR UNDERSTANDING OF PATHOGENESIS BY *Magnaporthe oryzae*

A combination of molecular genetics, genomics, and live cell imaging has enabled rapid progress in our understanding of rice blast infection. We now have a basic knowledge of how an appressorium is formed, how it develops turgor and how the re-polarisation process occurs to facilitate entry into the plant. However, there is much we still do not understand. The cell cycle control points that govern appressorium morphogenesis need precise definition and the genetic determinants need to be identified and characterised. These in turn need to be positioned in the context of the signalling pathways that we know regulate appressorium formation, the Pmk1 MAP kinase cascade in particular, but also the cAMP-dependent protein kinase A, and the protein kinase C/cell integrity pathways, so that the network and associated checkpoints that govern appressorium development can be clearly defined. This will require live cell imaging to define the co-localisation of individual components of these signalling pathways such that the spatial and temporal dynamics of the system can be understood. Definition of the Pmk1-dependent phosphorylation landscape of appressorium development[15] is a major advance that will enable the downstream targets of the pathway to be defined and connected with the transcriptional changes that have so far been identified (Osés-Ruiz et al., 2021).[37] However, a comprehensive analysis of Pmk1-dependent transcriptional regulators is required to fully define the hierarchy of control that leads to infection cell morphogenesis. Appressorium turgor generation also requires deeper biochemical analysis as the synthetic pathway for compatible solute generation is still relatively poorly understood. Turgor control will also require the histidine phosphorylation landscape to be defined so that the role of Sln1[81] can be fully understood. Appressorium re-polarisation will also require the septin interactome to be described in detail so that polarity determinants and early acting virulence factors can be identified and the role of septins more clearly understood.[82]

During invasive growth the major challenge will be to determine the functions of more than 500 effector proteins. This seems a daunting task at this stage, given that we understand very few effector functions so far and those that have been studied, such as AvrPi-zt, for example, can be complex involving multiple targets. Whether this is a common feature is currently unknown, but higher throughput gene functional analysis, perhaps using higher frequency CRISPR-Cas9 genome editing will be required along with advances in live cell imaging at scale, to achieve this goal. Understanding effector uptake, BIC formation and the precise delivery mechanism is also an important goal for future research. We need to understand the consequences of effector function in eliciting major changes in host cell organisation and organelle distribution, for example, and in determining how such a large amount of additional plant membrane membrane is made in an infected cell to accommodate growing invasive hyphae. In this article, we have predominantly reported studies using the expression of functional fluorescent proteins visualised by laser scanning confocal microscopy to perform live cell imaging of effector and regulator localisation and to examine the rice-*M. oryzae* interface.[23,27–31,83,84] Research questions regarding effector uptake and function, and host cellular responses during infection would, however, benefit greatly from advances in imaging platforms and microscopy techniques. Spinning disk confocal microscopy[85,86] with its

high temporal resolution, for example, is ideal for imaging the dynamics of fast-moving organelles such as mitochondria and endosomes during infection, which would greatly aid the analysis of effector delivery during infection. Multiphoton microscopy[83,87–91] which enables deep tissue imaging and minimises phototoxic damage, would particularly add value to the observation of structures located deeper in plant tissue such as the BIC to reveal its internal composition and the membrane dynamics of host-pathogen interactions. Light sheet microscopy[92,93] offers the benefit of long-term imaging due to low phototoxicity with a larger field of view. This could be applied, for instance, to monitoring hyphal development while looking at changes in host plant cell organisation, such as cytoskeletal re-modelling, or in tracking fluorescent effector protein movement away from initial sites of infection. Live cell-compatible super-resolution microscopy platforms including structured illumination microscopy (SIM)[94–96] and AiryScan microscopy[97] would furthermore allow examination of host-fungal interplay in greater detail, such as defining intricate details of the host endoplasmic reticulum during infection or localisation of proteins in plasmodesmata associated with immunity and the action of effectors in suppressing such responses (Fitzgibbon et al., 2010).[98]

Finally, these cell biology advances need to facilitate translation into new methods for disease control either via a more systematic effector-guided deployment strategy for major resistance genes in durable combinations, based on an understanding of the prevailing pathogen population, or by means of better, targeted antifungal compounds that have limited environmental impact and can be made in a sustainable manner. These tasks are equally daunting, but exciting too, and can build on recent advances in our understanding of pathogenesis that have been driven by advances in live cell imaging of blast infections.

ACKNOWLEDGEMENTS

We acknowledge funding from the Gatsby Charitable Foundation and the Biotechnology and Biological Sciences Research Council (BBSRC) grants BBS/E/J/000PR9797 and BB/V016342/1 to NJT. We also thank Alice Eseola for providing images of H1-GFP, and Matthew Wengler for providing us with the GFP-Atg8 strain to image.

DATA AVAILABILITY STATEMENT

Data sharing not applicable to this article as no data sets were generated or analysed during the current study.

ORCID

Berlaine G. Quime https://orcid.org/0009-0004-4537-0643
Lauren S. Ryder https://orcid.org/0000-0003-0370-5746
Nicholas J. Talbot https://orcid.org/0000-0001-6434-7757

REFERENCES

1. Dean, R., Van Kan, J. A., Pretorius, Z. A., Hammond-Kosack, K. E., Di Pietro, A., Spanu, P. D., Rudd, J. J., Dickman, M., Kahmann, R., & Ellis, J. (2012). The top 10 fungal pathogens in molecular plant pathology. *Molecular Plant Pathology*, *13*(4), 414–430.
2. Savary, S., Willocquet, L., Pethybridge, S. J., Esker, P., McRoberts, N., & Nelson, A. (2019). The global burden of pathogens and pests on major food crops. *Nature Ecology & Evolution*, *3*(3), 430–439. https://doi.org/10.1038/s41559-018-0793-y
3. Nalley, L., Tsiboe, F., Durand-Morat, A., Shew, A., & Thoma, G. (2016). Economic and Environmental Impact of Rice Blast Pathogen (*Magnaporthe oryzae*) Alleviation in the United States. *PLoS ONE*, *11*(12), e0167295. https://doi.org/10.1371/journal.pone.0167295
4. Wilson, R. A., & Talbot, N. J. (2009). Under pressure: Investigating the biology of plant infection by *Magnaporthe oryzae*. *Nature Reviews Microbiology*, *7*(3), 185–195.
5. Khush, G. S. (2005). What it will take to feed 5.0 billion rice consumers in 2030. *Plant Molecular Biology*, *59*, 1–6.
6. Kato, H., Yamamoto, M., Yamaguchi-Ozaki, T., Kadouchi, H., Iwamoto, Y., Nakayashiki, H., Tosa, Y., Mayama, S., & Mori, N. (2000). Pathogenicity, mating ability and DNA restriction fragment length polymorphisms of Pyricularia populations isolated from Gramineae, Bambusideae and Zingiberaceae plants. *Journal of General Plant Pathology*, *66*, 30–47.
7. Oh, H., Tosa, Y., Takabayashi, N., Nakagawa, S., Tomita, R., Don, L., Kusaba, M., Nakayashiki, H., & Mayama, S. (2002). Characterization of an Avena isolate of *Magnaporthe grisea* and identification of a locus conditioning its specificity on oat. *Canadian Journal of Botany*, *80*(10), 1088–1095.
8. Tosa, Y., Hirata, K., Tamba, H., Nakagawa, S., Chuma, I., Isobe, C., Osue, J., Urashima, A., Don, L., & Kusaba, M. (2004). Genetic constitution and pathogenicity of Lolium isolates of *Magnaporthe oryzae* in comparison with host species-specific pathotypes of the blast fungus. *Phytopathology*, *94*(5), 454–462.
9. Inoue, Y., Vy, T. T., Yoshida, K., Asano, H., Mitsuoka, C., Asuke, S., Anh, V. L., Cumagun, C. J., Chuma, I., & Terauchi, R. (2017). Evolution of the wheat blast fungus through functional losses in a host specificity determinant. *Science*, *357*(6346), 80–83.
10. Islam, M. T., Croll, D., Gladieux, P., Soanes, D. M., Persoons, A., Bhattacharjee, P., Hossain, M. S., Gupta, D. R., Rahman, M. M., & Mahboob, M. G. (2016). Emergence of wheat blast in Bangladesh was caused by a South American lineage of *Magnaporthe oryzae*. *BMC biology*, *14*, 1–11.
11. Islam, M. T., Kim, K.-H., & Choi, J. (2019). Wheat blast in Bangladesh: The current situation and future impacts. *The Plant Pathology Journal*, *35*(1), 1.
12. Latorre, S. M., Were, V. M., Foster, A. J., Langner, T., Malmgren, A., Harant, A., Asuke, S., Reyes-Avila, S., Gupta, D. R., Jensen, C., Ma, W., Mahmud, N. U., Mehebub, M. S., Mulenga, R. M., Muzahid, A. N. M., Paul, S. K., Rabby, S. M. F., Rahat, A. A. M., Ryder, L., … Kamoun, S. (2023). Genomic surveillance uncovers a pandemic clonal lineage of the wheat blast fungus. *PLoS Biology*, *21*(4):e3002052. https://doi.org/10.1371/journal.

pbio.3002052 Erratum in: PLoS Biol. 2023 Jul 19;21(7):e3002236. https://doi.org/10.1371/journal.pbio.3002236
13. Eseola, A. B., Ryder, L. S., Osés-Ruiz, M., Findlay, K., Yan, X., Cruz-Mireles, N., Molinari, C., Garduño-Rosales, M., & Talbot, N. J. (2021). Investigating the cell and developmental biology of plant infection by the rice blast fungus *Magnaporthe oryzae*. *Fungal Genetics and Biology*, *154*, 103562. https://doi.org/10.1016/j.fgb.2021.103562
14. Ryder, L. S., Lopez, S. G., Michels, L., Eseola, A. B., Sprakel, J., Ma, W., & Talbot, N. J. (2023). A molecular mechanosensor for real-time visualization of appressorium membrane tension in *Magnaporthe oryzae*. *Nature Microbiology*, *8*(8), 1508–1519. https://doi.org/10.1038/s41564-023-01430-x
15. Cruz-Mireles, N., Osés-Ruiz, M., Derbyshire, P., Jégousse, C., Ryder, L. S., Bautista, M. J. A., Eseola, A., Sklenar, J., Tang, B., Yan, X., Ma, W., Findlay, K. C., Were, V., MacLean, D., Talbot, N. J., & Menke, F. L. H. (2024). The phosphorylation landscape of infection-related development by the rice blast fungus. *Cell*, *187*(10), 2557–2573.e2518. https://doi.org/10.1016/j.cell.2024.04.007
16. Heath, M. C., Valent, B., Howard, R. J., & Chumley, F. G. (1990). Interactions of two strains of *Magnaporthe grisea* with rice, goosegrass, and weeping lovegrass. *Canadian Journal of Botany*, *68*(8), 1627–1637. https://doi.org/10.1139/b90-209
17. Koga, H., & Kobayashi, T. (1982). Comparison of the early infection process of *Pyricularia oryzae* Cav. in rice leaves of compatible and incompatible combinations. *Japanese Journal of Phytopathology*, *48*(4), 506–513.
18. Koga, H., Kobayashi, T., & Horino, O. (1982). Electron microscopical observation of rice leaves infected with *Pyricularia oryzae* Cav. in compatible and incompatible combinations I. Fine structure of invaded hyphae in host cells. *Japanese Journal of Phytopathology*, *48*(3), 281–289.
19. Peng, Y.-L., & Shishiyama, J. (1988). Temporal sequence of cytological events in rice leaves infected with *Pyricularia oryzae*. *Canadian Journal of Botany*, *66*(4), 730–735.
20. Peng, Y.-L., & Shishiyama, J. (1989). Timing of a cellular reaction in rice cultivars associated with differing degrees of resistance to Pyricularia oryzae. *Canadian Journal of Botany*, *67*(9), 2704–2710.
21. Koga, H. (1994). Hypersensitive death, autofluorescence, and ultrastructural changes in cells of leaf sheaths of susceptible and resistant near-isogenic lines of rice (Pi-zt) in relation to penetration and growth of Pyricularia oryzae. *Canadian Journal of Botany*, *72*(10), 1463–1477.
22. Sakamoto, M. (1949). On the new method of sheath-inoculation of rice plants with blast fungus, *Pyricularia oryzae* Cav. for the study of the disease-resistant nature of the plant. *Bulletin of the Institute for Agricultural Research Tohoku University, Japan*, *1*, 120–129.
23. Kankanala, P., Czymmek, K., & Valent, B. (2007). Roles for rice membrane dynamics and plasmodesmata during biotrophic invasion by the blast fungus. *The Plant Cell*, *19*(2), 706–724. https://doi.org/10.1105/tpc.106.046300
24. Jones, K., Kim, D. W., Park, J. S., & Khang, C. H. (2016). Live-cell fluorescence imaging to investigate the dynamics of plant cell death during infection by the rice blast fungus *Magnaporthe oryzae*. *BMC Plant Biology*, *16*(1), 69. https://doi.org/10.1186/s12870-016-0756-x
25. Shen, Q., Liang, M., Yang, F., Deng, Y. Z., & Naqvi, N. I. (2020). Ferroptosis contributes to developmental cell death in rice blast. *New Phytologist*, *227*(6), 1831–1846.
26. Giraldo, M. C., Dagdas, Y. F., Gupta, Y. K., Mentlak, T. A., Yi, M., Martinez-Rocha, A. L., Saitoh, H., Terauchi, R., Talbot, N. J., & Valent, B. (2013). Two distinct secretion systems facilitate tissue invasion by the rice blast fungus *Magnaporthe oryzae*. *Nature Communications*, *4*, 1996. https://doi.org/10.1038/ncomms2996
27. Khang, C. H., Berruyer, R., Giraldo, M. C., Kankanala, P., Park, S. Y., Czymmek, K., Kang, S., & Valent, B. (2010). Translocation of *Magnaporthe oryzae* effectors into rice cells and their subsequent cell-to-cell movement. *Plant Cell*, *22*(4), 1388–1403. https://doi.org/10.1105/tpc.109.069666
28. Mentlak, T. A., Kombrink, A., Shinya, T., Ryder, L. S., Otomo, I., Saitoh, H., Terauchi, R., Nishizawa, Y., Shibuya, N., Thomma, B. P. H. J., & Talbot, N. J. (2012). Effector-mediated suppression of chitin-triggered immunity by *Magnaporthe oryzae* Is necessary for rice blast disease. *The Plant Cell*, *24*(1), 322–335. https://doi.org/10.1105/tpc.111.092957
29. Mochizuki, S., Minami, E., & Nishizawa, Y. (2015). Live-cell imaging of rice cytological changes reveals the importance of host vacuole maintenance for biotrophic invasion by blast fungus, *Magnaporthe oryzae*. *MicrobiologyOpen*, *4*(6), 952–966. https://doi.org/10.1002/mbo3.304
30. Oliveira-Garcia, E., Tamang, T. M., Park, J., Dalby, M., Martin-Urdiroz, M., Rodriguez Herrero, C., Vu, A. H., Park, S., Talbot, N. J., & Valent, B. (2023). Clathrin-mediated endocytosis facilitates the internalization of *Magnaporthe oryzae* effectors into rice cells. *The Plant Cell*, *35*(7), 2527–2551. https://doi.org/10.1093/plcell/koad094
31. Yan, X., Tang, B., Ryder, L. S., MacLean, D., Were, V. M., Eseola, A. B., Cruz-Mireles, N., Ma, W., Foster, A. J., Osés-Ruiz, M., & Talbot, N. J. (2023). The transcriptional landscape of plant infection by the rice blast fungus *Magnaporthe oryzae* reveals distinct families of temporally co-regulated and structurally conserved effectors. *The Plant Cell*, *35*(5), 1360–1385. https://doi.org/10.1093/plcell/koad036
32. Hamer, J. E., Howard, R. J., Chumley, F. G., & Valent, B. (1988). A mechanism for surface attachment in spores of a plant pathogenic fungus. *Science*, *239*(4837), 288–290. https://doi.org/10.1126/science.239.4837.288
33. Fernandez, J., & Orth, K. (2018). Rise of a cereal killer: The biology of *Magnaporthe oryzae* biotrophic growth. *Trends in Microbiology*, *26*(7), 582–597. https://doi.org/10.1016/j.tim.2017.12.007
34. Howard, R. J., & Ferrari, M. A. (1989). Role of melanin in appressorium function. *Experimental Mycology*, *13*(4), 403–418.
35. Howard, R. J., & Valent, B. (1996). Breaking and entering: host penetration by the fungal rice blast pathogen *Magnaporthe grisea*. *Annual Review of Microbiology*, *50*(1996), 491–512. https://doi.org/10.1146/annurev.micro.50.1.491
36. Talbot, N. J. (2003). On the trail of a cereal killer: Exploring the biology of *Magnaporthe grisea*. *Annual Review of Microbiology*, *57*, 177–202. https://doi.org/10.1146/annurev.micro.57.030502.090957
37. Osés-Ruiz, M., Cruz-Mireles, N., Martin-Urdiroz, M., Soanes, D. M., Eseola, A. B., Tang, B., Derbyshire, P., Nielsen, M., Cheema, J., Were, V., Eisermann, I., Kershaw, M. J., Yan, X., Valdovinos-Ponce, G., Molinari, C., Littlejohn, G. R., Valent, B., Menke, F. L.

H., & Talbot, N. J. (2021). Appressorium-mediated plant infection by *Magnaporthe oryzae* is regulated by a Pmk1-dependent hierarchical transcriptional network. *Nature Microbiology*, *6*(11), 1383–1397. https://doi.org/10.1038/s41564-021-00978-w

38. de Jong, J. C., McCormack, B. J., Smirnoff, N., & Talbot, N. J. (1997). Glycerol generates turgor in rice blast. *Nature*, *389*(6648), 244–244. https://doi.org/10.1038/38418
39. Howard, R. J., Ferrari, M. A., Roach, D. H., & Money, N. P. (1991). Penetration of hard substrates by a fungus employing enormous turgor pressures. *PNAS*, *88*(24), 11281–11284. https://doi.org/10.1073/pnas.88.24.11281
40. Saunders, D. G., Dagdas, Y. F., & Talbot, N. J. (2010). Spatial uncoupling of mitosis and cytokinesis during appressorium-mediated plant infection by the rice blast fungus *Magnaporthe oryzae*. *Plant Cell*, *22*(7), 2417–2428. https://doi.org/10.1105/tpc.110.074492
41. Marroquin-Guzman, M., & Wilson, R. A. (2015). GATA-dependent glutaminolysis drives appressorium formation in *Magnaporthe oryzae* by suppressing TOR inhibition of cAMP/PKA signaling. *PLOS Pathogens*, *11*(4), e1004851. https://doi.org/10.1371/journal.ppat.1004851
42. Kershaw, M. J., & Talbot, N. J. (2009). Genome-wide functional analysis reveals that infection-associated fungal autophagy is necessary for rice blast disease. *Proceedings of the National Academy of Sciences*, *106*(37), 15967–15972.
43. Veneault-Fourrey, C., Barooah, M., Egan, M., Wakley, G., & Talbot, N. J. (2006). Autophagic fungal cell death is necessary for infection by the rice blast fungus. *Science*, *312*(5773), 580–583. https://doi.org/10.1126/science.1124550
44. Li, G., Dulal, N., Gong, Z., & Wilson, R. A. (2023). Unconventional secretion of *Magnaporthe oryzae* effectors in rice cells is regulated by tRNA modification and codon usage control. *Nature microbiology*, *8*(9), 1706–1716. https://doi.org/10.1038/s41564-023-01443-6
45. Liu, Q., Long, R., Lin, C., Bi, X., Liang, Z., & Deng, Y. Z. (2024). Phosphatidylethanolamines link ferroptosis and autophagy during appressorium formation of rice blast fungus. *Molecular Plant Pathology*, *25*(7), e13489. https://doi.org/10.1111/mpp.13489
46. Dagdas, Y. F., Yoshino, K., Dagdas, G., Ryder, L. S., Bielska, E., Steinberg, G., & Talbot, N. J. (2012). Septin-mediated plant cell invasion by the rice blast fungus, *Magnaporthe oryzae*. *Science*, *336*(6088), 1590–1595.
47. Dulal, N., Rogers, A. M., Proko, R., Bieger, B. D., Liyanage, R., Krishnamurthi, V. R., Wang, Y., & Egan, M. J. (2021). Turgor-dependent and coronin-mediated F-actin dynamics drive septin disc-to-ring remodeling in the blast fungus *Magnaporthe oryzae*. *Journal of Cell Science*, *134*(5), jcs251298.
48. Gupta, Y. K., Dagdas, Y. F., Martinez-Rocha, A.-L., Kershaw, M. J., Littlejohn, G. R., Ryder, L. S., Sklenar, J., Menke, F., & Talbot, N. J. (2015). Septin-dependent assembly of the exocyst is essential for plant infection by *Magnaporthe oryzae*. *The Plant Cell*, *27*(11), 3277–3289.
49. Sakulkoo, W., Osés-Ruiz, M., Oliveira Garcia, E., Soanes, D. M., Littlejohn, G. R., Hacker, C., Correia, A., Valent, B., & Talbot, N. J. (2018). A single fungal MAP kinase controls plant cell-to-cell invasion by the rice blast fungus. *Science*, *359*(6382), 1399–1403. https://doi.org/10.1126/science.aaq0892
50. Cruz-Mireles, N., Eseola, A. B., Osés-Ruiz, M., Ryder, L. S., & Talbot, N. J. (2021). From appressorium to transpressorium – Defining the morphogenetic basis of host cell invasion by the rice blast fungus. *PLOS Pathogens*, *17*(7), e1009779. https://doi.org/10.1371/journal.ppat.1009779
51. Ryder, L. S., Cruz-Mireles, N., Molinari, C., Eisermann, I., Eseola, A. B., & Talbot, N. J. (2022). The appressorium at a glance. *Journal of Cell Science*, *135*(14), jcs259857. https://doi.org/10.1242/jcs.259857
52. Koga, H., Dohi, K., Nakayachi, O., & Mori, M. (2004). A novel inoculation method of *Magnaporthe grisea* for cytological observation of the infection process using intact leaf sheaths of rice plants. *Physiological and Molecular Plant Pathology*, *64*(2), 67–72. https://doi.org/10.1016/j.pmpp.2004.07.002
53. de Jonge, R., Bolton, M. D., & Thomma, B. P. (2011). How filamentous pathogens co-opt plants: The ins and outs of fungal effectors. *Current Opinion in Plant Biology*, *14*(4), 400–406. https://doi.org/10.1016/j.pbi.2011.03.005
54. Yang, T., Song, L., Hu, J., Qiao, L., Yu, Q., Wang, Z., Chen, X., & Lu, G.-d. (2024). *Magnaporthe oryzae* effector AvrPik-D targets a transcription factor WG7 to suppress rice immunity. *Rice*, *17*(1), 14. https://doi.org/10.1186/s12284-024-00693-0
55. Zhang, S., & Xu, J.-R. (2014). Effectors and effector delivery in *Magnaporthe oryzae*. *PLOS Pathogens*, *10*(1), e1003826. https://doi.org/10.1371/journal.ppat.1003826
56. Tang, B., Yan, X., Ryder, L. S., Bautista, M. J. A., Cruz-Mireles, N., Soanes, D. M., Molinari, C., Foster, A. J., & Talbot, N. J. (2023). Rgs1 is a regulator of effector gene expression during plant infection by the rice blast fungus *Magnaporthe oryzae*. *Proceedings of the National Academy of Sciences*, *120*(12), e2301358120. https://doi.org/10.1073/pnas.2301358120
57. Mosquera, G., Giraldo, M. C., Khang, C. H., Coughlan, S., & Valent, B. (2009). Interaction transcriptome analysis identifies *Magnaporthe oryzae* BAS1-4 as Biotrophy-associated secreted proteins in rice blast disease. *Plant Cell*, *21*(4), 1273–1290. https://doi.org/10.1105/tpc.107.055228
58. Li, G., Gong, Z., Dulal, N., Marroquin-Guzman, M., Rocha, R. O., Richter, M., & Wilson, R. A. (2023). A protein kinase coordinates cycles of autophagy and glutaminolysis in invasive hyphae of the fungus *Magnaporthe oryzae* within rice cells. *Nature Communications*, *14*(1), 4146. https://doi.org/10.1038/s41467-023-39880-w
59. Wang, S., Boevink, P. C., Welsh, L., Zhang, R., Whisson, S. C., & Birch, P. R. J. (2017). Delivery of cytoplasmic and apoplastic effectors from Phytophthora infestans haustoria by distinct secretion pathways. *New Phytologist*, *216*(1), 205–215. https://doi.org/10.1111/nph.14696
60. Wang, H., Wang, S., Wang, W., Xu, L., Welsh, L. R. J., Gierlinski, M., Whisson, S. C., Hemsley, P. A., Boevink, P. C., & Birch, P. R. J. (2023). Uptake of oomycete RXLR effectors into host cells by clathrin-mediated endocytosis. *The Plant Cell*, *35*(7), 2504–2526. https://doi.org/10.1093/plcell/koad069
61. Ludwig, N., Reissmann, S., Schipper, K., Gonzalez, C., Assmann, D., Glatter, T., Moretti, M., Ma, L.-S., Rexer, K.-H., Snetselaar, K., & Kahmann, R. (2021). A cell surface-exposed protein complex with an essential virulence function in *Ustilago maydis*. *Nature Microbiology*, *6*(6), 722–730. https://doi.org/10.1038/s41564-021-00896-x
62. Lo Presti, L., & Kahmann, R. (2017). How filamentous plant pathogen effectors are translocated to host cells. *Current*

Opinion in Plant Biology, *38*, 19–24. https://doi.org/10.1016/j.pbi.2017.04.005

63. Chen, X. L., Shi, T., Yang, J., Shi, W., Gao, X., Chen, D., Xu, X., Xu, J. R., Talbot, N. J., & Peng, Y. L. (2014). N-glycosylation of effector proteins by an α-1,3-mannosyltransferase is required for the rice blast fungus to evade host innate immunity. *Plant Cell*, *26*(3), 1360–1376. https://doi.org/10.1105/tpc.114.123588
64. Yang, C., Yu, Y., Huang, J., Meng, F., Pang, J., Zhao, Q., Islam, M. A., Xu, N., Tian, Y., & Liu, J. (2019). Binding of the *Magnaporthe oryzae* Chitinase MoChi1 by a rice tetratricopeptide repeat protein allows free chitin to trigger immune responses. *The Plant Cell*, *31*(1), 172–188. https://doi.org/10.1105/tpc.18.00382
65. Hu, J., Liu, M., Zhang, A., Dai, Y., Chen, W., Chen, F., Wang, W., Shen, D., Telebanco-Yanoria, M. J., Ren, B., Zhang, H., Zhou, H., Zhou, B., Wang, P., & Zhang, Z. (2022). Co-evolved plant and blast fungus ascorbate oxidases orchestrate the redox state of host apoplast to modulate rice immunity. *Molecular Plant*, *15*(8), 1347–1366. https://doi.org/10.1016/j.molp.2022.07.001
66. Xu, G., Zhong, X., Shi, Y., Liu, Z., Jiang, N., Liu, J., Ding, B., Li, Z., Kang, H., Ning, Y., Liu, W., Guo, Z., Wang, G.-L., & Wang, X. (2020). A fungal effector targets a heat shock–dynamin protein complex to modulate mitochondrial dynamics and reduce plant immunity. *Science Advances*, *6*(48), eabb7719. https://doi.org/10.1126/sciadv.abb7719
67. Han, J., Wang, X., Wang, F., Zhao, Z., Li, G., Zhu, X., Su, J., & Chen, L. (2021). The fungal effector Avr-Pita suppresses innate immunity by increasing COX activity in rice mitochondria. *Rice*, *14*(1), 12. https://doi.org/10.1186/s12284-021-00453-4
68. Fujisaki, K., Abe, Y., Ito, A., Saitoh, H., Yoshida, K., Kanzaki, H., Kanzaki, E., Utsushi, H., Yamashita, T., Kamoun, S., & Terauchi, R. (2015). Rice Exo70 interacts with a fungal effector, AVR-Pii, and is required for AVR-Pii-triggered immunity. *The Plant Journal*, *83*(5), 875–887. https://doi.org/10.1111/tpj.12934
69. De la Concepcion, J. C., Fujisaki, K., Bentham, A. R., Cruz Mireles, N., Sanchez de Medina Hernandez, V., Shimizu, M., Lawson, D. M., Kamoun, S., Terauchi, R., & Banfield, M. J. (2022). A blast fungus zinc-finger fold effector binds to a hydrophobic pocket in host Exo70 proteins to modulate immune recognition in rice. *PNAS*, *119*(43), e2210559119. https://doi.org/10.1073/pnas.2210559119
70. Singh, R., Dangol, S., Chen, Y., Choi, J., Cho, Y.-S., Lee, J.-E., Choi, M.-O., & Jwa, N.-S. (2016). *Magnaporthe oryzae* effector AVR-Pii helps to establish compatibility by inhibition of the rice NADP-malic enzyme resulting in disruption of oxidative burst and host innate immunity. *Molecules and Cells*, *39*(5), 426–438. https://doi.org/10.14348/molcells.2016.0094
71. Park, C.-H., Chen, S., Shirsekar, G., Zhou, B., Khang, C. H., Songkumarn, P., Afzal, A. J., Ning, Y., Wang, R., Bellizzi, M., Valent, B., & Wang, G.-L. (2012). The *Magnaporthe oryzae* effector AvrPiz-t targets the RING E3 ubiquitin ligase APIP6 to suppress pathogen-associated molecular pattern–triggered immunity in rice. *The Plant Cell*, *24*(11), 4748–4762. https://doi.org/10.1105/tpc.112.105429
72. Park, C. H., Shirsekar, G., Bellizzi, M., Chen, S., Songkumarn, P., Xie, X., Shi, X., Ning, Y., Zhou, B., Suttiviriya, P., Wang, M., Umemura, K., & Wang, G.-L. (2016). The E3 ligase APIP10 connects the effector AvrPiz-t to the NLR receptor Piz-t in rice. *PLOS Pathogens*, *12*(3), e1005529. https://doi.org/10.1371/journal.ppat.1005529
73. Wang, R., Ning, Y., Shi, X., He, F., Zhang, C., Fan, J., Jiang, N., Zhang, Y., Zhang, T., Hu, Y., Bellizzi, M., & Wang, G.-L. (2016). Immunity to rice blast disease by suppression of effector-triggered necrosis. *Current Biology*, *26*(18), 2399–2411. https://doi.org/10.1016/j.cub.2016.06.072
74. Tang, M., Ning, Y., Shu, X., Dong, B., Zhang, H., Wu, D., Wang, H., Wang, G.-L., & Zhou, B. (2017). The Nup98 homolog APIP12 targeted by the effector AvrPiz-t is involved in rice basal resistance against *Magnaporthe oryzae*. *Rice*, *10*(1), 5. https://doi.org/10.1186/s12284-017-0144-7
75. Shi, X., Long, Y., He, F., Zhang, C., Wang, R., Zhang, T., Wu, W., Hao, Z., Wang, Y., Wang, G.-L., & Ning, Y. (2018). The fungal pathogen *Magnaporthe oryzae* suppresses innate immunity by modulating a host potassium channel. *PLOS Pathogens*, *14*(1), e1006878. https://doi.org/10.1371/journal.ppat.1006878
76. Guo, L., Cesari, S., de Guillen, K., Chalvon, V., Mammri, L., Ma, M., Meusnier, I., Bonnot, F., Padilla, A., Peng, Y. L., Liu, J., & Kroj, T. (2018). Specific recognition of two MAX effectors by integrated HMA domains in plant immune receptors involves distinct binding surfaces. *PNAS*, *115*(45), 11637–11642. https://doi.org/10.1073/pnas.1810705115
77. Maidment, J. H. R., Franceschetti, M., Maqbool, A., Saitoh, H., Jantasuriyarat, C., Kamoun, S., Terauchi, R., & Banfield, M. J. (2021). Multiple variants of the fungal effector AVR-Pik bind the HMA domain of the rice protein OsHIPP19, providing a foundation to engineer plant defense. *Journal of Biological Chemistry*, *296*, 100371. https://doi.org/10.1016/j.jbc.2021.100371
78. Maqbool, A., Saitoh, H., Franceschetti, M., Stevenson, C. E. M., Uemura, A., Kanzaki, H., Kamoun, S., Terauchi, R., & Banfield, M. J. (2015). Structural basis of pathogen recognition by an integrated HMA domain in a plant NLR immune receptor. *Elife*, *4*, e08709. https://doi.org/10.7554/eLife.08709
79. Were, V., Yan, X., Foster, A. J., Sklenar, J., Langner, T., Bentham, A., Zdrzałek, R., Ryder, L., Kaimenyi, D., Gomez De La Cruz, D., Gentle, A., Petit-Houdenot, Y., Eseola, A. B., Smoker, M., Bautista, M. J., Ma, W., Kourelis, J., Maclean, D., Banfield, M. J., … Talbot, N. J. (2024). The blast effector Pwl2 is a virulence factor that modifies the cellular localisation of host protein HIPP43 to suppress immunity. *BioRxiv*, 2024.2001.2020.576406. https://doi.org/10.1101/2024.01.20.576406
80. Zdrzałek, R., Xi, Y., Langner, T., Bentham, A. R., Petit-Houdenot, Y., De la Concepcion, J. C., Harant, A., Shimizu, M., Were, V., Talbot, N. J., Terauchi, R., Kamoun, S., & Banfield, M. J. (2024). Bioengineering a plant NLR immune receptor with a robust binding interface toward a conserved fungal pathogen effector. *Proceedings of the National Academy of Sciences*, *121*(28), e2402872121. https://doi.org/10.1073/pnas.2402872121
81. Ryder, L. S., Dagdas, Y. F., Kershaw, M. J., Venkataraman, C., Madzvamuse, A., Yan, X., Cruz-Mireles, N., Soanes, D. M., Oses-Ruiz, M., Styles, V., Sklenar, J., Menke, F. L. H., & Talbot, N. J. (2019). A sensor kinase controls turgor-driven plant infection by the rice blast fungus. *Nature*, *574*(7778), 423–427. https://doi.org/10.1038/s41586-019-1637-x
82. Foster, A. J., Martin-Urdiroz, M., Yan, X., Wright, H. S., Soanes, D. M., & Talbot, N. J. (2018). CRISPR-Cas9 ribonucleoprotein-mediated co-editing and counterselection in the rice blast fungus. *Scientific Reports*, *8*(1), 14355. https://doi.org/10.1038/s41598-018-32702-w

83. Czymmek, K. J., Bourett, T. M., Sweigard, J. A., Carroll, A., & Howard, R. J. (2002). Utility of cytoplasmic fluorescent proteins for live-cell imaging of *Magnaporthe grisea* in planta. *Mycologia*, *94*(2), 280–289. https://doi.org/10.1080/15572536.2003.11833234
84. Giraldo, M. C., & Valent, B. (2013). Filamentous plant pathogen effectors in action. *Nature Reviews Microbiology*, *11*(11), 800–814. https://doi.org/10.1038/nrmicro3119
85. Henty-Ridilla, J. L., Shimono, M., Li, J., Chang, J. H., Day, B., & Staiger, C. J. (2013). The plant actin cytoskeleton responds to signals from microbe-associated molecular patterns. *Plos Pathogens*, *9*(4), e1003290. https://doi.org/10.1371/journal.ppat.1003290
86. Oreopoulos, J., Berman, R., & Browne, M. (2014). Spinning-disk confocal microscopy: Present technology and future trends. *Methods in Cell Biology*, *123*, 153–175. https://doi.org/10.1016/b978-0-12-420138-5.00009-4
87. Bourett, T. M., Sweigard, J. A., Czymmek, K. J., Carroll, A., & Howard, R. J. (2002). Reef coral fluorescent proteins for visualizing fungal pathogens. *Fungal Genetics and Biology*, *37*(3), 211–220. https://doi.org/10.1016/s1087-1845(02)00524-8
88. Czymmek, K. J., Fogg, M., Powell, D. H., Sweigard, J., Park, S.-Y., & Kang, S. (2007). In vivo time-lapse documentation using confocal and multi-photon microscopy reveals the mechanisms of invasion into the Arabidopsis root vascular system by *Fusarium oxysporum*. *Fungal Genetics and Biology*, *44*(10), 1011–1023. https://doi.org/10.1016/j.fgb.2007.01.012
89. Larson, A. M. (2011). Multiphoton microscopy. *Nature Photonics*, *5*(1), 1–1. https://doi.org/10.1038/nphoton.an.2010.2
90. Mizuta, Y. (2021). Advances in two-photon imaging in plants. *Plant and Cell Physiology*, *62*(8), 1224–1230. https://doi.org/10.1093/pcp/pcab062
91. Mizuta, Y., Kurihara, D., & Higashiyama, T. (2015). Two-photon imaging with longer wavelength excitation in intact Arabidopsis tissues. *Protoplasma*, *252*(5), 1231–1240. https://doi.org/10.1007/s00709-014-0754-5
92. Keller, P. J., & Dodt, H. U. (2012). Light sheet microscopy of living or cleared specimens. *Current Opinion in Neurobiology*, *22*(1), 138–143. https://doi.org/10.1016/j.conb.2011.08.003
93. Ovečka, M., Sojka, J., Tichá, M., Komis, G., Basheer, J., Marchetti, C., Šamajová, O., Kuběnová, L., & Šamaj, J. (2022). Imaging plant cells and organs with light-sheet and super-resolution microscopy. *Plant Physiology*, *188*(2), 683–702. https://doi.org/10.1093/plphys/kiab349
94. Gustafsson, M. G. (2000). Surpassing the lateral resolution limit by a factor of two using structured illumination microscopy. *Journal of Microscopy*, *198*(Pt 2), 82–87. https://doi.org/10.1046/j.1365-2818.2000.00710.x
95. Lin, R., Kipreos, E. T., Zhu, J., Khang, C. H., & Kner, P. (2021). Subcellular three-dimensional imaging deep through multicellular thick samples by structured illumination microscopy and adaptive optics. *Nature Communications*, *12*(1), 3148. https://doi.org/10.1038/s41467-021-23449-6
96. Wu, Y., & Shroff, H. (2018). Faster, sharper, and deeper: Structured illumination microscopy for biological imaging. *Nature Methods*, *15*(12), 1011–1019. https://doi.org/10.1038/s41592-018-0211-z
97. Huff, J. (2015). The Airyscan detector from ZEISS: Confocal imaging with improved signal-to-noise ratio and super-resolution. *Nature Methods*, *12*(12), i–ii. https://doi.org/10.1038/nmeth.f.388
98. Fitzgibbon, J., Bell, K., King, E., & Oparka, K. (2010). Super-resolution imaging of plasmodesmata using three-dimensional structured illumination microscopy. *Plant Physiology*, *153*(4), 1453–1463. https://doi.org/10.1104/pp.110.157941

How to cite this article: Quime, B. G., Ryder, L. S., & Talbot, N. J. (2025). Live cell imaging of plant infection provides new insight into the biology of pathogenesis by the rice blast fungus *Magnaporthe oryzae*. *Journal of Microscopy*, *297*, 274–288. https://doi.org/10.1111/jmi.13382

Appendix Table 1 Fluorescence screening and GFP copy number determination in rice cv. Kitaake T_0 lines expressing GFP-tagged subcellular markers.

ID	Species	Backbone	Accession	Code	Construct	Generation	Clone No.	Fluorescence	GFP copy no.
OST67_1	*O. sativa*	pGWB502	Kitaake	SLNT67	35S:OsAra6:GFP:Nos	T0	1-1	+	2
OST67_2	*O. sativa*	pGWB502	Kitaake	SLNT67	35S:OsAra6:GFP:Nos	T0	1-2	-	
OST67_3	*O. sativa*	pGWB502	Kitaake	SLNT67	35S:OsAra6:GFP:Nos	T0	1-3	-	
OST67_4	*O. sativa*	pGWB502	Kitaake	SLNT67	35S:OsAra6:GFP:Nos	T0	1-4	-	
OST67_5	*O. sativa*	pGWB502	Kitaake	SLNT67	35S:OsAra6:GFP:Nos	T0	4-1	-	
OST67_6	*O. sativa*	pGWB502	Kitaake	SLNT67	35S:OsAra6:GFP:Nos	T0	4-2	-	
OST67_7	*O. sativa*	pGWB502	Kitaake	SLNT67	35S:OsAra6:GFP:Nos	T0	4-3	+	21
OST67_8	*O. sativa*	pGWB502	Kitaake	SLNT67	35S:OsAra6:GFP:Nos	T0	4-4	+	23
OST67_9	*O. sativa*	pGWB502	Kitaake	SLNT67	35S:OsAra6:GFP:Nos	T0	5-1	-	
OST67_10	*O. sativa*	pGWB502	Kitaake	SLNT67	35S:OsAra6:GFP:Nos	T0	7-1	-	
OST67_11	*O. sativa*	pGWB502	Kitaake	SLNT67	35S:OsAra6:GFP:Nos	T0	9-1	-	
OST67_12	*O. sativa*	pGWB502	Kitaake	SLNT67	35S:OsAra6:GFP:Nos	T0	13-1	-	
OST67_13	*O. sativa*	pGWB502	Kitaake	SLNT67	35S:OsAra6:GFP:Nos	T0	14-1	-	
OST67_14	*O. sativa*	pGWB502	Kitaake	SLNT67	35S:OsAra6:GFP:Nos	T0	15-1	+	1
OST67_15	*O. sativa*	pGWB502	Kitaake	SLNT67	35S:OsAra6:GFP:Nos	T0	15-2	+	3
OST67_16	*O. sativa*	pGWB502	Kitaake	SLNT67	35S:OsAra6:GFP:Nos	T0	17-1	-	
OST70_1	*O. sativa*	pICSL4723	Kitaake	SLNT70	35S:LTI6b TMD:GFP:Nos	T0	1-1	-	
OST70_2	*O. sativa*	pICSL4723	Kitaake	SLNT70	35S:LTI6b TMD:GFP:Nos	T0	1-2	-	
OST70_3	*O. sativa*	pICSL4723	Kitaake	SLNT70	35S:LTI6b TMD:GFP:Nos	T0	1-3	+	1
OST70_4	*O. sativa*	pICSL4723	Kitaake	SLNT70	35S:LTI6b TMD:GFP:Nos	T0	1-4	-	
OST70_5	*O. sativa*	pICSL4723	Kitaake	SLNT70	35S:LTI6b TMD:GFP:Nos	T0	2-1	-	0
OST70_6	*O. sativa*	pICSL4723	Kitaake	SLNT70	35S:LTI6b TMD:GFP:Nos	T0	3-1	-	
OST70_7	*O. sativa*	pICSL4723	Kitaake	SLNT70	35S:LTI6b TMD:GFP:Nos	T0	3-2	-	
OST70_8	*O. sativa*	pICSL4723	Kitaake	SLNT70	35S:LTI6b TMD:GFP:Nos	T0	3-3	-	

ID	Species	Backbone	Accession	Code	Construct	Generation	Clone No.	Fluorescence	GFP copy no.
OST70_9	*O. sativa*	pICSL4723	Kitaake	SLNT70	35S:LTI6b TMD:GFP:Nos	T0	5-1	-	
OST70_10	*O. sativa*	pICSL4723	Kitaake	SLNT70	35S:LTI6b TMD:GFP:Nos	T0	6-1	-	
OST70_11	*O. sativa*	pICSL4723	Kitaake	SLNT70	35S:LTI6b TMD:GFP:Nos	T0	6-2	-	
OST70_12	*O. sativa*	pICSL4723	Kitaake	SLNT70	35S:LTI6b TMD:GFP:Nos	T0	6-3	-	
OST70_13	*O. sativa*	pICSL4723	Kitaake	SLNT70	35S:LTI6b TMD:GFP:Nos	T0	8-1	+	1
OST70_14	*O. sativa*	pICSL4723	Kitaake	SLNT70	35S:LTI6b TMD:GFP:Nos	T0	8-2	+	1
OST70_15	*O. sativa*	pICSL4723	Kitaake	SLNT70	35S:LTI6b TMD:GFP:Nos	T0	8-3	+	1
OST70_16	*O. sativa*	pICSL4723	Kitaake	SLNT70	35S:LTI6b TMD:GFP:Nos	T0	8-4	+	1
OST70_17	*O. sativa*	pICSL4723	Kitaake	SLNT70	35S:LTI6b TMD:GFP:Nos	T0	9-1	-	
OST70_18	*O. sativa*	pICSL4723	Kitaake	SLNT70	35S:LTI6b TMD:GFP:Nos	T0	10-1	-	
OST70_19	*O. sativa*	pICSL4723	Kitaake	SLNT70	35S:LTI6b TMD:GFP:Nos	T0	10-2	+	2
OST70_20	*O. sativa*	pICSL4723	Kitaake	SLNT70	35S:LTI6b TMD:GFP:Nos	T0	10-3	-	
OST70_21	*O. sativa*	pICSL4723	Kitaake	SLNT70	35S:LTI6b TMD:GFP:Nos	T0	10-4	-	
OST70_22	*O. sativa*	pICSL4723	Kitaake	SLNT70	35S:LTI6b TMD:GFP:Nos	T0	12-1	-	
OST70_23	*O. sativa*	pICSL4723	Kitaake	SLNT70	35S:LTI6b TMD:GFP:Nos	T0	13-1	+	3
OST70_24	*O. sativa*	pICSL4723	Kitaake	SLNT70	35S:LTI6b TMD:GFP:Nos	T0	13-2	+	3
OST70_25	*O. sativa*	pICSL4723	Kitaake	SLNT70	35S:LTI6b TMD:GFP:Nos	T0	13-3	+	3
OST70_26	*O. sativa*	pICSL4723	Kitaake	SLNT70	35S:LTI6b TMD:GFP:Nos	T0	14-1	+	6
OST70_27	*O. sativa*	pICSL4723	Kitaake	SLNT70	35S:LTI6b TMD:GFP:Nos	T0	14-2	+	2
OST70_28	*O. sativa*	pICSL4723	Kitaake	SLNT70	35S:LTI6b TMD:GFP:Nos	T0	14-3	-	
OST70_29	*O. sativa*	pICSL4723	Kitaake	SLNT70	35S:LTI6b TMD:GFP:Nos	T0	15-1	-	
OST70_30	*O. sativa*	pICSL4723	Kitaake	SLNT70	35S:LTI6b TMD:GFP:Nos	T0	16-1	+	3
OST70_31	*O. sativa*	pICSL4723	Kitaake	SLNT70	35S:LTI6b TMD:GFP:Nos	T0	16-2	+	3
OST70_32	*O. sativa*	pICSL4723	Kitaake	SLNT70	35S:LTI6b TMD:GFP:Nos	T0	17-1	-	
OST70_33	*O. sativa*	pICSL4723	Kitaake	SLNT70	35S:LTI6b TMD:GFP:Nos	T0	18-1	+	6
OST70_34	*O. sativa*	pICSL4723	Kitaake	SLNT70	35S:LTI6b TMD:GFP:Nos	T0	19-1	-	
OST70_35	*O. sativa*	pICSL4723	Kitaake	SLNT70	35S:LTI6b TMD:GFP:Nos	T0	20-1	-	
OST70_36	*O. sativa*	pICSL4723	Kitaake	SLNT70	35S:LTI6b TMD:GFP:Nos	T0	21-1	+	1

ID	Species	Backbone	Accession	Code	Construct	Generation	Clone No.	Fluorescence	GFP copy no.
OST70_37	*O. sativa*	pICSL4723	Kitaake	SLNT70	35S:LTI6b TMD:GFP:Nos	T0	21-2	+	2
OST70_38	*O. sativa*	pICSL4723	Kitaake	SLNT70	35S:LTI6b TMD:GFP:Nos	T0	21-3	-	
OST70_39	*O. sativa*	pICSL4723	Kitaake	SLNT70	35S:LTI6b TMD:GFP:Nos	T0	22-1	-	
OST70_40	*O. sativa*	pICSL4723	Kitaake	SLNT70	35S:LTI6b TMD:GFP:Nos	T0	22-2	-	
OST70_41	*O. sativa*	pICSL4723	Kitaake	SLNT70	35S:LTI6b TMD:GFP:Nos	T0	22-3	-	
OST70_42	*O. sativa*	pICSL4723	Kitaake	SLNT70	35S:LTI6b TMD:GFP:Nos	T0	23-1	-	
OST70_43	*O. sativa*	pICSL4723	Kitaake	SLNT70	35S:LTI6b TMD:GFP:Nos	T0	24-1	-	
OST70_44	*O. sativa*	pICSL4723	Kitaake	SLNT70	35S:LTI6b TMD:GFP:Nos	T0	25-1	-	
OST70_45	*O. sativa*	pICSL4723	Kitaake	SLNT70	35S:LTI6b TMD:GFP:Nos	T0	25-2	-	
OST70_46	*O. sativa*	pICSL4723	Kitaake	SLNT70	35S:LTI6b TMD:GFP:Nos	T0	26-1	-	
OST70_47	*O. sativa*	pICSL4723	Kitaake	SLNT70	35S:LTI6b TMD:GFP:Nos	T0	26-2	-	
OST70_48	*O. sativa*	pICSL4723	Kitaake	SLNT70	35S:LTI6b TMD:GFP:Nos	T0	26-3	+	1
OST70_49	*O. sativa*	pICSL4723	Kitaake	SLNT70	35S:LTI6b TMD:GFP:Nos	T0	27-1	-	
OST70_50	*O. sativa*	pICSL4723	Kitaake	SLNT70	35S:LTI6b TMD:GFP:Nos	T0	27-2	-	
OST70_51	*O. sativa*	pICSL4723	Kitaake	SLNT70	35S:LTI6b TMD:GFP:Nos	T0	28-1	+	2
OST70_52	*O. sativa*	pICSL4723	Kitaake	SLNT70	35S:LTI6b TMD:GFP:Nos	T0	29-1	-	
OST70_53	*O. sativa*	pICSL4723	Kitaake	SLNT70	35S:LTI6b TMD:GFP:Nos	T0	30-1	+	1
OST70_54	*O. sativa*	pICSL4723	Kitaake	SLNT70	35S:LTI6b TMD:GFP:Nos	T0	30-2	-	
OST70_55	*O. sativa*	pICSL4723	Kitaake	SLNT70	35S:LTI6b TMD:GFP:Nos	T0	31-1	-	
OST70_56	*O. sativa*	pICSL4723	Kitaake	SLNT70	35S:LTI6b TMD:GFP:Nos	T0	31-2	-	
OST70_57	*O. sativa*	pICSL4723	Kitaake	SLNT70	35S:LTI6b TMD:GFP:Nos	T0	31-3	-	
OST70_58	*O. sativa*	pICSL4723	Kitaake	SLNT70	35S:LTI6b TMD:GFP:Nos	T0	31-4	-	
OST70_59	*O. sativa*	pICSL4723	Kitaake	SLNT70	35S:LTI6b TMD:GFP:Nos	T0	32-1	-	
OST70_60	*O. sativa*	pICSL4723	Kitaake	SLNT70	35S:LTI6b TMD:GFP:Nos	T0	34-1	-	
OST70_61	*O. sativa*	pICSL4723	Kitaake	SLNT70	35S:LTI6b TMD:GFP:Nos	T0	35-1	-	
OST70_62	*O. sativa*	pICSL4723	Kitaake	SLNT70	35S:LTI6b TMD:GFP:Nos	T0	36-1	-	
OST70_63	*O. sativa*	pICSL4723	Kitaake	SLNT70	35S:LTI6b TMD:GFP:Nos	T0	37-1	-	
OST70_64	*O. sativa*	pICSL4723	Kitaake	SLNT70	35S:LTI6b TMD:GFP:Nos	T0	38-1	-	

ID	Species	Backbone	Accession	Code	Construct	Generation	Clone No.	Fluorescence	GFP copy no.
OST70_65	*O. sativa*	pICSL4723	Kitaake	SLNT70	35S:LTI6b TMD:GFP:Nos	T0	39-1	-	
OST70_66	*O. sativa*	pICSL4723	Kitaake	SLNT70	35S:LTI6b TMD:GFP:Nos	T0	39-2	-	
OST70_67	*O. sativa*	pICSL4723	Kitaake	SLNT70	35S:LTI6b TMD:GFP:Nos	T0	40-1	+	2
OST70_68	*O. sativa*	pICSL4723	Kitaake	SLNT70	35S:LTI6b TMD:GFP:Nos	T0	41-1	-	
OST71_1	*O. sativa*	pICSL4723	Kitaake	SLNT71	35S:COXIV:GFP:Nos	T0	1-1	-	
OST71_2	*O. sativa*	pICSL4723	Kitaake	SLNT71	35S:COXIV:GFP:Nos	T0	1-2	+	2
OST71_3	*O. sativa*	pICSL4723	Kitaake	SLNT71	35S:COXIV:GFP:Nos	T0	1-3	+	2
OST71_4	*O. sativa*	pICSL4723	Kitaake	SLNT71	35S:COXIV:GFP:Nos	T0	1-4	-	
OST71_5	*O. sativa*	pICSL4723	Kitaake	SLNT71	35S:COXIV:GFP:Nos	T0	2-1	+	1
OST71_6	*O. sativa*	pICSL4723	Kitaake	SLNT71	35S:COXIV:GFP:Nos	T0	2-2	-	
OST71_7	*O. sativa*	pICSL4723	Kitaake	SLNT71	35S:COXIV:GFP:Nos	T0	3-1	+	1
OST71_8	*O. sativa*	pICSL4723	Kitaake	SLNT71	35S:COXIV:GFP:Nos	T0	4-1	-	
OST71_9	*O. sativa*	pICSL4723	Kitaake	SLNT71	35S:COXIV:GFP:Nos	T0	4-2	+	2
OST71_10	*O. sativa*	pICSL4723	Kitaake	SLNT71	35S:COXIV:GFP:Nos	T0	5-1	+	1
OST71_11	*O. sativa*	pICSL4723	Kitaake	SLNT71	35S:COXIV:GFP:Nos	T0	5-2	+	1
OST71_12	*O. sativa*	pICSL4723	Kitaake	SLNT71	35S:COXIV:GFP:Nos	T0	6-1	+	3
OST71_13	*O. sativa*	pICSL4723	Kitaake	SLNT71	35S:COXIV:GFP:Nos	T0	7-1	-	
OST71_14	*O. sativa*	pICSL4723	Kitaake	SLNT71	35S:COXIV:GFP:Nos	T0	8-1	+	1
OST71_15	*O. sativa*	pICSL4723	Kitaake	SLNT71	35S:COXIV:GFP:Nos	T0	8-2	+	1
OST71_16	*O. sativa*	pICSL4723	Kitaake	SLNT71	35S:COXIV:GFP:Nos	T0	8-3	+	1
OST71_17	*O. sativa*	pICSL4723	Kitaake	SLNT71	35S:COXIV:GFP:Nos	T0	8-4	-	
OST71_18	*O. sativa*	pICSL4723	Kitaake	SLNT71	35S:COXIV:GFP:Nos	T0	10-1	+	1
OST71_19	*O. sativa*	pICSL4723	Kitaake	SLNT71	35S:COXIV:GFP:Nos	T0	10-2	+	1
OST71_20	*O. sativa*	pICSL4723	Kitaake	SLNT71	35S:COXIV:GFP:Nos	T0	11-1	+	1
OST71_21	*O. sativa*	pICSL4723	Kitaake	SLNT71	35S:COXIV:GFP:Nos	T0	12-1	+	1
OST71_22	*O. sativa*	pICSL4723	Kitaake	SLNT71	35S:COXIV:GFP:Nos	T0	12-2	+	1
OST71_23	*O. sativa*	pICSL4723	Kitaake	SLNT71	35S:COXIV:GFP:Nos	T0	13-1	+	1
OST71_24	*O. sativa*	pICSL4723	Kitaake	SLNT71	35S:COXIV:GFP:Nos	T0	13-2	+	1

ID	Species	Backbone	Accession	Code	Construct	Generation	Clone No.	Fluorescence	GFP copy no.
OST71_25	*O. sativa*	pICSL4723	Kitaake	SLNT71	35S:COXIV:GFP:Nos	T0	13-3	+	1
OST71_26	*O. sativa*	pICSL4723	Kitaake	SLNT71	35S:COXIV:GFP:Nos	T0	13-4	+	1
OST71_27	*O. sativa*	pICSL4723	Kitaake	SLNT71	35S:COXIV:GFP:Nos	T0	14-1	+	1
OST71_28	*O. sativa*	pICSL4723	Kitaake	SLNT71	35S:COXIV:GFP:Nos	T0	15-1	+	1
OST71_29	*O. sativa*	pICSL4723	Kitaake	SLNT71	35S:COXIV:GFP:Nos	T0	16-1	-	
OST71_30	*O. sativa*	pICSL4723	Kitaake	SLNT71	35S:COXIV:GFP:Nos	T0	16-2	-	
OST71_31	*O. sativa*	pICSL4723	Kitaake	SLNT71	35S:COXIV:GFP:Nos	T0	16-3	-	
OST71_32	*O. sativa*	pICSL4723	Kitaake	SLNT71	35S:COXIV:GFP:Nos	T0	17-1	+	1
OST71_33	*O. sativa*	pICSL4723	Kitaake	SLNT71	35S:COXIV:GFP:Nos	T0	17-2	+	1
OST71_34	*O. sativa*	pICSL4723	Kitaake	SLNT71	35S:COXIV:GFP:Nos	T0	17-3	+	1
OST71_35	*O. sativa*	pICSL4723	Kitaake	SLNT71	35S:COXIV:GFP:Nos	T0	17-4	+	1
OST71_36	*O. sativa*	pICSL4723	Kitaake	SLNT71	35S:COXIV:GFP:Nos	T0	18-1	-	
OST71_37	*O. sativa*	pICSL4723	Kitaake	SLNT71	35S:COXIV:GFP:Nos	T0	19-1	-	
OST71_38	*O. sativa*	pICSL4723	Kitaake	SLNT71	35S:COXIV:GFP:Nos	T0	21-1	+	1
OST71_39	*O. sativa*	pICSL4723	Kitaake	SLNT71	35S:COXIV:GFP:Nos	T0	21-2	+	1
OST71_40	*O. sativa*	pICSL4723	Kitaake	SLNT71	35S:COXIV:GFP:Nos	T0	22-1	+	1
OST71_41	*O. sativa*	pICSL4723	Kitaake	SLNT71	35S:COXIV:GFP:Nos	T0	22-2	+	1
OST71_42	*O. sativa*	pICSL4723	Kitaake	SLNT71	35S:COXIV:GFP:Nos	T0	23-1	-	
OST71_43	*O. sativa*	pICSL4723	Kitaake	SLNT71	35S:COXIV:GFP:Nos	T0	24-1	-	
OST71_44	*O. sativa*	pICSL4723	Kitaake	SLNT71	35S:COXIV:GFP:Nos	T0	25-1	+	1
OST71_45	*O. sativa*	pICSL4723	Kitaake	SLNT71	35S:COXIV:GFP:Nos	T0	26-1	-	
OST71_46	*O. sativa*	pICSL4723	Kitaake	SLNT71	35S:COXIV:GFP:Nos	T0	27-1	-	
OST71_47	*O. sativa*	pICSL4723	Kitaake	SLNT71	35S:COXIV:GFP:Nos	T0	28-1	-	
OST71_48	*O. sativa*	pICSL4723	Kitaake	SLNT71	35S:COXIV:GFP:Nos	T0	29-1	-	
OST71_49	*O. sativa*	pICSL4723	Kitaake	SLNT71	35S:COXIV:GFP:Nos	T0	30-1	-	
OST71_50	*O. sativa*	pICSL4723	Kitaake	SLNT71	35S:COXIV:GFP:Nos	T0	31-1	+	2
OST71_51	*O. sativa*	pICSL4723	Kitaake	SLNT71	35S:COXIV:GFP:Nos	T0	32-1	-	
OST71_52	*O. sativa*	pICSL4723	Kitaake	SLNT71	35S:COXIV:GFP:Nos	T0	33-1	-	

ID	Species	Backbone	Accession	Code	Construct	Generation	Clone No.	Fluorescence	GFP copy no.
OST71_53	*O. sativa*	pICSL4723	Kitaake	SLNT71	35S:COXIV:GFP:Nos	T0	34-1	+	4
OST71_54	*O. sativa*	pICSL4723	Kitaake	SLNT71	35S:COXIV:GFP:Nos	T0	35-1	+	1
OST71_55	*O. sativa*	pICSL4723	Kitaake	SLNT71	35S:COXIV:GFP:Nos	T0	36-1	-	
OST73_1	*O. sativa*	pICSL4723	Kitaake	SLNT73	ZmUbi:GFP:Ara7:Nos	T0	1-1	-	
OST73_2	*O. sativa*	pICSL4723	Kitaake	SLNT73	ZmUbi:GFP:Ara7:Nos	T0	2-1	-	
OST73_3	*O. sativa*	pICSL4723	Kitaake	SLNT73	ZmUbi:GFP:Ara7:Nos	T0	3-1	-	
OST73_4	*O. sativa*	pICSL4723	Kitaake	SLNT73	ZmUbi:GFP:Ara7:Nos	T0	3-2	-	
OST73_5	*O. sativa*	pICSL4723	Kitaake	SLNT73	ZmUbi:GFP:Ara7:Nos	T0	4-1	-	
OST73_6	*O. sativa*	pICSL4723	Kitaake	SLNT73	ZmUbi:GFP:Ara7:Nos	T0	4-2	-	
OST73_7	*O. sativa*	pICSL4723	Kitaake	SLNT73	ZmUbi:GFP:Ara7:Nos	T0	4-3	-	
OST73_8	*O. sativa*	pICSL4723	Kitaake	SLNT73	ZmUbi:GFP:Ara7:Nos	T0	4-4	+	1
OST73_9	*O. sativa*	pICSL4723	Kitaake	SLNT73	ZmUbi:GFP:Ara7:Nos	T0	5-1	+	3
OST73_10	*O. sativa*	pICSL4723	Kitaake	SLNT73	ZmUbi:GFP:Ara7:Nos	T0	5-2	+	1
OST73_11	*O. sativa*	pICSL4723	Kitaake	SLNT73	ZmUbi:GFP:Ara7:Nos	T0	5-3	-	
OST73_12	*O. sativa*	pICSL4723	Kitaake	SLNT73	ZmUbi:GFP:Ara7:Nos	T0	5-4	-	
OST73_13	*O. sativa*	pICSL4723	Kitaake	SLNT73	ZmUbi:GFP:Ara7:Nos	T0	6-1	-	
OST73_14	*O. sativa*	pICSL4723	Kitaake	SLNT73	ZmUbi:GFP:Ara7:Nos	T0	6-2	+	1
OST73_15	*O. sativa*	pICSL4723	Kitaake	SLNT73	ZmUbi:GFP:Ara7:Nos	T0	6-3	-	
OST73_16	*O. sativa*	pICSL4723	Kitaake	SLNT73	ZmUbi:GFP:Ara7:Nos	T0	7-1	+	2
OST73_17	*O. sativa*	pICSL4723	Kitaake	SLNT73	ZmUbi:GFP:Ara7:Nos	T0	7-2	-	
OST73_18	*O. sativa*	pICSL4723	Kitaake	SLNT73	ZmUbi:GFP:Ara7:Nos	T0	8-1	-	
OST73_19	*O. sativa*	pICSL4723	Kitaake	SLNT73	ZmUbi:GFP:Ara7:Nos	T0	8-2	-	
OST73_20	*O. sativa*	pICSL4723	Kitaake	SLNT73	ZmUbi:GFP:Ara7:Nos	T0	8-3	-	
OST73_21	*O. sativa*	pICSL4723	Kitaake	SLNT73	ZmUbi:GFP:Ara7:Nos	T0	9-1	-	
OST73_22	*O. sativa*	pICSL4723	Kitaake	SLNT73	ZmUbi:GFP:Ara7:Nos	T0	10-1	+	2
OST73_23	*O. sativa*	pICSL4723	Kitaake	SLNT73	ZmUbi:GFP:Ara7:Nos	T0	10-2	-	
OST73_24	*O. sativa*	pICSL4723	Kitaake	SLNT73	ZmUbi:GFP:Ara7:Nos	T0	11-1	-	
OST73_25	*O. sativa*	pICSL4723	Kitaake	SLNT73	ZmUbi:GFP:Ara7:Nos	T0	12-1	+	1

ID	Species	Backbone	Accession	Code	Construct	Generation	Clone No.	Fluorescence	GFP copy no.
OST73_26	*O. sativa*	pICSL4723	Kitaake	SLNT73	ZmUbi:GFP:Ara7:Nos	T0	12-2	+	1
OST73_27	*O. sativa*	pICSL4723	Kitaake	SLNT73	ZmUbi:GFP:Ara7:Nos	T0	12-3	-	
OST73_28	*O. sativa*	pICSL4723	Kitaake	SLNT73	ZmUbi:GFP:Ara7:Nos	T0	14-1	+	2
OST73_29	*O. sativa*	pICSL4723	Kitaake	SLNT73	ZmUbi:GFP:Ara7:Nos	T0	15-1	+	1
OST73_30	*O. sativa*	pICSL4723	Kitaake	SLNT73	ZmUbi:GFP:Ara7:Nos	T0	16-1	-	
OST73_31	*O. sativa*	pICSL4723	Kitaake	SLNT73	ZmUbi:GFP:Ara7:Nos	T0	16-2	+	3
OST73_32	*O. sativa*	pICSL4723	Kitaake	SLNT73	ZmUbi:GFP:Ara7:Nos	T0	16-3	+	3
OST73_33	*O. sativa*	pICSL4723	Kitaake	SLNT73	ZmUbi:GFP:Ara7:Nos	T0	17-1	-	
OST73_34	*O. sativa*	pICSL4723	Kitaake	SLNT73	ZmUbi:GFP:Ara7:Nos	T0	17-2	+	1
OST73_35	*O. sativa*	pICSL4723	Kitaake	SLNT73	ZmUbi:GFP:Ara7:Nos	T0	18-1	+	1
OST73_36	*O. sativa*	pICSL4723	Kitaake	SLNT73	ZmUbi:GFP:Ara7:Nos	T0	19-1	+	2
OST73_37	*O. sativa*	pICSL4723	Kitaake	SLNT73	ZmUbi:GFP:Ara7:Nos	T0	19-2	+	2
OST73_38	*O. sativa*	pICSL4723	Kitaake	SLNT73	ZmUbi:GFP:Ara7:Nos	T0	19-3	+	2
OST73_39	*O. sativa*	pICSL4723	Kitaake	SLNT73	ZmUbi:GFP:Ara7:Nos	T0	20-1	+	2
OST73_40	*O. sativa*	pICSL4723	Kitaake	SLNT73	ZmUbi:GFP:Ara7:Nos	T0	21-1	-	
OST73_41	*O. sativa*	pICSL4723	Kitaake	SLNT73	ZmUbi:GFP:Ara7:Nos	T0	22-1	-	
OST73_42	*O. sativa*	pICSL4723	Kitaake	SLNT73	ZmUbi:GFP:Ara7:Nos	T0	24-1	+	2
OST73_43	*O. sativa*	pICSL4723	Kitaake	SLNT73	ZmUbi:GFP:Ara7:Nos	T0	24-2	+	2
OST73_44	*O. sativa*	pICSL4723	Kitaake	SLNT73	ZmUbi:GFP:Ara7:Nos	T0	24-3	+	2
OST73_45	*O. sativa*	pICSL4723	Kitaake	SLNT73	ZmUbi:GFP:Ara7:Nos	T0	24-4	+	2
OST73_46	*O. sativa*	pICSL4723	Kitaake	SLNT73	ZmUbi:GFP:Ara7:Nos	T0	25-1	-	
OST73_47	*O. sativa*	pICSL4723	Kitaake	SLNT73	ZmUbi:GFP:Ara7:Nos	T0	25-2	-	
OST73_48	*O. sativa*	pICSL4723	Kitaake	SLNT73	ZmUbi:GFP:Ara7:Nos	T0	26-1	-	
OST73_49	*O. sativa*	pICSL4723	Kitaake	SLNT73	ZmUbi:GFP:Ara7:Nos	T0	26-2	+	1
OST73_50	*O. sativa*	pICSL4723	Kitaake	SLNT73	ZmUbi:GFP:Ara7:Nos	T0	27-1	-	
OST73_51	*O. sativa*	pICSL4723	Kitaake	SLNT73	ZmUbi:GFP:Ara7:Nos	T0	28-1	-	
OST73_52	*O. sativa*	pICSL4723	Kitaake	SLNT73	ZmUbi:GFP:Ara7:Nos	T0	29-1	-	
OST73_53	*O. sativa*	pICSL4723	Kitaake	SLNT73	ZmUbi:GFP:Ara7:Nos	T0	29-2	+	1

ID	Species	Backbone	Accession	Code	Construct	Generation	Clone No.	Fluorescence	GFP copy no.
OST73_54	*O. sativa*	pICSL4723	Kitaake	SLNT73	ZmUbi:GFP:Ara7:Nos	T0	29-3	-	
OST73_55	*O. sativa*	pICSL4723	Kitaake	SLNT73	ZmUbi:GFP:Ara7:Nos	T0	30-1	-	
OST73_56	*O. sativa*	pICSL4723	Kitaake	SLNT73	ZmUbi:GFP:Ara7:Nos	T0	30-2	+	1
OST73_57	*O. sativa*	pICSL4723	Kitaake	SLNT73	ZmUbi:GFP:Ara7:Nos	T0	30-3	-	
OST73_58	*O. sativa*	pICSL4723	Kitaake	SLNT73	ZmUbi:GFP:Ara7:Nos	T0	30-4	-	
OST73_59	*O. sativa*	pICSL4723	Kitaake	SLNT73	ZmUbi:GFP:Ara7:Nos	T0	31-1	-	
OST73_60	*O. sativa*	pICSL4723	Kitaake	SLNT73	ZmUbi:GFP:Ara7:Nos	T0	31-2	-	
OST73_61	*O. sativa*	pICSL4723	Kitaake	SLNT73	ZmUbi:GFP:Ara7:Nos	T0	31-3	-	
OST73_62	*O. sativa*	pICSL4723	Kitaake	SLNT73	ZmUbi:GFP:Ara7:Nos	T0	32-1	-	
OST73_63	*O. sativa*	pICSL4723	Kitaake	SLNT73	ZmUbi:GFP:Ara7:Nos	T0	33-1	+	3
OST73_64	*O. sativa*	pICSL4723	Kitaake	SLNT73	ZmUbi:GFP:Ara7:Nos	T0	34-1	-	
OST74_1	*O. sativa*	pICSL4723	Kitaake	SLNT74	ZmUbi:LifeAct:GFP:Nos	T0	1-1	-	
OST74_2	*O. sativa*	pICSL4723	Kitaake	SLNT74	ZmUbi:LifeAct:GFP:Nos	T0	1-2	-	
OST74_3	*O. sativa*	pICSL4723	Kitaake	SLNT74	ZmUbi:LifeAct:GFP:Nos	T0	2-1	+	1
OST74_4	*O. sativa*	pICSL4723	Kitaake	SLNT74	ZmUbi:LifeAct:GFP:Nos	T0	2-2	-	
OST74_5	*O. sativa*	pICSL4723	Kitaake	SLNT74	ZmUbi:LifeAct:GFP:Nos	T0	3-1	-	
OST74_6	*O. sativa*	pICSL4723	Kitaake	SLNT74	ZmUbi:LifeAct:GFP:Nos	T0	3-2	-	
OST74_7	*O. sativa*	pICSL4723	Kitaake	SLNT74	ZmUbi:LifeAct:GFP:Nos	T0	4-1	+	1
OST74_8	*O. sativa*	pICSL4723	Kitaake	SLNT74	ZmUbi:LifeAct:GFP:Nos	T0	5-1	+	1
OST74_9	*O. sativa*	pICSL4723	Kitaake	SLNT74	ZmUbi:LifeAct:GFP:Nos	T0	5-2	+	1
OST74_10	*O. sativa*	pICSL4723	Kitaake	SLNT74	ZmUbi:LifeAct:GFP:Nos	T0	5-3	+	1
OST74_11	*O. sativa*	pICSL4723	Kitaake	SLNT74	ZmUbi:LifeAct:GFP:Nos	T0	5-4	+	1
OST74_12	*O. sativa*	pICSL4723	Kitaake	SLNT74	ZmUbi:LifeAct:GFP:Nos	T0	6-1	+	less than 1
OST74_13	*O. sativa*	pICSL4723	Kitaake	SLNT74	ZmUbi:LifeAct:GFP:Nos	T0	6-2	+	less than 1
OST74_14	*O. sativa*	pICSL4723	Kitaake	SLNT74	ZmUbi:LifeAct:GFP:Nos	T0	6-3	+	less than 1
OST74_15	*O. sativa*	pICSL4723	Kitaake	SLNT74	ZmUbi:LifeAct:GFP:Nos	T0	7-1	+	1
OST74_16	*O. sativa*	pICSL4723	Kitaake	SLNT74	ZmUbi:LifeAct:GFP:Nos	T0	8-1	-	
OST74_17	*O. sativa*	pICSL4723	Kitaake	SLNT74	ZmUbi:LifeAct:GFP:Nos	T0	9-1	+	1

ID	Species	Backbone	Accession	Code	Construct	Generation	Clone No.	Fluorescence	GFP copy no.
OST74_18	*O. sativa*	pICSL4723	Kitaake	SLNT74	ZmUbi:LifeAct:GFP:Nos	T0	10-1	-	
OST74_19	*O. sativa*	pICSL4723	Kitaake	SLNT74	ZmUbi:LifeAct:GFP:Nos	T0	11-1	+	1
OST74_20	*O. sativa*	pICSL4723	Kitaake	SLNT74	ZmUbi:LifeAct:GFP:Nos	T0	11-2	+	1
OST74_21	*O. sativa*	pICSL4723	Kitaake	SLNT74	ZmUbi:LifeAct:GFP:Nos	T0	12-1	+	2
OST74_22	*O. sativa*	pICSL4723	Kitaake	SLNT74	ZmUbi:LifeAct:GFP:Nos	T0	13-1	+	2
OST74_23	*O. sativa*	pICSL4723	Kitaake	SLNT74	ZmUbi:LifeAct:GFP:Nos	T0	13-2	-	
OST74_24	*O. sativa*	pICSL4723	Kitaake	SLNT74	ZmUbi:LifeAct:GFP:Nos	T0	13-3	+	2
OST74_25	*O. sativa*	pICSL4723	Kitaake	SLNT74	ZmUbi:LifeAct:GFP:Nos	T0	13-4	+	2
OST74_26	*O. sativa*	pICSL4723	Kitaake	SLNT74	ZmUbi:LifeAct:GFP:Nos	T0	14-1	+	2
OST74_27	*O. sativa*	pICSL4723	Kitaake	SLNT74	ZmUbi:LifeAct:GFP:Nos	T0	15-1	+	1
OST74_28	*O. sativa*	pICSL4723	Kitaake	SLNT74	ZmUbi:LifeAct:GFP:Nos	T0	16-1	+	1
OST74_29	*O. sativa*	pICSL4723	Kitaake	SLNT74	ZmUbi:LifeAct:GFP:Nos	T0	17-1	-	
OST74_30	*O. sativa*	pICSL4723	Kitaake	SLNT74	ZmUbi:LifeAct:GFP:Nos	T0	17-2	-	
OST74_31	*O. sativa*	pICSL4723	Kitaake	SLNT74	ZmUbi:LifeAct:GFP:Nos	T0	17-3	+	1
OST74_32	*O. sativa*	pICSL4723	Kitaake	SLNT74	ZmUbi:LifeAct:GFP:Nos	T0	17-4	+	1
OST74_33	*O. sativa*	pICSL4723	Kitaake	SLNT74	ZmUbi:LifeAct:GFP:Nos	T0	19-1	+	2
OST74_34	*O. sativa*	pICSL4723	Kitaake	SLNT74	ZmUbi:LifeAct:GFP:Nos	T0	19-2	+	2
OST74_35	*O. sativa*	pICSL4723	Kitaake	SLNT74	ZmUbi:LifeAct:GFP:Nos	T0	19-3	+	2
OST74_36	*O. sativa*	pICSL4723	Kitaake	SLNT74	ZmUbi:LifeAct:GFP:Nos	T0	19-4	-	
OST74_37	*O. sativa*	pICSL4723	Kitaake	SLNT74	ZmUbi:LifeAct:GFP:Nos	T0	21-1	-	
OST74_38	*O. sativa*	pICSL4723	Kitaake	SLNT74	ZmUbi:LifeAct:GFP:Nos	T0	22-1	+	1
OST74_39	*O. sativa*	pICSL4723	Kitaake	SLNT74	ZmUbi:LifeAct:GFP:Nos	T0	22-2	+	1
OST74_40	*O. sativa*	pICSL4723	Kitaake	SLNT74	ZmUbi:LifeAct:GFP:Nos	T0	23-1	+	1
OST74_41	*O. sativa*	pICSL4723	Kitaake	SLNT74	ZmUbi:LifeAct:GFP:Nos	T0	23-2	-	
OST74_42	*O. sativa*	pICSL4723	Kitaake	SLNT74	ZmUbi:LifeAct:GFP:Nos	T0	24-1	+	1
OST74_43	*O. sativa*	pICSL4723	Kitaake	SLNT74	ZmUbi:LifeAct:GFP:Nos	T0	24-2	+	2
OST74_44	*O. sativa*	pICSL4723	Kitaake	SLNT74	ZmUbi:LifeAct:GFP:Nos	T0	24-3	-	
OST74_45	*O. sativa*	pICSL4723	Kitaake	SLNT74	ZmUbi:LifeAct:GFP:Nos	T0	24-4	-	

ID	Species	Backbone	Accession	Code	Construct	Generation	Clone No.	Fluorescence	GFP copy no.
OST74_46	*O. sativa*	pICSL4723	Kitaake	SLNT74	ZmUbi:LifeAct:GFP:Nos	T0	29-1	-	
OST74_47	*O. sativa*	pICSL4723	Kitaake	SLNT74	ZmUbi:LifeAct:GFP:Nos	T0	31-1	-	
OST80_1	*O. sativa*	pICSL4723	Kitaake	SLNT80	35S:NLS:GFP:Nos	T0	1-1	+	2
OST80_2	*O. sativa*	pICSL4723	Kitaake	SLNT80	35S:NLS:GFP:Nos	T0	1-2	+	2
OST80_3	*O. sativa*	pICSL4723	Kitaake	SLNT80	35S:NLS:GFP:Nos	T0	1-3	+	2
OST80_4	*O. sativa*	pICSL4723	Kitaake	SLNT80	35S:NLS:GFP:Nos	T0	1-4	+	2
OST80_5	*O. sativa*	pICSL4723	Kitaake	SLNT80	35S:NLS:GFP:Nos	T0	2-1	+	2
OST80_6	*O. sativa*	pICSL4723	Kitaake	SLNT80	35S:NLS:GFP:Nos	T0	2-2	+	2
OST80_7	*O. sativa*	pICSL4723	Kitaake	SLNT80	35S:NLS:GFP:Nos	T0	2-3	+	2
OST80_8	*O. sativa*	pICSL4723	Kitaake	SLNT80	35S:NLS:GFP:Nos	T0	3-1	+	2
OST80_9	*O. sativa*	pICSL4723	Kitaake	SLNT80	35S:NLS:GFP:Nos	T0	4-1	-	
OST80_10	*O. sativa*	pICSL4723	Kitaake	SLNT80	35S:NLS:GFP:Nos	T0	4-2	-	
OST80_11	*O. sativa*	pICSL4723	Kitaake	SLNT80	35S:NLS:GFP:Nos	T0	5-1	+	1
OST80_12	*O. sativa*	pICSL4723	Kitaake	SLNT80	35S:NLS:GFP:Nos	T0	5-2	-	
OST80_13	*O. sativa*	pICSL4723	Kitaake	SLNT80	35S:NLS:GFP:Nos	T0	5-3	+	3
OST80_14	*O. sativa*	pICSL4723	Kitaake	SLNT80	35S:NLS:GFP:Nos	T0	5-4	+	2
OST80_15	*O. sativa*	pICSL4723	Kitaake	SLNT80	35S:NLS:GFP:Nos	T0	6-1	-	
OST80_16	*O. sativa*	pICSL4723	Kitaake	SLNT80	35S:NLS:GFP:Nos	T0	6-2	+	1
OST80_17	*O. sativa*	pICSL4723	Kitaake	SLNT80	35S:NLS:GFP:Nos	T0	6-3	+	1
OST80_18	*O. sativa*	pICSL4723	Kitaake	SLNT80	35S:NLS:GFP:Nos	T0	6-4	+	3
OST80_19	*O. sativa*	pICSL4723	Kitaake	SLNT80	35S:NLS:GFP:Nos	T0	7-1	+	3
OST80_20	*O. sativa*	pICSL4723	Kitaake	SLNT80	35S:NLS:GFP:Nos	T0	8-1	-	
OST80_21	*O. sativa*	pICSL4723	Kitaake	SLNT80	35S:NLS:GFP:Nos	T0	8-1	+	1
OST80_22	*O. sativa*	pICSL4723	Kitaake	SLNT80	35S:NLS:GFP:Nos	T0	8-2	+	7
OST80_23	*O. sativa*	pICSL4723	Kitaake	SLNT80	35S:NLS:GFP:Nos	T0	11-1	-	
OST80_24	*O. sativa*	pICSL4723	Kitaake	SLNT80	35S:NLS:GFP:Nos	T0	12-1	+	3
OST80_25	*O. sativa*	pICSL4723	Kitaake	SLNT80	35S:NLS:GFP:Nos	T0	13-1	+	1
OST80_26	*O. sativa*	pICSL4723	Kitaake	SLNT80	35S:NLS:GFP:Nos	T0	13-2	-	

ID	Species	Backbone	Accession	Code	Construct	Generation	Clone No.	Fluorescence	GFP copy no.
OST80_27	*O. sativa*	pICSL4723	Kitaake	SLNT80	35S:NLS:GFP:Nos	T0	15-1	+	6 to 7
OST80_28	*O. sativa*	pICSL4723	Kitaake	SLNT80	35S:NLS:GFP:Nos	T0	16-1	-	
OST80_29	*O. sativa*	pICSL4723	Kitaake	SLNT80	35S:NLS:GFP:Nos	T0	17-1	+	1
OST80_30	*O. sativa*	pICSL4723	Kitaake	SLNT80	35S:NLS:GFP:Nos	T0	19-1	+	1
OST80_31	*O. sativa*	pICSL4723	Kitaake	SLNT80	35S:NLS:GFP:Nos	T0	19-2	+	1
OST80_32	*O. sativa*	pICSL4723	Kitaake	SLNT80	35S:NLS:GFP:Nos	T0	20-1	-	
OST80_33	*O. sativa*	pICSL4723	Kitaake	SLNT80	35S:NLS:GFP:Nos	T0	21-1	+	2
OST80_34	*O. sativa*	pICSL4723	Kitaake	SLNT80	35S:NLS:GFP:Nos	T0	24-1	+	2
OST80_35	*O. sativa*	pICSL4723	Kitaake	SLNT80	35S:NLS:GFP:Nos	T0	25-1	+	2
OST80_36	*O. sativa*	pICSL4723	Kitaake	SLNT80	35S:NLS:GFP:Nos	T0	25-2	+	2
OST80_37	*O. sativa*	pICSL4723	Kitaake	SLNT80	35S:NLS:GFP:Nos	T0	27-1	-	
OST80_38	*O. sativa*	pICSL4723	Kitaake	SLNT80	35S:NLS:GFP:Nos	T0	27-2	-	
OST80_39	*O. sativa*	pICSL4723	Kitaake	SLNT80	35S:NLS:GFP:Nos	T0	28-1	-	
OST80_40	*O. sativa*	pICSL4723	Kitaake	SLNT80	35S:NLS:GFP:Nos	T0	28-2	-	
OST80_41	*O. sativa*	pICSL4723	Kitaake	SLNT80	35S:NLS:GFP:Nos	T0	29-1	+	1
OST80_42	*O. sativa*	pICSL4723	Kitaake	SLNT80	35S:NLS:GFP:Nos	T0	29-2	+	1
OST80_43	*O. sativa*	pICSL4723	Kitaake	SLNT80	35S:NLS:GFP:Nos	T0	29-3	-	
OST80_44	*O. sativa*	pICSL4723	Kitaake	SLNT80	35S:NLS:GFP:Nos	T0	29-4	-	
OST80_45	*O. sativa*	pICSL4723	Kitaake	SLNT80	35S:NLS:GFP:Nos	T0	30-1	+	1
OST80_46	*O. sativa*	pICSL4723	Kitaake	SLNT80	35S:NLS:GFP:Nos	T0	30-2	+	1
OST80_47	*O. sativa*	pICSL4723	Kitaake	SLNT80	35S:NLS:GFP:Nos	T0	30-3		
OST80_48	*O. sativa*	pICSL4723	Kitaake	SLNT80	35S:NLS:GFP:Nos	T0	31-1	+	1
OST80_49	*O. sativa*	pICSL4723	Kitaake	SLNT80	35S:NLS:GFP:Nos	T0	32-1	+	1
OST80_50	*O. sativa*	pICSL4723	Kitaake	SLNT80	35S:NLS:GFP:Nos	T0	33-1	-	
OST80_51	*O. sativa*	pICSL4723	Kitaake	SLNT80	35S:NLS:GFP:Nos	T0	34-1	-	
OST80_52	*O. sativa*	pICSL4723	Kitaake	SLNT80	35S:NLS:GFP:Nos	T0	34-2	+	1
OST80_53	*O. sativa*	pICSL4723	Kitaake	SLNT80	35S:NLS:GFP:Nos	T0	35-1	+	2
OST80_54	*O. sativa*	pICSL4723	Kitaake	SLNT80	35S:NLS:GFP:Nos	T0	36-1	+	1

ID	Species	Backbone	Accession	Code	Construct	Generation	Clone No.	Fluorescence	GFP copy no.
OST80_55	*O. sativa*	pICSL4723	Kitaake	SLNT80	35S:NLS:GFP:Nos	T0	37-1	+	1
OST80_56	*O. sativa*	pICSL4723	Kitaake	SLNT80	35S:NLS:GFP:Nos	T0	37-2	+	1
OST81_1	*O. sativa*	pICSL4723	Kitaake	SLNT81	ZmUbi:GFP:35S	T0	1-1	-	
OST81_2	*O. sativa*	pICSL4723	Kitaake	SLNT81	ZmUbi:GFP:35S	T0	2-1	+	2
OST81_3	*O. sativa*	pICSL4723	Kitaake	SLNT81	ZmUbi:GFP:35S	T0	3-1	+	1
OST81_4	*O. sativa*	pICSL4723	Kitaake	SLNT81	ZmUbi:GFP:35S	T0	4-1	+	1
OST81_5	*O. sativa*	pICSL4723	Kitaake	SLNT81	ZmUbi:GFP:35S	T0	4-2	+	1
OST81_6	*O. sativa*	pICSL4723	Kitaake	SLNT81	ZmUbi:GFP:35S	T0	4-3	+	1
OST81_7	*O. sativa*	pICSL4723	Kitaake	SLNT81	ZmUbi:GFP:35S	T0	4-4	+	1
OST81_8	*O. sativa*	pICSL4723	Kitaake	SLNT81	ZmUbi:GFP:35S	T0	5-1	+	7
OST81_9	*O. sativa*	pICSL4723	Kitaake	SLNT81	ZmUbi:GFP:35S	T0	6-1	+	1
OST81_10	*O. sativa*	pICSL4723	Kitaake	SLNT81	ZmUbi:GFP:35S	T0	6-2	+	1
OST81_11	*O. sativa*	pICSL4723	Kitaake	SLNT81	ZmUbi:GFP:35S	T0	6-3	+	1
OST81_12	*O. sativa*	pICSL4723	Kitaake	SLNT81	ZmUbi:GFP:35S	T0	7-1	+	3
OST81_13	*O. sativa*	pICSL4723	Kitaake	SLNT81	ZmUbi:GFP:35S	T0	7-2	+	3
OST81_14	*O. sativa*	pICSL4723	Kitaake	SLNT81	ZmUbi:GFP:35S	T0	7-3	+	3
OST81_15	*O. sativa*	pICSL4723	Kitaake	SLNT81	ZmUbi:GFP:35S	T0	7-4	+	2
OST81_16	*O. sativa*	pICSL4723	Kitaake	SLNT81	ZmUbi:GFP:35S	T0	8-1	++	3
OST81_17	*O. sativa*	pICSL4723	Kitaake	SLNT81	ZmUbi:GFP:35S	T0	8-2	+	3
OST81_18	*O. sativa*	pICSL4723	Kitaake	SLNT81	ZmUbi:GFP:35S	T0	10-1	+	2
OST81_19	*O. sativa*	pICSL4723	Kitaake	SLNT81	ZmUbi:GFP:35S	T0	11-1	+	3
OST81_20	*O. sativa*	pICSL4723	Kitaake	SLNT81	ZmUbi:GFP:35S	T0	11-2	+	3
OST81_21	*O. sativa*	pICSL4723	Kitaake	SLNT81	ZmUbi:GFP:35S	T0	12-1	-	
OST81_22	*O. sativa*	pICSL4723	Kitaake	SLNT81	ZmUbi:GFP:35S	T0	12-2	+	14
OST81_23	*O. sativa*	pICSL4723	Kitaake	SLNT81	ZmUbi:GFP:35S	T0	12-3	+	3
OST81_24	*O. sativa*	pICSL4723	Kitaake	SLNT81	ZmUbi:GFP:35S	T0	13-1	+	1
OST81_25	*O. sativa*	pICSL4723	Kitaake	SLNT81	ZmUbi:GFP:35S	T0	13-2	+	1
OST81_26	*O. sativa*	pICSL4723	Kitaake	SLNT81	ZmUbi:GFP:35S	T0	14-1	-	

ID	Species	Backbone	Accession	Code	Construct	Generation	Clone No.	Fluorescence	GFP copy no.
OST81_27	*O. sativa*	pICSL4723	Kitaake	SLNT81	ZmUbi:GFP:35S	T0	14-2	-	
OST81_28	*O. sativa*	pICSL4723	Kitaake	SLNT81	ZmUbi:GFP:35S	T0	14-3	-	
OST81_29	*O. sativa*	pICSL4723	Kitaake	SLNT81	ZmUbi:GFP:35S	T0	15-1	+	1
OST118_1	*O. sativa*	pVKH18	Kitaake	SLNT118	35S:STtmd:GFP:Nos*	T0	1-1	-	
OST118_2	*O. sativa*	pVKH18	Kitaake	SLNT118	35S:STtmd:GFP:Nos	T0	1-2	-	
OST118_3	*O. sativa*	pVKH18	Kitaake	SLNT118	35S:STtmd:GFP:Nos	T0	1-3	-	
OST118_4	*O. sativa*	pVKH18	Kitaake	SLNT118	35S:STtmd:GFP:Nos	T0	1-4	-	
OST118_5	*O. sativa*	pVKH18	Kitaake	SLNT118	35S:STtmd:GFP:Nos	T0	1-5	ER-like	
OST118_6	*O. sativa*	pVKH18	Kitaake	SLNT118	35S:STtmd:GFP:Nos	T0	1-6	-	
OST118_7	*O. sativa*	pVKH18	Kitaake	SLNT118	35S:STtmd:GFP:Nos	T0	1-7	-	
OST118_8	*O. sativa*	pVKH18	Kitaake	SLNT118	35S:STtmd:GFP:Nos	T0	1-8	-	
OST118_9	*O. sativa*	pVKH18	Kitaake	SLNT118	35S:STtmd:GFP:Nos	T0	1-9	-	
OST118_10	*O. sativa*	pVKH18	Kitaake	SLNT118	35S:STtmd:GFP:Nos	T0	1-10	+	2
OST118_11	*O. sativa*	pVKH18	Kitaake	SLNT118	35S:STtmd:GFP:Nos	T0	1-11	-	
OST118_12	*O. sativa*	pVKH18	Kitaake	SLNT118	35S:STtmd:GFP:Nos	T0	1-12	-	
OST118_13	*O. sativa*	pVKH18	Kitaake	SLNT118	35S:STtmd:GFP:Nos	T0	1-13	-	
OST118_14	*O. sativa*	pVKH18	Kitaake	SLNT118	35S:STtmd:GFP:Nos	T0	1-14	ER-like	
OST118_15	*O. sativa*	pVKH18	Kitaake	SLNT118	35S:STtmd:GFP:Nos	T0	2-1	ER-like	
OST118_16	*O. sativa*	pVKH18	Kitaake	SLNT118	35S:STtmd:GFP:Nos	T0	2-2	-	
OST118_17	*O. sativa*	pVKH18	Kitaake	SLNT118	35S:STtmd:GFP:Nos	T0	2-3	ER-like	
OST118_18	*O. sativa*	pVKH18	Kitaake	SLNT118	35S:STtmd:GFP:Nos	T0	2-4	ER-like	
OST118_19	*O. sativa*	pVKH18	Kitaake	SLNT118	35S:STtmd:GFP:Nos	T0	2-5	-	
OST118_20	*O. sativa*	pVKH18	Kitaake	SLNT118	35S:STtmd:GFP:Nos	T0	2-6	ER-like	
OST118_21	*O. sativa*	pVKH18	Kitaake	SLNT118	35S:STtmd:GFP:Nos	T0	2-7	ER-like	
OST118_22	*O. sativa*	pVKH18	Kitaake	SLNT118	35S:STtmd:GFP:Nos	T0	2-8	-	
OST118_23	*O. sativa*	pVKH18	Kitaake	SLNT118	35S:STtmd:GFP:Nos	T0	2-9	ER-like	
OST118_24	*O. sativa*	pVKH18	Kitaake	SLNT118	35S:STtmd:GFP:Nos	T0	2-10	ER-like	
OST118_25	*O. sativa*	pVKH18	Kitaake	SLNT118	35S:STtmd:GFP:Nos	T0	2-11	ER-like	

ID	Species	Backbone	Accession	Code	Construct	Generation	Clone No.	Fluorescence	GFP copy no.
OST118_26	*O. sativa*	pVKH18	Kitaake	SLNT118	35S:STtmd:GFP:Nos	T0	2-12	+	2
OST118_27	*O. sativa*	pVKH18	Kitaake	SLNT118	35S:STtmd:GFP:Nos	T0	2-13	-	
OST118_28	*O. sativa*	pVKH18	Kitaake	SLNT118	35S:STtmd:GFP:Nos	T0	2-14	+	46
OST118_29	*O. sativa*	pVKH18	Kitaake	SLNT118	35S:STtmd:GFP:Nos	T0	3-1	-	
OST118_30	*O. sativa*	pVKH18	Kitaake	SLNT118	35S:STtmd:GFP:Nos	T0	3-2	ER-like	
OST118_31	*O. sativa*	pVKH18	Kitaake	SLNT118	35S:STtmd:GFP:Nos	T0	3-3	ER-like	
OST118_32	*O. sativa*	pVKH18	Kitaake	SLNT118	35S:STtmd:GFP:Nos	T0	3-4	-	
OST118_33	*O. sativa*	pVKH18	Kitaake	SLNT118	35S:STtmd:GFP:Nos	T0	3-5	-	
OST118_34	*O. sativa*	pVKH18	Kitaake	SLNT118	35S:STtmd:GFP:Nos	T0	3-6	ER-like	4
OST118_35	*O. sativa*	pVKH18	Kitaake	SLNT118	35S:STtmd:GFP:Nos	T0	3-7	ER-like	6
OST118_36	*O. sativa*	pVKH18	Kitaake	SLNT118	35S:STtmd:GFP:Nos	T0	3-8	ER-like	4
OST118_37	*O. sativa*	pVKH18	Kitaake	SLNT118	35S:STtmd:GFP:Nos	T0	3-9	ER-like	
OST118_38	*O. sativa*	pVKH18	Kitaake	SLNT118	35S:STtmd:GFP:Nos	T0	3-10	ER-like	
OST118_39	*O. sativa*	pVKH18	Kitaake	SLNT118	35S:STtmd:GFP:Nos	T0	3-11	-	
OST118_40	*O. sativa*	pVKH18	Kitaake	SLNT118	35S:STtmd:GFP:Nos	T0	3-12	-	
OST118_41	*O. sativa*	pVKH18	Kitaake	SLNT118	35S:STtmd:GFP:Nos	T0	3-13	-	
OST118_42	*O. sativa*	pVKH18	Kitaake	SLNT118	35S:STtmd:GFP:Nos	T0	3-14	-	
OST118_43	*O. sativa*	pVKH18	Kitaake	SLNT118	35S:STtmd:GFP:Nos	T0	3-15	-	
OST118_44	*O. sativa*	pVKH18	Kitaake	SLNT118	35S:STtmd:GFP:Nos	T0	4-1	-	
OST118_45	*O. sativa*	pVKH18	Kitaake	SLNT118	35S:STtmd:GFP:Nos	T0	4-2	-	
OST118_46	*O. sativa*	pVKH18	Kitaake	SLNT118	35S:STtmd:GFP:Nos	T0	4-3	-	
OST118_47	*O. sativa*	pVKH18	Kitaake	SLNT118	35S:STtmd:GFP:Nos	T0	4-4	-	
OST118_48	*O. sativa*	pVKH18	Kitaake	SLNT118	35S:STtmd:GFP:Nos	T0	4-5	-	
OST118_49	*O. sativa*	pVKH18	Kitaake	SLNT118	35S:STtmd:GFP:Nos	T0	4-6	-	
OST118_50	*O. sativa*	pVKH18	Kitaake	SLNT118	35S:STtmd:GFP:Nos	T0	4-7	ER-like	
OST118_51	*O. sativa*	pVKH18	Kitaake	SLNT118	35S:STtmd:GFP:Nos	T0	4-8	-	
OST118_52	*O. sativa*	pVKH18	Kitaake	SLNT118	35S:STtmd:GFP:Nos	T0	4-9	-	
OST118_53	*O. sativa*	pVKH18	Kitaake	SLNT118	35S:STtmd:GFP:Nos	T0	4-10	-	

ID	Species	Backbone	Accession	Code	Construct	Generation	Clone No.	Fluorescence	GFP copy no.
OST118_54	*O. sativa*	pVKH18	Kitaake	SLNT118	35S:STtmd:GFP:Nos	T0	4-11	-	
OST118_55	*O. sativa*	pVKH18	Kitaake	SLNT118	35S:STtmd:GFP:Nos	T0	4-12	-	
OST118_56	*O. sativa*	pVKH18	Kitaake	SLNT118	35S:STtmd:GFP:Nos	T0	5-1	+	3
OST118_57	*O. sativa*	pVKH18	Kitaake	SLNT118	35S:STtmd:GFP:Nos	T0	5-2	+	3
OST118_58	*O. sativa*	pVKH18	Kitaake	SLNT118	35S:STtmd:GFP:Nos	T0	5-3	+	5
OST118_59	*O. sativa*	pVKH18	Kitaake	SLNT118	35S:STtmd:GFP:Nos	T0	5-4	-	
OST118_60	*O. sativa*	pVKH18	Kitaake	SLNT118	35S:STtmd:GFP:Nos	T0	5-5	-	
OST118_61	*O. sativa*	pVKH18	Kitaake	SLNT118	35S:STtmd:GFP:Nos	T0	5-6	ER-like	
OST118_62	*O. sativa*	pVKH18	Kitaake	SLNT118	35S:STtmd:GFP:Nos	T0	5-7	ER-like	
OST118_63	*O. sativa*	pVKH18	Kitaake	SLNT118	35S:STtmd:GFP:Nos	T0	5-8	-	
OST118_64	*O. sativa*	pVKH18	Kitaake	SLNT118	35S:STtmd:GFP:Nos	T0	5-9	-	
OST118_65	*O. sativa*	pVKH18	Kitaake	SLNT118	35S:STtmd:GFP:Nos	T0	5-10	ER-like	7
OST117_1	*O. sativa*	pAGM4723_ccdB	Kitaake	SLNT117	ZmUbi:GFP:PTS1	T0	1-1	+	14
OST117_2	*O. sativa*	pAGM4723_ccdB	Kitaake	SLNT117	ZmUbi:GFP:PTS1	T0	1-2	+	18
OST117_3	*O. sativa*	pAGM4723_ccdB	Kitaake	SLNT117	ZmUbi:GFP:PTS1	T0	1-3	+	2
OST117_4	*O. sativa*	pAGM4723_ccdB	Kitaake	SLNT117	ZmUbi:GFP:PTS1	T0	1-4	+	1
OST117_5	*O. sativa*	pAGM4723_ccdB	Kitaake	SLNT117	ZmUbi:GFP:PTS1	T0	1-5	+	15
OST117_6	*O. sativa*	pAGM4723_ccdB	Kitaake	SLNT117	ZmUbi:GFP:PTS1	T0	1-6	+	16
OST117_7	*O. sativa*	pAGM4723_ccdB	Kitaake	SLNT117	ZmUbi:GFP:PTS1	T0	1-7	+	11
OST117_8	*O. sativa*	pAGM4723_ccdB	Kitaake	SLNT117	ZmUbi:GFP:PTS1	T0	1-8	+	15
OST117_9	*O. sativa*	pAGM4723_ccdB	Kitaake	SLNT117	ZmUbi:GFP:PTS1	T0	2-1	+	9
OST117_10	*O. sativa*	pAGM4723_ccdB	Kitaake	SLNT117	ZmUbi:GFP:PTS1	T0	2-2	+	5
OST117_11	*O. sativa*	pAGM4723_ccdB	Kitaake	SLNT117	ZmUbi:GFP:PTS1	T0	2-3	-	
OST117_12	*O. sativa*	pAGM4723_ccdB	Kitaake	SLNT117	ZmUbi:GFP:PTS1	T0	2-4	+	17
OST117_13	*O. sativa*	pAGM4723_ccdB	Kitaake	SLNT117	ZmUbi:GFP:PTS1	T0	2-5	+	17
OST117_14	*O. sativa*	pAGM4723_ccdB	Kitaake	SLNT117	ZmUbi:GFP:PTS1	T0	2-6	+	17
OST117_15	*O. sativa*	pAGM4723_ccdB	Kitaake	SLNT117	ZmUbi:GFP:PTS1	T0	2-7	+	2
OST117_16	*O. sativa*	pAGM4723_ccdB	Kitaake	SLNT117	ZmUbi:GFP:PTS1	T0	2-8	+	2

ID	Species	Backbone	Accession	Code	Construct	Generation	Clone No.	Fluorescence	GFP copy no.
OST117_17	*O. sativa*	pAGM4723_ccdB	Kitaake	SLNT117	ZmUbi:GFP:PTS1	T0	2-9	+	11
OST117_18	*O. sativa*	pAGM4723_ccdB	Kitaake	SLNT117	ZmUbi:GFP:PTS1	T0	2-10	-	
OST117_19	*O. sativa*	pAGM4723_ccdB	Kitaake	SLNT117	ZmUbi:GFP:PTS1	T0	3-1	+	6
OST117_20	*O. sativa*	pAGM4723_ccdB	Kitaake	SLNT117	ZmUbi:GFP:PTS1	T0	3-2	+	6
OST117_21	*O. sativa*	pAGM4723_ccdB	Kitaake	SLNT117	ZmUbi:GFP:PTS1	T0	3-3	+	3
OST117_22	*O. sativa*	pAGM4723_ccdB	Kitaake	SLNT117	ZmUbi:GFP:PTS1	T0	3-4	+	3
OST117_23	*O. sativa*	pAGM4723_ccdB	Kitaake	SLNT117	ZmUbi:GFP:PTS1	T0	3-5	+	3
OST117_24	*O. sativa*	pAGM4723_ccdB	Kitaake	SLNT117	ZmUbi:GFP:PTS1	T0	3-6	+	7
OST117_25	*O. sativa*	pAGM4723_ccdB	Kitaake	SLNT117	ZmUbi:GFP:PTS1	T0	3-7	+	3
OST117_26	*O. sativa*	pAGM4723_ccdB	Kitaake	SLNT117	ZmUbi:GFP:PTS1	T0	3-8	-	
OST117_27	*O. sativa*	pAGM4723_ccdB	Kitaake	SLNT117	ZmUbi:GFP:PTS1	T0	3-9	-	
OST117_28	*O. sativa*	pAGM4723_ccdB	Kitaake	SLNT117	ZmUbi:GFP:PTS1	T0	4-1	+	9
OST117_29	*O. sativa*	pAGM4723_ccdB	Kitaake	SLNT117	ZmUbi:GFP:PTS1	T0	4-2	+	9
OST117_30	*O. sativa*	pAGM4723_ccdB	Kitaake	SLNT117	ZmUbi:GFP:PTS1	T0	4-3	+	3
OST117_31	*O. sativa*	pAGM4723_ccdB	Kitaake	SLNT117	ZmUbi:GFP:PTS1	T0	4-4	+	8
OST117_32	*O. sativa*	pAGM4723_ccdB	Kitaake	SLNT117	ZmUbi:GFP:PTS1	T0	4-5	-	
OST117_33	*O. sativa*	pAGM4723_ccdB	Kitaake	SLNT117	ZmUbi:GFP:PTS1	T0	4-6	+	43
OST117_34	*O. sativa*	pAGM4723_ccdB	Kitaake	SLNT117	ZmUbi:GFP:PTS1	T0	4-7	+	8
OST117_35	*O. sativa*	pAGM4723_ccdB	Kitaake	SLNT117	ZmUbi:GFP:PTS1	T0	4-8	+	16
OST117_36	*O. sativa*	pAGM4723_ccdB	Kitaake	SLNT117	ZmUbi:GFP:PTS1	T0	4-9	+	16
OST117_37	*O. sativa*	pAGM4723_ccdB	Kitaake	SLNT117	ZmUbi:GFP:PTS1	T0	4-10	-	
OST117_38	*O. sativa*	pAGM4723_ccdB	Kitaake	SLNT117	ZmUbi:GFP:PTS1	T0	4-11	+	6
OST117_39	*O. sativa*	pAGM4723_ccdB	Kitaake	SLNT117	ZmUbi:GFP:PTS1	T0	4-12	+	16
OST117_40	*O. sativa*	pAGM4723_ccdB	Kitaake	SLNT117	ZmUbi:GFP:PTS1	T0	4-13	+	17
OST117_41	*O. sativa*	pAGM4723_ccdB	Kitaake	SLNT117	ZmUbi:GFP:PTS1	T0	4-14	+	10
OST117_42	*O. sativa*	pAGM4723_ccdB	Kitaake	SLNT117	ZmUbi:GFP:PTS1	T0	4-15	+	14
OST117_43	*O. sativa*	pAGM4723_ccdB	Kitaake	SLNT117	ZmUbi:GFP:PTS1	T0	4-16	+	3
OST123_1	*O. sativa*	pAGM4723_ccdB	Kitaake	SLNT123	ZmUbi:AtWAK2:GFP:HDEL	T0	1-1	+	15

ID	Species	Backbone	Accession	Code	Construct	Generation	Clone No.	Fluorescence	GFP copy no.
OST123_2	*O. sativa*	pAGM4723_ccdB	Kitaake	SLNT123	ZmUbi:AtWAK2:GFP:HDEL	T0	1-3	+	15
OST123_3	*O. sativa*	pAGM4723_ccdB	Kitaake	SLNT123	ZmUbi:AtWAK2:GFP:HDEL	T0	2-1	+	12
OST123_4	*O. sativa*	pAGM4723_ccdB	Kitaake	SLNT123	ZmUbi:AtWAK2:GFP:HDEL	T0	14-1	+	1
OST123_5	*O. sativa*	pAGM4723_ccdB	Kitaake	SLNT123	ZmUbi:AtWAK2:GFP:HDEL	T0	15-1	+	6
OST123_6	*O. sativa*	pAGM4723_ccdB	Kitaake	SLNT123	ZmUbi:AtWAK2:GFP:HDEL	T0	15-3	+	6
OST123_7	*O. sativa*	pAGM4723_ccdB	Kitaake	SLNT123	ZmUbi:AtWAK2:GFP:HDEL	T0	17-1	+	4
OST123_8	*O. sativa*	pAGM4723_ccdB	Kitaake	SLNT123	ZmUbi:AtWAK2:GFP:HDEL	T0	17-3	+	4
OST123_9	*O. sativa*	pAGM4723_ccdB	Kitaake	SLNT123	ZmUbi:AtWAK2:GFP:HDEL	T0	17-4	+	4

Appendix Table 2 Fluorescence screening and GFP copy number determination in barley cv. Golden Promise T_0 lines expressing GFP-tagged subcellular markers.

ID	Species	Backbone	Accession	Code	Construct	Generation	Clone No.	Fluorescence	GFP copy no.
HVT67_1	*H. vulgare*	pGWB502	Golden Promise	SLNT67	35S:OsAra6:GFP:Nos	T0	1-1	+	
HVT67_2	*H. vulgare*	pGWB502	Golden Promise	SLNT67	35S:OsAra6:GFP:Nos	T0	2-1	-	
HVT67_3	*H. vulgare*	pGWB502	Golden Promise	SLNT67	35S:OsAra6:GFP:Nos	T0	2-2	-	
HVT67_4	*H. vulgare*	pGWB502	Golden Promise	SLNT67	35S:OsAra6:GFP:Nos	T0	3-1	-	
HVT67_5	*H. vulgare*	pGWB502	Golden Promise	SLNT67	35S:OsAra6:GFP:Nos	T0	4-1	-	
HVT67_6	*H. vulgare*	pGWB502	Golden Promise	SLNT67	35S:OsAra6:GFP:Nos	T0	4-2	-	
HVT70_1	*H. vulgare*	pICSL4723	Golden Promise	SLNT70	35S:LTI6b TMD:GFP:Nos	T0	1-1	+	4
HVT70_2	*H. vulgare*	pICSL4723	Golden Promise	SLNT70	35S:LTI6b TMD:GFP:Nos	T0	1-2	-	
HVT70_3	*H. vulgare*	pICSL4723	Golden Promise	SLNT70	35S:LTI6b TMD:GFP:Nos	T0	1-3	-	
HVT70_4	*H. vulgare*	pICSL4723	Golden Promise	SLNT70	35S:LTI6b TMD:GFP:Nos	T0	1-4	-	
HVT70_5	*H. vulgare*	pICSL4723	Golden Promise	SLNT70	35S:LTI6b TMD:GFP:Nos	T0	2-1	-	2
HVT70_6	*H. vulgare*	pICSL4723	Golden Promise	SLNT70	35S:LTI6b TMD:GFP:Nos	T0	2-2	-	
HVT70_7	*H. vulgare*	pICSL4723	Golden Promise	SLNT70	35S:LTI6b TMD:GFP:Nos	T0	3-1	-	3
HVT70_8	*H. vulgare*	pICSL4723	Golden Promise	SLNT70	35S:LTI6b TMD:GFP:Nos	T0	3-2	-	
HVT70_9	*H. vulgare*	pICSL4723	Golden Promise	SLNT70	35S:LTI6b TMD:GFP:Nos	T0	4-1	-	
HVT70_10	*H. vulgare*	pICSL4723	Golden Promise	SLNT70	35S:LTI6b TMD:GFP:Nos	T0	4-2	-	
HVT70_11	*H. vulgare*	pICSL4723	Golden Promise	SLNT70	35S:LTI6b TMD:GFP:Nos	T0	4-3	+	3
HVT70_12	*H. vulgare*	pICSL4723	Golden Promise	SLNT70	35S:LTI6b TMD:GFP:Nos	T0	5-1	+	1
HVT70_13	*H. vulgare*	pICSL4723	Golden Promise	SLNT70	35S:LTI6b TMD:GFP:Nos	T0	5-2	+	1
HVT70_14	*H. vulgare*	pICSL4723	Golden Promise	SLNT70	35S:LTI6b TMD:GFP:Nos	T0	6-1	+	2
HVT70_15	*H. vulgare*	pICSL4723	Golden Promise	SLNT70	35S:LTI6b TMD:GFP:Nos	T0	6-2	+	1
HVT70_16	*H. vulgare*	pICSL4723	Golden Promise	SLNT70	35S:LTI6b TMD:GFP:Nos	T0	6-3	+	1
HVT70_17	*H. vulgare*	pICSL4723	Golden Promise	SLNT70	35S:LTI6b TMD:GFP:Nos	T0	6-4	+	1
HVT70_18	*H. vulgare*	pICSL4723	Golden Promise	SLNT70	35S:LTI6b TMD:GFP:Nos	T0	7-1	+	4
HVT70_19	*H. vulgare*	pICSL4723	Golden Promise	SLNT70	35S:LTI6b TMD:GFP:Nos	T0	7-2	-	

ID	Species	Backbone	Accession	Code	Construct	Generation	Clone No.	Fluorescence	GFP copy no.
HVT70_20	*H. vulgare*	pICSL4723	Golden Promise	SLNT70	35S:LTI6b TMD:GFP:Nos	T0	7-3	-	
HVT70_21	*H. vulgare*	pICSL4723	Golden Promise	SLNT70	35S:LTI6b TMD:GFP:Nos	T0	7-4	-	
HVT70_22	*H. vulgare*	pICSL4723	Golden Promise	SLNT70	35S:LTI6b TMD:GFP:Nos	T0	8-1	+	1
HVT70_23	*H. vulgare*	pICSL4723	Golden Promise	SLNT70	35S:LTI6b TMD:GFP:Nos	T0	9-1	+	1
HVT70_24	*H. vulgare*	pICSL4723	Golden Promise	SLNT70	35S:LTI6b TMD:GFP:Nos	T0	10-1	+	2
HVT70_25	*H. vulgare*	pICSL4723	Golden Promise	SLNT70	35S:LTI6b TMD:GFP:Nos	T0	11-1	+	1
HVT71_1	*H. vulgare*	pICSL4723	Golden Promise	SLNT71	35S:COXIV:GFP:Nos	T0	1-1	-	3
HVT71_2	*H. vulgare*	pICSL4723	Golden Promise	SLNT71	35S:COXIV:GFP:Nos	T0	2-1	+	2
HVT71_3	*H. vulgare*	pICSL4723	Golden Promise	SLNT71	35S:COXIV:GFP:Nos	T0	3-1	-	
HVT71_4	*H. vulgare*	pICSL4723	Golden Promise	SLNT71	35S:COXIV:GFP:Nos	T0	3-2	-	3
HVT71_5	*H. vulgare*	pICSL4723	Golden Promise	SLNT71	35S:COXIV:GFP:Nos	T0	3-3	-	
HVT71_6	*H. vulgare*	pICSL4723	Golden Promise	SLNT71	35S:COXIV:GFP:Nos	T0	3-4	-	
HVT71_7	*H. vulgare*	pICSL4723	Golden Promise	SLNT71	35S:COXIV:GFP:Nos	T0	4-1	+	1
HVT71_8	*H. vulgare*	pICSL4723	Golden Promise	SLNT71	35S:COXIV:GFP:Nos	T0	4-2	-	
HVT71_9	*H. vulgare*	pICSL4723	Golden Promise	SLNT71	35S:COXIV:GFP:Nos	T0	4-3	-	
HVT71_10	*H. vulgare*	pICSL4723	Golden Promise	SLNT71	35S:COXIV:GFP:Nos	T0	5-1	+	2
HVT71_11	*H. vulgare*	pICSL4723	Golden Promise	SLNT71	35S:COXIV:GFP:Nos	T0	5-2	-	
HVT71_12	*H. vulgare*	pICSL4723	Golden Promise	SLNT71	35S:COXIV:GFP:Nos	T0	5-3	-	
HVT71_13	*H. vulgare*	pICSL4723	Golden Promise	SLNT71	35S:COXIV:GFP:Nos	T0	6-1	+	1
HVT71_14	*H. vulgare*	pICSL4723	Golden Promise	SLNT71	35S:COXIV:GFP:Nos	T0	6-2	+	3
HVT71_15	*H. vulgare*	pICSL4723	Golden Promise	SLNT71	35S:COXIV:GFP:Nos	T0	6-3	+	2
HVT71_16	*H. vulgare*	pICSL4723	Golden Promise	SLNT71	35S:COXIV:GFP:Nos	T0	6-4	+	1
HVT71_17	*H. vulgare*	pICSL4723	Golden Promise	SLNT71	35S:COXIV:GFP:Nos	T0	7-1	+	2
HVT71_18	*H. vulgare*	pICSL4723	Golden Promise	SLNT71	35S:COXIV:GFP:Nos	T0	9-1	+	1
HVT71_19	*H. vulgare*	pICSL4723	Golden Promise	SLNT71	35S:COXIV:GFP:Nos	T0	10-1	-	6
HVT71_20	*H. vulgare*	pICSL4723	Golden Promise	SLNT71	35S:COXIV:GFP:Nos	T0	11-1	-	
HVT71_21	*H. vulgare*	pICSL4723	Golden Promise	SLNT71	35S:COXIV:GFP:Nos	T0	12-1	+	1
HVT71_22	*H. vulgare*	pICSL4723	Golden Promise	SLNT71	35S:COXIV:GFP:Nos	T0	12-2	-	0

ID	Species	Backbone	Accession	Code	Construct	Generation	Clone No.	Fluorescence	GFP copy no.
HVT71_23	*H. vulgare*	pICSL4723	Golden Promise	SLNT71	35S:COXIV:GFP:Nos	T0	12-3	-	
HVT71_24	*H. vulgare*	pICSL4723	Golden Promise	SLNT71	35S:COXIV:GFP:Nos	T0	13-1	+	1
HVT71_25	*H. vulgare*	pICSL4723	Golden Promise	SLNT71	35S:COXIV:GFP:Nos	T0	13-2	+	1
HVT71_26	*H. vulgare*	pICSL4723	Golden Promise	SLNT71	35S:COXIV:GFP:Nos	T0	13-3	+	1
HVT71_27	*H. vulgare*	pICSL4723	Golden Promise	SLNT71	35S:COXIV:GFP:Nos	T0	13-4	+	1
HVT73_1	*H. vulgare*	pICSL4723	Golden Promise	SLNT73	ZmUbi:GFP:Ara7:Nos	T0	1-1	+	1
HVT73_2	*H. vulgare*	pICSL4723	Golden Promise	SLNT73	ZmUbi:GFP:Ara7:Nos	T0	1-2	-	
HVT73_3	*H. vulgare*	pICSL4723	Golden Promise	SLNT73	ZmUbi:GFP:Ara7:Nos	T0	1-3	-	
HVT73_4	*H. vulgare*	pICSL4723	Golden Promise	SLNT73	ZmUbi:GFP:Ara7:Nos	T0	1-4	-	
HVT73_5	*H. vulgare*	pICSL4723	Golden Promise	SLNT73	ZmUbi:GFP:Ara7:Nos	T0	2-1	+	1
HVT73_6	*H. vulgare*	pICSL4723	Golden Promise	SLNT73	ZmUbi:GFP:Ara7:Nos	T0	3-1	+	1
HVT73_7	*H. vulgare*	pICSL4723	Golden Promise	SLNT73	ZmUbi:GFP:Ara7:Nos	T0	3-2	-	
HVT73_8	*H. vulgare*	pICSL4723	Golden Promise	SLNT73	ZmUbi:GFP:Ara7:Nos	T0	3-3	-	
HVT73_9	*H. vulgare*	pICSL4723	Golden Promise	SLNT73	ZmUbi:GFP:Ara7:Nos	T0	3-4	-	
HVT73_10	*H. vulgare*	pICSL4723	Golden Promise	SLNT73	ZmUbi:GFP:Ara7:Nos	T0	4-1	+	1
HVT73_11	*H. vulgare*	pICSL4723	Golden Promise	SLNT73	ZmUbi:GFP:Ara7:Nos	T0	4-2	-	
HVT73_12	*H. vulgare*	pICSL4723	Golden Promise	SLNT73	ZmUbi:GFP:Ara7:Nos	T0	5-1	+	1
HVT73_13	*H. vulgare*	pICSL4723	Golden Promise	SLNT73	ZmUbi:GFP:Ara7:Nos	T0	5-2	-	
HVT73_14	*H. vulgare*	pICSL4723	Golden Promise	SLNT73	ZmUbi:GFP:Ara7:Nos	T0	5-3	-	
HVT73_15	*H. vulgare*	pICSL4723	Golden Promise	SLNT73	ZmUbi:GFP:Ara7:Nos	T0	5-4	-	
HVT73_16	*H. vulgare*	pICSL4723	Golden Promise	SLNT73	ZmUbi:GFP:Ara7:Nos	T0	6-1	+	1
HVT73_17	*H. vulgare*	pICSL4723	Golden Promise	SLNT73	ZmUbi:GFP:Ara7:Nos	T0	7-1	+	1
HVT73_18	*H. vulgare*	pICSL4723	Golden Promise	SLNT73	ZmUbi:GFP:Ara7:Nos	T0	7-2	-	
HVT73_19	*H. vulgare*	pICSL4723	Golden Promise	SLNT73	ZmUbi:GFP:Ara7:Nos	T0	7-3	-	
HVT73_20	*H. vulgare*	pICSL4723	Golden Promise	SLNT73	ZmUbi:GFP:Ara7:Nos	T0	8-1	+	1
HVT73_21	*H. vulgare*	pICSL4723	Golden Promise	SLNT73	ZmUbi:GFP:Ara7:Nos	T0	8-2	-	
HVT73_22	*H. vulgare*	pICSL4723	Golden Promise	SLNT73	ZmUbi:GFP:Ara7:Nos	T0	8-3	-	
HVT73_23	*H. vulgare*	pICSL4723	Golden Promise	SLNT73	ZmUbi:GFP:Ara7:Nos	T0	8-4	-	

ID	Species	Backbone	Accession	Code	Construct	Generation	Clone No.	Fluorescence	GFP copy no.
HVT73_24	*H. vulgare*	pICSL4723	Golden Promise	SLNT73	ZmUbi:GFP:Ara7:Nos	T0	9-1	-	
HVT73_25	*H. vulgare*	pICSL4723	Golden Promise	SLNT73	ZmUbi:GFP:Ara7:Nos	T0	9-2	-	
HVT73_26	*H. vulgare*	pICSL4723	Golden Promise	SLNT73	ZmUbi:GFP:Ara7:Nos	T0	9-3	-	
HVT73_27	*H. vulgare*	pICSL4723	Golden Promise	SLNT73	ZmUbi:GFP:Ara7:Nos	T0	10-1	+	1
HVT73_28	*H. vulgare*	pICSL4723	Golden Promise	SLNT73	ZmUbi:GFP:Ara7:Nos	T0	11-1	+	1
HVT73_29	*H. vulgare*	pICSL4723	Golden Promise	SLNT73	ZmUbi:GFP:Ara7:Nos	T0	11-2	+	1
HVT74_1	*H. vulgare*	pICSL4723	Golden Promise	SLNT74	ZmUbi:LifeAct:GFP:Nos	T0	1-1	+	1
HVT74_2	*H. vulgare*	pICSL4723	Golden Promise	SLNT74	ZmUbi:LifeAct:GFP:Nos	T0	1-2	+	1
HVT74_3	*H. vulgare*	pICSL4723	Golden Promise	SLNT74	ZmUbi:LifeAct:GFP:Nos	T0	1-3	+	1
HVT74_4	*H. vulgare*	pICSL4723	Golden Promise	SLNT74	ZmUbi:LifeAct:GFP:Nos	T0	2-1	-	
HVT74_5	*H. vulgare*	pICSL4723	Golden Promise	SLNT74	ZmUbi:LifeAct:GFP:Nos	T0	2-2	+	1
HVT74_6	*H. vulgare*	pICSL4723	Golden Promise	SLNT74	ZmUbi:LifeAct:GFP:Nos	T0	2-3	-	
HVT74_7	*H. vulgare*	pICSL4723	Golden Promise	SLNT74	ZmUbi:LifeAct:GFP:Nos	T0	3-1	-	
HVT74_8	*H. vulgare*	pICSL4723	Golden Promise	SLNT74	ZmUbi:LifeAct:GFP:Nos	T0	3-2	-	
HVT74_9	*H. vulgare*	pICSL4723	Golden Promise	SLNT74	ZmUbi:LifeAct:GFP:Nos	T0	4-1	-	
HVT74_10	*H. vulgare*	pICSL4723	Golden Promise	SLNT74	ZmUbi:LifeAct:GFP:Nos	T0	4-2	-	
HVT74_11	*H. vulgare*	pICSL4723	Golden Promise	SLNT74	ZmUbi:LifeAct:GFP:Nos	T0	5-1	+	1
HVT74_12	*H. vulgare*	pICSL4723	Golden Promise	SLNT74	ZmUbi:LifeAct:GFP:Nos	T0	5-2	+	1
HVT74_13	*H. vulgare*	pICSL4723	Golden Promise	SLNT74	ZmUbi:LifeAct:GFP:Nos	T0	6-1	+	1
HVT74_14	*H. vulgare*	pICSL4723	Golden Promise	SLNT74	ZmUbi:LifeAct:GFP:Nos	T0	7-1	+	1
HVT74_15	*H. vulgare*	pICSL4723	Golden Promise	SLNT74	ZmUbi:LifeAct:GFP:Nos	T0	7-2	+	1
HVT74_16	*H. vulgare*	pICSL4723	Golden Promise	SLNT74	ZmUbi:LifeAct:GFP:Nos	T0	7-3	+	1
HVT74_17	*H. vulgare*	pICSL4723	Golden Promise	SLNT74	ZmUbi:LifeAct:GFP:Nos	T0	7-4	+	1
HVT74_18	*H. vulgare*	pICSL4723	Golden Promise	SLNT74	ZmUbi:LifeAct:GFP:Nos	T0	8-1	-	0
HVT74_19	*H. vulgare*	pICSL4723	Golden Promise	SLNT74	ZmUbi:LifeAct:GFP:Nos	T0	9-1	+	1
HVT74_20	*H. vulgare*	pICSL4723	Golden Promise	SLNT74	ZmUbi:LifeAct:GFP:Nos	T0	9-2	+	1
HVT80_1	*H. vulgare*	pICSL4723	Golden Promise	SLNT80	35S:NLS:GFP:Nos	T0	1-1	-	
HVT80_2	*H. vulgare*	pICSL4723	Golden Promise	SLNT80	35S:NLS:GFP:Nos	T0	1-2	-	

ID	Species	Backbone	Accession	Code	Construct	Generation	Clone No.	Fluorescence	GFP copy no.
HVT80_3	*H. vulgare*	pICSL4723	Golden Promise	SLNT80	35S:NLS:GFP:Nos	T0	1-3	-	
HVT80_4	*H. vulgare*	pICSL4723	Golden Promise	SLNT80	35S:NLS:GFP:Nos	T0	1-4	-	
HVT80_5	*H. vulgare*	pICSL4723	Golden Promise	SLNT80	35S:NLS:GFP:Nos	T0	2-1	+	3
HVT80_6	*H. vulgare*	pICSL4723	Golden Promise	SLNT80	35S:NLS:GFP:Nos	T0	3-1	+	1
HVT80_7	*H. vulgare*	pICSL4723	Golden Promise	SLNT80	35S:NLS:GFP:Nos	T0	3-2	+	1
HVT80_8	*H. vulgare*	pICSL4723	Golden Promise	SLNT80	35S:NLS:GFP:Nos	T0	3-3	+	1
HVT80_9	*H. vulgare*	pICSL4723	Golden Promise	SLNT80	35S:NLS:GFP:Nos	T0	3-4	-	
HVT80_10	*H. vulgare*	pICSL4723	Golden Promise	SLNT80	35S:NLS:GFP:Nos	T0	4-1	-	
HVT80_11	*H. vulgare*	pICSL4723	Golden Promise	SLNT80	35S:NLS:GFP:Nos	T0	4-2	-	
HVT80_12	*H. vulgare*	pICSL4723	Golden Promise	SLNT80	35S:NLS:GFP:Nos	T0	5-1	-	
HVT80_13	*H. vulgare*	pICSL4723	Golden Promise	SLNT80	35S:NLS:GFP:Nos	T0	5-2	-	
HVT80_14	*H. vulgare*	pICSL4723	Golden Promise	SLNT80	35S:NLS:GFP:Nos	T0	5-3	-	
HVT80_15	*H. vulgare*	pICSL4723	Golden Promise	SLNT80	35S:NLS:GFP:Nos	T0	5-4	+	1
HVT80_16	*H. vulgare*	pICSL4723	Golden Promise	SLNT80	35S:NLS:GFP:Nos	T0	6-1	+	1
HVT80_17	*H. vulgare*	pICSL4723	Golden Promise	SLNT80	35S:NLS:GFP:Nos	T0	6-2	-	
HVT80_18	*H. vulgare*	pICSL4723	Golden Promise	SLNT80	35S:NLS:GFP:Nos	T0	7-1	-	
HVT80_19	*H. vulgare*	pICSL4723	Golden Promise	SLNT80	35S:NLS:GFP:Nos	T0	7-2	-	
HVT80_20	*H. vulgare*	pICSL4723	Golden Promise	SLNT80	35S:NLS:GFP:Nos	T0	8-1	-	
HVT80_21	*H. vulgare*	pICSL4723	Golden Promise	SLNT80	35S:NLS:GFP:Nos	T0	8-2	-	
HVT80_22	*H. vulgare*	pICSL4723	Golden Promise	SLNT80	35S:NLS:GFP:Nos	T0	9-1	+	1
HVT80_23	*H. vulgare*	pICSL4723	Golden Promise	SLNT80	35S:NLS:GFP:Nos	T0	9-2	-	
HVT80_24	*H. vulgare*	pICSL4723	Golden Promise	SLNT80	35S:NLS:GFP:Nos	T0	10-1	-	
HVT80_25	*H. vulgare*	pICSL4723	Golden Promise	SLNT80	35S:NLS:GFP:Nos	T0	11-1	+	1
HVT80_26	*H. vulgare*	pICSL4723	Golden Promise	SLNT80	35S:NLS:GFP:Nos	T0	12-1	-	
HVT80_27	*H. vulgare*	pICSL4723	Golden Promise	SLNT80	35S:NLS:GFP:Nos	T0	12-2	-	
HVT80_28	*H. vulgare*	pICSL4723	Golden Promise	SLNT80	35S:NLS:GFP:Nos	T0	13-1	+	1
HVT80_29	*H. vulgare*	pICSL4723	Golden Promise	SLNT80	35S:NLS:GFP:Nos	T0	13-2	-	
HVT80_30	*H. vulgare*	pICSL4723	Golden Promise	SLNT80	35S:NLS:GFP:Nos	T0	14-1	+	1

ID	Species	Backbone	Accession	Code	Construct	Generation	Clone No.	Fluorescence	GFP copy no.
HVT81_1	*H. vulgare*	pICSL4723	Golden Promise	SLNT81	ZmUbi:GFP:35S	T0	1-1	+	1
HVT81_2	*H. vulgare*	pICSL4723	Golden Promise	SLNT81	ZmUbi:GFP:35S	T0	1-2	-	
HVT81_3	*H. vulgare*	pICSL4723	Golden Promise	SLNT81	ZmUbi:GFP:35S	T0	1-3	+	1
HVT81_4	*H. vulgare*	pICSL4723	Golden Promise	SLNT81	ZmUbi:GFP:35S	T0	1-4	+	1
HVT81_5	*H. vulgare*	pICSL4723	Golden Promise	SLNT81	ZmUbi:GFP:35S	T0	1-5	-	
HVT81_6	*H. vulgare*	pICSL4723	Golden Promise	SLNT81	ZmUbi:GFP:35S	T0	1-6	-	
HVT81_7	*H. vulgare*	pICSL4723	Golden Promise	SLNT81	ZmUbi:GFP:35S	T0	2-1	+	1
HVT81_8	*H. vulgare*	pICSL4723	Golden Promise	SLNT81	ZmUbi:GFP:35S	T0	2-2	+	1
HVT81_9	*H. vulgare*	pICSL4723	Golden Promise	SLNT81	ZmUbi:GFP:35S	T0	2-3	-	
HVT81_10	*H. vulgare*	pICSL4723	Golden Promise	SLNT81	ZmUbi:GFP:35S	T0	3-1	+	1
HVT81_11	*H. vulgare*	pICSL4723	Golden Promise	SLNT81	ZmUbi:GFP:35S	T0	3-2	+	1
HVT81_12	*H. vulgare*	pICSL4723	Golden Promise	SLNT81	ZmUbi:GFP:35S	T0	3-3	-	
HVT81_13	*H. vulgare*	pICSL4723	Golden Promise	SLNT81	ZmUbi:GFP:35S	T0	3-4	-	
HVT81_14	*H. vulgare*	pICSL4723	Golden Promise	SLNT81	ZmUbi:GFP:35S	T0	3-5	-	
HVT81_15	*H. vulgare*	pICSL4723	Golden Promise	SLNT81	ZmUbi:GFP:35S	T0	3-6	-	
HVT81_16	*H. vulgare*	pICSL4723	Golden Promise	SLNT81	ZmUbi:GFP:35S	T0	4-1	+	1
HVT81_17	*H. vulgare*	pICSL4723	Golden Promise	SLNT81	ZmUbi:GFP:35S	T0	4-2	+	2
HVT81_18	*H. vulgare*	pICSL4723	Golden Promise	SLNT81	ZmUbi:GFP:35S	T0	4-3	-	
HVT81_19	*H. vulgare*	pICSL4723	Golden Promise	SLNT81	ZmUbi:GFP:35S	T0	4-4	+	1
HVT81_20	*H. vulgare*	pICSL4723	Golden Promise	SLNT81	ZmUbi:GFP:35S	T0	4-5	-	
HVT81_21	*H. vulgare*	pICSL4723	Golden Promise	SLNT81	ZmUbi:GFP:35S	T0	4-6	-	
HVT81_22	*H. vulgare*	pICSL4723	Golden Promise	SLNT81	ZmUbi:GFP:35S	T0	5-1	-	
HVT81_23	*H. vulgare*	pICSL4723	Golden Promise	SLNT81	ZmUbi:GFP:35S	T0	5-2	-	
HVT81_24	*H. vulgare*	pICSL4723	Golden Promise	SLNT81	ZmUbi:GFP:35S	T0	5-3	+	1
HVT81_25	*H. vulgare*	pICSL4723	Golden Promise	SLNT81	ZmUbi:GFP:35S	T0	5-4	+	1
HVT81_26	*H. vulgare*	pICSL4723	Golden Promise	SLNT81	ZmUbi:GFP:35S	T0	6-1	-	
HVT81_27	*H. vulgare*	pICSL4723	Golden Promise	SLNT81	ZmUbi:GFP:35S	T0	6-2	-	
HVT81_28	*H. vulgare*	pICSL4723	Golden Promise	SLNT81	ZmUbi:GFP:35S	T0	7-1	+	1

ID	Species	Backbone	Accession	Code	Construct	Generation	Clone No.	Fluorescence	GFP copy no.
HVT81_29	*H. vulgare*	pICSL4723	Golden Promise	SLNT81	ZmUbi:GFP:35S	T0	7-2	-	
HVT81_30	*H. vulgare*	pICSL4723	Golden Promise	SLNT81	ZmUbi:GFP:35S	T0	7-3	-	
HVT81_31	*H. vulgare*	pICSL4723	Golden Promise	SLNT81	ZmUbi:GFP:35S	T0	7-4	-	
HVT81_32	*H. vulgare*	pICSL4723	Golden Promise	SLNT81	ZmUbi:GFP:35S	T0	7-5	+	1
HVT81_33	*H. vulgare*	pICSL4723	Golden Promise	SLNT81	ZmUbi:GFP:35S	T0	7-6	-	